

UNCLASSIFIED

AD 283 911

*Reproduced
by the*

**ARMED SERVICES TECHNICAL INFORMATION AGENCY
ARLINGTON HALL STATION
ARLINGTON 12, VIRGINIA**



UNCLASSIFIED

7

NOTICE: When government or other drawings, specifications or other data are used for any purpose other than in connection with a definitely related government procurement operation, the U. S. Government thereby incurs no responsibility, nor any obligation whatsoever; and the fact that the Government may have formulated, furnished, or in any way supplied the said drawings, specifications, or other data is not to be regarded by implication or otherwise as in any manner licensing the holder or any other person or corporation, or conveying any rights or permission to manufacture, use or sell any patented invention that may in any way be related thereto.

62-4-6

Technical Report: NAVTRADEVCEEN 801A

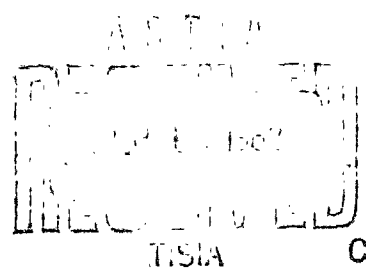
283 911

SIX-DEGREE-OF-FREEDOM EQUATIONS OF MOTION FOR
A MANEUVERING RE-ENTRY VEHICLE

John M. Schuler
Francis E. Pritchard

Cornell Aeronautical Laboratory, Inc.
of Cornell University
Buffalo 21, New York

15 June 1962



Prepared for

U. S. NAVAL TRAINING DEVICE CENTER
Port Washington, New York

Contract N61339-801

ASTIA
ALOG

283 911

**SIX-DEGREE-OF-FREEDOM EQUATIONS OF MOTION FOR
A MANEUVERING RE-ENTRY VEHICLE**

ABSTRACT

Equations of motion for a re-entry vehicle are developed for use with a digitally operated, fixed-base simulator. The equations provide:

1. Six-degrees-of-freedom for a vehicle of non-varying mass whose trajectory and orientation are given with respect to a spherical, rotating earth.
2. An inverse-square gravitational force, a rotating atmosphere, and relevant atmospheric properties.
3. Aerodynamic forces and moments in coefficient form, and reaction control moments.

The only restriction on attitude, maneuver, or flight path is that flights directly over the North and South poles are excluded.

The equations, as described, have been programmed on an IBM 704 and specific solutions were obtained to show effects of maneuvers, pilot's inputs, different geophysical models, and mathematical simplifications.

The report contains descriptive chapters on geophysics and aerodynamics and control which are especially pertinent to re-entry simulation. In addition, Appendices extend the equations for varying mass, large thrust, and earth oblateness with related effects.

Reproduction of this publication
in whole or in part is permitted
for any purpose of the United
States Government

F O R E W O R D

The application of high speed general purpose type digital computers to real time simulation was pioneered by the Naval Training Device Center and continued with the development of UDOTT (Universal Digital Operational Flight Trainer Tool) under joint sponsorship with the Air Force, Wright Air Development Division. UDOTT simulated a subsonic F9F and a supersonic F100 aircraft. The present study was initiated as a continuation of this development, to further explore the capabilities and requirements of real-time digital simulation in other areas.

The scope of the study was limited to an investigation of the equations of motion required for manned hypersonic flight and the possible simplification of these equations for computation in a digital computer for real-time simulation. A hypothetical vehicle was generated to be studied and to further limit the scope of the study, only the re-entry portion of the flight was to be considered. The study did have the advantage that simulation for training may be limited in frequency and response to those equations to which a pilot can be expected to react.

The present study concludes that considerable simplification can be effected in the general sense and additional simplification may be tolerable in specific training areas. However, the full flight dynamics of piloted hypersonic or near-orbital vehicles over the complete flight regime from boost, through orbit, re-entry and landing are too complex for simulation on UDOTT or present state-of-the-art computers. The study suggests that a breakdown into simpler regimes of limited complexity may be necessary to train for portions of the total flight. The possibility exists that high speed magnetic tape storage of portions of the program with entry into the computer during transitions from one phase to another would permit a continuous simulation as perceived by the pilot.



MILTON FISCHER

Head, Computer Branch

U.S. Naval Training Device Center

NAVTRADEV CEN 801A

TABLE OF CONTENTS

<u>Section</u>		<u>Page</u>
	FOREWORD	i
	TABLE OF CONTENTS	iii
	LIST OF TABLES	v
	LIST OF ILLUSTRATIONS	vi
	SYMBOLS AND DEFINITIONS	vii
I	INTRODUCTION	1
	1.1 Background	1
	1.2 Purpose	2
	1.3 Approach	3
	1.4 References	7
II	GEOPHYSICS.	9
	2.1 Introduction	9
	2.2 The Motions, Shape, and Gravitational Field of the Earth	11
	2.3 The Atmosphere.	16
	2.4 References	24
III	EQUATIONS OF MOTION.	28
	3.1 Introduction	28
	3.2 Vector Equations - Basic Principles and Concepts	29
	3.3 Axis Systems, Coordinates, and Transformations	34
	3.4 Matrix Equations	38
	3.5 References	50
IV	AERODYNAMICS AND CONTROL	56
	4.1 Introduction	56
	4.2 Flight Spectrum and Corridor	57
	4.3 General Aerodynamics for Re-Entry Vehicle	63
	4.4 Methods of Handling Aerodynamic Data	69
	4.5 Vehicle Control	72
	4.6 References	74

NAVTRADEV CEN 801A

<u>Section</u>		<u>Page</u>
V	SOLUTIONS OF EQUATIONS OF MOTION	80
	5.1 Conditions for Solution	80
	5.2 Re-Entry Solutions	84
	5.3 Roll Maneuver and Turn During Re-Entry	89
VI	SIMPLIFICATION OF EQUATIONS OF MOTION	98
	6.1 Introduction	98
	6.2 Simplifying Assumptions for Derivation of Equations of Motion	98
	6.3 Effect of Simplifications in Equations of Motion	100
VII	CONCLUSION	107
	7.1 Introduction	107
	7.2 Geophysical Data	107
	7.3 Coordinates and Axes for Integration	110
	7.4 Aerodynamic Representation	111
	7.5 Required Equations	112
	7.6 Conclusions	114
 <u>Appendix</u>		
A	SUMMARY OF EQUATIONS OF MOTION IN ALGEBRAIC FORM	115
	A.1 Equations of Motion	115
	A.2 Transformation Matrices	120
B	EXTENSION OF THE EQUATIONS TO LARGE THRUST AND VARIABLE MASS	122
	B.1 The General Vector Equations	122
	B.2 Application of Equations to Rocket Vehicles	125
	B.3 References	129
C	EXTENSION OF EQUATIONS FOR EARTH OBLATENESS AND SURFACE ABERRATIONS.	130
	C.1 Extension for First-Order Oblateness	130
	C.2 Special Surface Aberrations	137
	C.3 References	138

NAVTRADEV CEN 801A

Appendix

Page

D	SUMMARY OF DIGITAL TECHNIQUES USED IN PROGRAM	140
D. 1	General Mathematical Techniques	140
D. 2	Numerical Integration	142
D. 3	Obtaining Solutions of Equations of Motion	146
D. 4	References	149

LIST OF TABLES

Table

Page

5. 1	Comparison of Three Basic Cases.	90
5. 2	Effect of Attitude Perturbations on Trajectory Parameters	90
6. 1	Comparison of Simplification Solutions	104
6. 2	Effect of Simplifications on Short Period Dynamic Response .	104

NAVTRADEVGEN 801A

LIST OF ILLUSTRATIONS

<u>Figure</u>		<u>Page</u>
2. 1	Atmospheric Temperature Models.	25
2. 2	Atmospheric Density Models	26
2. 3	Atmospheric Wind Profile Models.	27
3. 1	Inertial, Earth, and Body Coordinate Systems.	51
3. 2	Coordinates for Relative Motion Over the Earth	52
3. 3	Orientation Angles	53
3. 4	Angular Displacements and Corresponding Angular Velocities.	54
3. 5	Orientation of Body, Stability, and Wind Axes; Conventions for Linear and Angular Velocities and for Control Surface Deflections	55
4. 1	h - V Diagram for the Study Vehicle	76
4. 2	Approximate Footprint for the Study Vehicle	77
4. 3	Newtonian Hypersonic Lift and Drag Characteristics	78
4. 4	Typical Normal Force Characteristics for Hypersonic Glider	79
5. 1	Three View of Typical Re-Entry Vehicle	91
5. 2	Longitudinal Aerodynamics - Trimmed Condition	92
5. 3	Equatorial Re-Entry Solution - Case I	93
5. 4	Atlantic Missile Range Re-Entry Solution - Case II	93
5. 5	Turning Re-Entry Solution - Case III	94
5. 6	Comparison of Three Basic Cases	95
5. 7	Angle of Attack Perturbations	96
5. 8	Short Period Transient, Roll Angle Input - Case III.	97
5. 9	Short Period Transient, Angle of Attack Perturbation	97
5. 10	Short Period Transient, Bank Angle Perturbation	97
5. 11	Short Period Transient, Sideslip Perturbation.	97
6. 1	Effect of $(\dot{V}_a)_g = (\dot{V})_g$ Simplification on Short Period Transient	105
6. 2	Effect of Angular Velocity Simplification on Trajectory Parameters	105
6. 3	Effect of Constant Gravitational Acceleration on Trajectory Parameters	106
6. 4	Effect of Earth Rotation on Trajectory Parameters	106
D. 1	Simplified Diagram of Computer Program	151

NAVTRADEVCEEN 801A

SYMBOLS AND DEFINITIONS

Symbols, definitions, and conventions are illustrated in Figures 3.1 through 3.5 and elsewhere in the report.

AXES

The following axes are right-handed orthogonal sets with origin at the center of gravity (c. g.), and a longitudinal plane of mirror symmetry for the aircraft is assumed.

Wind Axes

x_w directed along the relative wind
 y_w normal to the wind and in a plane normal to the plane of symmetry
 z_w normal to the wind and in the plane of symmetry, directed "down"
 B origin in space

Stability Axes

x_s in the plane of symmetry and coincident with the projection of the wind in that plane
 y_s normal to the plane of symmetry, directed along the right wing
 z_s in the plane of symmetry, directed "down"
 B origin in space

Body Axes

x in the plane of symmetry, directed toward the nose of the aircraft
 y normal to the plane of symmetry, directed along the right wing
 z in the plane of symmetry, directed "down"
 B origin in space

Earth-Surface Axes

x_{ES} perpendicular to the direction of the local gravitational force, directed north
 y_{ES} perpendicular to the direction of the local gravitational force, directed east
 z_{ES} coincident with the direction of the gravitational force, directed toward the earth
 B origin in space

NAVTRADEV CEN 801A

The following axes are right-hand orthogonal sets, with origin at the center of the earth.

Earth Axes

X_E	in the equatorial plane, normally passing through the zero meridian (Greenwich)
Y_E	in the equatorial plane
Z_E	normal to the equatorial plane, passing through the North Pole
E	origin in space.

Earth-Centered Inertial Axes

X_0	in the equatorial plane, normally in the direction of vernal equinox
Y_0	in the equatorial plane
Z_0	normal to the equatorial plane, passing through the North Pole
E	origin in space

The following axis system is assumed to be fixed with respect to the "fixed stars", and for practical purposes, its origin may be considered to be the center of the sun.

Inertial Axes

X_I	parallel to X_0 , normal in the direction of the vernal equinox
Y_I	parallel to Y_0
Z_I	parallel to Z_0
I	origin in space

DIMENSIONAL UNITS

distance - feet
time - seconds
angle - radians (unless otherwise noted)
force - lbs
moment - ft-lbs
mass - slugs

The angles (λ , ν , α , β , δ) and angular rates ($\dot{\rho}$, \dot{q} , \dot{r}) are presented in units of deg and deg/sec in the time histories and some figures. However, in all other cases (equations, derivatives, etc.) the standard dimensions given in the above table are used. Any deviation always has the proper units denoted.

NOTATION

$[\]$	matrix
$(\bar{\quad})$	vector (superposed bar)
$(\frac{d}{dt})_i, (\cdot)_i$	time rate of change with respect to the "i" axes
t	time

SYMBOLS

\bar{M}	linear momentum of the body
\bar{H}	angular momentum of the body about the c. g.
$\bar{F}; F_x, F_y, F_z$	sum of forces on the body; body axes components
$\bar{M}; M_x, M_y, M_z$	sum of moments on the body about the c. g. ; body axes components
m	mass of vehicle
$\bar{I}; I_x, I_y, I_z, I_{xz}$	moment of inertia operator relative to c. g. ; body axes components
$\bar{V}; u, v, w$	inertial velocity of body axes (not including earth's orbital velocity); body axes components
$\bar{\omega}; p, q, r$	inertial angular velocity; body axes components
$\bar{V}_E; V_\psi, V_\lambda, -V_r$	relative velocity of body with respect to earth, earth-surface axes components
\bar{V}_{er}	inertial velocity of body due to earth rotation
$\bar{\omega}_E; p_E, q_E, r_E$	angular velocity of body with respect to earth; body axes components
$\bar{\Omega}$	inertial angular velocity of the earth
\bar{r}	position vector
\bar{r}_{IE}	position of earth with respect to inertial axes
\bar{r}_{IB}	position of body with respect to inertial axes
\bar{r}_{EB}	position of body with respect to earth axes
$\bar{W}; W_\psi, W_\lambda, -W_r$	velocity of wind with respect to earth, earth-surface axes components
$\bar{\mu}; \mu_x, \mu_y, \mu_z$	gust velocity, body axes components
$\bar{V}_a; u_a, v_a, w_a$	velocity of body axes with respect to air, body axes components
$\bar{\omega}_a; p_a, q_a, r_a$	angular velocity of body axes with respect to the local air, body axes components
\bar{F}_a, \bar{M}_a	aerodynamic forces and moments
\bar{F}_g, \bar{M}_g	gravitational forces and moments
\bar{F}_T, \bar{M}_T	forces and moments due to thrust or reaction controls
L, D	lift, drag
λ, ψ	longitude, latitude

NAVTRADEVGEN 801A

V_T	tangential velocity over the earth's surface
ψ_T	heading angle of trajectory over the earth's surface
γ	climb or flight path angle
h	altitude
R_0	radius of earth
ψ, θ, ϕ	normal Euler angles of body axes with respect to earth-surface axes
ψ_s, θ_s, ϕ_s	special Euler angles
α	angle of attack
β	sideslip (angle)
$\delta_e, \delta_a, \delta_r$	elevator, aileron, and rudder deflections
S, b, c	wing area, span, and reference chord
C_x, C_y, C_z	force coefficients, body axes
C_l, C_m, C_n	moment coefficients, body axes
C_L, C_D	lift and drag coefficients, wind axes
g_0	acceleration of gravity at sea level
ρ	atmospheric density
a	speed of sound
T	atmospheric temperature
P	atmospheric pressure
M	Mach number, V_a/a
Re	Reynolds number
$q_i = \frac{1}{2} \rho V_a^2$	incompressible dynamic pressure
C_p	pressure coefficient, $\frac{P - P_{STATIC}}{q_i}$
\dot{Q}	stagnation point heat transfer rate
R	nose radius
ω_n	natural frequency (undamped)
ζ	damping ratio

NAVTRADEVCEEN 801A

LIST OF MATRICES

Body Axes

$$[F] = \begin{bmatrix} F_x \\ F_y \\ F_z \end{bmatrix}$$

external forces

$$[M] = \begin{bmatrix} L \\ M \\ N \end{bmatrix}$$

external moments about c. g.

$$[V] = \begin{bmatrix} u \\ v \\ w \end{bmatrix}$$

components of inertial angular velocity

$$[\omega] = \begin{bmatrix} p \\ q \\ r \end{bmatrix}$$

components of inertial angular velocity

$$[I] = \begin{bmatrix} I_x & 0 & -I_{xz} \\ 0 & I_y & 0 \\ -I_{xz} & 0 & I_z \end{bmatrix}$$

moments and products of inertial about the c. g. - $x-z$ symmetry assumed

$$[\omega_E] = \begin{bmatrix} p_E \\ q_E \\ r_E \end{bmatrix}$$

components of angular velocity with respect to earth axes

$$[V_a] = \begin{bmatrix} u_a \\ v_a \\ w_a \end{bmatrix}$$

components of velocity of c. g. with respect to air

$$[\omega_a] = \begin{bmatrix} p_a \\ q_a \\ r_a \end{bmatrix}$$

components of angular velocity with respect to air

$$[\mu] = \begin{bmatrix} \mu_x \\ \mu_y \\ \mu_z \end{bmatrix}$$

components of velocity of the air with respect to the earth axes - the increment over and above general air mass motions (gusts, etc.) - defined with respect to aircraft

$$[C_F] = \begin{bmatrix} C_x \\ C_y \\ C_z \end{bmatrix}$$

aerodynamic force coefficients

$$[C_M] = \begin{bmatrix} C_L \\ C_m \\ C_N \end{bmatrix}$$

aerodynamic moment coefficients

Earth Axes

$$[\Omega] = \begin{bmatrix} 0 \\ 0 \\ \Omega \end{bmatrix}$$

angular velocity of earth with respect to inertial space

$$[r_{EB}] = \begin{bmatrix} X_{EB} \\ Y_{EB} \\ Z_{EB} \end{bmatrix}$$

components of the position of the c. g. with respect to earth axes

Earth-Surface Axes

$$[V_E] = \begin{bmatrix} V_\psi \\ V_\lambda \\ -V_\tau \end{bmatrix}$$

components of the velocity of the c. g. with respect to earth axes

$$[V_{er}] = \begin{bmatrix} 0 \\ V_{er} \\ 0 \end{bmatrix}$$

the inertial velocity of the vehicle due to earth rotation: $V_{er} = \Omega r_{EB} \cos \psi$

$$[W] = \begin{bmatrix} W_\psi \\ W_\lambda \\ -W_\tau \end{bmatrix}$$

components of velocity of the air - general northward, eastward (westerly), and upward air mass motions (winds, etc.) - defined with respect to the earth

$$[(r_{EB})_{ES}] = \begin{bmatrix} 0 \\ 0 \\ r_{EB} \end{bmatrix}$$

components of the position vector of the body axes with respect to earth axes

Orientation Angles

$$[E_{ES-E}] = \begin{bmatrix} h \\ \nu \\ \lambda \end{bmatrix}$$

position coordinates of the earth-surface axes with respect to earth axes: h , altitude; λ , longitude; ν , latitude

$$[E_{B-ES}] = \begin{bmatrix} \phi \\ \theta \\ \psi \end{bmatrix}$$

successive rotations defining the orientation of the body axes with respect to earth-surface axes: ψ , azimuth ("yaw"); θ , elevation ("pitch"); ϕ , bank angle ("roll")

$$[E_s] = \begin{bmatrix} \phi_s \\ \theta_s \\ \psi_s \end{bmatrix}$$

alternate rotations defining the orientation of body axes with respect to earth-surface axes - used for dives, spins, high angle of attack re-entries, etc.: ψ_s , wing azimuth or spin angle ("roll"); θ_s , nose tilt ("pitch"); ϕ_s , wing tilt ("yaw")

Transformations

$$[L_{B-ES}] = [\phi] [\theta] [\psi]$$

transformation from earth-surface to body axes

$$[L_s] = [I^n] [\phi_s] [\theta_s] [\psi_s]$$

alternate transformation from earth-surface to body axes - used for $\bullet \rightarrow \pm 90^\circ$

$$[L_{B-ES}] = [L_s] = [L_{ij}]$$

$i = 1, 2, 3; j = 1, 2, 3$

$$[L_{ES-E}] = [I^n] [\nu] [\lambda]$$

transformation from earth axes to earth-surface axes

$$[L_{B-E}] = [L_{B-ES}] [L_{ES-E}]$$

transformation from earth to body axes

$$[L_{B-W}] = [\alpha] [\beta]$$

transformation from wind axes to body axes

$$[\phi] = \begin{bmatrix} 1 & 0 & 0 \\ 0 & \cos \phi & \sin \phi \\ 0 & -\sin \phi & \cos \phi \end{bmatrix} \quad [1''] = \begin{bmatrix} 0 & 0 & 1 \\ 0 & 1 & 0 \\ -1 & 0 & 0 \end{bmatrix}$$

$$[\theta] = \begin{bmatrix} \cos \theta & 0 & -\sin \theta \\ 0 & 1 & 0 \\ \sin \theta & 0 & \cos \theta \end{bmatrix} \quad [\psi] = \begin{bmatrix} \cos \psi & 0 & \sin \psi \\ 0 & 1 & 0 \\ -\sin \psi & 0 & \cos \psi \end{bmatrix}$$

$$[\nu] = \begin{bmatrix} \cos \nu & \sin \nu & 0 \\ -\sin \nu & \cos \nu & 0 \\ 0 & 0 & 1 \end{bmatrix} \quad [\lambda] = \begin{bmatrix} \cos \lambda & \sin \lambda & 0 \\ -\sin \lambda & \cos \lambda & 0 \\ 0 & 0 & 1 \end{bmatrix}$$



$[1'']$ is a 90° negative (counterclockwise) about the y -axis.
 $[\phi_s]$, $[\theta_s]$, and $[\nu_s]$ have the same form as $[\phi]$, $[\theta]$, and $[\nu]$, respectively.

$$[\beta] = \begin{bmatrix} \cos \beta & -\sin \beta & 0 \\ \sin \beta & \cos \beta & 0 \\ 0 & 0 & 1 \end{bmatrix}$$

$$[\alpha] = \begin{bmatrix} \cos \alpha & 0 & -\sin \alpha \\ 0 & 1 & 0 \\ \sin \alpha & 0 & \cos \alpha \end{bmatrix}$$

Operators

The general matrix

$$[r_p] = \begin{bmatrix} x \\ y \\ z \end{bmatrix}$$

is used to illustrate matrix operational notation.

Cross Product Operator:

$$[r_p \times] = \begin{bmatrix} 0 & -z & y \\ z & 0 & -x \\ -y & x & 0 \end{bmatrix}$$

Transpose:

$$[r_p]' = [x \ y \ z]$$

Derivative:

$$[\dot{r}_p] = \begin{bmatrix} \dot{x} \\ \dot{y} \\ \dot{z} \end{bmatrix}$$

Inverse:

$$[I] = [L_{\theta-\epsilon}] [L_{\theta-\epsilon}]^{-1}, [I] \text{ is the unity matrix.}$$

$$[L_{\theta-\epsilon}]^{-1} = [L_{\theta-\epsilon}]' = [L_{\epsilon-\theta}] \text{ for orthogonal transformations.}$$

Combinations and Special Matrices

$$[C] = \begin{bmatrix} \frac{1}{\cos \theta} & 0 & 0 \\ 0 & 1 & 0 \\ \frac{\sin \theta}{\cos \theta} & 0 & 1 \end{bmatrix}$$

$[C_s]$ is the same function of θ_s , as $[C]$ is of θ

$$[(\Omega)_{ES}] = \begin{bmatrix} \Omega \cos \psi \\ 0 \\ -\Omega \sin \psi \end{bmatrix}$$

$$[(\omega_{ES-E})_{ES}] = \begin{bmatrix} 0 \\ -\dot{\psi} \\ 0 \end{bmatrix} + [I^*] [\psi] \begin{bmatrix} 0 \\ 0 \\ \dot{\lambda} \end{bmatrix} = \begin{bmatrix} \dot{\lambda} \cos \psi \\ -\dot{\psi} \\ -\dot{\lambda} \sin \psi \end{bmatrix}$$

$$[(V_{er})_E] = [\Omega \times] [r_{EB}] = \Omega \begin{bmatrix} -Y_{EB} \\ X_{EB} \\ 0 \end{bmatrix}$$

$$[(\dot{V}_{er})_E] = [\Omega \times] [(V_E)_E] = \Omega \begin{bmatrix} -\dot{Y}_{EB} \\ \dot{X}_{EB} \\ 0 \end{bmatrix}$$

$$[L_{ES-E}] [(\dot{V}_{er})_E] = [(\Omega)_{ES} \dot{\lambda}] [V_E] = \Omega \begin{bmatrix} 0 & \sin \psi & 0 \\ -\sin \psi & 0 & -\cos \psi \\ 0 & \cos \psi & 0 \end{bmatrix} \begin{bmatrix} V_{\psi} \\ V_{\lambda} \\ -V_r \end{bmatrix}$$

$$[(\omega_{ES-E})_{ES}^X] = \begin{bmatrix} 0 & \lambda \sin \psi & -\dot{\psi} \\ -\lambda \sin \psi & 0 & -\lambda \cos \psi \\ \dot{\psi} & \lambda \cos \psi & 0 \end{bmatrix}$$

$$[I]^{-1} = \begin{bmatrix} \frac{I_z}{I_x I_z - I_x^2} & 0 & \frac{I_{xz}}{I_x I_z - I_x^2} \\ 0 & \frac{1}{I_y} & 0 \\ \frac{I_{xz}}{I_x I_z - I_x^2} & 0 & \frac{I_x}{I_x I_z - I_x^2} \end{bmatrix}$$

SECTION I
INTRODUCTION

1.1 BACKGROUND

The rocket engine, with its tremendous thrust capabilities, has produced a quantum jump in the possible aircraft flight speeds. Hypersonic flight for manned aircraft, at speeds near orbital velocity, can now be considered practical, and manned space vehicles are predicted for the near future. Hypersonic aircraft, with range capabilities from a few thousand miles to a few rotations of the earth, are the first breed of vehicles being considered. Examples are the X-15 airplane and the vehicles being developed under the Mercury and Dyna-Soar programs.

The role of man in hypervelocity flight vehicles has been the object of considerable interest and conjecture. Traditionally, man has been an element in the primary airplane control loop, but recent trends place more reliance on automatic controls and relatively less on man for the primary control function. This trend has been necessary because of man's limitations and the more stringent control requirements, rather than because of a desire to relieve or replace man's functions. Man's performance as an element in a control system is in certain ways very poor: his motor actions are power limited and slow; he requires an environment carefully controlled in temperature, pressure, and physical and chemical composition; and his tolerance to accelerations or situations producing mental stresses is limited. But in other ways his performance is unexcelled: he is extremely adaptable and is able to accept a multitude of different kinds of inputs, organize them, and interpret their meaning in terms of corrective action; man represents an extremely capable and efficient logical computer. Thus, if man's capabilities are to be efficiently employed, we must provide him with environmental conditions compatible with good performance and present him with the proper cues so that he can perform assigned tasks. These assigned tasks must be compatible with his limited motor capabilities. For man to perform effectively, he must not be overloaded with stabilization and control tasks which could be better performed by automatic devices; rather, enough of his potential must be reserved for tasks which utilize his unique decision making and adaptive capabilities.

Generalities of the foregoing type are rather easily come by, but it is not such a simple matter to specify the requirements for a particular vehicle or particular situation or set of circumstances. If one is dealing with hardware, one can usually find a mathematical model with which to represent the system and which describes system performance with sufficient accuracy to provide the system designer with all the information he needs to come up with a satisfactory design. However, man is so complex an element that such an approach cannot be used. Instead; one tries to accumulate data on particular details of the problem. For example, dimensional data on various pilots is used to design the physical layout of a cockpit and enough flexibility is built in to provide for the deviation from the normal values. Another approach has been to try to characterize man's actions under very special circumstances by an equation. Thus, work has been done on defining transfer functions for the human pilot in order to determine how he operates as a stabilizing device in an airplane, and what the characteristics of the airplane should be without the man in the loop. However, these are very specialized studies related to very particular circumstances. More generally, a large body of information has been collected by

engineers, psychologists, and bio-medical people. Based on past experience, one uses this data to try to design a compatible man-machine system. Then one builds such a system and modifies it to correct the errors.

Simulators offer a useful tool in system design. Rather elaborate simulation facilities can often be justified because of the expense involved in building, operating, and testing prototype flight systems. There are three types of simulators. One is the research simulator which is used to obtain general characteristics and data not related to specific systems. The variable stability airplane is a good example of such a research simulator. Another type of simulator is the design or development simulator used in the design of a specific vehicle. Finally we have the training simulator which is used to actually train pilots or improve their proficiency in flying specific airplanes. All three types of simulators are needed for hypervelocity flight vehicles. Much work has been done in this field, particularly in connection with the X-15, Dyna-Soar and Mercury projects; more is needed.

The Naval Training Device Center has sponsored, as a joint Navy and Air Force project, the development of a high-speed general purpose digital computer for application to real time simulation. The concepts were originated at the Moore School of Electrical Engineering, University of Pennsylvania; the Sylvania Electronic Systems Division of Sylvania Electric Products, Inc. developed the concepts into UDofTT (Universal Digital Operational Flight Trainer Tool). UDofTT consists primarily of the stored program digital computer, two aircraft cockpit mock-ups, and control consoles. This facility, located at Garden City, Long Island, is being used as a research tool for investigation of various real time simulation problems. The Naval Training Device Center, as part of a program to exploit the capabilities of UDofTT, has sponsored at the Flight Research Department of the Cornell Aeronautical Laboratory, Inc. a study of the equations of motion required to simulate the re-entry and landing of manned hypersonic flight vehicles of the Dyna-Soar type.

1.2 PURPOSE

The end objective of performing this study, as alluded to previously, is to determine the feasibility of using UDofTT as a piloted simulator for hypersonic flight vehicles. However, the specific results of this study, as presented in this report, are not intended to answer this question directly, but rather are intended to present just the necessary facts relative to the equations of motion.

On the surface, it might appear that six-degree-of-freedom equations of motion for a re-entry vehicle would not be substantially different from those for a supersonic fighter. However, a more careful examination of the problem shows this not to be the case. The new geophysical aspects entering the problem, such as spheroidal earth, earth rotation, wind gradients, atmospheric properties at high altitudes, and gravitational gradients, all complicate the equations of motion. The large variations in vehicle attitude often associated with re-entry (e. g. , angles of attack to 90°) and the non-linearities associated with hypersonic aerodynamics complicate the aerodynamic representation. Furthermore, the extreme speeds and altitudes characteristic of re-entry pose severe requirements on computational accuracy for solving the equations.

Recognizing that most of the complexity is introduced by the new

dimensions associated with near orbital and re-entry flight, it became the purpose of this study to investigate primarily these regions of flight. Also, in recognition of the complexity of the problem, it became the purpose of this study to find what simplifications could be made in the equations and still retain adequate simulation. Furthermore, since the equations were to be developed for a piloted maneuvering vehicle in which the primary emphasis was on the piloting problem (in other words, the solution was required to be accurate only so far as it affected the behavior of the pilot), it was recognized that analysis of the pilot's task would have an important influence on the required accuracy of the equations and the acceptability of the various simplifications.

Thus, the purpose of this study is to provide a set of equations of motion suitable for simulating manned hypersonic flight on a digital computer such as UDOFTT. Since the simulation is concerned primarily with the piloting task, the equations are intended to represent the re-entry and landing portion of the flight regime. Because the new aspects of the problem are associated with the near orbital portions of this flight regime, most of the study has been concerned with such problems. Little work has been done on low speed problems as these are already well understood.

Also, since the configurations and missions of hypersonic vehicles are not at present well defined, and since there are still large areas of hypersonic flight about which little is known, it is not reasonable to expect that any one particular set of equations will satisfy all requirements. For this reason, it is important to summarize the basis on which the recommended equations have been formulated and to summarize methods by which they can be extended, simplified, or altered to account for future changes in the circumstances governing their use. To this intent, sections on geophysics and aerodynamics, a complete derivation of the equations of motion, and appendices on extension of the equations have been included in this report.

1.3 APPROACH

The primary tasks in this study have been to derive equations of motion for a maneuvering re-entry vehicle, program these equations for solutions on an IBM 704 digital computer, and compute solutions of these equations to determine the effects of various parameters in the equations and the effects of making various simplifying assumptions in the equations. Early in the study, visits were made to several aircraft companies and NASA to discuss pertinent work being done on re-entry, with respect to both the simulation problem and the characteristics of manned hypersonic aircraft. The information so obtained was of real value in guiding the direction of study. The one outstanding finding was that (though several groups had attempted or were starting programs to solve the complete equations of motion for hypersonic flight) no such program existed in a developed state*. Numerous re-entry programs existed, but all

* Since completion of this study, the recently completed work of Brown, Brulle and Griffin was uncovered and their basic development of the equations of motion parallels closely the present work. While Brown et al. develop a generalized computer program in great detail, the present work was directed toward simplifying the equations to facilitate their solution on a real time digital computer.

Brown, R. C., R. V. Brulle and G. D. Griffin: "Six-Degree-of-Freedom Flight-Path Study Generalized Computer Program - Part I, Problem Formulation: WADD Technical Report 60-781, November 1960.

NAVTRADEVGEN 801A

involved substantial simplifying assumptions, primarily in the degrees of freedom considered or in the representation of the earth's shape, rotation, and gravitational force. It was apparent from our own initial efforts and from discussion with other people in the field that the task of developing, programming, and checking out complete equations of motion for a maneuvering hypersonic aircraft was no mean feat and that finding acceptable simplifications in the equations was of paramount importance.

Accordingly, equations of motion were derived which represented the conditions of near orbital and re-entry flight as completely as possible, but with certain notable exceptions. The earth was assumed spherical and no thrust or mass variations were included in the equations. Earth oblateness was excluded (both the geometric effect and the gravitational field effect) because it complicated the process of checking out the computer program and analyzing the results, and because sufficient work has been done by other investigators to show when oblateness has to be included. Variable mass and thrust were excluded arbitrarily because the vehicle was assumed to be a boost glider that was unpowered during re-entry, though this would not exclude the concept of a landing engine.

A typical re-entry vehicle configuration was selected for study - one with a low aspect ratio modified delta wing with vertical tails mounted at the wing tips and with fuselage above the wing. Estimates of lift, drag, and inertial characteristics were obtained and an idealized control system was selected to provide control of angle of attack, sideslip, and bank angle. The rapid dynamic response so obtained would be similar to the response that could be realized if the vehicle had an adaptive control system. Thus, though no aerodynamic moments as such were included, a useful and reasonable simulation of the over-all aerodynamic characteristics was obtained.

The principal area of interest for this study was defined as the re-entry and landing of hypersonic flight vehicles; more precisely, flight below 300,000 feet of altitude and less than 26,000 ft/sec (approximate circular orbital velocity). Accordingly, the geophysical models of interest are those for the earth's shape, the gravitational field, and the atmospheric density, temperature, winds, and turbulence (gusts). There is adequate data to formulate tentative models, within the defined limits, for all but atmospheric winds and turbulence. Existent data on winds at high altitudes is mostly for the northern hemisphere, particularly over the United States; almost no data is available on turbulence at high altitudes. Most of the atmospheric data is based on mean values and the data on temporal variations, particularly short time variations, is fragmentary. In Section II of this report, the present status of our knowledge of the pertinent geophysical characteristics is summarized, and mean or typical models are formulated for these characteristics. The air has been treated in this study as a normal continuum since free molecular flow effects do not take on significance until altitudes above 300,000 feet are reached (References 1.4, 1.5, 2.5).

A complete formulation of the aerodynamic characteristics for hypersonic vehicles cannot be made at the present time; adequate theory and data are not available. Even an attempt to discuss the available material is far beyond the scope of this investigation. However, enough effort was devoted to aerodynamics so as to define the over-all problem. Re-entry aerodynamics

NAVTRADEVCCEN 801A

is complex, more so than that for low speeds because of the new facets involved. There are three basic aspects: (1) lift and drag, the performance parameters which govern the vehicle's trajectory and provide path control, and the vehicle's deceleration which must be maintained within limits tolerable to the pilot; (2) aerodynamic heating, essentially a local flow problem which poses limits on the allowable flight regime; (3) stability and control characteristics, involving complex over-all flow problems, which can be expected to lead to stringent requirements for automatic control and limits on the allowable flight regime. The aerodynamic problem is compounded by the following aspect. We are dealing with a many faceted air: subsonic, transonic, supersonic, and hypersonic flow; ionization and dissociation, both laminar and turbulent boundary layers, and free molecular flow at the higher altitudes. We are dealing with a strongly non-linear problem: the basic non-linear nature of hypersonic flow and the high angles of attack contemplated in re-entry will cause severe non-linear stability and control problems. Furthermore, in hypersonic flight the problems associated with performance, heating, and stability and control are intimately related and cannot be treated independently, and their solutions are not mutually compatible. If the past can be used as an indicator, vehicle configurations will be established principally by performance and heating considerations, leaving stability and control to make the most of a poor situation. On this basis, we can expect stringent requirements for automatic control; should the automatic control system fail, it will be enough to just return man safely to earth - if even that is possible.

Much of the available data on projected manned hypersonic vehicles is classified, but the general aerodynamic characteristics can be formulated based on the available unclassified theory and experimental data. The vehicle's basic over-all characteristics at hypersonic speeds (lift, drag, stability derivatives) are similar to those at lower speeds, but non-linear effects are abnormally strong. We have attempted in this study to formulate a guide for suitably representing the aerodynamic data in the equations of motion, based on the requirements of the simulation task.

As for the control problem, it will be severe since the uncontrolled vehicle can be expected to have poor stability and control characteristics and both aerodynamic and reaction controls will be necessary. An adaptive control approach will very likely be used because of the extremes involved in the control problem. Achieving adequate reliability will be difficult. Performance and aerodynamic heating will enter the control problem in the form of energy management and temperature control systems and pilot's displays. A unified approach will be needed for the whole control problem, including flight controls, energy management system (including propulsion), temperature control system, navigation and guidance system, and the pilot with his displays and controls. In this study, we have not considered all these problems in detail. Rather, we have tried to formulate the equations of motion so that the necessary data (variables and quantities) would be available for the pilot's displays and the various systems.

The derived equations were programmed on an IBM 704 digital computer, and a fourth order Runge-Kutta numerical integration scheme was used to solve the equation. Work was done on a more sophisticated integration technique utilizing a "predictor-corrector" integration formula which automatically varied the integration time interval. However, there was insufficient time to develop

the numerical error criteria required to adjust the time interval, and the straight Runge-Kutta integration technique was used for all the solutions obtained in this study. Considerable difficulty was encountered in checking the equations as programmed on the IBM 704. The normal difficulties (eliminating mistakes in the equations and the program) were compounded by the difficulty in obtaining a satisfactory numerical integration technique. It was estimated that if the Runge-Kutta method was used and the control system parameters were selected to give good handling qualities, it would take 10 hours of computing time to solve for one re-entry - a prohibitively long time. This long computing time evolved because the integration time interval had to be short enough to compute the fastest mode of motion present in the equations (the longitudinal and lateral short period motions which for good handling qualities would have 0.5 cps natural frequencies). If such solutions had been computed, it was not certain that they would have been correct because of the round-off errors in the integration of the variables describing the trajectory of the vehicle. The scope of the work did not permit an extensive study to solve these difficulties so a useful expedient was adopted. It was reasoned that the combined dynamics of airplane and pilot, as the pilot tried to control his trajectory in re-entry would have a much lower effective natural frequency than that of the airplane alone. It was determined that a .05 cps natural frequency was typical of the control-fixed longitudinal short period mode for a re-entry vehicle at 250,000 feet of altitude (Reference 1.6). Accordingly, the control system parameters were selected to provide a 0.7 damping ratio (ζ) and .05 cps natural frequency (ω_n) in the angle of attack, sideslip, and bank angle modes. By this reduction in short period natural frequency from 0.5 cps to .05 cps, the computing time for a re-entry was reduced to about one hour. A further reduction to about 20 minutes was effected by the following computational expedient. For those portions of the re-entry where no short period response were being excited by command inputs and the control system was simply regulating, an integration time interval was selected just small enough to provide a stable computation. Then when command inputs were inserted, simulating positive pilot control action, the time interval was decreased to obtain an accurate computation of the short period motions. In this manner it was possible, using the Runge-Kutta integration technique, to obtain a reasonably short computing time for re-entries and at the same time compute accurately both short period and long period or trajectory motions.

Considerable thought was given as to what solutions should be computed. It was clear that because of the purpose of this study, it was not necessary to hold the re-entry to any precise limits. Any solution which approximated re-entry conditions would satisfy, but on the other hand it was necessary that the solutions encompass all the elements that would actually be encountered (e. g., non-equatorial flight, skips during re-entry, both lateral and longitudinal maneuvers, excitation of both short and long period dynamic modes and their interaction). It was also necessary to obtain some measure of significance of the various effects in relation to the piloting problem, particularly to assess the quantitative significance of simplifications in the equations of motion. Accordingly, three basic solutions or cases were selected for study: (1) an equatorial re-entry at constant angle of attack, (2) a similar re-entry but aligned down the Atlantic Missile Range, and (3) a re-entry initially like (2), but in which a 45° banked turn was initiated at the bottom of the first skip and held for the duration of the solution. Perturbations about Case (1) were made in which the angle of attack (α), the bank angle (ϕ), and sideslip (β) were

varied. These perturbation solutions provided a measure of the effectiveness and sensitivity of the pilot's control over the vehicle's trajectory. The effect of short period dynamics was determined by effecting the banked turn and the perturbations in α , β , and ϕ by step command inputs, all at the bottom of the first skip.

It would have been desirable to compute additional types of solutions (particularly re-entries from the recovery ceiling, re-entries for different α 's and L/D's, and re-entries with winds and gusts), but shortage of time precluded such solutions.

The programmed equations included certain initial simplifications: no earth oblateness, no thrust, constant mass. The effects of oblateness are determinable from the literature, and their pertinence to the simulation problem is discussed in this report (Section 6.2). Thrust and variable mass are outside the scope of this study, but methods for their inclusion in the equations of motion are discussed in Appendix B. Study of simplifications in the equations of motion, other than these two initial ones, has been effected by computing solutions on the IBM 704 with the simplified equations and comparing these solutions to those obtained with the complete equations. It was not possible to study the effect of each individual term in the equations - far too lengthy a process. Instead, the effect of various groups of terms with some physical significance were examined (e.g., the effect of earth rotation in the equations for $\dot{\alpha}$ and $\dot{\beta}$); and also, total effects of certain quantities were examined (e.g., the effect of neglecting earth rotation entirely). It was necessary to assess the effect of a simplification from two standpoints: first, from the effect on the over-all trajectory; and second, from the effect on the short period motions. Also, it was necessary to consider interaction of the two effects. Evaluation of whether a simplification was allowable or not was primarily based on how it affected the piloting task. Here, the perturbation solutions (Case (3) with variations in α , ϕ , and β) helped to give some quantitative measure of the importance of a change in the solution; but at the same time, experience and knowledge of airplane handling qualities and the piloting task were also important.

Recognizing that many problems have not received adequate evaluation in this study and that concepts change rapidly, we do not consider the equations developed in this report as necessarily optimum nor have we attempted to be completely explicit in the formulation. Accordingly, we have attempted to denote the shortcomings of the equations, to point out possible methods for improvement, and to show in what areas there is insufficient knowledge for definitive formulation.

1.4 REFERENCES

- 1.1 Allen, H. Julian: "Hypersonic Flight and the Re-entry Problem (Twenty-First Wright Brothers Lecture)" Journal of the Aeronautical Sciences, April 1958.

NAVTRADEVCEEN 801A

- 1.2 Wargo, Julian J.: "UDOF TT - A Digital Computer Controlled Flight Simulator-Trainer." General Telephone and Electronics Corporation, G. T. & E. Research and Development Journal, January 1961.
- 1.3 Wychorski, Henry J.: "Reproduction of Aircraft Dynamic Response in Real-Time by a Digital Computer System." Aerospace Engineering, May 1961.
- 1.4 Gazley, Carl Jr.: Atmospheric Entry of Manned Vehicles. Rand Corporation Report No. RM-2579, January 20, 1960.
- 1.5 Probststein, Ronald F.: Shock Wave and Flow Field Development in Hypersonic Re-entry. American Rocket Society Paper No. 1110-60, Presented at ARS Semi-Annual Meeting, May 9 - 12, 1960. (ARS J., Feb. 1961)
- 1.6 Etkin, B.: Longitudinal Dynamics of a Lifting Vehicle in a Circular Orbit. University of Toronto, Institute of Aerophysics, Report No. 65 (AFOSR TN 60-191), February 1960.

SECTION II
GEOPHYSICS

2.1 INTRODUCTION

Since any geophysical property of the earth may have many different mathematical models of varying complexity depending upon application, the properties which affect atmospheric re-entry flight have been studied with the objectives of this project as a guide; that is, the formulation of re-entry vehicle equations of motion suitable for use with a fixed-base flight simulator driven by a digital computer. It is for the purpose of defining adequate models of the pertinent geophysical properties that this section is included.

All geophysical elements usually modeled for the study of normal atmospheric flight must be considered; but, in addition, some of these concepts must be extended and other completely new concepts added. In other words, the operation of a re-entry vehicle within the normal flight range is just one segment of a wider range of operation which begins with orbital conditions and ultimately ends with low subsonic velocities near the surface of the earth. In the paragraphs which follow, a qualitative discussion of various phases of re-entry is given.

In a near-orbital condition (defined here as an orbit whose lifetime is only a few revolutions) the major force acting on a re-entry vehicle is the gravitational force which is essentially balanced by the so-called centrifugal force due to the vehicle's velocity. Present also are the very small aerodynamic forces drag and lift. It is the drag force which causes inevitable orbital decay while the lift force produces "long" and "short" period oscillations analogous to the usual low altitude longitudinal flight oscillations. The analysis of Reference 1.6 shows that the period of the "long" period oscillation approaches orbital period and, in variance with its name, the period of the "short" period oscillation approaches infinity as altitude increases. As small as the aerodynamic forces are, however, they completely mask any effects of lunar and solar gravitational fields, the earth's magnetic field, radiation pressures, atomic particle and micrometeorite collisions, and other lesser effects.

The gravity and drag forces are probably more important in this near-orbital condition. Accurate description of the vehicle's orbital lifetime, a function of drag, is dependent upon adequate knowledge of air density and accurate determination of vehicle velocity with respect to the air. The former requires a good model of density while the latter requires that the atmosphere rotate with the earth. This means that the earth's angular velocity should be included with the equations of motion. There are smaller periodic and secular (non-periodic) drag effects, but they are not discussed here.

The largest single external force acting on an orbiting vehicle is gravity. As such, it affects all flight near the earth. With regard to an orbital vehicle, the earth's true gravitational field produces some small perturbation effects due to the oblateness in addition to the usual radially directed force. The perturbations are periodic and secular with secular motions such as regression of

nodes* and precession of the line of apsides** being most important. Further information can be obtained from Reference 2.1. As a consequence of their magnitudes, the gravitationally-induced periodic effects are negligible and the secular effects become important only for an extended stay in orbit. Since an extended stay in orbit is not at all likely for a re-entry vehicle, the gravitational effects of oblateness are probably not important in this study.

The most important effect of the earth's oblateness is due to the geometry involved. The path of an orbiting vehicle near the earth or one re-entering the atmosphere is affected because the oblateness causes periodic changes in atmospheric density for the orbiting vehicle and similar but not necessarily periodic changes in density for a re-entering vehicle. Earth oblateness also produces, in analysis, a vehicle location problem because pseudo-spherical*** coordinates (μ, ν, λ) such as derived in Section III no longer give the vehicle's location with respect to the earth. Oblateness can cause latitude errors of nearly 12 miles on the earth's surface and differences of about 6.5 miles in altitude when compared with a mean spherical earth.

As the vehicle penetrates deeper into the sensible atmosphere, the phase actually called re-entry begins. During the re-entry the most severe aerodynamic effects, deceleration and heating, occur. Drag is indirectly responsible for both, in the sense that deceleration is proportional to drag and the vehicle's kinetic energy is, through the mechanism of drag, converted to heat. Lift force is an important moderating factor during re-entry because it can be controlled to decrease decelerations and heating rates. However, lift can, and usually does, cause some "skipping" which is the "long" period oscillation mentioned previously, and an increase of total heat input. In addition, lift provides the capability for correcting certain miscalculations or errors made previously during re-entry. It becomes apparent that geophysical properties must be adequately modeled for the re-entry phase, especially the atmospheric density and temperature models which are very necessary for computation of aerodynamic forces. Earth rotation, too, with the corresponding atmospheric rotation, grows increasingly more important as the vehicle's inertial velocity decreases in re-entry.

The final phase of a re-entry might be described as "normal flight" because the vehicle is operating at velocities and altitudes common to ordinary high performance aircraft. Here, restrictions are relaxed on requirements of some of the geophysical properties; for example, the gravitational acceleration could be taken as constant and the earth's shape can be considered spherical, for at this velocity and altitude the vehicle's range is short. However, it may be desirable to evaluate the effect of winds and gusts upon the vehicle. The large scale winds probably would cause deviations from the desired path while gusts could

* The line of nodes is the line which connects points of intersection of the orbit and the equatorial plane.

** The line of apsides is the major axis of the elliptical orbit, the line connecting the apogee and perigee which are respectively the farthest and the nearest points from the center of the gravitational field.

*** The variables (μ, ν, λ) are called pseudo-spherical because the usual spherical coordinates are equivalent to $(r_{EB}, 90^\circ - \nu, \lambda)$ in the derivation of Section III.

cause difficult and dangerous handling problems for the pilot of a re-entry vehicle, especially if the vehicle is marginally stable.

Any set of geophysical properties chosen for equations of motion of a re-entry vehicle would be consistent in themselves and therefore "correct". For a flight simulator, however, the geophysical modeling should be made as nearly "real" as possible. The simulator models should provide, simply and adequately, the realism needed throughout the various phases of re-entry flight. The next sections provide a description of the various geophysical properties of the earth. The problem will be divided into two major categories: first, the motions, size and shape, and gravitational field of the earth; and second, the earth's atmosphere.

2.2 THE MOTIONS, SHAPE, AND GRAVITATIONAL FIELD OF THE EARTH

In order that accurate equations of motion for a vehicle may be written, the equations must be referred to an inertial frame. For orbital or re-entry studies a convenient reference frame would be centered in the earth and possibly rotating with the earth. However, this earth-centered frame is not an inertial frame because the earth is not fixed in space. It is possible to refer all motions of a vehicle to such an earth-centered frame provided the motions of the earth are known.

The two principal motions of the earth which might significantly affect the equations of motion are:

1. rotation about its axis, and
2. revolution about the sun.

These motions will be discussed in detail later with emphasis placed upon applicability of the motion to this study. Additional information is given by Parvin, Reference 2.2.

It is necessary to know the shape or figure of the earth so that the position of an orbiting or re-entry vehicle may be accurately described. Generally, this is a more difficult situation to resolve mathematically than the motions of the earth. Altitude can be obtained in terms of the vehicle's spherical coordinates for an earth-centered frame by knowing the magnitude of the radius vector and the radius of the earth at some point on its surface. It is the model of the earth's size and shape which defines the radius of the earth. Altitude is used in preference to the radius vector magnitude because the earth's surface provides a convenient reference for altitude determination, the concept of altitude has been in general use for aeronautical work since the earliest days of flight, and atmospheric properties, as described in Section 2.3 for example, are presented in terms of altitude. Unfortunately, altitude must be described mathematically in a different way for each model of the shape of the earth, although the definition of altitude remains the same in each case. Altitude is generally defined as the height of a vehicle above some reference spheroid, measured normal to the local surface of the spheroid.

Latitude and longitude of the vehicle are mathematically described, like altitude, differently for each earth-shape model. In general, there exists more than one definition of latitude, but usually only one definition of longitude. The

latter may be accounted for by the assumed axially symmetric figure for the earth. Longitude is defined as the angle between the projection of the radius vector on the equatorial plane and some reference direction in that plane which is usually the direction of the line from the earth's center through Greenwich, England. Two definitions of latitude are given here. Geocentric latitude, as its name may imply, is the angular measure from the equatorial plane to the radius vector of some point using the earth center as vertex for the angle. Geodetic latitude is the angle between the equatorial plane and the line to the given point which is normal to the reference spheroid. A more complete analysis of the vehicle position problem is given in Appendix C.

In many analyses of flight the acceleration of gravity can be taken as a constant without serious restriction; however, to study the motions of a vehicle during atmospheric re-entry and during its orbital and boost phases, a more accurate description of this acceleration is undoubtedly necessary. The possibilities include a simple inverse-square variation and the more complicated but more nearly correct oblate spheroidal variation which has a non-radial component. An adequate description of gravitational acceleration for use with a re-entry flight simulator has been an objective of this study and is reported here.

2.2.1 Earth Motions

The earth's rotation is clearly the most significant of all its motions so far as equations of motion for a hypersonic re-entry are concerned. Rotation about the earth's polar axis is a full 360° each day in a counterclockwise sense when viewed from above the North Pole. With respect to the so-called "fixed" stars, a 360° rotation is described as a sidereal day which is 23 hours, 56 minutes, 4.09 seconds in length. With respect to the sun, however, the full rotation of the earth is more than 360° in space. The solar day is, therefore, longer than the sidereal day by the time required for the extra rotation: about 4 minutes, but not exactly so because each solar day is of different duration. This effect is due to the earth's orbital motion about the sun. The durations mentioned above are in terms of mean solar time, which is identical with ordinary civil time except for its reference. Mean solar time will be used in all discussions henceforth.

One complete revolution of the earth in its orbit about the sun, with respect to inertial space, requires 365.256,360,42 mean solar days* and is called a sidereal year. The orbit is slightly elliptical with an eccentricity of 0.0167272, and the earth's revolution is counterclockwise when viewed from above the North Pole. It is because the earth's orbital motion and its rotation are in the same direction that the solar day is longer than the sidereal day. In addition, the ellipticity of the orbit means that the earth moves along in its path a different angular distance each solar day, thus accounting for the variable length of the solar day mentioned in the preceding paragraph. The aphelion, or the greatest distance from the sun, is 1.519×10^{11} meters while the perihelion, the least distance, is 1.469×10^{11} meters. A situation of importance is that throughout the earth's orbital motion the sun's gravity will attract the earth and any body near it (e. g., a re-entry vehicle) with nearly equal forces.

* The mean solar day, which has a constant length, represents the average of all true solar days during one revolution of the earth about the sun.

An elementary mathematical study of the earth's motions will show that only two motions, the earth's rotation around its polar axis and its revolution about the sun, have any appreciable effects that need be considered in the study of a re-entry vehicle. That is, precession and nutation of the polar axis, etc. can be neglected. The preceding paragraph concludes with a verbal argument for neglecting the translational motions of the earth, and Section 3.2.1 contains a mathematical description of the same argument. The result, then, is that the earth's sidereal rotation is the only motion that need be considered. Since the earth completes one rotation in space each 23 hours, 56 minutes, 4.09 seconds, its angular velocity is

$$\Omega = 0.004178075 \text{ deg/sec.}$$

The earth's angular velocity is very slowly decreasing with time, but this secular variation of Ω is of no concern here. Thus, by neglecting the earth's revolution about the sun and using the sidereal rotation, a non-rotating reference frame whose origin is fixed at the center of the earth may be used as an inertial frame.

The earth's angular velocity causes a vehicle moving northward to appear to veer eastward unless it is constrained to the earth's surface. This apparent acceleration, that must be considered if one attempts to use the rotating earth as an inertial frame, is called the Coriolis acceleration. In vector notation, the acceleration is stated as the cross product

$$\vec{A}_c = -2\vec{\Omega} \times \vec{V}_E \quad (2.1)$$

in which \vec{V}_E is the vector velocity with respect to the rotating earth. This Coriolis acceleration, a component of the total acceleration, is a direct consequence of twice differentiating the vehicle's position vector, \vec{r}_{EB} , when the position vector is expressed with components in an earth-centered frame rotating at angular velocity $\vec{\Omega}$ in inertial space.

Model of Earth's Motion: The earth's angular velocity given above was rounded off to the value

$$\Omega = 0.004178 \text{ deg/sec}$$

for obtaining the solutions of Sections V and VI.

2.2.2 The Size and Shape of the Earth

Neglecting surface irregularities of large and small scale, the earth is oblate spheroidal; that is, its polar radius (coincident with the axis of rotation) is smaller than its equatorial radius. It is possible to mathematically define the spheroid as an ellipsoid of revolution symmetric about the polar axis. In terms of the equatorial radius (a), flattening (ϵ), and geocentric latitude (ψ), the radius of the earth is:

$$R_{\psi} = \sqrt{\frac{a^2}{\cos^2 \psi} + \frac{a^2(1-\epsilon)^2}{\sin^2 \psi}} \quad (2.2)$$

for which adaptation of Kaula's data (Reference 2.3) gives

$$\epsilon \triangleq \frac{a-b}{a} = \frac{1}{298.24}$$

$$a = 6,378,163 \text{ meters} = 20,925,732 \text{ feet.}$$

For comparison with the equatorial radius, the polar radius (b) can be computed using a and ϵ :

$$b = 6,356,777 \text{ meters} = 20,855,567 \text{ feet.}$$

This oblate spheroidal representation of the earth's size and shape is adequate (or more than adequate) for nearly all applications. Equation 2.2 can be simplified, if desired, by obtaining its power series expansion in terms of flattening and using only a few terms of the expansion.

If a less precise model of the earth's size and shape will suffice, the earth can be considered spherical. It is best, then, to choose some mean radius for the earth in terms of the equatorial and polar radii given above. Many mean radii can be defined according to various criteria; however, a suitable mean is that which makes the volumes of sphere and spheroid equal:

$$R_0 = a(1-\epsilon)^{1/3} \approx a(1-\frac{1}{3}\epsilon) \quad (2.3)$$

$$\approx 20,902,343 \text{ feet}$$

Since the earth's geometric shape affects aerodynamic forces on a vehicle (indirectly through altitude dependent atmospheric properties such as density and temperature), in a particular case one might prefer a "mean" radius chosen to provide a better value of altitude (\mathcal{L}) and geocentric radius ($r_{g,0} = \mathcal{L} + R_0$) than that given by Eq. 2.3. This would be especially true for re-entries confined to equatorial or polar regions where the earth radius most differs from the mean of Eq. 2.3.

A more precise description of the shape of the earth has been obtained recently from studies of the motions of artificial satellites. Although gravity measurements at the earth's surface have for years indicated the presence of large-scale undulations of the surface, data was sufficiently scarce to prevent good estimates of the magnitude and extent of the undulations. The artificial satellites have produced good gravitational data which can be analyzed to obtain a description of the earth's shape. This data has verified that the equator is not circular, but slightly elliptical, making the earth more nearly a triaxial ellipsoid. In addition, the "pear-shaped" figure of the earth was "found" by analyzing satellite tracking data. In general, these more precise models of the earth are unnecessary for work involving equations of motion of re-entry vehicles.

Model of Size and Shape: The solutions of the equations of motion presented in this report have been computed using a spherical earth model whose radius is:

$$R_0 = 20,860,000 \text{ feet.}$$

This value is somewhat less than that indicated by Eq. 2.3, but this does not affect the significance of the solutions.

2.2.3 The Gravitational Field

The earth's gravitational field is in reality an extremely complex thing which depends entirely on mass distribution. It is possible, however, to express mathematically the gravitational potential to any degree of precision with a summation of spherical harmonics for the potential:

$$U = \sum_{n=0}^{\infty} \sum_{m=0}^n \frac{1}{r_{EB}^{n+1}} P_n^m(\sin \psi) (A_n^m \cos m\lambda + B_n^m \sin m\lambda) \quad (2.4)$$

in which any term, U_n^m , is of degree n and order m, and $P_n^m(\sin \psi)$ is the associated Legendre function. Recent studies of artificial satellite motions and other geodetic data have resulted in evaluation of this potential function to terms of $m = n = 8$ (see Kaula, Reference 2.3). Gravitational acceleration is then obtained as the gradient of the potential.

Certainly, so complete a description of the gravitational field as is given above is not needed for the equations of motion developed in Section III. The potential function can be considerably simplified by neglecting the dependence on longitude (λ), a reasonable assumption for the earth. In this case, the potential function, in an alternate notation, is

$$U = \frac{Gm_e}{r_{EB}} \sum_{n=0}^{\infty} J_n \left(\frac{a}{r_{EB}}\right)^n P_n^0(\sin \psi) \quad (2.5)$$

in which G is the universal gravitational constant, m_e is the mass of the earth, r_{EB} is the magnitude of the position vector a is the equatorial radius, and the J's are constants which specify the magnitude of the deviations from spherical (i. e., for $n \geq 2$). Kaula (Reference 2.3) states the following values:

$$\begin{aligned} a &= 6,378,163 \text{ meters} = 20,925,732 \text{ feet} \\ Gm_e &= +3.98602 \times 10^{14} \text{ m}^3/\text{sec}^2 = 1.40765 \times 10^{16} \text{ ft}^3/\text{sec}^2 \\ J_0 &= 1 \\ J_1 &= 0 \\ J_2 &= -1082.61 \times 10^{-6} \\ J_3 &= +2.05 \times 10^{-6*} \\ J_4 &= +1.43 \times 10^{-6} \end{aligned}$$

Actually, he gives values for J_6 and J_7 but the corresponding errors are large relative to the coefficients themselves and, therefore, the coefficients are not listed here.

Probably the most widely used description for the earth's gravitational field is the familiar inverse-square acceleration whose potential is given by

$$U = \frac{Gm_e}{r_{EB}} \quad (2.6)$$

* This is the term which results from the earth's "pear shaped" figure. The small or stemmed end of the pear is at the North Pole.

which is simply the zero order term ($n = 0$) of the two more precise formulations given by Equations 2.4 and 2.5. The gradient of this potential gives the following expression with its equivalent in terms of acceleration of gravity at mean sea level:

$$\bar{g} = -\frac{Gm_{\oplus}}{r_{EB}^3} \bar{r}_{EB} = -g_0 \left(\frac{R_0}{r_{EB}} \right)^2 \frac{\bar{r}_{EB}}{r_{EB}} \quad (2.7)$$

This equation clearly indicates that Gm_{\oplus} and $g_0 R_0^2$ are equal in magnitude. Thus, by using the value for Gm_{\oplus} given above and the value for R_0 from Eq. 2.3, the sea level gravitational acceleration can be evaluated:

$$g_0 = \frac{Gm_{\oplus}}{R_0^2} = 32.318 \text{ ft/sec}^2 \quad (2.8)$$

Of course, the expression can be used to obtain R_0 if g_0 is available.

Usually an inverse-square law for gravity is modeled in conjunction with a spherically shaped earth. Because there is a possibility that an inverse-square law would be used with an oblate spheroidal shape for the earth, it is important to specify what earth radius should be used to find g_0 . Since the J_2 term of Eq. 2.5 is the predominant deviation from the spherical field, the other higher order terms can be ignored; therefore, the radius at which the second harmonic (J_2) term is zero ($\psi \approx \pm 35.3^\circ$) should be used with Eq. 2.8 above.

Model of the Gravitational Acceleration: For the solutions presented in Sections V and VI of this report, an inverse-square gravitational acceleration (consistent with the spherical shape) is used. The sea level gravity is specified:

$$g_0 = 32.17 \text{ ft/sec}^2$$

a value somewhat lower than given by Eq. 2.8.

2.3 THE ATMOSPHERE

This section, which describes the atmosphere and models of some of its properties, begins with a discussion of general properties and atmospheric shells; then narrows considerably to physical properties of the atmosphere which affect the description of a re-entry flight, the temperature, density, winds and gusts.

2.3.1 General Discussion

The atmosphere is a very complex body of matter which can be analyzed (Reference 2.4) according to its various:

1. Physical qualities (density, pressure, temperature),
2. Chemical qualities (composition, dissociation, molecular weight),
3. Electrical and nuclear qualities (ionization, aurora),
4. Motions (jet stream, turbulence),
5. Biological aspects (physiological effects upon man), and
6. Technical aspects (aerodynamic forces and heating).

The physical qualities, motions, and the technical aspects are most important from the point of view of the equations of motion for a re-entry vehicle. However, in the real situation, each of the six points above can be important. Pressure, density, and temperature are variable with altitude; and, in fact, temperature is commonly used as a basis for dividing the atmosphere into nearly concentric, approximately spherical, contiguous shells having indistinct boundaries (called pauses*) at various altitudes. The usual division of the atmosphere into shells, with a short description of some corresponding atmospheric motions, temperature gradients, and technical aspects, follows.

Troposphere: Winds and turbulence are prevalent; jet streams exist near the tropopause which is at about 45,000 feet. The temperature gradient is negative. This is the region of greatest air density. Air breathing engines are used and aerodynamic control of flight vehicles is not only possible but advantageous.

Stratosphere: In the lower regions jet streams exist, but the upper regions are calm. There is no weather. The stratopause is placed at about 100,000 feet, which also represents an approximate practical limit for ordinary air breathing engines. In the upper regions of the stratosphere, aerodynamic controls tend to be ineffective, which necessitates the use of reaction controls. The temperature gradient is approximately zero.

From this point the division is not nearly so well defined. Reference 2.5 summarizes many different approaches to further shell separation which depend upon temperature, composition, ionization, etc. Here, the breakdown will follow that given in Reference 2.4, Table 3 - 7A, which is a breakdown based upon a composite of properties:

Chemosphere: In the upper region, which has a negative temperature gradient, there is some turbulence and ionization begins. The lower region has a positive temperature gradient. The chemosphere is aerodynamically a slip flow region in which high glide-vehicle velocities are feasible. The region has high-velocity geostrophic winds, but very low density. The chemopause is at 260,000 feet.

Ionosphere: The atmosphere is increasingly ionized with altitude in this region due to solar ultraviolet radiation. There is probably some slight turbulence with increasing wind velocities but, like the chemosphere, the density is so small that the net effect on a re-entry vehicle is negligible. This is a region of free molecular flow. Temporary earth satellites are possible.

* Pause, with the prefixed root word, is used to indicate the upper boundary of a region (e. g., tropopause is the boundary between the troposphere and stratosphere).

Ionosphere: (continued)	The temperature gradient is positive. The ionopause is at approximately 250 miles.
Mesosphere and Exosphere:	These regions were essentially unexplored and relatively little was known about them before the era of earth satellites. They are what could be called regions of near-space flight although there is some remaining atmosphere of ionized particles, and radiation belts are present. Satellite lifetimes are indefinite. These regions are, however, of no interest in the usual re-entry problem.

The above description should provide a rudimentary understanding of the environment for near orbital and re-entry flights.

2.3.2 Density and Temperature

Since density and temperature are physically interdependent, this section will discuss both. The density is an atmospheric property which is of great importance in flight. For a given velocity, the aerodynamic forces and moments acting on the vehicle are proportional to the density. This explains the relative ineffectiveness of aerodynamic control during the first portions of a re-entry: even with the vehicle's great speed, the density is too small to provide the necessary control. Physically, the atmospheric temperature has little effect on a re-entry vehicle; but from the analysis point of view, temperature is needed so that speed of sound and hence Mach number can be calculated for use with the vehicle aerodynamic representation.

Various methods are used to obtain the atmospheric density and temperature data depending upon the altitude range of interest. In the lower regions of the atmosphere (the troposphere and most of the stratosphere) where "air-breathing" aircraft can be used, the data is generally very good. Both mean properties and variations can be adequately measured. In the very high atmosphere (the ionosphere and above) earth satellites are used for determining atmospheric properties. Although satellite data is difficult to analyze, it produces good results not only for mean values of the properties but also for variations of these properties. The most difficult altitude range (roughly the entire chemosphere) lies between these two extremes where neither ordinary aircraft nor satellite can operate. Here rockets, balloons and other very ingenious methods are used but there has been relatively little data obtained. However, this scant data for the chemosphere can be used to help interpolate between the regions on either side whose properties are more precisely known.

The interrelationship between the measured quantities (usually pressure, density and speed of sound) and the desired quantities requires knowledge of the mean molecular weight, ratio of specific heats, and the universal gas constant. It is assumed that the universal gas constant applies everywhere. The ratio of specific heats is very nearly constant to about 90 kilometers ($\approx 300,000$ ft); above this altitude, the speed of sound tends to lose significance and little is known of the ratio of specific heats. Measurements indicate that the mean molecular weight is also nearly constant to an altitude of about 90 kilometers but decreases, in a fashion not well known, above this altitude. Actually then, the pressure, density and speed of sound measurements provide reasonably good

determinations of all atmospheric properties below 90 kilometers, the altitude range of most interest in this study.

The U.S. Extension to the ICAO Standard Atmosphere, Reference 2.6, tabulates 17 important atmospheric properties to an altitude of about 90 kilometers and continues the tabulation to 300 kilometers for some of the 17. In the region from sea level to about 500,000 feet, the variation of density can be described as roughly exponential; it decreases by a factor of approximately ten for each 54,000-foot increase in altitude. Figure 2.2 shows the density variation with altitude to 450,000 feet as assumed by Reference 2.6. Figure 2.1 shows the assumed piece-wise linear variation of temperature with altitude given in Reference 2.6.

Density and Temperature Models: Of the physical properties of the atmosphere, the density is the most important to the description of the aerodynamic forces acting on a re-entry vehicle. The lift, drag, and stability and control characteristics of the re-entry vehicle depend heavily upon dynamic pressure which is a function of density as well as the velocity of the relative wind. Similarly, the calculation of Mach number requires an accurately developed model of atmospheric temperature. Each of these physical properties is modeled as a function of geometric altitude to 300,000 feet and the models are described in the following paragraphs.

The basic source of data for both density and temperature is the U.S. Extension to the ICAO Standard Atmosphere (1958), Reference 2.6. This work tabulates atmospheric properties to 300,000 geometric meters and correspondingly to 1,000,000 geometric feet. There are other sources of such data; but for altitudes below about 300,000 feet, there is very little difference among them. The density model is essentially based upon Table IV B, page 199; and the temperature model is based entirely upon Table IV A, page 185, Reference 2.6.

Since above an altitude of about 300,000 feet there is no meaning to the speed of sound and there is little aerodynamic heating for the slowly decelerating vehicle, the temperature model is developed accurately to an altitude of 300,000 feet and no higher. The speed of sound is needed to evaluate Mach number which, in turn, is needed to evaluate the aerodynamic coefficients; however, the aerodynamic effects are so small at altitudes above 300,000 feet that accuracy in the temperature model is not important there.

Figure 2.1 shows the variation of kinetic temperature, T , in degrees Rankine with the altitude, h , in geometric feet. The speed of sound is defined as:

$$a = \sqrt{\frac{\gamma R^*}{M} T} \quad (2.9)$$

in which, to an altitude of nearly 300,000 feet, the following values hold:

$\gamma = 1.4$, the ratio of specific heats of air for altitudes

$M = 28.966$, the mean molecular weight

NAVTRADEVCEEN 801A

$R^* = 49719.64 \text{ ft-lb} / \text{ }^\circ\text{R slug}$, the universal gas constant

T = temperature in degrees Rankine

This reduces to the expression programmed with the equations of motion:

$$a = 49.1 \sqrt{T} \tag{2.10}$$

Because the temperature function is made up of straight line segments only, it is programmed in the IBM 704 at just the break points, and the IBM 704 linearly interpolates between these values which are tabulated below.

$h \sim$ Geometric Feet	$T \sim$ Degrees Rankine
0	518.688
36,500	389.988
82,000	389.988
156,000	508.788
175,000	508.788
250,000	354.35

(2.11)

For altitudes above 250,000 feet, the constant value $T = 354.35 \text{ }^\circ\text{R}$ is used.

Since in this study the primary interest in atmospheric density lies in the region below 300,000 feet, special effort has been applied toward obtaining a good empirical fit of the standard atmosphere density data of Reference 2.6 below 300,000 feet. The data is exponential in character; hence the empirical model is composed of three exponential segments, two of constant slope (on a plot of ρ versus $\log \rho$) separated by a segment whose slope is a function of altitude. This approach allows the use of a fixed coefficient, the value of density at sea level, for the exponential function.

The empirical model is plotted in Figure 2.2 along with a plot of the standard atmosphere data. It can be seen that the model of density used in this program fits the standard atmosphere very well at altitudes below 300,000 feet. The plot is, however, extended to higher altitudes to show that the model is still good up to 450,000 feet. The equations which is programmed and has been used to obtain the solutions of Sections V and VI is:

$$\rho = \rho_0 \exp\left(-\frac{h}{31600 - x}\right) \tag{2.12}$$

in which

$$x = \begin{cases} 0, & 0 \leq h < 25000 \text{ ft} \\ 0.2 h - 5000, & 25000 \text{ ft} \leq h \leq 65000 \text{ ft} \\ 8000, & 65000 \text{ ft} < h \end{cases}$$

$$\rho_0 = 0.002378 \text{ slugs/ft}^3$$

The value for ρ_0 is the one that has been the standard for years and does not exactly agree with that of Reference 2.6 (given as .0023769). Also, at $h = 25,000 \text{ ft}$

and $h = 65,000$ feet, the empirical model has slope discontinuities, but the curve itself is continuous throughout. At the time this density model was devised, it was thought that an exponential having a slope which was a function of altitude would be the best way to fit the curvature of the standard atmosphere data. It is felt now, however, that three exponential segments, each having a different constant slope and a different coefficient, would be equally good.

The atmospheric pressure is required for the description of rocket thrust in the atmosphere as in Appendix B. Pressure, P , may be obtained from the equation of state for a perfect gas:

$$P = 3090.24 \rho T \text{ lb/ft}^2 \quad (2.13)$$

in which density, ρ , and temperature, T , are given by the models described in this section. Above 300,000 feet the temperature is not significant to the specification of the forces on the vehicle, so the temperature model used in this study (Figure 2.1), as a matter of convenience, neglects any variation of T above 300,000 feet.

2.3.3 Winds and Gusts

It is conceivable that a wind, such as a jet stream, could produce a substantial change in a vehicle's path. It is conceivable also that turbulence, or gusts, could produce severe short period vehicle motions which would make piloting and control difficult. Each of these possibilities should be considered important to the over-all description of re-entry vehicle flight for a simulator.

The motions of the atmosphere, called circulations, are described in Chapter VII of Reference 2.7. The primary circulation is that which exchanges air between high and low latitudes. It is, by nature, a thermal circulation composed of three meridian cells of flow which is heavily modified by the earth's rotation and its radiative heat loss. This atmospheric circulation accounts for the general westerly surface winds in the middle latitudes and the easterly surface winds in the polar and equatorial zones. In the upper troposphere the wind direction is variable with season, being westerly in winter and easterly in summer (Reference 2.5). Differences in temperature between the oceans and the land masses, in certain regions, cause circulations to and from summer-heated and winter-cooled continents. These are called monsoon circulations. Similar to these circulations are the minor circulations which result from a variety of local situations and are diurnal in character. The circulations described in this paragraph are always present because of the earth's surface features and the influx of solar energy, but they are often completely masked by large perturbations in the air flow associated, at the surface, with cyclones and anticyclones which produce daily weather changes.

The westerly winds of the upper troposphere, mentioned in the preceding paragraph, prevail at all latitudes and are often concentrated in one or more jet streams. A jet stream is a pronounced concentration of west-to-east flow in a narrow band centered just below the tropopause in the middle latitudes around the earth. It appears as a fast-moving meandering stream whose position varies considerably. The meandering can be associated with the cyclones and anticyclones of the air near the earth's surface. Of the two jet streams which are ordinarily present in the upper troposphere (two in each hemisphere), the most northerly one (the one found near the border of the United States and Canada in the summer) is the stronger.

NAVTRADEVGEN 801A

At much higher altitudes the data on wind velocities is very sketchy because of the measurement techniques required. Basically, the summer winds in the region from 100,000 to 200,000 feet are easterly, averaging about 100 feet per second; and from 200,000 to 300,000 feet the winds gradually become westerly, approaching a peak velocity slightly above 300,000 feet. In winter the winds are westerly, peaking at about 200 feet per second at an altitude of 200,000 feet. Chapter VII of Reference 2.7 and Chapter V of Reference 2.5 contain more information about winds at these high altitudes.

The description of the general winds presented in the preceding three paragraphs is simply an averaged condition based upon as much data as is available. In the atmosphere at the earth's surface, and especially throughout the troposphere, the daily weather variations produce great changes in the wind velocity and direction at a given location. Thus, a general wind profile, as developed for this program is only a long-term average of the mean wind measured on many different occasions.

Near the earth's surface at any particular time, the wind can be considered a combination of a vector mean wind and the superimposed turbulence (gusts). To simplify matters, the vector mean wind is assumed constant over the field of interest, and gust velocity amplitude probability distribution is assumed Gaussian. This latter basic assumption allows the statistical description of turbulence. Studies of data have shown that, except for very low altitudes, the assumption is adequate. In addition, indications are that turbulence takes the form of individual patches or fields throughout which it is reasonable to assume that spatial homogeneity* and isotropy** hold. Caution must be exercised when using approximations of homogeneity and isotropy. For example, isotropy is a poor approximation for certain kinds of clear air turbulence and for turbulence under 1000 feet altitude.

One patch or field of turbulence is different from another if the root-mean-square velocities and the velocity spectra are different. Some factors which affect turbulence intensities (velocities) and spectra are:

1. Weather
2. Terrain features
3. Altitude above terrain
4. Flight path direction relative to terrain
5. Magnitude of the mean wind
6. Direction of the mean wind relative to terrain
7. Temperature gradient.

This listing is not meant to be in order of importance of the factors as present knowledge of atmospheric turbulence is insufficient for such a classification. References 2.8 and 2.9 give more details.

* Spatial homogeneity means that the statistical properties (root-mean-square gust velocity and gust velocity spectrum) are the same at each point in the field; that is, the coordinate axes may be translated without effect. Temporal homogeneity (stationarity) may be assumed when the statistical properties of the field do not change with time.

** Isotropy means that the statistical properties are independent of angular orientation; that is, the coordinate axes may be rotated without effect.

There is considerable gust data for altitudes in the middle regions of troposphere, but for very low altitudes below a few hundred feet and for high altitudes near and above the jet stream, data is scarce. The most severe conditions are probably met in low altitude approach and landing, and though data in this region is meager, what there is should suffice for the simulation problem. Turbulence associated with jet stream shears, though not well known except that its intensity is high, is probably much less a problem because of the higher air-speeds and the less exacting pilot tasks at jet stream altitudes.

Wind and Gust Models: The winds around the earth are variable in direction and velocity, dependent upon location, and dependent upon seasonal and diurnal effects. It is, therefore, difficult to do much more than develop a model based upon large-scale general winds though this may be somewhat unrealistic. The model presented below is developed so that it is a function of latitude and altitude only. The wind direction is always the same; the function gives magnitude only. The basic source of wind data is Reference 2.5 which presents data in tabular and graphical form. A gust model has not been programmed; however, a usable model is described.

For the wind model, attention was centered upon mean winter winds in the 30 to 45 degree north latitude region. In this region the dependence of wind direction and velocity upon longitude is needlessly complex for simulator purposes. Hence, the directional data was ignored and the magnitude data was graphically averaged and used as if it were completely zonal; that is, in a direction parallel to lines of latitude. Data is presented for altitudes to 100,000 feet in the Vector Mean Wind Table of Reference 2.5. For altitudes from 100,000 to 300,000 feet, available data is much less complete and is given (Reference 2.5) in zonal form only. Here again, much averaging was done to put the data in useful form for this study. The result of the graphical averaging is the general winter wind profile shown as the solid line in Figure 2.3. The profile gives the wind velocity magnitude with respect to the local surface of the earth as a function of altitude, h , for the 30 to 45 degree latitude zone. The wind is assumed to be always westerly (from the west) in both north and south latitudes. The profile accounts for the jet stream, and the general geostrophic winds at higher altitudes.

An empirical fit for the wind profile is also plotted in Figure 2.3 as the dashed line. This equation is:

$$W_{\lambda} = \left[30 + \frac{17,280}{144 + (35 - .001 h)^4} + \frac{300,000}{1500 + (20 - .0001 h)^4} \right] |\sin 2\mu| \quad (2.14)$$

where W_{λ} is the westerly component of the wind velocity (ft/sec) with respect to the local earth's surface.

The wind velocity matrix $[W]$ has northward and upward components also, which in this study are assumed identically zero. The absolute value of the sine of twice the latitude angle produces the variation of wind velocity with latitude. The magnitude of the wind velocity is zero at the equator, reaches a maximum at 45° north or south latitudes, and is zero again at the poles. This variation is in rough agreement with the measured variation of zonal wind magnitudes at various latitudes.

No gust velocity model was programmed in this study, but such a model can be devised by suitably modifying the output of a digital random function generating

NAVTRADEV CEN 801A

subroutine using some digital filtering technique to obtain the correct gust frequency spectrum. The filtered output is then scaled to the desired level and used directly as μ_x , μ_y , and μ_z .

2.4 REFERENCES

- 2.1 Geyling, F. T.: "Fundamental Satellite Perturbations." ARS Journal, Vol. 30, No. 11, November 1960.
- 2.2 Parvin, Richard H.: "The Earth in Inertial Space." Aerospace Engineering, Part I, Vol. 18, No. 4, April 1959; Part II, Vol. 18, No. 5, May 1959.
- 2.3 Kaula, W. M.: A Geoid and World Geodetic System Based on a Combination of Gravimetric, Astro-Geodetic, and Satellite Data. NASA Technical Note D-702, May 1961.
- 2.4 Ehricke, Krafft A.: Space Flight, I, Environment and Celestial Mechanics. D. Van Nostrand Company, Inc., Princeton, N. J., 1960.
- 2.5 Air Force Cambridge Research Center, USAF ARDC: Handbook of Geophysics. Revised Edition, the MacMillan Company, New York, 1960.
- 2.6 Minzner, R. A.; W.S. Ripley; T.P. Condron: U.S. Extension to the ICAO Standard Atmosphere. Air Force Cambridge Research Center, USAF ARDC, U.S. Government Printing Office, Washington, D. C., 1958.
- 2.7 Kuiper, Gerard P. Editor: The Earth as a Planet. The University of Chicago Press, Chicago, Illinois, 1954.
- 2.8 Notess, C. B.: Analysis of Turbulence Data Measured in Flight at Altitudes Up to 1600 Feet Above Three Different Types of Terrain. Cornell Aeronautical Laboratory, Inc., Report No. TE-1215-F-1, February 1959.
- 2.9 Etkin, Bernard: Dynamics of Flight. John Wiley and Sons, Inc., New York, 1959.

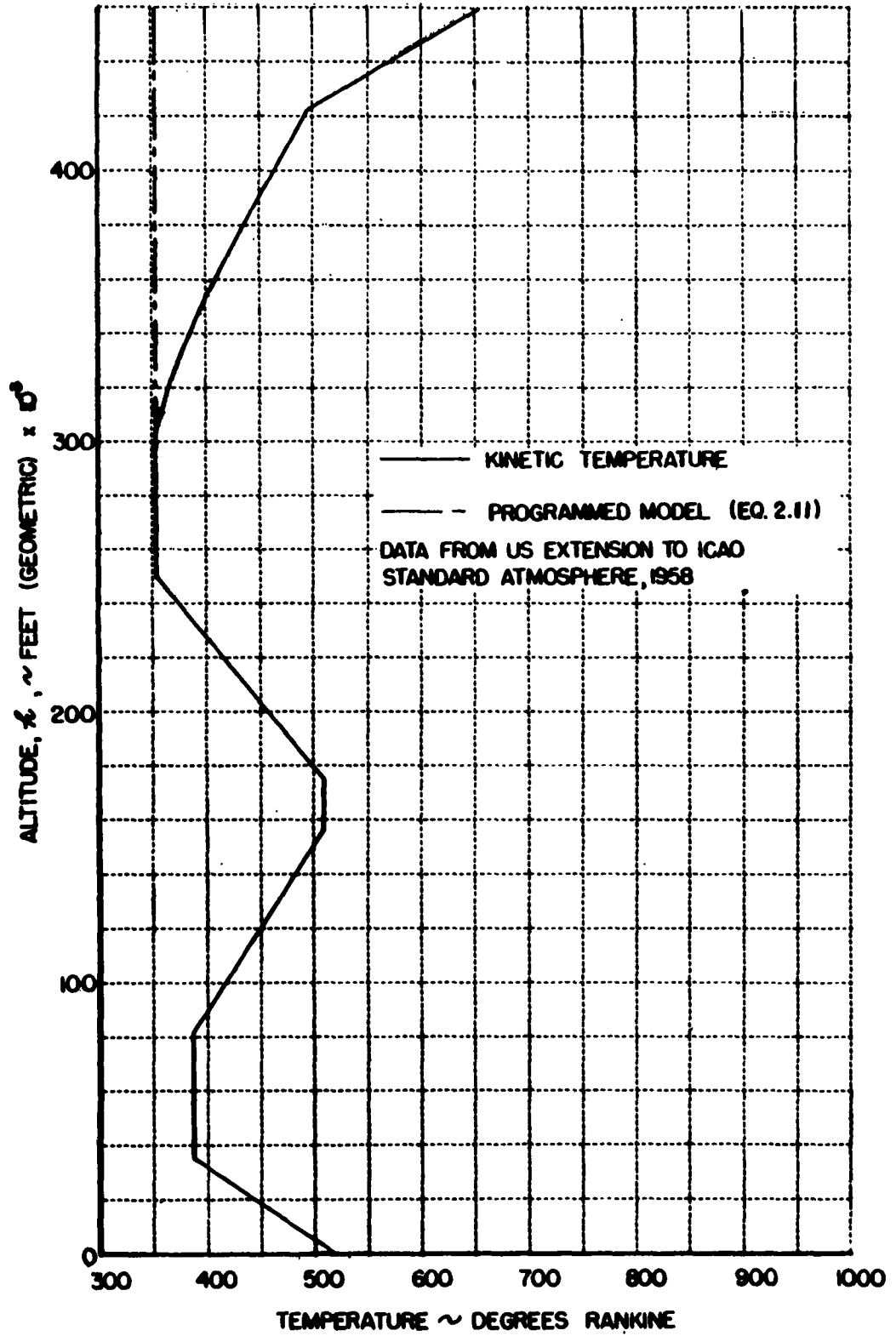


FIGURE 2.1 ATMOSPHERIC TEMPERATURE MODELS

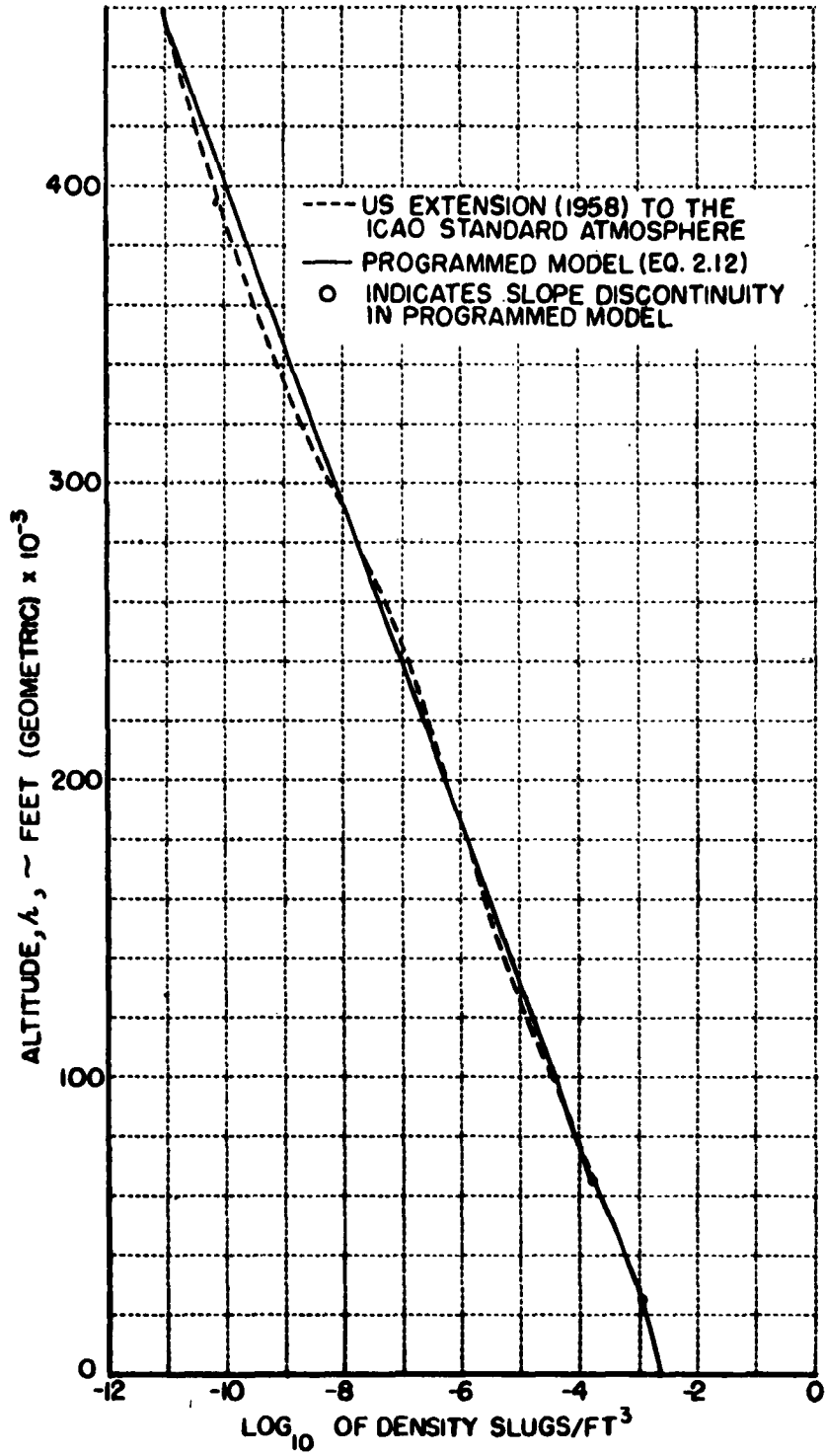


FIGURE 2.2 ATMOSPHERIC DENSITY MODELS

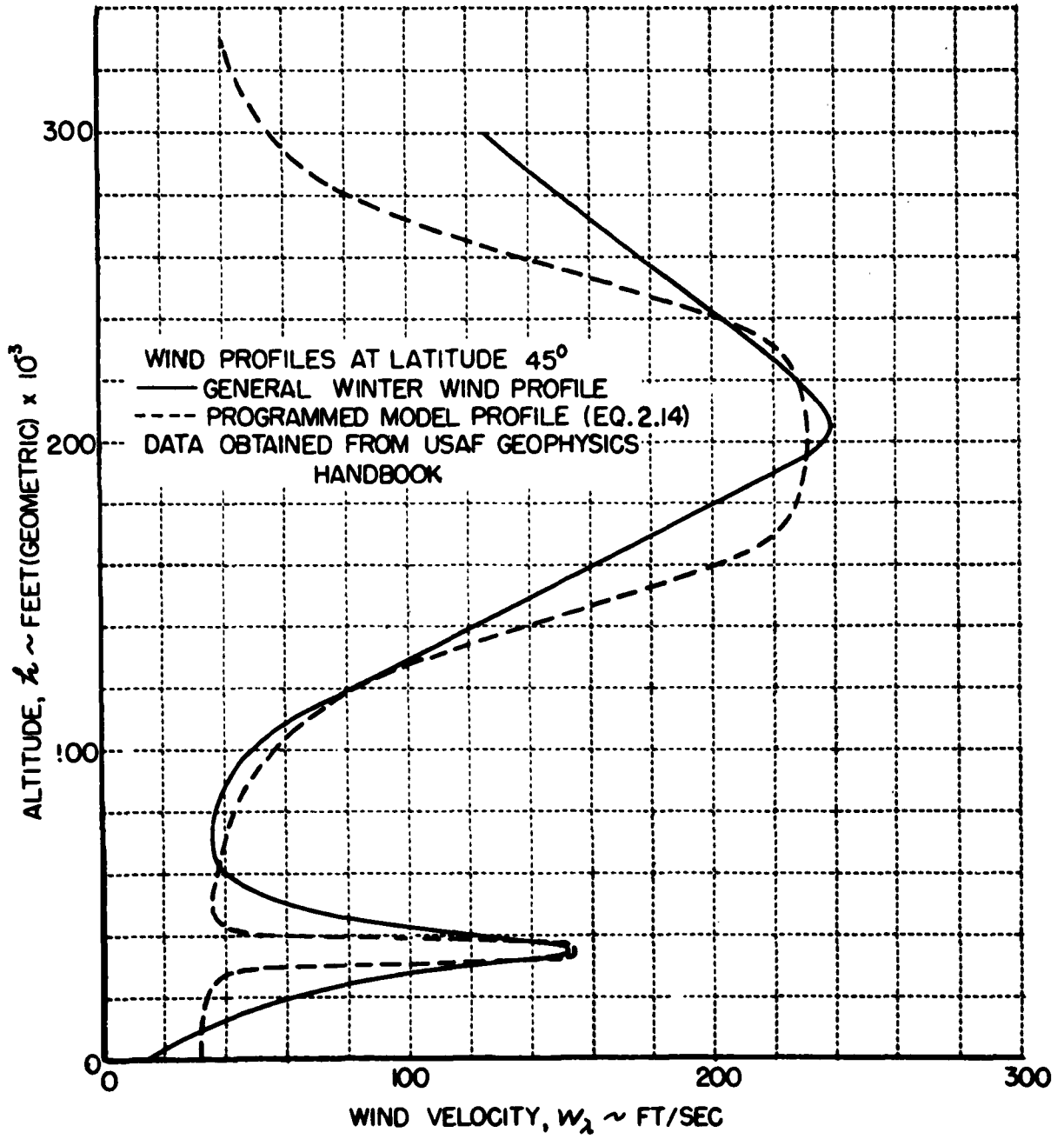


FIGURE 2.3 ATMOSPHERIC WIND PROFILE MODELS

SECTION III
EQUATIONS OF MOTION

3.1 INTRODUCTION

The general purpose of this study is to develop equations of motion suitable for simulating the re-entry and landing problem for a manned hypervelocity boost glider, and particularly for application to flight simulators using digital computers. The equations of motion as derived for use in this study, as distinguished from those suitable for a simulator, accent the new dimensions assumed in dealing with space flight and hypervelocity vehicles; and their purpose is to determine how these new dimensions must be handled. As such, these equations embody many new concepts not normally found in flight simulator equations. On the other hand, many characteristics commonly included in simulator equations will not be found in the equations used in this study. It is not the purpose of this study to investigate matters which are already well understood, but rather to investigate the new facets being introduced. The complete equations of motion describing the flight of boost glide space vehicles, including both the attitude and trajectory problems, are exceedingly complex. Thus, this study is essentially limited to piloted flight - the over-all re-entry and landing problem - and emphasis is placed on determining what simplifications can be made in the complete equations with the piloting task in mind.

The equations of motion as derived for this study include the following characteristics and limitations:

1. Six rigid-body degrees of freedom for the over-all vehicle,
2. A spherical earth rotating with constant angular velocity,
3. Flight limited to sub-orbital speeds and below 300,000 feet of altitude,
4. No restrictions on the vehicle's attitude,
5. No restrictions on the vehicle's trajectory within (3) except that flights directly over the North and South Poles are excluded,
6. Non-varying mass (i. e., limited power),
7. Aerodynamic and reaction controls,
8. Non-linear aerodynamics,
9. Undisturbed atmosphere rotates with the earth,
10. Winds defined in terms of northward, eastward and upward components as functions of altitude, latitude and longitude,
11. Gusts or turbulence defined in terms of the vehicle - lateral, normal, and head-on components,
12. Gravitational force field for a spherical earth, and
13. Air density and temperature variable with altitude.

None of the restrictions listed will compromise the objectives of this study, but the restriction to a non-varying mass (6), and to a spherical earth (2) and (12), might seriously hamper extension of the equations to the full flight of sub- or near-orbital vehicles. Accordingly, methods for including the rapidly varying mass and large thrust forces associated with boosted flight are developed in Appendix B, and methods for including earth oblateness and surface aberrations are developed in Appendix C.

The restrictions placed on the flight range are compatible with atmospheric

flight, but preclude flight where the aerodynamic forces are negligible. For flight outside the atmosphere, many effects become important (e. g., gravitational aberrations, radiation pressures, magnetic fields) which are missing in the equations used in this study, and which even the smallest aerodynamic forces and moments would completely mask. The restriction to non-polar flight is an artificial one produced by using latitude as a variable. If polar flights are required in any particular application, one of two methods developed in this study can be used to remove this restriction: (1) the method used to handle a 90° side-slip, which involves using direction cosines instead of angles in some relations, or (2) the method used to handle vehicle attitude, which involves switching to an alternate axis system.

The general development of the equations begins by setting forth basic principles and concepts, which are formulated most conveniently in vector notation. Next follows the selection of the axis systems, coordinates, and transformations which are necessary to develop the equations in detail. Finally the detailed equations are developed in matrix form. The extensive use of matrix algebra is dictated by its concise form and the ease with which matrix equations can be incorporated into a digital computer program, the method selected for solving the equations in this study. Since the algebraic form of the equations is of some interest, the matrix equations have been expanded and are presented in Appendix A.

3.2 VECTOR EQUATIONS – BASIC PRINCIPLES AND CONCEPTS

This section is concerned with the application of the laws of mechanics to the dynamical description of the vehicle, and its relative motion with respect to the earth and the atmosphere. The fundamental assumption is that the vehicle may be treated as a rigid body.

3.2.1 Equations of Motion

The derivation starts with the assumption of Newton's Laws of Motion for a particle and their extension to a system of particles. The inertial frame is taken as fixed with respect to the "fixed stars", and secondary (moving) reference frames are defined by the earth and the vehicle. Coordinate systems and position vectors for these reference frames are shown in Figure 3.1, and it should be noted that X_0 , Y_0 , and Z_0 are parallel to X_I , Y_I , and Z_I , respectively.

The basic vector equations of motion for a body or system of mass particles, where the moments of forces and moments of momentum are restricted specifically to be taken about the c. g., are written following Reference 3.1 as

$$\left(\frac{d\bar{M}}{dt} \right)_I = \bar{F}_I \quad (3.1)$$

$$\left(\frac{d\bar{H}}{dt} \right)_I = \bar{M}_I \quad (3.2)$$

where the derivatives are taken with respect to inertial space as denoted by the "I" subscript. The forces exerted by the sun, moon and stars – called the astronomical forces – are separated from those exerted by the earth as

$$\bar{F}_I = \bar{F} + \bar{F}_{\text{astronomical}}$$

$$\bar{M}_I = \bar{M} + \bar{M}_{\text{astronomical}}$$

Treating the body as a constant mass, and writing the force equation in terms of the position vectors, we obtain

$$\left(\frac{d\bar{M}}{dt}\right)_I = m(\ddot{\bar{r}}_{IB})_I = m(\ddot{\bar{r}}_{IE})_I + m(\ddot{\bar{r}}_{EB})_I = \bar{F} + \bar{F}_{\text{astronomical}} \quad (3.3)$$

Consider the force on the body (vehicle) due to the sun, the largest astronomical force. Applying the inverse square law of gravitation yields

$$\left(\ddot{\bar{r}}_{IE}\right)_I = \frac{F_{\text{sun (on earth)}}}{m \text{ (of earth)}} \bar{I}_{ES} = \frac{F_{\text{sun (on vehicle)}}}{m \text{ (of vehicle)}} \left(\frac{r_{SB}}{r_{SE}}\right)^2 \bar{I}_{ES}$$

where \bar{I}_{ES} is a unit vector in the earth to sun direction

\bar{I}_{BS} is a unit vector in the body to sun direction

r_{SB} is the distance from sun to body

r_{SE} is the distance from sun to earth

F_{sun} is the force exerted by the sun.

Since $(r_{SB}/r_{SE})^2 \cong 1$ and $\bar{I}_{ES} \cong \bar{I}_{BS}$, then

$$m(\ddot{\bar{r}}_{IE})_I = F_{\text{sun (on vehicle)}} \bar{I}_{BS} = \bar{F}_{\text{sun}}$$

Extending the results to all other astronomical bodies yields:

$$m(\ddot{\bar{r}}_{IE})_I = \bar{F}_{\text{astronomical}} \quad (3.4)$$

By definition, the origin of the body axes are the c. g., so that

$$\bar{M}_I = \bar{M} \text{ since } \bar{M}_{\text{astronomical}} \cong 0^* \quad (3.5)$$

Now, subtracting Equation (3.4) from (3.3) and using (3.5) in (3.2) yields the following:

$$m(\ddot{\bar{r}}_{EB})_I = \bar{F} \quad (3.6)$$

$$\left(\frac{d\bar{M}}{dt}\right)_I = \bar{M} \quad (3.7)$$

* The equality is exact for a spherical mass distribution.

Thus, for motions near the earth, we can treat the earth's center as an inertial reference provided the gravitational forces of all celestial bodies other than the earth are excluded. In this manner, X_0 , Y_0 , and Z_0 can be considered the inertial frame.*

The equations of motion can be written in more explicit form using body reference quantities as follows.

$$\overline{m} = m \overline{V} \quad (3.8)$$

$$\overline{N} = \overline{I} \overline{\omega} \quad (3.9)$$

where \overline{I} is the moment of inertia operator (Reference 3.1)** and the inertial frame is the pseudo-inertial earth-centered reference frame. The general equations of motion for the vehicle when treated as a rigid body follow. The equations are extended to deal with variable mass in Appendix B.

$$m(\dot{\overline{V}})_B + \overline{\omega} \times m \overline{V} = \overline{F} \quad (3.10)$$

$$\overline{I} \dot{\overline{\omega}} + \overline{\omega} \times \overline{I} \overline{\omega} = \overline{M} \quad (3.11)$$

$$\overline{V} = \int_0^t (\dot{\overline{V}})_B d\tau + \overline{V}_0 \quad (3.12)$$

$$\overline{\omega} = \int_0^t \dot{\overline{\omega}} d\tau + \overline{\omega}_0 \quad (3.13)$$

(No subscript is needed on $\dot{\overline{\omega}}$ since $(\dot{\overline{\omega}})_E = (\dot{\overline{\omega}})_B$).

The integrals for \overline{V} and $\overline{\omega}$ must be interpreted with care, since general vector integration is not definable (Reference 3.2). These integrals imply integration of the components of $(\dot{\overline{V}})_B$ and $\dot{\overline{\omega}}$ in the body axes.

3.2.2 Kinematics Relative to the Earth

It is necessary to describe the trajectory of the vehicle and the rotation of the vehicle relative to the earth, that is, with respect to the X_E , Y_E , Z_E frame which rotates with, and is fixed in, the earth. The relative linear and angular velocities of the vehicle may be expressed as:

$$\overline{V}_E = \overline{V} - \overline{V}_{er} \quad (3.14)$$

$$\overline{\omega}_E = \overline{\omega} - \overline{\Omega} \quad (3.15)$$

* This does not imply that the earth is travelling in a straight line and is a true inertial reference. The approximation is much better than that. It implies that the acceleration of the earth and the vehicle due to astronomical forces are equal, that the acceleration of the vehicle relative to the earth arises entirely from earth forces.

** \overline{I} is a dyad or second order tensor and Equation (3.9) would be written as

$\overline{N} = \overline{I} \cdot \overline{\omega}$ in the notation of Reference 3.2.

where the velocity due to earth rotation is

$$\bar{V}_{Er} = -\bar{\Omega} \times \bar{r}_{EB} \quad (3.16)$$

The position of the vehicle is obtained from

$$\left(\dot{\bar{r}}_{EB}\right)_E = \bar{V}_E \quad (3.17)$$

so that

$$\bar{r}_{EB} = \int_0^t \bar{V}_E d\tau + \bar{r}_{EB_0} \quad (3.18)$$

The integral for \bar{r}_{EB} implies integration of the components of \bar{V}_E in earth axes, and \bar{r}_{EB_0} is a vector fixed in the earth axes which denotes the initial position of the vehicle at $t = 0$.

3.2.3 Kinematics Relative to the Air

In order to determine the aerodynamic forces on the vehicle, it is necessary to describe the motions of the vehicle relative to the air. The undisturbed air is assumed to rotate with the earth, and two types of disturbance velocities are superimposed on the general rotating atmosphere:

1. general air mass motions or winds, \bar{W} , which are defined with respect to the earth, and
2. rapid air mass motions or gusts, $\bar{\mu}$, which are defined with respect to the airplane.

The reason for this duality is that the accelerations and the velocities of the air relative to the vehicle must be specified in order to determine the aerodynamic forces. This is an extremely complex problem where the winds are specified relative to the earth, as it requires determining nine velocity gradients with respect to the airplane (i. e., $\partial w_x/\partial x$, $\partial w_y/\partial x$, ..., $\partial w_x/\partial y$, ..., etc.) and their time derivatives. Where the winds are expressed in terms of empirical geophysical data, this represents a fantastically complicated computing problem. In order to avoid this situation, several assumptions are made:

1. The air motions can be separated into low frequency motions (winds, \bar{W}) and high frequency motions (gusts and turbulence, $\bar{\mu}$).
2. The gradients of the low frequency winds are small enough to be neglected.
3. The high frequency air motions, gusts and turbulence, can be specified directly in terms of components in the body reference frame.

These three assumptions rest on relatively firm ground. A fourth assumption, not so firmly grounded, that one would like to make is:

4. The relative accelerations of the low frequency winds, and also those due to the rotating atmosphere, may be neglected in determining the accelerations of the air relative to the vehicle.

This fourth assumption will be investigated in the course of this study to see

if it really is valid.

The velocity of the vehicle relative to the air (measured at the c. g.) and its time rate of change in the body axes frame are given as:

$$\bar{V}_a = \bar{V} - \bar{V}_{er} - \bar{W} - \bar{\mu} \quad (3.19)$$

$$(\dot{\bar{V}}_a)_B = (\dot{\bar{V}})_B - (\dot{\bar{V}}_{er})_{ES} - (\dot{\bar{W}})_{ES} - (\dot{\bar{\mu}})_B + \bar{\omega}_{B-ES} \times (\bar{V}_{er} + \bar{W}) \quad (3.20)$$

in which $\bar{\omega}_{B-ES}$ is the angular velocity of the body axes frame relative to the earth-surface frame. The angular velocity of the airplane with respect to the air (measured at the c. g.) would be given, in the absence of any assumptions, as

$$\bar{\omega}_a = \bar{\omega} - \bar{\omega}_w - \bar{\omega}_\mu - \bar{\Omega}$$

However, assumption (2) implies that $\bar{\omega}_w = 0$. Furthermore, the present knowledge of atmospheric turbulence does not provide any data on $\bar{\omega}_\mu$, so that perforce, $\bar{\omega}_\mu = 0$. Thus we are led to the equation

$$\bar{\omega}_a = \bar{\omega}_E = \bar{\omega} - \bar{\Omega} \quad (3.21)$$

3.2.4 Forces and Moments

The forces and moments acting on the vehicle can be grouped functionally.

\bar{F}_a	\bar{M}_a	aerodynamic forces and moments
\bar{F}_g	\bar{M}_g	gravitational forces and moments
\bar{F}_T	\bar{M}_T	thrust and engine forces and moments (power), and reaction controls
$\Delta \bar{F}$	$\Delta \bar{M}$	other forces and moments.

The aerodynamic forces are generally functions of air density, air velocity, and aerodynamic coefficients. The gravitational forces are generally functions of the position of the vehicle with respect to the earth. \bar{F}_T and \bar{M}_T are forces and moments expressed directly in dimensional units (lb and ft-lb) and are functions of some arbitrary control. $\Delta \bar{F}$ and $\Delta \bar{M}$ are reserved for additional terms which may arise, say from a booster or rotating machinery.

3.2.5 Measured Accelerations

The accelerations that would be felt by the pilot or measured by accelerometers (three components) placed at the c. g. of the aircraft are given by the external forces (i. e., they do not include the gravitational force) as follows.

$$\bar{\pi} = (\bar{F} - \bar{F}_g) / m = (\bar{F}_a + \bar{F}_T) / m$$

Now, if the accelerations are measured at some place other than the c. g. of the aircraft (as would usually be the case), the effects of rotation must be included. If the instruments are located with respect to the c. g. by the position vector \bar{r}_i , then the acceleration of \bar{r}_i is given as:

$$(\ddot{\bar{r}}_i)_I = (\ddot{\bar{r}}_i)_B + \dot{\bar{\omega}} \times \bar{r}_i + 2\bar{\omega} \times (\dot{\bar{r}}_i)_B + \bar{\omega} \times (\bar{\omega} \times \bar{r}_i)$$

For a rigid body (no flexibility)

$$(\ddot{\mathbf{r}}_i)_B = (\dot{\mathbf{r}}_i)_B = 0$$

Thus $\bar{\mathbf{a}}_i$, the measured acceleration, is given as

$$\bar{\mathbf{a}}_i = (\bar{\mathbf{F}} - \bar{\mathbf{F}}_g) / m + \dot{\bar{\boldsymbol{\omega}}} \times \bar{\mathbf{r}}_i + \bar{\boldsymbol{\omega}} \times (\bar{\boldsymbol{\omega}} \times \bar{\mathbf{r}}_i)$$

3.3 AXIS SYSTEMS, COORDINATES, AND TRANSFORMATIONS

Matrix notation is fundamental to the description of coordinate systems and their transformations, and hence, is used extensively in this development. The assumption of a spherical earth is inherent in the development, but the approach can be extended to include oblateness as outlined in Appendix C.

3.3.1 Earth-Surface Axes

Spherical coordinates have been selected for defining the position of the vehicle with respect to the earth. Such coordinates have an obvious disadvantage: a singularity exists at the poles and precludes polar flights. On the other hand, these are the coordinates commonly used in both terrestrial navigation and in celestial mechanics; and, as will be discussed in Section 3.3.2, they are the means for removing an even more embarrassing singularity. Accordingly, "earth-surface axes" (X_{ES} , Y_{ES} , and Z_{ES}) are defined as shown in Figure 3.2. The X_{ES} and Y_{ES} axes are parallel to the earth's surface (directed north and east, respectively), and the Z_{ES} axis points toward the earth's center; but the origin of the earth-surface axes is located at the vehicle's c.g. and not on the earth's surface. Since the earth is considered spherical, the orientation of these axes is described by the longitude (λ) and the latitude (ψ) of the vehicle, and their position is described by these same quantities and the magnitude of the radius vector (r_{EB}). The position could be described alternatively by components in the earth axes (X_{EB} , Y_{EB} , and Z_{EB}).

Convenient relative velocity components are defined by the earth-surface axes: the vehicle's velocity north (V_ψ) and east (V_λ), and its rate of climb (V_r). The relative tangential or horizontal velocity vector ($\bar{\mathbf{V}}_T$) is described in magnitude (V_T) by the vector sum of V_ψ and V_λ , and in direction by the flight-path heading angle (ψ_T). The flight-path angle (γ) is the angle between $\bar{\mathbf{V}}_T$ and $\bar{\mathbf{V}}_E$.

3.3.2 Orientation of Body Axes

Conventional body axes (x , y , z) are selected to represent the vehicle. The method of orienting these axes in conventional airplane dynamics is well established (e.g., Reference 3.3): three sequential rotations or Euler angles (γ , θ , and ϕ) are used to rotate from inertial axes to body axes. This same conventional scheme has been used by Patha in Reference 3.4 to handle the larger problem associated with hypervelocity vehicles, but it leads to serious difficulty. A singularity occurs whenever the x -axis is parallel to the polar axis, a likely situation in any re-entry and landing trajectory. Patha solves this problem by re-orienting the fixed reference frame each time a singularity is approached; but in so doing, the orientation angles lose their physical significance. The approach taken here is to introduce additional orientation angles (five in all), thus strategically locating the singularities where they will do the least harm. In addition, an alternate set of orientation angles is resorted to whenever the

singularities are approached, but once passed, the original angles are restored. This scheme was suggested by Patha's re-orientation scheme, but has the additional advantage of retaining the physical significance of the angles.

The usual definition of the orientation angles (ψ , θ , and ϕ) is made as shown in Figure 3.3a, except the reference frame is the earth-surface axes rather than the earth or inertial axes. Thus the usual significance of these angles is still retained: ψ is the heading from north, θ is elevation from the local horizontal, and ϕ is the bank angle from the local horizontal.

The singularities occur for a vertical attitude ($\theta = \pm 90^\circ$). Since $\theta = 90^\circ$ is a possible re-entry attitude, it is deemed necessary to provide for this case, and also concurrently the case of $\theta = -90^\circ$ which might occur in a spin. Accordingly, a second set of "special orientation angles" is defined (ψ_s , θ_s , and ϕ_s) as shown in Figures 3.3b and 3.3c, which is used only when $\theta \rightarrow -90^\circ$ (nose down) or $\theta \rightarrow +90^\circ$ (nose up). These angles can be thought of as being the same angles as the normal ones, except the reference position of the vehicle is with the nose pointed straight down. Alternatively, these angles can be thought of as providing the azimuth of the pilot's head (ψ_s), the elevation of the pilot's head (θ_s), and the wing tilt angle (ϕ_s). In terms of nose position, θ_s gives the upward tilt from straight down (θ near -90°) or the downward tilt from straight up (θ near $+90^\circ$); ϕ_s gives the leftward tilt from straight down, and $\phi_s - 180^\circ$ gives the leftward tilt from straight up. These are relatively significant quantities when the attitude of the vehicle is vertical (nose down or nose up). But it is perhaps more important that this particular selection of the alternate "special orientation angles" is most easily incorporated into the equations of motion.

The method for switching from one set of axes to the other employs a criteria based on θ . When θ reaches some large negative or positive value, say $|\theta| = 70^\circ$, the coordinates are switched from ψ , θ , and ϕ to ψ_s , θ_s , and ϕ_s . Then when θ again reduces, say to $|\theta| = 50^\circ$, the coordinates are switched back. Different switching values of $|\theta|$ are used so that small oscillations will not cause continual switching of coordinates.

The angles ψ , θ , and ϕ (alternatively ψ_s , θ_s , and ϕ_s) are only part of the general problem, orienting the body axes with respect to the earth-surface axes. It still remains to orient these latter axes with respect to the earth axes and the inertial axes. The earth-surface axes and the earth axes are related by the longitude (λ) and the latitude (ν); the earth axes and the inertial axes, by the angle Ωt . The angle Ωt is only of interest if celestial navigation is specifically included. The complete orientation problem (for normal ψ , θ , and ϕ) is depicted in Figure 3.4. The sequence of rotations (orthogonal transformations) going from earth to body axes is as follows:

1. a rotation λ about Z_E to X_1, Y_1, Z_1
2. a rotation ν about $-Y_1$ to X_2, Y_2, Z_2
3. a -90° rotation about Y_1 to X_{ES}, Y_{ES}, Z_{ES}
4. a rotation ψ about Z_{ES} to x_1, y_1, z_1
5. a rotation θ about y_1 to x_2, y_2, z_2
6. a rotation ϕ about x_1 to x, y, z

To complete the picture, the sequence for the special orientation angles (ψ_s, θ_s, ϕ_s) is unchanged through rotation (3), and continues as:

4. a rotation ψ_s about z_{ES} to x_1, y_1, z_1
5. a rotation θ_s about y_1 to x_2, y_2, z_2
6. a rotation ϕ_s about x_2 to x_3, y_3, z_3
7. a -90° rotation about y_3 to x, y, z

3.3.3 Wind, Stability, and Body Axes

The wind axes and stability axes are defined in the conventional manner, as shown in Figure 3.5. The only unusual characteristic is that these axes are defined by the vector \vec{V}_a , as distinct from the usual vector \vec{V} . The body axes are located with origin at the c.g. and x and z are in the (assumed) plane of symmetry; but the "incidence" of x is essentially arbitrary, and may be set at any convenient value. The sequence of rotations (orthogonal transformations) relating the axes, going from wind to stability to body axes, is as follows:

1. a rotation β about z_w to x_s, y_s, z_s
2. a rotation α about y_s to x, y, z

3.3.4 Coordinate Transformations

It is necessary to define coordinate transformations between the various axis systems. These are defined in terms of the direction cosine matrices, and differentials are used to avoid including origin shifts in the basic definitions.

Earth axes to earth-surface axes:

$$\begin{bmatrix} dx_{ES} \\ dy_{ES} \\ dz_{ES} \end{bmatrix} = [L_{ES-E}] \begin{bmatrix} dX_E \\ dY_E \\ dZ_E \end{bmatrix} \quad (3.22)$$

Earth-surface axes to body axes:

$$\begin{bmatrix} dx \\ dy \\ dz \end{bmatrix} = [L_{B-ES}] \begin{bmatrix} dx_{ES} \\ dy_{ES} \\ dz_{ES} \end{bmatrix} \quad (3.23)$$

Earth axes to body axes:

$$\begin{bmatrix} dx \\ dy \\ dz \end{bmatrix} = [L_{B-E}] \begin{bmatrix} dX_E \\ dY_E \\ dZ_E \end{bmatrix} \quad (3.24)$$

and

$$[L_{B-E}] = [L_{B-ES}] [L_{ES-E}] \quad (3.25)$$

Wind axes to body axes:

$$\begin{bmatrix} dx \\ dy \\ dz \end{bmatrix} = [L_{B-W}] \begin{bmatrix} dx_w \\ dy_w \\ dz_w \end{bmatrix} \quad (3.26)$$

The foregoing transformations are orthogonal, each matrix element being the cosine of the angle between the corresponding axes. These can be handled directly in terms of direction cosines, but the approach taken here is to express the direction cosines in terms of specific angles - Euler angles or orientation angles - which have some general physical significance. The orientation angles are defined in the previous section, and it remains to define the transformations in terms of these angles:

$$[L_{ES-E}] = [1''] [\nu] [\lambda] \quad (3.27)$$

$$[L_{B-ES}] = [\phi] [\theta] [\psi] \quad (3.28)$$

$$[L_{B-W}] = [\alpha] [\beta] \quad (3.29)$$

And the transformations representing the individual rotations (single angle transformations) are listed as follows:

$$[\lambda] = \begin{bmatrix} \cos \lambda & \sin \lambda & 0 \\ -\sin \lambda & \cos \lambda & 0 \\ 0 & 0 & 1 \end{bmatrix} \quad [\nu] = \begin{bmatrix} \cos \nu & 0 & \sin \nu \\ 0 & 1 & 0 \\ -\sin \nu & 0 & \cos \nu \end{bmatrix}$$

$$[1''] = \begin{bmatrix} 0 & 0 & 1 \\ 0 & 0 & 1 \\ -1 & 0 & 0 \end{bmatrix} \quad [\psi] = \begin{bmatrix} \cos \psi & \sin \psi & 0 \\ -\sin \psi & \cos \psi & 0 \\ 0 & 0 & 1 \end{bmatrix}$$

$$[\theta] = \begin{bmatrix} \cos \theta & 0 & -\sin \theta \\ 0 & 1 & 0 \\ \sin \theta & 0 & \cos \theta \end{bmatrix} \quad [\phi] = \begin{bmatrix} 1 & 0 & 0 \\ 0 & \cos \phi & \sin \phi \\ 0 & -\sin \phi & \cos \phi \end{bmatrix}$$

$$[\beta] = \begin{bmatrix} \cos \beta & -\sin \beta & 0 \\ \sin \beta & \cos \beta & 0 \\ 0 & 0 & 1 \end{bmatrix} \quad [\alpha] = \begin{bmatrix} \cos \alpha & 0 & -\sin \alpha \\ 0 & 1 & 0 \\ \sin \alpha & 0 & \cos \alpha \end{bmatrix}$$

The definitions are not complete without specifying the range for each of the angles:

$$\begin{aligned} -180^\circ < \lambda &\leq 180^\circ; & -90^\circ &\leq \nu &\leq 90^\circ \\ 0 &\leq \psi < 360^\circ; & -90^\circ &\leq \theta &\leq 90^\circ; & -180^\circ < \phi &\leq 180^\circ \\ -180^\circ < \beta &\leq 180^\circ; & -90^\circ &\leq \alpha &\leq 90^\circ \end{aligned}$$

In addition, the transformations for the "special orientation angles" must be defined. The symbol $[L_s]$ is used to describe the $[L_{B-ES}]$ matrix when this matrix is defined in terms of the special orientation angles (ψ_s, θ_s, ϕ_s).

$$[L_s] = [L_{B-ES}] \quad (3.30)$$

$$[L_s] = [I''] [\phi_s] [\theta_s] [\psi_s] \quad (3.31)$$

The functional form of the $[\phi_s]$, $[\theta_s]$ and $[\psi_s]$ matrices is identical to that of the $[\phi]$, $[\theta]$, and $[\psi]$ matrices (the trigonometric functions of corresponding elements), and the range of ψ_s , θ_s , and ϕ_s are the same as those for ψ , θ , and ϕ , respectively.

Finally, it should be noted that the stability axes are the intermediate axes between the wind axes and the body axes.

$$\begin{bmatrix} dx \\ dy \\ dz \end{bmatrix} = [\alpha] \begin{bmatrix} dx_s \\ dy_s \\ dz_s \end{bmatrix} \quad \text{or} \quad \begin{bmatrix} dx_s \\ dy_s \\ dz_s \end{bmatrix} = [\beta] \begin{bmatrix} dx_w \\ dy_w \\ dz_w \end{bmatrix} \quad (3.32)$$

3.4 MATRIX EQUATIONS

The basic principles and concepts have been developed, using primarily vector notation. Axis systems have been selected for describing the various physical quantities, and methods for transforming quantities from one axis system to the next have been defined. The next step is to write the detailed equations describing the kinematic and dynamic behavior of the vehicle. Matrix algebra is used almost exclusively, in order to keep the development tractable, and because matrix equations are easily adapted to digital computers.

3.4.1 Equations of Motion

The equations of motion are written in body axes. The linear and angular momenta (from Equations 3.8 and 3.9) are written as

$$[M] = m[V] \quad (3.33)$$

$$[N] = [I][\omega] \quad (3.34)$$

where

$$[V] = \begin{bmatrix} u \\ v \\ w \end{bmatrix}, \quad [\omega] = \begin{bmatrix} p \\ q \\ r \end{bmatrix}, \quad [I] = \begin{bmatrix} I_x & 0 & -I_{xz} \\ 0 & I_y & 0 \\ -I_{xz} & 0 & I_z \end{bmatrix}$$

The form of $[I]$ implies that $x-z$ is a plane of symmetry.

The notation generally adopted is that the primary symbol refers to a specific type of quantity (e.g., V for the velocity of the body), and the subscript indicates the reference frame involved (e.g., V_E for the velocity of the body with respect to the earth axes) - no subscript usually implying an inertial reference.

The equations of motion are obtained (from Equations 3.10 and 3.11) as

$$m [a] = m [\dot{V}] + m [\omega \times] [V] = [F] \quad (3.35)$$

$$[I][\dot{\omega}] + [\omega \times][I][\omega] = [M] \quad (3.36)$$

where

$$[a] = \begin{bmatrix} a_x \\ a_y \\ a_z \end{bmatrix}, \quad [F] = \begin{bmatrix} F_x \\ F_y \\ F_z \end{bmatrix}, \quad [M] = \begin{bmatrix} M_x \\ M_y \\ M_z \end{bmatrix}$$

and $[\omega \times]$ is an operational form for the vector cross product $\bar{\omega} \times$ (see Reference 3.5).

$$[\omega \times] = \begin{bmatrix} 0 & -r & q \\ r & 0 & -p \\ -q & p & 0 \end{bmatrix}$$

Note that the dot (e.g., in $[\dot{V}]$) indicates a scalar differentiation of the individual elements, not a vector differentiation.

The above equations (3.35 and 3.36) can be expressed in a form suitable for integration as follows.

$$[\dot{V}] = \frac{1}{m}[F] - [\omega \times][V] \quad (3.37)$$

$$[\dot{\omega}] = [I]^{-1} \{ [M] - [\omega \times][I][\omega] \} \quad (3.38)$$

where

$$[I]^{-1} = \begin{bmatrix} I_z/I & 0 & I_{xz}/I \\ 0 & 1/I_y & 0 \\ I_{xz}/I & 0 & I_x/I \end{bmatrix}, \quad I = I_x I_y - I_{xz}^2$$

The velocities are integrated in the body axis system (following Equations 3.12 and 3.13) giving

$$[V] = \int_0^t [\dot{V}] d\tau + [V_0] \quad (3.39)$$

$$[\omega] = \int_0^t [\dot{\omega}] d\tau + [\omega_0] \quad (3.40)$$

3.4.2 Trajectory Kinematics

The motions of the vehicle relative to the earth are described primarily in terms of quantities measured in the earth-surface axes (see Figure 3.2). The

relative velocity of the vehicle is written (from Equation 3.14) as

$$[V_E] = [L_{B-ES}]' [V] - [V_{er}] \quad (3.41)$$

where

$$[V_E] = \begin{bmatrix} V_\lambda \\ V_\psi \\ -V_r \end{bmatrix} \quad [V_{er}] = \begin{bmatrix} 0 \\ V_{er} \\ 0 \end{bmatrix}$$

and the prime denotes the transpose (i. e., for an orthogonal matrix the inverse is equal to the transpose; e. g., $[L_{ES-B}] = [L_{B-ES}]^{-1} = [L_{B-ES}]'$). We find, from Equation 3.16, that

$$V_{er} = \Omega r_{EB} \cos \psi \quad (3.42)$$

The magnitudes of the tangential velocity (V_T) and the relative velocity (V_E), and the azimuth of the tangential velocity (ψ_T) and the elevation of the relative velocity or the climb angle (σ) are given by

$$V_T = \sqrt{V_\psi^2 + V_\lambda^2} ; V_T > 0 \quad (3.43)$$

$$V_E = \sqrt{V_T^2 + V_r^2} ; V_E > 0 \quad (3.44)$$

$$\psi_T = \sin^{-1} \frac{V_\lambda}{V_T} ; 0 \leq \psi_T < 360^\circ \left\{ \begin{array}{l} \text{Quad.} \\ V_\psi \quad + \quad - \quad - \quad + \\ V_\lambda \quad + \quad + \quad - \quad - \end{array} \right. \quad (3.45)$$

$$\sigma = \sin^{-1} \frac{V_r}{V_E} ; \begin{array}{l} 0 < \sigma \leq 90^\circ \quad \text{for } V_r > 0 \\ 0 > \sigma \geq -90^\circ \quad \text{for } V_r < 0 \end{array} \quad (3.46)$$

The position of the vehicle is described in terms of the latitude (ψ), the longitude (λ), and the altitude (h). These are obtained by integrating \vec{V}_E as in Equation 3.18, but in spherical coordinates.

$$[E_{ES-E}] = \int_0^t [\dot{E}_{ES-E}] d\tau + [E_{ES-E_0}] \quad (3.47)$$

where

$$[E_{ES-E}] = \begin{bmatrix} h \\ \psi \\ \lambda \end{bmatrix}$$

$$\dot{h} = V_p \quad (3.48)$$

$$\dot{\psi} = \frac{V_\psi}{r_{EB}} \quad (3.49)$$

$$\dot{\lambda} = \frac{V_\lambda}{r_{EB}} \cos \psi \quad (3.50)$$

$$r_{EB} = h + R_0 \quad (3.51)$$

3.4.3 Vehicle Orientation

The angular position of the vehicle is described by the various orientation angles; specifically the orientation of the body axes with respect to the earth-surface axes is specified by the Euler angles ψ , θ , and ϕ (or the special angles ψ_s , θ_s , and ϕ_s). These angles are obtained from the angular velocity relationships.

"Normal" Euler Angles: The angular velocity of the body axes can be expressed as the sum of the angular velocity of the earth axes ($\bar{\Omega}$), the angular velocity of the earth-surface axes with respect to the earth axes ($\bar{\omega}_{ES-E}$), and the angular velocity of the body axes with respect to the earth-surface axes ($\bar{\omega}_{B-ES}$).

$$\bar{\omega} = \bar{\omega}_{B-ES} + \bar{\omega}_{ES-E} + \bar{\Omega}$$

Further subdivision can be achieved by introducing the angular velocity vectors representing the time rates of change of the orientation angles.

$$\bar{\omega}_E = (\dot{\phi} + \dot{\theta} + \dot{\psi}) + (\dot{\psi} + \dot{\lambda}) + \bar{\Omega} \quad (3.52)$$

It is convenient to introduce the angular velocity of the vehicle relative to the earth ($\bar{\omega}_E$, as defined previously by Equation 3.15) so that

$$\bar{\omega}_E = \dot{\phi} + \dot{\theta} + \dot{\psi} + \dot{\psi} + \dot{\lambda} \quad (3.53)$$

Now this vector equations can be written in matrix form, transforming all components to body axes, as follows.

$$[\omega_E] = \begin{bmatrix} \dot{\phi} \\ 0 \\ 0 \end{bmatrix} + [\phi] \begin{bmatrix} 0 \\ \dot{\theta} \\ 0 \end{bmatrix} + [\phi][\theta] \begin{bmatrix} 0 \\ 0 \\ \dot{\psi} \end{bmatrix} + [L_{B-ES}] \left(\begin{bmatrix} 0 \\ -\dot{\psi} \\ 0 \end{bmatrix} + [I''] [\psi] \begin{bmatrix} 0 \\ 0 \\ \dot{\lambda} \end{bmatrix} \right) \quad (3.54)$$

$$[\omega_E] = \begin{bmatrix} \dot{\phi} \\ 0 \\ 0 \end{bmatrix} + [\phi] \begin{bmatrix} 0 \\ \dot{\theta} \\ 0 \end{bmatrix} + [\phi][\theta] \begin{bmatrix} 0 \\ 0 \\ \dot{\psi} \end{bmatrix} + [L_{B-ES}] [(\omega_{ES-E})_{ES}] \quad (3.54a)$$

where

$$[\omega_E] = \begin{bmatrix} p_E \\ q_E \\ r_E \end{bmatrix}$$

Equation 3.54 can be solved for the rates of change of the Euler angles as

$$[\dot{E}_{B-E3}] = \begin{bmatrix} \dot{\phi} \\ \dot{\theta} \\ \dot{\psi} \end{bmatrix} = [A] [\omega_E] - [B] \begin{bmatrix} 0 \\ -\dot{\psi} \\ \dot{\lambda} \end{bmatrix} \quad (3.55)$$

where

$$\begin{aligned} [A] &= [C] [\Theta]' [\Phi]' \\ [B] &= [C] [\Psi] [I''] [\nu] \end{aligned}$$

and

$$[C] = \begin{bmatrix} 1/\cos \Theta & 0 & 0 \\ 0 & 1 & 0 \\ \sin \Theta / \cos \Theta & 0 & 1 \end{bmatrix}$$

Finally, the desired Euler angles are obtained by integrating Equation 3.55.

$$[E_{B-E3}] = \begin{bmatrix} \phi \\ \theta \\ \psi \end{bmatrix} = \int_0^t [\dot{E}_{B-E3}] dt + [E_{B-E3_0}] \quad (3.56)$$

The angular velocity of the body axes with respect to earth axes is obtained by writing Equation 3.15 as

$$[\omega_E] = [\omega] - [L_{B-E}] [\Omega] \quad (3.57)$$

"Special" Euler Angles: The "special" Euler angles are treated in exactly the same manner as the normal ones, with the following results:

$$[\dot{E}_s] = \begin{bmatrix} \dot{\phi}_s \\ \dot{\theta}_s \\ \dot{\psi}_s \end{bmatrix} = [A_s] [I''^s] [\omega_E] - [B_s] \begin{bmatrix} 0 \\ -\dot{\psi} \\ \dot{\lambda} \end{bmatrix} \quad (3.55s)$$

where

$$\begin{aligned} [A_s] &= [C_s] [\Theta_s]' [\Phi_s]' \\ [B_s] &= [C_s] [\Psi_s] [I''^s] [\nu] \end{aligned}$$

$$[E_s] = \begin{bmatrix} \phi_s \\ \theta_s \\ \psi_s \end{bmatrix} = \int_0^t [\dot{E}_s] d\tau + [E_{s_0}] \quad (3.56s)$$

The functional forms of the "s" matrices are identical with those for the normal system, and the only change that is introduced in the equations is the insertion of the $[I'']$ matrix in the equations for $[\dot{E}_s]$. Of course, though the functional form of $[L_s]$ is different from $[L_{\theta-ES}]$, these two matrices are actually equal by definition.

The similarity between the equations and the matrices associated with the two sets of angles makes it very convenient and easy to switch from one set to the other; and it is for this very reason that ϕ_s , θ_s , and ψ_s are defined as they are. In a digital computer the same storage locations and the same operations can be used for the normal and the special sets. It is only necessary to make the one modification going from Equation 3.55 to 3.55s, and to compute the "initial conditions" required for Equation 3.56 or 3.56s.

Interchange Between "Normal" and "Special" Angles: As mentioned in Section 3.3.2, the switching criteria are based on the value of θ , and two values are used in the criteria.

θ_1 - the value of θ for which the change is made from the ϕ, θ, ψ set to the ϕ_s, θ_s, ψ_s set.

θ_2 - the value of θ for which the change is made from the ϕ_s, θ_s, ψ_s set back to the ϕ, θ, ψ set.

In order to avoid continual switching due to small oscillations,

$$|\theta_2| < |\theta_1| \quad (3.58)$$

The two matrices, $[L_{\theta-ES}]$ and $[L_s]$, are written out in partial detail in order to clearly show the relationships used to calculate the starting values when switching occurs.

$$[L_{\theta-ES}] = \begin{bmatrix} \cos \theta \cos \psi & \cos \theta \sin \psi & -\sin \theta \\ L_{21} & L_{22} & \sin \phi \cos \theta \\ L_{31} & L_{32} & \cos \phi \cos \theta \end{bmatrix}$$

$$[L_s] = \begin{bmatrix} L_{s11} & L_{s21} & \cos \phi_s \cos \theta_s \\ L_{s21} & L_{s22} & \sin \phi_s \cos \theta_s \\ -\cos \theta_s \cos \psi_s & -\cos \theta_s \sin \psi_s & \sin \theta_s \end{bmatrix}$$

It should be noted that the elements in these two matrixes are always equal,

$$L_{ij} = L_{s_{ij}}$$

When switching from the ϕ, θ, ψ set to the ϕ_s, θ_s, ψ_s set, the values of ϕ, θ, ψ are known and it is necessary to compute the corresponding values of ϕ_s, θ_s, ψ_s . These values are computed by equating appropriate elements of the $[L_{\theta-ES}]$ and $[L_s]$ matrices.

$$\theta_s = \sin^{-1}(\cos \phi, \cos \theta) = \sin^{-1} L_{33}; \quad \begin{matrix} 0 < \theta_s < 90^\circ, \text{ for } L_{33} > 0 \\ 0 > \theta_s > -90^\circ, \text{ for } L_{33} < 0 \end{matrix} \quad (3.59)$$

$$\phi_s = \sin^{-1} \left(\frac{\sin \phi \cos \theta}{\cos \theta_s} \right) = \sin^{-1} \left(\frac{L_{33}}{\cos \theta_s} \right); \quad \left\{ \begin{array}{l} \text{QUAD. I II III IV} \\ L_{13} \quad + \quad - \quad - \quad + \\ L_{23} \quad + \quad + \quad - \quad - \end{array} \right\} \quad (3.60)$$

$$\psi_s = \sin^{-1} \left(\frac{-L_{32}}{\cos \theta_s} \right); \quad \left\{ \begin{array}{l} \text{QUAD. I II III IV} \\ L_{31} \quad - \quad + \quad + \quad - \\ L_{32} \quad - \quad - \quad + \quad + \end{array} \right\} \quad (3.61)$$

When switching from the θ_s, ϕ_s, ψ_s set to the ϕ, θ, ψ set, the values of θ_s, ϕ_s, ψ_s are known and it is necessary to compute the corresponding values of ϕ, θ, ψ . The approach is the same as before.

$$\theta = \sin^{-1}(-\cos \phi_s \cos \theta_s) = \sin^{-1}(-L_{s_{13}}); \quad \begin{matrix} 0 < \theta < 90^\circ, \text{ for } L_{s_{13}} < 0 \\ 0 > \theta > -90^\circ, \text{ for } L_{s_{13}} > 0 \end{matrix} \quad (3.62)$$

$$\phi = \sin^{-1} \left(\frac{\sin \phi_s \cos \theta_s}{\cos \theta} \right) = \sin^{-1} \left(\frac{L_{s_{23}}}{\cos \theta} \right); \quad \left\{ \begin{array}{l} \text{QUAD. I II III IV} \\ L_{s_{23}} \quad + \quad + \quad - \quad - \\ L_{s_{33}} \quad + \quad - \quad - \quad + \end{array} \right\} \quad (3.63)$$

$$\psi = \sin^{-1} \left(\frac{L_{s_{12}}}{\cos \theta} \right); \quad \left\{ \begin{array}{l} \text{QUAD. I II III IV} \\ L_{s_{11}} \quad + \quad - \quad - \quad + \\ L_{s_{12}} \quad + \quad + \quad - \quad - \end{array} \right\} \quad (3.64)$$

The switching time for a continuous solution of the equation, such as would be obtained on an analog computer, would be that time at which $|\theta| = |\theta_s|$ or $|\phi| = |\phi_s|$ occurred, depending on which set of angles was being used at the

time. For digital computation, however, it is more convenient to define a test value of Θ , and then switch coordinates at the end of the first time interval for which the test shows switching is needed. Also, since

$$L_{13} = L_{s,13} = -\sin \Theta$$

it is more convenient to apply the test criteria to L_{13} and $L_{s,13}$ rather than Θ directly, as follows:

- (a) Switch from ϕ, θ, ψ to ϕ_s, θ_s, ψ_s when $|L_{13}| > L_{13T} = \sin \Theta_{1T}$
- (b) Switch from ϕ_s, θ_s, ψ_s to ϕ, θ, ψ when $|L_{s,13}| < |L_{s,13T}| = \sin \Theta_{2T}$

The values of Θ_{1T} and Θ_{2T} which have been selected in the present study are

$$\Theta_{1T} = 70^\circ, \quad \Theta_{2T} = 50^\circ.$$

3.4.4 Relative-Wind Kinematics

The relative wind is defined by the inertial velocity of the vehicle and by the motions of the air due to earth rotation, winds and gusts. The specification of these quantities follows from the development in Section 3.2.3.

The velocity of the air due to earth rotation, as measured at the origin of the earth-surface axes and in terms of components in these axes, is

$$[V_{er}] = \begin{bmatrix} 0 \\ V_{er} \\ 0 \end{bmatrix} \quad (3.65)$$

where

$$V_{er} = \Omega r_{eB} \cos \psi$$

The general air mass motions, or winds, are also measured with respect to the earth and are expressed in terms of components of earth-surface axes as

$$[W] = \begin{bmatrix} W_p \\ W_\lambda \\ -W_r \end{bmatrix} \quad (3.66)$$

In the given order, these components represent northward, eastward, and upward (+ W_r) air mass velocities. The rapid air mass motions, or gusts, are defined with respect to the vehicle and are, therefore, expressed in terms of components of the body axes as

$$[U] = \begin{bmatrix} u_x \\ u_y \\ u_z \end{bmatrix} \quad (3.67)$$

The components represent, in order, the head-on, lateral, and normal gust velocities.

Using the three quantities defined above, the velocity of the vehicle with respect to the air is obtained from Equation 3.19 and with components in body axes as

$$\begin{bmatrix} V_a \\ v_a \\ w_a \end{bmatrix} = \begin{bmatrix} u_a \\ v_a \\ w_a \end{bmatrix} = [V] - [L_{B-ES}] \left\{ [V_{er}] + [W] \right\} - [\mu] \quad (3.68)$$

in which the matrix L_{B-ES} transforms V_{er} and W from earth-surface axes to body axes. The airspeed (V_a), the angle of attack (α), and sideslip (β) are given by

$$V_a = \sqrt{u_a^2 + v_a^2 + w_a^2}, \quad V_a > 0 \quad (3.69)$$

$$\beta = \sin^{-1} \frac{v_a}{V_a}; \quad \left\{ \begin{array}{c} \text{QUAD.} \\ u_a \\ v_a \end{array} \begin{array}{cccc} \text{I} & \text{II} & \text{III} & \text{IV} \\ + & - & - & + \\ + & + & - & - \end{array} \right\} \quad (3.70)$$

$$\alpha = \sin^{-1} \frac{w_a}{V_a \cos \beta}; \quad \begin{array}{l} 0 < \alpha \leq 90^\circ \text{ for } w_a > 0 \\ 0 > \alpha \geq -90^\circ \text{ for } w_a < 0 \\ \alpha = 0 \text{ for } \beta = \pm 90^\circ \end{array} \quad (3.71)$$

Figure 3.5 shows the velocity vector, \vec{V}_a , and indicates the reference directions for positive α and β .

In Section IV, it is shown that aerodynamic representation of the vehicle requires, in addition to V_a , α , and β , the variables $\dot{\alpha}$ and $\dot{\beta}$ which are used with the derivatives associated with non-stationary flow or lags (downwash lags). The solution for $\dot{\alpha}$ and $\dot{\beta}$ is one of the stickiest algebraic problems in the whole development, and has been neglected by other authors (e.g., Reference 3.4). To solve for $\dot{\alpha}$ and $\dot{\beta}$, the air velocity in wind axes

$$[V_w] = \begin{bmatrix} V_a \\ 0 \\ 0 \end{bmatrix} = [L_{B-W}]' [V_a]$$

is differentiated and arranged to obtain:

$$\begin{bmatrix} \dot{V}_a \\ V_a \dot{\beta} \\ V_a \dot{\alpha} \cos \beta \end{bmatrix} = [L_{B-W}]' [\dot{V}_a] = [L_{B-W}]' \begin{bmatrix} \dot{u}_a \\ \dot{v}_a \\ \dot{w}_a \end{bmatrix} \quad (3.72)$$

To find $[\dot{V}_a]$, Equation 3.20 is rewritten in slightly different form as

$$(\dot{V}_a)_B = (\dot{V})_B - (\dot{V}_{er})_E - (\dot{W})_{ES} - \bar{\omega}_{ES-E} \times \bar{W} - (\dot{\mu})_B + \bar{\omega}_E \times (\bar{V}_{er} + \bar{W}) \quad (3.20a)$$

When written in matrix form, Equation (3.20a) becomes

$$\begin{aligned} [\dot{V}_a] &= [\dot{V}] - [L_{B-ES}] \left\{ [L_{ES-E}] [(\dot{V}_{er})_E] + [W] \right\} \\ &\quad - [L_{B-ES}] [(\omega_{ES-E})_{ES} \times] [W] - [\dot{\mu}] + [\omega_E \times] [L_{B-ES}] \left\{ [V_{er}] + [W] \right\} \end{aligned} \quad (3.73)$$

Certain matrices in this equation are specially synthesized

1. $[(\omega_{ES-E})_{ES} \times]$
2. $[L_{ES-E}] [(\dot{V}_{er})_E]$

and both are defined in the List of Matrices near the front of this report. Now $\dot{\beta}$ and $\dot{\alpha} \cos \beta$ can be expressed explicitly from Equation 3.72 in terms of \dot{u}_a , \dot{v}_a , and \dot{w}_a as

$$\dot{\beta} = \frac{1}{V_a} (-\dot{u}_a \sin \beta \cos \alpha + \dot{v}_a \cos \beta - \dot{w}_a \sin \beta \sin \alpha) \quad (3.74)$$

$$\dot{\alpha} \cos \beta = \frac{1}{V_a} (-\dot{u}_a \sin \alpha + \dot{w}_a \cos \alpha) \quad (3.75)$$

and the velocity components are obtained from Equation 3.73. The quantity $\dot{\alpha} \cos \beta$ is obtained, instead of $\dot{\alpha}$, in order that Equation 3.75 may still be evaluated at $\beta = \pm 90^\circ$.

The angular velocity of the vehicle relative to the air is expressed from Equation 3.21 in body axes as

$$[\omega_a] = \begin{bmatrix} p_a \\ q_a \\ r_a \end{bmatrix} = [\omega] - [L_{B-E}] [\omega] = [\omega_E] \quad (3.76)$$

The components of $[\omega_a]$ are needed for the aerodynamic representation of the vehicle.

3.4.5 Forces and Moments

Following the general description of vector forces and moments given in Section 3.2.4, the forces and moments can be expressed in body axis components as

$$[F] = [F_a] + [F_g] + [F_T] + [\Delta F] \quad (3.77)$$

$$[M] = [M_a] + [M_g] + [M_T] + [\Delta M] \quad (3.78)$$

For present purposes, we assume there is no thrust, no gravitational torque about the c.g., and hence set

$$[F_T] = 0, [\Delta F] = 0, [M_g] = 0, [\Delta M] = 0$$

Appendices B and C provide methods for handling the forces and moments which by assumption have been neglected here, especially those due to thrust and gravity.

Aerodynamic forces and moments are expressed in the usual coefficient form in body axes

$$[F_a] = \frac{1}{2} \rho V_a^2 S [C_F] \quad (3.79)$$

$$[M_a] = \frac{1}{2} \rho V_a^2 S [L][C_M] \quad (3.80)$$

where

ρ = air density, a function of altitude given by Equation 2.12

V_a = airspeed, given by Equation 3.69

S = the vehicle's wing area

$[L] = \begin{bmatrix} b & 0 & 0 \\ 0 & c & 0 \\ 0 & 0 & b \end{bmatrix}$ = the characteristic length matrix with reference span b , and reference chord c

$[C_F] = \begin{bmatrix} C_x \\ C_y \\ C_z \end{bmatrix}$ = the aerodynamic force coefficient matrix in body axes

$[C_M] = \begin{bmatrix} C_{Ll} \\ C_{ml} \\ C_{nl} \end{bmatrix}$ = the aerodynamic moment coefficient matrix in body axes.

The matrices $[C_F]$ and $[C_M]$, in general, are complex functions of the variables $M, \alpha, \beta, \dot{\alpha}, \dot{\beta}, \delta_e, \delta_a, \delta_r, p_a, q_a, r_a$ and others. There

is a peculiarity in the digital computer program, however, which precludes the dependency of $[C_F]$ upon $\dot{\alpha}$ and $\dot{\beta}$. This arises because of computation order in the program: $[C_F]$ is required to compute $[F]$ which, in turn, is required to compute $[\dot{V}]$. Then $[\dot{V}]$ is used to compute $[\dot{V}_e]$ and hence $\dot{\alpha}$ and $\dot{\beta}$. Thus, though $\dot{\alpha}$ and $\dot{\beta}$ may be used to compute $[C_M]$, they are not available for computing $[C_F]$. The simplified diagram of the computer program, Figure D.1 of Appendix D, shows the computational order and illustrates the situation. This situation causes no hardship since C_{L_x} and $C_{y_{\beta}}$ are not normally even considered in the equations of motion. In the event that terms such as these should be needed in some unusual case, then either numerical differentiation or iteration of the force equation will have to be resorted to.

The gravitational force, included here as that due to an inverse-square field, can be expressed as follows:

$$[(F_g)_{es}] = -\pi g_0 \frac{R_0^2}{(r_{e0})^3} [(r_{e0})_{es}] = \pi g_0 \left(\frac{R_0}{r_{e0}} \right)^2 \begin{bmatrix} 0 \\ 0 \\ 1 \end{bmatrix}$$

and

$$[F_g] = [L_{B-es}] [(F_g)_{es}]$$

therefore,

$$[F_g] = \pi g_0 \left(\frac{R_0}{r_{e0}} \right)^2 \begin{bmatrix} L_{13} \\ L_{23} \\ L_{33} \end{bmatrix} \quad (3.81)$$

In these equations:

$[(F_g)_{es}]$ = the gravitational force matrix in the earth-surface axes,

π = the mass of the vehicle,

g_0 = the sea level value of gravitational acceleration,

R_0 = the radius of the (assumed spherical) earth,

$[(r_{e0})_{es}]$ = the matrix representing the vector from the earth center to the vehicle in earth-surface axes; and

$\begin{bmatrix} L_{13} \\ L_{23} \\ L_{33} \end{bmatrix}$ = the column matrix of the 13, 23, and 33 elements of $[L_{B-es}]$.

The corresponding equations for the gravitational force of an oblate spheroidal earth are presented in Appendix C.

Small moments due to rocket thrust can be applied to re-entry vehicles to provide for a lack of aerodynamic control moments at very high altitudes. These moments would be supplied by a reaction controller, and one form for such a control system is developed in Section 5.1.7 (Equation 5.8) where the elements of the matrix

$$[M_T] = \begin{bmatrix} L_T \\ M_T \\ N_T \end{bmatrix}$$

are made functions of α , β , δ , their derivatives, and command inputs. The more general problem of forces and moments due to rocket thrust are treated in Appendix B.

3.5 REFERENCES

- 3.1 Schuler, John M.: Vector Equations of Motion for a Rigid Body. Cornell Aeronautical Laboratory Memorandum FRM No. 251, June 1956.
- 3.2 Coburn, Nathaniel: Vector and Tensor Analysis. The Macmillan Company, New York, 1955.
- 3.3 Rhoads, Donald W. and John M. Schuler: "A Theoretical and Experimental Study of Airplane Dynamics in Large-Disturbance Maneuvers." Journal of the Aeronautical Sciences, July 1957.
- 3.4 Patha, John T.: Dynamics of a Rigid Body with Six Degrees of Freedom Including Effects of Nonlinear Aerodynamic Terms, Automatic Control Command, Rapidly Varying Mass, Earth Rotation, and Earth Oblateness. Boeing Airplane Company Document No. D5-5639, October 1959.
- 3.5 Frazer, R.A.; W.J. Duncan; A.R. Collar: Elementary Matrices. Cambridge University Press, 1950.

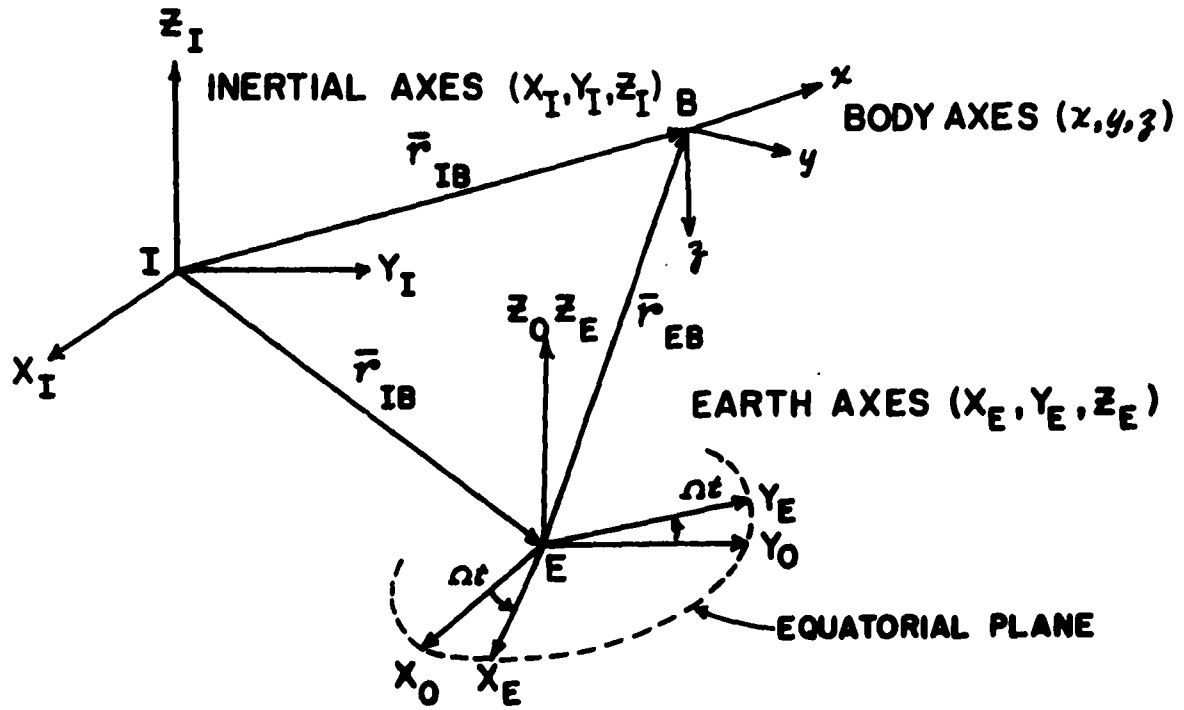


FIGURE 3.1 INERTIAL, EARTH, AND BODY COORDINATE SYSTEMS

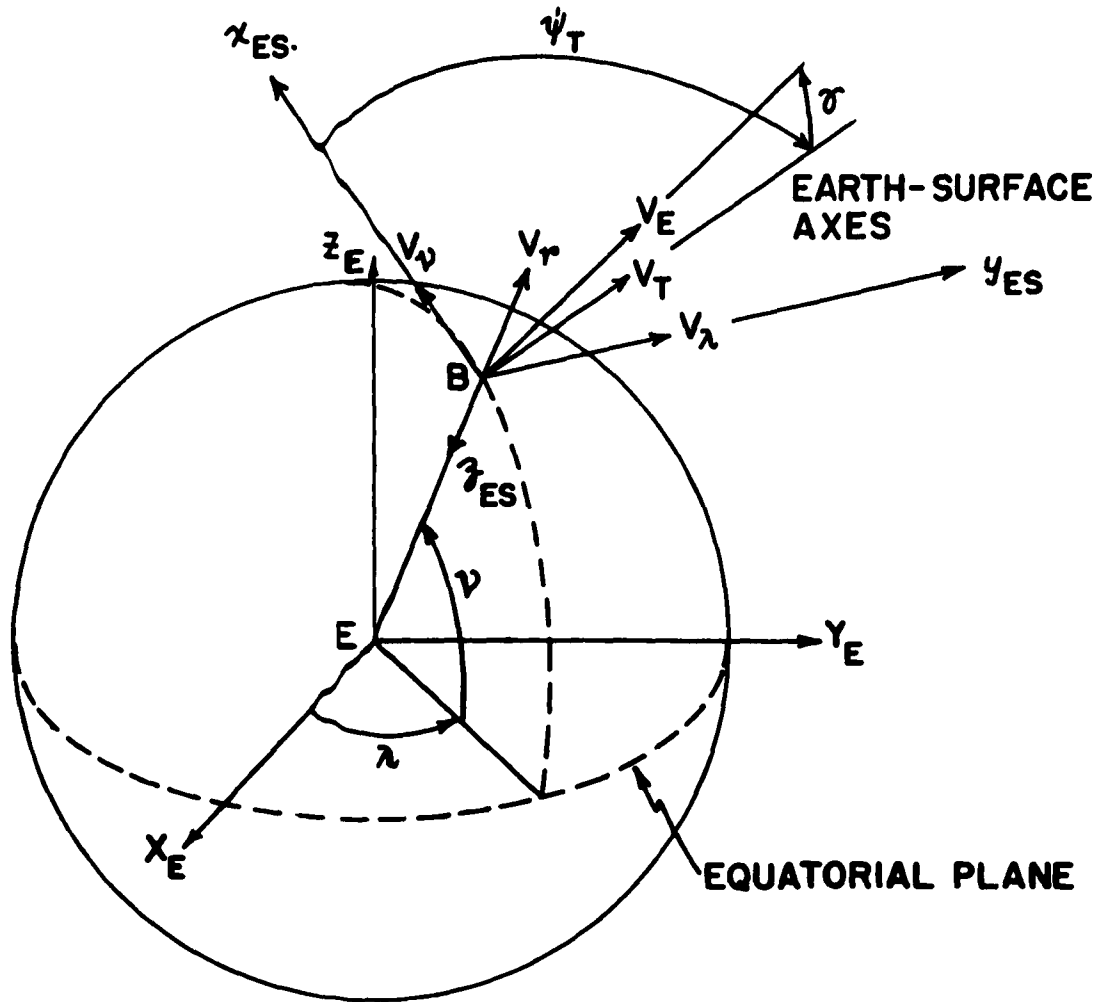
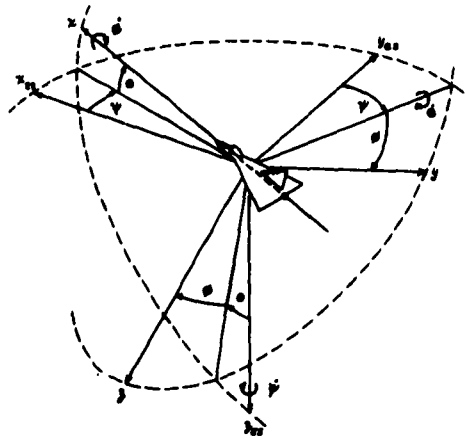
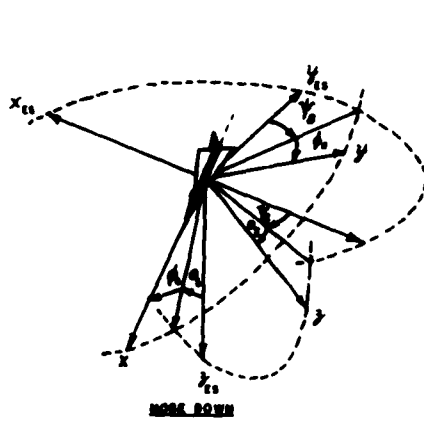


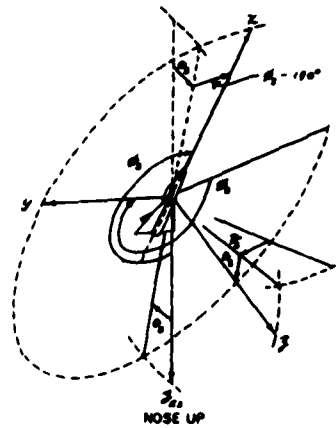
FIGURE 3.2 COORDINATES FOR RELATIVE MOTION OVER THE EARTH



a. Normal Orientation Angles



b. Special Orientation Angles



c. Special Orientation Angles

FIGURE 3.3 ORIENTATION ANGLES

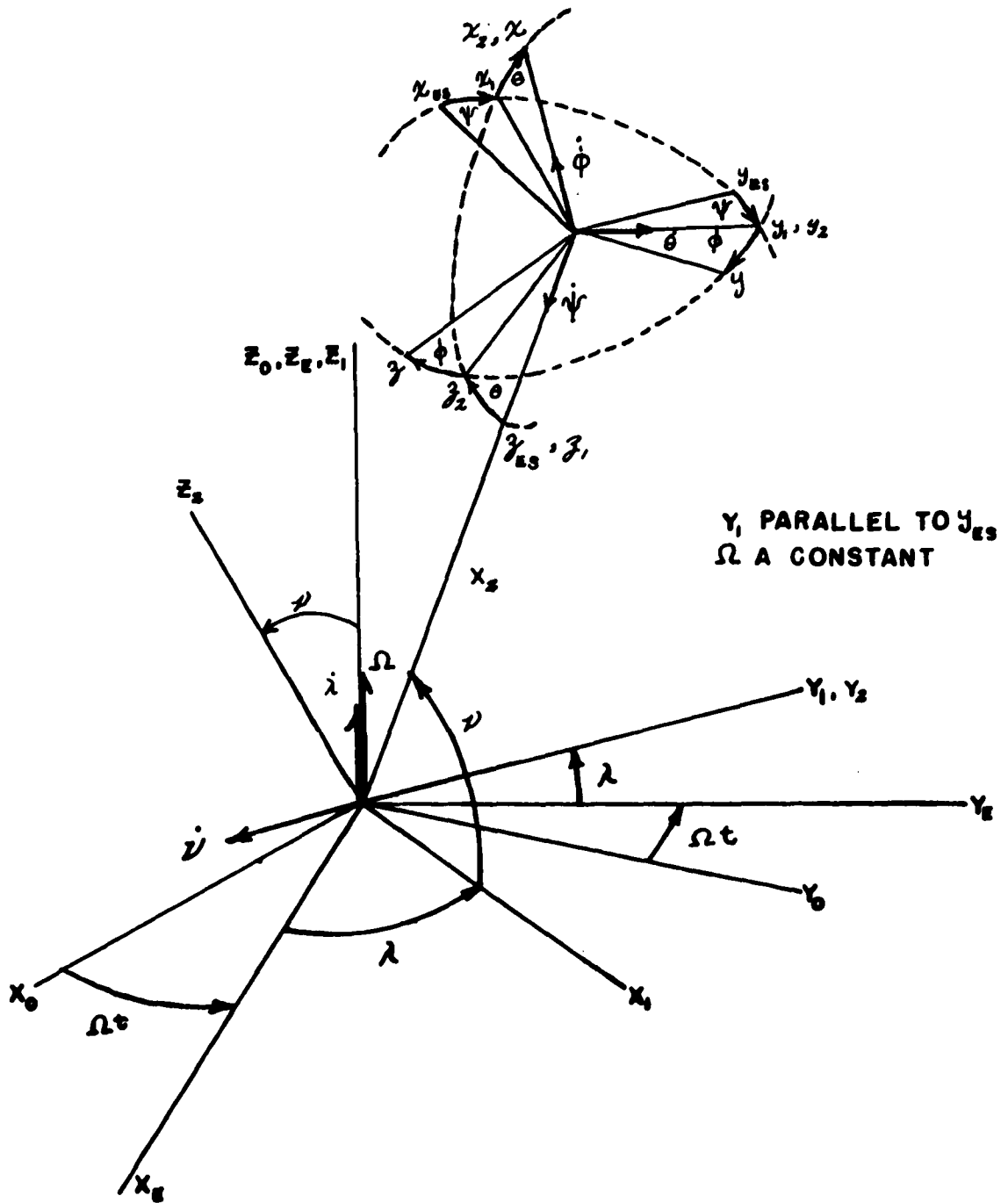


FIGURE 3. 4 ANGULAR DISPLACEMENTS AND CORRESPONDING ANGULAR VELOCITIES

$$\delta_e = \delta_{ec} = \frac{\delta_{aL} + \delta_{aR}}{2}$$

$$\delta_a = \delta_{aL} - \delta_{aR}$$

$$\delta_r = \frac{1}{2}(\delta_{rL} + \delta_{rR})$$

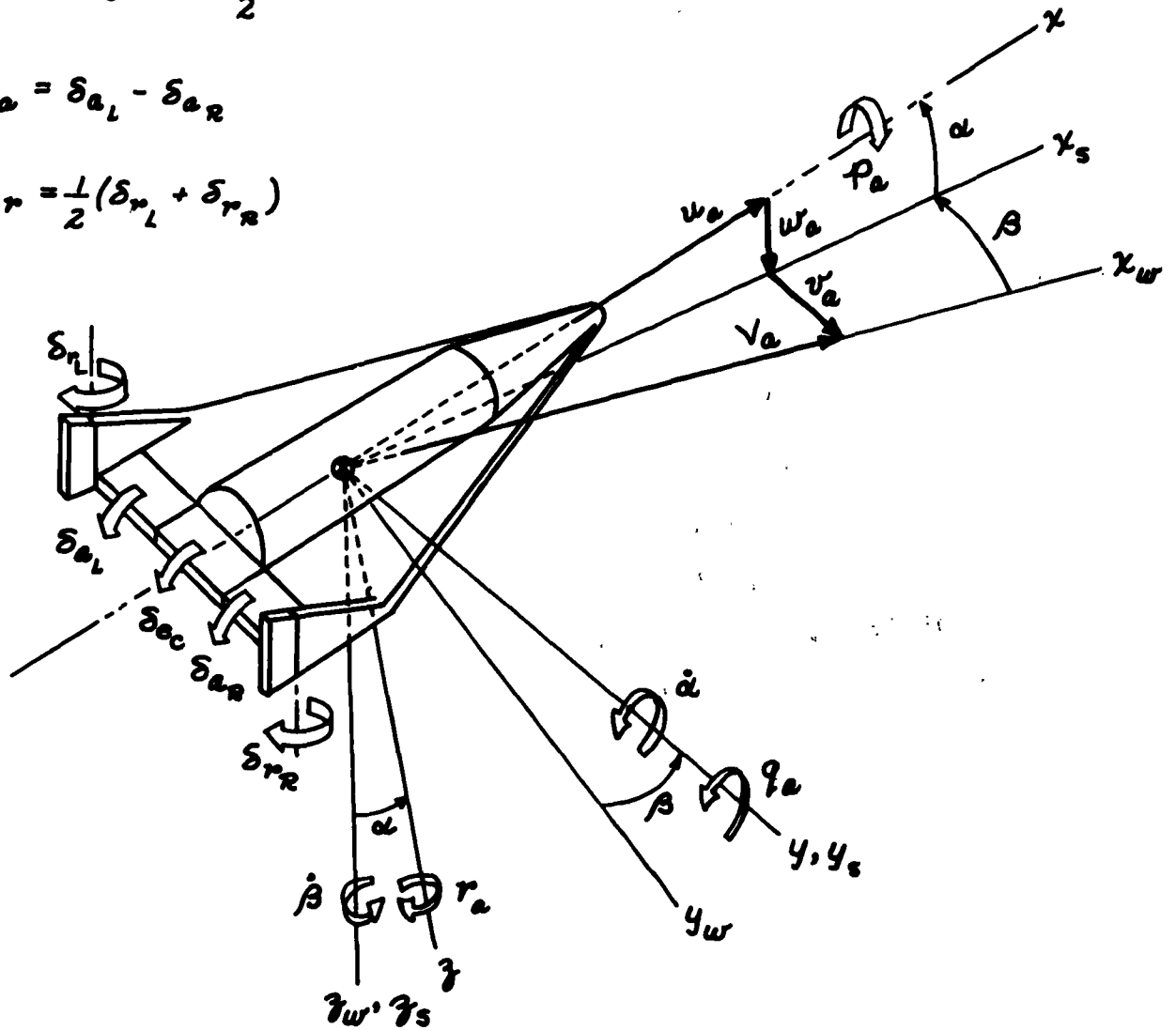


FIGURE 3.5 ORIENTATION OF BODY, STABILITY, AND WIND AXES; CONVENTIONS FOR LINEAR AND ANGULAR VELOCITIES AND FOR CONTROL SURFACE DEFLECTIONS

NAVTRADEVGEN 801A
SECTION IV
AERODYNAMICS AND CONTROL

4.1 INTRODUCTION

The basic purpose of this section is to describe methods for representing the aerodynamic data in the equations of motion. This description could embrace not only the equations for the forces and moments on the aircraft, but also the equations for aerodynamic heating, structural temperatures, aero-thermo-elasticity, control system characteristics - that is, the whole dynamic problem. However, such description is considerably beyond the scope of the present work; our principal concern is with the forces and moments related to the rigid-body motions of the aircraft.

Before considering the equations for the forces and moments, it is necessary to define flight boundaries and operating limitations. Then the general aerodynamic characteristics of re-entry vehicles can be considered as a prelude to formulating equations for representing the aerodynamic data. Three types of simulation can be considered: (1) trajectory studies which require knowledge of just C_L and C_D ; (2) studies of rotational motions or attitude dynamics which assume a pre-programmed trajectory or just a constant flight condition; (3) complete representation for full simulation of the vehicle's flight. The significance of the vehicle control problem must not be missed since this represents the pilot's task - the real measure of what is needed in the simulation.

Despite the voluminous publications on hypersonic vehicles and aerodynamics and despite the rapid growth of theory and experimental data, hypersonic flight still remains much of a mystery and it is not possible to characterize hypersonic aerodynamics definitively in any general sense. Perhaps good definition will not be achieved until we have actually tested hypersonic aircraft in flight. The best one can do is to represent the data obtained from the existing estimation methods even though they be inadequate, make educated guesses based on past experience, and hope that enough tolerance for error has been allowed. Thus, the presentation of numerical data has not been considered important in this study; rather, forms of equations have been developed which should be suitable for representing the estimated aerodynamic characteristics of particular aircraft as they are developed. In this manner, the functional equations provide some measure of the complexity of the problem and of the requirements for simulation.

The aircraft control problem contains many unknowns and is very much dependent on configuration details; at the same time the aircraft control characteristics determine to a large extent just what aerodynamic representation is needed. The following general criteria have been adopted (Reference 4.5 describes detailed requirements):

1. The aircraft will have an automatic control system which will provide the pilot with good control of the whole flight of the aircraft.
2. The aircraft will have a stability augmentation system (minimum automatic control system) which will provide the pilot with good handling qualities throughout the flight envelope.
3. Direct manual control will be an emergency condition only,

and under these conditions only minimum flyable handling qualities can be expected.

Pilot task analysis is the key factor - it determines the formulation of the problem.

4.2 FLIGHT SPECTRUM AND CORRIDOR

The flight spectrum can be broken into four general regions: boost, en-route cruise (sub-orbital, orbital or super-orbital), re-entry, and landing. Boosted flight may include pilot control, particularly in the event boost is aborted. The pilot's job during cruise depends on the task he is given, and may include the initiation of re-entry (the transition from cruise to re-entry). Transition is critical because it governs the piloting task during re-entry. Transition may be effected by firing retro-rockets, by aerodynamic means, or by both combined. Re-entry poses a piloting task under all circumstances; even with fully automatic control, the pilot must monitor the re-entry and be prepared to take over if a malfunction occurs or if unforeseen circumstances require a change in plans. The landing problem for a hypersonic aircraft will not be much different from that for contemporary high-speed aircraft, though the piloting requirements will probably be more stringent because speeds will be higher and less power will be available (thrust and duration for landing engines will be kept small because of the severe penalty incurred from excess weight).

Re-entry, the flight region of primary concern in this study, has the purpose of landing the aircraft on a given spot. The range achieved following re-entry is very sensitive to small changes in re-entry velocity and flight path angle, so what would seem to be minor effects (such as earth oblateness) can take on significance. In order to minimize the uncertainties, it would be desirable to minimize range during re-entry and hence minimize dispersion. The use of maximum re-entry angles (γ_{RE}) are thus implied, and the analysis of Lees, Hartwig and Cohen (Reference 4.7) shows that angles up to $\gamma_{RE} = -6^\circ$ are feasible. To achieve such a γ_{RE} will require large retro-rockets, the maximum use of drag, and possibly negative lift (inverted flight). Precise control in this transition region will be required, including precise attitude control. Aerodynamic moments will be small, and primary control will be by inertial devices or reaction jets. Though not a problem analyzed here in detail, it should be recognized that how the aircraft is controlled during this transition from cruise to re-entry will have a profound influence on re-entry. Very stringent requirements will be placed on time or spatial position, re-entry angle, attitude, and proper performance of the task.

The "h-V diagram" is a useful and commonly used tool for representing the flight spectrum in re-entry (e.g., see Figure 4.1 in this report, also Reference 4.2 and Batdorf in Reference 4.6). On this diagram one can plot the various operating characteristics and limit lines: equilibrium flight or glide conditions, heating limits, structural limits, maneuver limits, and aerodynamic limits. These define the corridor for safe flight. The h-V diagram is essentially a state diagram which defines the energy of the system - potential vs. kinetic. In addition to the h-V information, information is needed on the trajectory and how to control it - the range problem. Range control is a complex problem, especially since at high speeds the range is very sensitive to minor changes in atmospheric characteristics or aircraft characteristics and flight condition (e.g., the range is indeterminate if $V > V_c$ and h is high enough, i.e., $R \rightarrow \infty$). Range control is the objective of what has been called "energy management"; many concepts for energy

management systems have been proposed and studied (e.g., Reference 4.3). Here we are not concerned with the energy management system per se, but only with the variables that affect it; we are not concerned with how to control range, but rather with the variables needed for range control and the accurate computation of range given the proper control. The pertinent aspects of energy management, the state in h-V space and the trajectory or range in physical space are described very briefly in the following sections. More comprehensive treatment of energy management is found in References 4.3, 4.4, and 4.13. This last paper by Yoler includes a concise review of the whole performance problem.

4.2.1 Equilibrium Conditions

Equilibrium flight assumes a balance of gravity, lift and "centrifugal force" - the acceleration due to rotating around the earth. Equilibrium flight, a concept valid only for small flight path angles, is characterized by the following simple equations:

$$L = W \left(1 - \frac{V^2}{gr} \right) \quad (4.1)$$

where

L = lift

W = weight

r = vehicle geocentric radius \cong earth radius

$\frac{V^2}{gr}$ = "centrifugal force"

If a non-rotating earth is assumed, then Equation 4.1 may be written as

$$\frac{W}{C_L S} = \frac{\frac{1}{2} \rho V^2}{1 - \frac{V^2}{gr}} \quad (4.2)$$

and the right-hand side is completely determined for any given h and V since ρ can be obtained from the standard atmosphere. Thus, curves of constant $W/C_L S$ can be plotted on the h-V diagram, or curves of constant C_L can be plotted for a particular aircraft. Equilibrium glide curves for the study aircraft are shown in Figure 4.1 for two cases: (1) $C_L = .7$ which is characteristic of C_{LMAX} ; (2) C_L for $\alpha = 15^\circ$ which is characteristic of L/D_{MAX} and hence the minimum equilibrium C_L for re-entry.

If earth rotation is included, then Equation 4.2 becomes

$$\frac{W}{C_L S} = \frac{\frac{1}{2} \rho V_a^2}{1 - \frac{V^2}{gr}} \quad (4.3)$$

and V_a may be computed to sufficient accuracy from the relation

$$V^2 = V_a^2 + V_{er}^2 + 2 V_{er} V_a \sin \psi_T \quad (4.4)$$

where

ψ_T = azimuth angle of flight path

V_{er} = velocity due to earth rotation at the particular latitude, $\Omega r \cos \psi$

Equation 4.4 may be solved for V_T to yield

$$V_a = -V_{er} \sin \gamma_T \pm \sqrt{V^2 - V_{er}^2 \cos^2 \gamma_T} \quad (4.5)$$

and the + sign is used except when both $\gamma_T > 180^\circ$ and $V_a < -V_{er} \sin \gamma_T$. Since V_{er} is a function of latitude, it is clear that a single h-V diagram cannot account properly for the difference between inertial and relative velocity except in the case of a nearly equatorial re-entry. However, by using an average value of V_{er} , an acceptably accurate picture will usually be obtained. An upper bound for the error is shown in Figure 4.1 by the equilibrium glide curve for an eastward equatorial re-entry.

The range for an equilibrium glide can be roughly approximated by the equation

$$R = \frac{1}{2} r \left(\frac{L}{D} \right) \ln \left(\frac{1}{1 - \frac{V_0^2}{gR}} \right) \quad (4.6)$$

where V_0 = initial velocity at start of glide.

It is seen that while C_L controls the profile in the h-V plane, it is L/D that controls the range. Thus, a high L/D max is needed in order to have a large range, and control of L/D is needed in order to control the range or to vary the landing spot.

4.2.2 Aerodynamic Heating

To a great extent the aerodynamic heating depends on the aircraft shape and physical characteristics: the shape and thickness of the nose, wing and tail leading edges, etc.; the range of α and β allowed in flight; the structure and method of cooling it. The basic problem in flight is to keep the temperatures at various critical points on the aircraft less than the allowable limit temperatures. Various temperature-limit lines (T_{LIMIT} lines) can be plotted on the h-V diagram, and these will usually depend on α or C_L . The calculation of T_{LIMIT} lines is complicated; however, theoretical heat transfer rates for simple shapes and conditions do give an insight to the problem. Lees (Reference 4.12) gives an equation developed from the Fay-Riddell results for the stagnation-point heat-transfer rate (convective):

$$\dot{Q}_s = C \sqrt{\frac{\rho}{R}} V_a^3 \quad (4.7)$$

where

C = constant depending on the characteristics of the air and the shape of the surface

R = radius of curvature of the surface.

A curve for $\dot{Q}_s = 200 \text{ Btu/sec-ft}^2$ has been plotted on the h-V diagram in Figure 4.1 to typify a heating limit curve for the study vehicle. This curve represents \dot{Q}_s for the nose of the vehicle which has been assumed to have a radius

$$R = .5 \text{ feet}$$

and the constant, C , according to Lees, is

$$C = 2^{1/2} K_{EARTH}$$

$\mathcal{E} = 1$ for axially symmetric flow

$$K_{EARTH} = 15.5.$$

Of course, skin and structural temperatures depend on more than just heat transfer rates. Not only must convective, conductive and radiative heat transfer rates be known, but also the heat flux through the structure must be known, and the effect of cooling by ablation or other methods must be included in order to solve for the actual temperatures.

4.2.3 Structural Limits

A number of limitations fall in the structural category: air loads, maneuver loads, flutter (particularly panel flutter). The structural problem has been summarized by Batdorf in Reference 4.6, and References 4.1, 4.2 and 4.4 contain analyses of the maneuver loads problem. The primary influence on the structural limits is the dynamic pressure (q_i), so that lines of constant q_i in the h-V plane are typical of structural limit lines. A curve for $q_i = 500$ psf has been plotted on Figure 4.1 and is typical of a structural limit line for a re-entry glider with low wing loading. For an actual aircraft the structural limit lines, as in the case of T_{LIMIT} lines, depend on the vehicle's attitude and flight condition. In particular, heating is significant since high temperatures and high stress combine to give critical conditions.

4.2.4 Maneuver Limits

The maneuver limits for a re-entry vehicle are similar to those of a conventional aircraft (load factor or "g" limits), but an additional curve appears on the h-V diagram called the "recovery ceiling". A recovery ceiling, as it might appear, is sketched on the h-V diagram of Figure 4.1. The recovery ceiling is defined as the maximum allowable altitude (potential energy) for horizontal flight (apogee) at a particular velocity. If this altitude is exceeded, then on re-entry the vehicle will exceed one of the flight boundaries - burn up, break up, or crash into the ground. This will be true if the recovery ceiling is exceeded for the given velocity, irrespective of the direction of flight (i. e., horizontal flight is only the least critical case). The recovery ceiling is primarily of interest to the boost phase of hypersonic flight. It is desirable to avoid crossing this boundary at any time during boost, so that abortion and subsequent re-entry are always safe.

Because of the low values of L/D in hypersonic flight, drag is an important factor in the maneuver loads. The maximum load factor (maximum total "g") on the h-V diagram is essentially a line of constant q_i for any given angle of attack. Maneuver load boundaries are discussed further in References 4.2 and 4.4.

4.2.5 Stability and Control

The over-all problem of stability and control is a complex one, involving handling qualities under various types of operation (automatic control, manual control with stability augmentation, direct manual control), maneuver limits (accelerations on the pilot), attitude and control limits (stability, heating, and control authority), and range control (energy management). The stability and control problem is intimately linked with the whole flight spectrum, and what

limitations will be imposed by these problems are not presently clear. This is, in fact, the purpose behind the present study: to develop equations which can be used to help define the critical stability and control problems. However, certain characteristics are fundamental and can be described with present knowledge.

The basic problem is that of providing control of angle of attack (α) and bank angle (ϕ) in such a way as to satisfy the handling qualities requirements, performance requirements, and heating limitations, and do this for each of the control modes (automatic, manual, etc.). The angle of attack range during re-entry is limited at the low end by α for L/D_{\max} , at the high end by stability and control limitations; contrary to normal flight, re-entry flight occurs essentially on the "back-side of the power-required curve". The reason is that for $\alpha < \alpha_{L/D_{\max}}$ heating increases drastically (Reference 4.3). It is desirable to have α range from $\alpha_{L/D_{\max}}$ to $\alpha_{C_{L_{\max}}}$, and from Figure 4.3, this corresponds to roughly $15^\circ < \alpha < 50^\circ$. It would be of value to obtain maximum C_D with $L/D = 0$ (i. e., $\alpha = 90^\circ$), but it is unlikely that the severe stability and control problems presented by flight at $\alpha = 90^\circ$ would justify it. Achieving $\alpha = 50^\circ$ is difficult enough.

Range and altitude control is achieved principally through bank angle (ϕ). Though the equilibrium glide is continually discussed as the mode for flight during re-entry, it is a condition which is virtually impossible to achieve except for a non-lifting vehicle. The actual flight path achieved involves skipping (See Figure 5.3 for example). The first skip is essentially impossible to avoid (the first overshoot below equilibrium glide), but the best method of damping the skip is by banking. That is, ϕ is used to reduce "lift" (normal to the earth) while maintaining drag. Thus ϕ becomes effectively a control for L' and L'/D independent of α (L' denotes the effective lift normal to the earth). In addition to its function as an altitude control, ϕ controls the lateral range.

The manner in which α and ϕ control the over-all aircraft motions can be seen from the following simplified equations of motion in which the effects of earth rotation (among others) have been neglected.

$$L \cos \phi = W \left(1 - \frac{V^2}{gr} \right) + \underline{m V \dot{\gamma}} \quad (4.8)$$

$$L \sin \phi = m V \dot{\psi}_T \quad (4.9)$$

$$m \dot{V} = D \quad (4.10)$$

where

γ = the flight path elevation angle, assumed small

$\dot{\psi}_T$ = the flight heading angle.

The underlined term ($m V \dot{\gamma}$) is zero for equilibrium glide by definition ($\dot{\gamma} = 0$). The range, from the initial conditions, is given approximately by

$$\begin{aligned} X &= \int_0^{t_1} V \cos \psi_T dt \\ Y &= \int_0^{t_1} V \sin \psi_T dt \end{aligned} \quad (4.11)$$

where X and Y are the longitudinal and lateral range, respectively. Now it is clear that $L \cos \phi$ takes the place of L in the equilibrium glide equation (Equation 4.1). L/D_{\max} still produces the maximum range, but the total range is reduced by banking. It can be shown that $\phi = 45^\circ$ produces approximately the

maximum lateral range. By banking successively left and right while holding a high α , the longitudinal range can be decreased without changing heading. The effect of ϕ control on range is sketched in Figure 4.2 (including two digital solutions for the study vehicle), and the envelope of possible landing points (called a foot print) is indicated for the particular initial re-entry condition.

The method of controlling the skip - of damping the hypersonic phugoid - is readily apparent. $L \cos \phi$ controls $\dot{\gamma}$ (Equation 4.8), and so once $\dot{\gamma} = 0$ at the bottom of the first skip then ϕ can be controlled to hold $\dot{\gamma} \cong 0$ and maintain $\dot{\gamma} \cong 0$. Thus, α can be used to control range, through D , and ϕ used to control h through $L \cos \phi$. Such control takes on particular significance for super-orbital re-entry ($V > V_c$). Here negative "lift" (L') is needed to stay in the atmosphere (Reference 4.7), and inverted flight ($\phi = 180^\circ$) is the only reasonable method of achieving it since the use of negative α creates many problems (heating, structural, negative "g" on the pilot).^{*} For sub-orbital re-entries $\phi < 90^\circ$ would normally prevail; though if the aircraft were permitted to start skipping out, then inverted flight ($\phi = 180^\circ$) would be required. Such a technique might be used to gain altitude. Roll rates ($\dot{\phi}$) for controlling range might be quite low, but high rates (as measured by the required aerodynamic or aileron control power) may be needed for controlling the skip.

4.2.6 Pilot's Displays

Certain quantities (\mathcal{K} , V , α , etc.) take on particular significance in terms of the piloting task in re-entry. Once initiated, the piloting task in re-entry is essentially that of controlling the trajectory through the attitude of the aircraft while staying within a limited h - V corridor. The pilot must be supplied with information on range, the aircraft's attitude, and the corridor (output, input, and constraints). The essential features of this control problem, the energy management problem, have already been summarized briefly using simplified equations and concepts to demonstrate the gross effects. There is considerable literature on energy management; Reference 4.3 (Unclassified) gives a good comprehensive treatment of the problem and includes many detailed results. Three primary displays are suggested in Reference 4.3: a range display showing the estimated footprint and the vehicle track on it, an h - V display with the various limits and the predicted path in h - V space, and an attitude display similar to the one presently used but with sensitivities increased where precise attitude control is required. The problem of how to measure, process, and compute the necessary quantities should not be minimized; it is an extremely difficult one. However, the problem for this study is a different one; it is the problem of computing from the equations of motion the quantities necessary to simulate the displays. It is logical to include α and ϕ in the primary display, perhaps also $\dot{\gamma}$ and \mathcal{T} . In addition to the normal aircraft instruments, there will be a need for instruments associated with special problems and equipment (i. e., energy management system, propulsion system, reaction controls, life support systems, etc.). Thus a simulator will have to include not only the equations of motion for the vehicle, but also equations for computing all the displayed quantities for the subsystems and any special sensors required (e. g., ones to measure skin temperatures at critical points on the vehicle). The equations of motion developed in this report have

* An interesting possibility is suggested. By flying at escape velocity (36,000 fps) in inverted flight, a normal one-g environment would be achieved for personnel in the airplane.

been derived with these facts in mind. Especially, the axis systems and variables used or solved for in the equations were selected to provide the required data as expeditiously as possible.

4.3 GENERAL AERODYNAMICS FOR RE-ENTRY VEHICLE

The aerodynamic problem for a re-entry vehicle is essentially that of determining the aerodynamic forces and moments acting on the vehicle as a function of the parameters (flight condition, attitude, and shape) that affect these forces and moments. It is not possible to give explicit functions for the force and moments except for a particular vehicle. However, functional forms can be given, and to this intent we start with some definitions and assumptions. We assign an axis system (X, Y, Z) with specified origin, and then write the forces and moments in terms of the air density, velocity, and the vehicle's wing area, span, and chord.

$$[F] = \frac{1}{2} \rho V_a^2 S [C_F] + [F_T]; [M] = \frac{1}{2} \rho V_a^2 S [L] [C_M] + [M_T] \quad (4.12)$$

where $[C_F] = \begin{bmatrix} C_x \\ C_y \\ C_z \end{bmatrix}$, $[C_M] = \begin{bmatrix} C_{Ll} \\ C_{Ml} \\ C_{Nl} \end{bmatrix}$, $[L] = \begin{bmatrix} b & 0 & 0 \\ 0 & c & 0 \\ 0 & 0 & b \end{bmatrix}$

F_T and M_T are reaction forces and moments due to thrust and reaction controls which are not conveniently expressed in coefficient form. The forces and moments can be sub-divided into certain groups with which certain parameters can be associated. Without loss of generality, we may write the forces and moments in differential form:

$$[d C_F] = \begin{bmatrix} C_{xM} & C_{xR_0} \\ C_{yM} & C_{yR_0} \\ C_{zM} & C_{zR_0} \end{bmatrix} \begin{bmatrix} dM \\ dR_0 \end{bmatrix} + \begin{bmatrix} C_{x\beta} & C_{x\dot{\beta}} \\ C_{y\beta} & C_{y\dot{\beta}} \\ C_{z\beta} & C_{z\dot{\beta}} \end{bmatrix} \begin{bmatrix} d\beta \\ d\dot{\beta} \end{bmatrix} + \begin{bmatrix} C_{x\delta_0} & C_{x\delta_a} & C_{x\delta_r} \\ C_{y\delta_0} & C_{y\delta_a} & C_{y\delta_r} \\ C_{z\delta_0} & C_{z\delta_a} & C_{z\delta_r} \end{bmatrix} \begin{bmatrix} d\delta_0 \\ d\delta_a \\ d\delta_r \end{bmatrix}$$

$$+ \frac{1}{2V_a} \begin{bmatrix} C_{x\dot{\rho}} & C_{x\dot{\gamma}} & C_{x\dot{r}} \\ C_{y\dot{\rho}} & C_{y\dot{\gamma}} & C_{y\dot{r}} \\ C_{z\dot{\rho}} & C_{z\dot{\gamma}} & C_{z\dot{r}} \end{bmatrix} \begin{bmatrix} b & 0 & 0 \\ 0 & c & 0 \\ 0 & 0 & b \end{bmatrix} \begin{bmatrix} d\dot{\rho}_a \\ d\dot{\gamma}_a \\ d\dot{r}_a \end{bmatrix}$$

$$+ \frac{1}{2V_a} \begin{bmatrix} C_{x\dot{\delta}} & C_{x\dot{\beta}} & C_{x\dot{\delta}_0} \\ C_{y\dot{\delta}} & C_{y\dot{\beta}} & C_{y\dot{\delta}_0} \\ C_{z\dot{\delta}} & C_{z\dot{\beta}} & C_{z\dot{\delta}_0} \end{bmatrix} \begin{bmatrix} c & 0 & \dots \\ 0 & b & \dots \\ 0 & 0 & \dots \end{bmatrix} \begin{bmatrix} d\dot{\delta} \\ d\dot{\beta} \\ d\dot{\delta}_0 \\ \vdots \end{bmatrix}$$

$$+ \frac{1}{2V_a} \begin{bmatrix} C_{x\delta_{Li}} & \dots & \dots \\ \dots & C_{y\delta_{Li}} & \dots \\ \dots & \dots & C_{z\delta_{Li}} \end{bmatrix} \begin{bmatrix} d\delta_{Li} \\ \vdots \\ d\delta_{Si} \\ \vdots \end{bmatrix} + \begin{bmatrix} C_{x\epsilon} \\ C_{y\epsilon} \\ C_{z\epsilon} \end{bmatrix} dt$$

$$[C_F] = \begin{bmatrix} C_x(M) \\ 0 \\ C_z(M) \end{bmatrix} + \begin{bmatrix} \Delta C_x(\alpha, M) \\ 0 \\ \Delta C_z(\alpha, M) \end{bmatrix} + \begin{bmatrix} 0 \\ C_{y\beta}(\alpha, M) \\ 0 \end{bmatrix} \beta + \begin{bmatrix} \Delta C_x(s_\theta, \alpha, M) \\ 0 \\ \Delta C_z(s_\theta, \alpha, M) \end{bmatrix} \quad (4.16)$$

$$\begin{aligned} [C_M] &= \begin{bmatrix} 0 \\ C_m(M) \\ 0 \end{bmatrix} + \begin{bmatrix} 0 \\ \Delta C_m(\alpha, M) \\ 0 \end{bmatrix} + \begin{bmatrix} C_{L\beta}(\alpha, M) \\ 0 \\ C_{m\beta}(\alpha, M) \end{bmatrix} \beta \\ &+ \begin{bmatrix} 0 \\ \Delta C_m(s_\theta, \alpha, M) \\ 0 \end{bmatrix} + \begin{bmatrix} C_{Ls_\theta}(\alpha, M) & C_{Ls_r}(\alpha, M) \\ C_{ms_\theta}(\alpha, M) & C_{ms_r}(\alpha, M) \end{bmatrix} \begin{bmatrix} s_\theta \\ s_r \end{bmatrix} \\ &+ \frac{1}{2V_a} \begin{bmatrix} C_{Lp}(\alpha, M) & 0 & C_{Lr}(\alpha, M) \\ C_{mp}(\alpha, M) & C_{m\dot{q}}(\alpha, M) & C_{mr}(\alpha, M) \end{bmatrix} \begin{bmatrix} p \\ q \\ r \end{bmatrix} \\ &+ \frac{1}{2V_a} \begin{bmatrix} 0 & C_{L\dot{\beta}}(\alpha, M) \\ C_{m\dot{\beta}}(\alpha, M) & C_{m\dot{\beta}}(\alpha, M) \end{bmatrix} \begin{bmatrix} \dot{\beta} \\ \dot{\beta} \end{bmatrix} \quad (4.17) \end{aligned}$$

Equations 4.16 and 4.17 include the terms that will normally be encountered; additional terms which may be needed in special cases are discussed below. The notation implies incrementals (in theory resulting from each successive integration in Equation 4.14). For non-linear terms, the increment is attributed to the first variable that it is said to be a function of [e.g., $\Delta C_m(\alpha, M)$ is the increment in C_m due to α with $\beta, s_\theta, s_a, s_r$, etc. all zero, and it is a function of M and non-linear in α]. For linear terms the increment is attributed to the variable with respect to which the partial differentiation is taken. Aeroelasticity may be accounted for in the derivatives (quasi-static effects). Control interaction between ailerons and elevator (common for delta wings) is included. If configuration changes (e.g., flaps and gear) have significant effects, appropriate terms must be added. For large sideslip angles or aileron deflections, pitching moment increments may be required [i.e., $\Delta C_m(\beta, \alpha, M)$ and $\Delta C_m(s_\theta, s_\alpha, \alpha, M)$, respectively], and C_L and C_m may show non-linearity with β or s_θ . Except for unusual effects peculiar to a particular airplane (e.g., wing drooping at transonic speeds), Equations 4.16 and 4.17 should be adequate to cope with all significant aerodynamic data for $M < M_R$.

In the hypersonic region, $M > M_R$, the non-linear effects associated with hypersonic flow become important (References 4.8 and 4.9 describe the general characteristics). The elements of the phenomena may be shown as follows. The linearized theory for supersonic flow (given for example in Reference 4.10) gives for the pressure coefficient

$$C_p = \frac{2\theta}{\sqrt{M^2-1}} \quad (4.18)$$

where θ is the flow deflection angle from free stream (positive if the normal to the surface points upstream). The simple Newtonian expression for the hypersonic pressure coefficient is given as

$$C_p = 2 \sin^2 \delta \quad (4.19)$$

where δ is the angle the surface makes with the oncoming flow (Newtonian theory does not specify flow on the back surface - ambient or less). Consider what happens as Mach number becomes large:

$$C_{P\text{SUPERSONIC}} \rightarrow 0 \text{ AS } M \rightarrow \infty$$

$$C_{P\text{HYPERSONIC}} \text{ BECOMES VALID}$$

The same phenomena is demonstrated for the lift on a two-dimensional flat plate:

$$C_L (\text{SUPERSONIC}) = \frac{4\alpha}{\sqrt{M^2-1}} \quad (4.20)$$

$$C_L (\text{HYPERSONIC}) = C_N \cos \alpha = 2 \sin^2 \alpha \cos \alpha \quad (4.21)$$

One can see that at high Mach numbers Equation 4.21 effectively adds a correction to Equation 4.20; that is, the sum of the two terms would give the correct answer. Furthermore, for small α the sum of Equations 4.20 and 4.21 would also give the correct answer at supersonic speeds. This formulation suggests that appropriate expressions for the hypersonic forces and moments can be obtained by adding corrective terms to the expressions for the supersonic forces and moments. This, in fact, does prove to be a convenient method of handling the data; but the problem is considerably more complicated than Equations 4.18 through 4.21 indicate.

The significant factors affecting the representation of hypersonic aerodynamics may be summarized briefly as follows.

Mach Number Independence: The changes in the aerodynamic coefficients with Mach number are very small and can generally be neglected.

Viscous Effects: Reynolds numbers are low, boundary layers are large, and there is strong shock-wave boundary-layer interaction. As a result the aerodynamic coefficients and particularly the drag coefficient are dependent on altitude. The effect is demonstrated by the data in Figure 4.4.

Longitudinal Trim: The data of Figure 4.3 shows that $\alpha \rightarrow 50^\circ$ for $C_{L\text{MAX}}$. At hypersonic speeds the center of pressure is near the centroid of area, much farther aft than at subsonic speeds so that large nose-up moments will be required for trim. These may be difficult to achieve without variable geometry. The most efficient method would be to extend a nose surface; a simpler way would be to tip up the nose. Conversely, the basic configuration could be designed to trim at high angles of attack at hypersonic speeds, and then tail surfaces could be extended (perhaps folding out from vertical fins) at lower speeds to provide the needed stability. The primary effect of the geometric change would be on C_x , C_z , and C_m but other derivatives such as $C_{L\beta}$ might also be strongly affected.

Non-linearities in Statics: As evidenced by the data of Figure 4.3, it will be necessary to represent all the forces and moments as function of angle of attack. However, it is clear that any lifting surface will have strongly non-linear properties. Accordingly, the forces and moments will all have to be represented as functions of the two attitude variables α and β over the expected range of these variables.

Non-linearities in Control Effectiveness: The forces and moments due to control surface deflection will be found strongly non-linear. For example, in the

study configuration (see Figure 5.1) the elevator effectiveness is small for $-\delta_e > \alpha$ (shielded by the wing), but increases rapidly as the elevator is deflected down, $-\delta_e < \alpha$. The rolling and yawing moments due to aileron deflection (differential elevator deflection, δ_a) will be non-linear with δ_a and will depend strongly on α and δ_e and less strongly on β . The vertical tails will be ineffective at small angles of sideslip unless the rudders are deflected differentially outboard ($\delta_{r_L} > 0$; $\delta_{r_R} < 0$) in their neutral position, and it may be expected that only outboard rudder motions will be used (for a single tail, a split trailing edge, opening to a wedge at hypersonic speeds, could give the same effect). Thus the rolling and yawing moments due to rudder deflection (δ_r) will be strongly non-linear with δ_r , α , and β . What is true for the study vehicle is typical of what can be expected: control effectiveness will be non-linear, will be affected by attitude (α and β), and there will be strong interactions of the controls; furthermore the static stability of the vehicle ($C_{m_{\dot{\alpha}}}$, $C_{n_{\dot{\beta}}}$, $C_{l_{\dot{\beta}}}$) will also be a function of control surface deflections.

Rotary Derivatives: Only small values of the non-dimensional or reduced rotation rates ($p b / 2V$, $q c / 2V$, ... $\dot{\alpha} c / 2V$) will be encountered at hypersonic speeds, and aerodynamic damping will be minimal. Etkin has shown this to be true for the longitudinal short period mode (Reference 1.6), and the same can be assumed for lateral or coupled motions. Accordingly, only rough approximations for the rotary derivatives (C_{l_p} , C_{n_p} , C_{m_q} , ... $C_{m_{\dot{\alpha}}}$, etc.) will be needed. Certainly they can be linearized with respect to rotation and at most made functions of α and β (just α if β is not too large).

Heating Effects: Substantial structural deflections may be caused by aerodynamic heating, and if so, then the effect of such deformations will have to be included in the aerodynamic forces and moments. It can be surmised that only the moments due to such deformations will be significant. It may not be sufficient to consider equilibrium or steady state conditions, more likely, it will be necessary to include degrees of freedom associated with heating. The significance of deformations due to heating will depend on the particular configuration; but, in general, if such deformations are significant it will be necessary to compute transient temperatures, then the deformations, and finally the corresponding aerodynamic moments.

From the foregoing discussion of the various factors affecting the representation of hypersonic aerodynamics, it is clear that most of the problems are intimately associated with the specific vehicle configuration employed. However, one can formulate the likely functional dependencies by making certain assumptions, and thus indicate the problems which are likely to be encountered. With the study configuration in mind (shown in Figure 5.1), the following assumptions are made to arrive at an aerodynamic representation for hypersonic flight.

1. Mach number independence
2. Viscous and dissociation effects depend on altitude alone
3. Variable nose tip-up is used to trim at high α
4. Rudders are deflected outboard (towed out) to maintain directional stability and rudder effectiveness
5. Moderate sideslip angles (β)
6. Heating is symmetric and produces only symmetric deflections of the structure (good only for small β) and these deflections can be characterized by modes.

The following notation is adopted:

- δ_N nose tip-up deflection
- δ_{RD} differential antisymmetric rudder deflection
- δ_{α_i} deflection of the i^{th} mode due to heating

The aerodynamic force and moment coefficients for hypersonic speeds can now be written in functional form, where terms and functional dependencies that are likely to be of lesser significance are omitted.

$$\begin{aligned}
 [C_F] = & \begin{bmatrix} C_{x_1}(\lambda) \\ 0 \\ C_{z_1}(\lambda) \end{bmatrix} + \begin{bmatrix} \Delta C_x(\alpha, \lambda) \\ 0 \\ \Delta C_z(\alpha, \lambda) \end{bmatrix} + \begin{bmatrix} \Delta C_x(\beta, \alpha) \\ \Delta C_y(\beta, \alpha) \\ \Delta C_z(\beta, \alpha) \end{bmatrix} + \begin{bmatrix} \Delta C_x(\delta_\alpha, \alpha) \\ 0 \\ \Delta C_z(\delta_\alpha, \alpha) \end{bmatrix} \\
 & + \begin{bmatrix} 0 \\ \Delta C_y(\delta_N, \alpha, \beta) \\ 0 \end{bmatrix} + \begin{bmatrix} \Delta C_x(\delta_N, \alpha) \\ 0 \\ \Delta C_z(\delta_N, \alpha) \end{bmatrix} + \begin{bmatrix} \Delta C_x(\delta_{RD}, \alpha) \\ \Delta C_y(\delta_{RD}, \delta_N, \beta, \alpha) \\ \Delta C_z(\delta_{RD}, \alpha) \end{bmatrix}
 \end{aligned}
 \tag{4.22}$$

$$\begin{aligned}
 [C_m] = & \begin{bmatrix} 0 \\ C_{m_1}(\lambda) \\ 0 \end{bmatrix} + \begin{bmatrix} 0 \\ \Delta C_m(\alpha, \lambda) \\ 0 \end{bmatrix} + \begin{bmatrix} \Delta C_L(\beta, \alpha) \\ \Delta C_m(\beta, \alpha) \\ \Delta C_n(\beta, \alpha) \end{bmatrix} + \begin{bmatrix} 0 \\ \Delta C_m(\delta_\alpha, \alpha, \lambda) \\ 0 \end{bmatrix} \\
 & + \begin{bmatrix} \Delta C_L(\delta_\alpha, \delta_\alpha, \alpha) \\ \Delta C_m(\delta_\alpha, \delta_\alpha, \alpha) \\ \Delta C_n(\delta_\alpha, \delta_\alpha, \alpha) \end{bmatrix} + \begin{bmatrix} \Delta C_L(\delta_N, \beta, \alpha) \\ 0 \\ \Delta C_n(\delta_N, \beta, \alpha) \end{bmatrix} + \begin{bmatrix} \Delta C_L(\delta_N, \beta, \alpha) \\ \Delta C_m(\delta_N, \beta, \alpha) \\ \Delta C_n(\delta_N, \beta, \alpha) \end{bmatrix} \\
 & + \begin{bmatrix} \Delta C_L(\delta_{RD}, \delta_N, \beta, \alpha) \\ \Delta C_m(\delta_{RD}, \beta, \alpha) \\ \Delta C_n(\delta_{RD}, \delta_N, \beta, \alpha) \end{bmatrix} + \begin{bmatrix} \Delta C_L(\delta_{\alpha_i}, \beta, \alpha) \\ \Delta C_m(\delta_{\alpha_i}, \delta_\alpha, \alpha) \\ \Delta C_n(\delta_{\alpha_i}, \beta, \alpha) \end{bmatrix} \\
 & + \frac{1}{2V_\infty} \begin{bmatrix} C_{L_p}(\alpha) & 0 & C_{L_r}(\alpha) \\ 0 & C_{m_q}(\alpha) & 0 \\ C_{n_p}(\alpha) & 0 & C_{n_r}(\alpha) \end{bmatrix} [L] \begin{bmatrix} p_\alpha \\ q_\alpha \\ r_\alpha \end{bmatrix}
 \end{aligned}
 \tag{4.23}$$

Again, the notation is such that the first variable in the incremental term is the one to which the effect is attributed [i.e., $\Delta C_L(\delta_N, \beta, \alpha)$ mean the change in C_L due to δ_N , and this is non-linear with δ_N and is a function of β and α]. It should be noted that the conventional derivatives may have contributions from many sources. For example, it is implied that $C_{n_p} = \partial C_n / \partial p$ will be affected by β , α , δ_α , δ_N , δ_{RD} , δ_N , and δ_{RD} . The representation will require, in some cases, generating functions of four variables. The δ_{α_i}

must come from equations determined by a detailed analysis of the aero-thermo-elastic properties of the vehicle.

Having developed one general formulation for the aerodynamic forces at subsonic, transonic, and supersonic speeds and a second general formulation for hypersonic speeds, we may well ask how does one combine the two? The supersonic derivatives, which are needed only for moderate angle of attack, should be asymptotic to the hypersonic values at some low altitude, say between 150,000 and 200,000 feet where the Reynolds number is still large. Thus, the supersonic values can be used as the basis for hypersonic forces and moments, and the additional effects associated with hypersonic flight can be added to the supersonic formulation for $M > M_{\infty}$ (it is presumed that $M > M_{\infty}$ at altitudes above 200,000 feet where h begins to have an effect). Where such a scheme is not possible because of peculiarities in the flight profile, it may be necessary to make the formulation continuous with Mach number for all M . This is discussed in further detail in Section 4.4.

4.4 METHODS OF HANDLING AERODYNAMIC DATA

In this section the actual methods for handling the aerodynamic data relative to the functional dependencies are discussed, and equations and numerical data are presented from which some appreciation of the magnitudes of the various effects can be obtained. Then the data required for various types of simulation are discussed. In particular, three types of simulation are considered in which the requirements are formulated by the task being simulated: trajectory control, attitude control, complete simulation.

4.4.1 Aerodynamic Data

As pointed out in Section 4.3, the aerodynamic data for flight at subsonic, transonic, and low supersonic speeds is essentially linear and depends principally on M and α . As velocity increases to hypersonic speeds, non-linearity predominates and the stability derivative concept is no longer valid. However, for very small disturbances (in α , β , δ_e , etc.) the aerodynamic characteristics at hypersonic speeds are similar to those for lower speeds, and the values of the supersonic stability derivatives approach the hypersonic values in somewhat of an asymptotic fashion. The Vetter scale (after Hans Vetter of Douglas Aircraft who originated it) provides a very useful way of plotting the data so that the pertinent aspects of the various flow regimes are put in proper perspective. The Vetter scale is given by the following formula:

$$\begin{aligned} \chi &= M \quad \text{for } 0 < M < 1 \\ \chi &= 2 - \frac{1}{M} \quad \text{for } 1 < M < \infty \end{aligned}$$

where χ is the abscissa. The Vetter scale compresses the whole Mach number range into a finite scale, and its utility becomes apparent when one considers the following characteristics.

Prandtl-Glauert Rule:

$$\frac{C_{L\alpha}}{(C_{L\alpha})_{M=0}} = \frac{1}{\sqrt{1-M^2}} \approx 1 + \frac{1}{2} M^2 \quad (\text{for } M < 1) \quad (4.24)$$

Linearized Two-Dimensional Supersonic Wing Theory:

$$\frac{C_{L\alpha}}{(C_{L\alpha})_{M=\sqrt{\lambda}}} = \frac{1}{\sqrt{M^2-1}} \approx \frac{1}{M} \left[1 + \frac{1}{2} \left(\frac{1}{M} \right)^2 \right] \quad (\text{for } M > 1) \quad (4.25)$$

Data for the normal force as a function of M , α , and β are shown in Figure 4.4 for a typical hypersonic glider and serve to illustrate most of the problems that are encountered. Part a shows that the Vetter plot of $-C_{z\alpha}$ is a nicely behaved function. Part b shows the effect of α and $-C_{z\alpha}$. The presence of hypersonic effects is dependent on α ; for large α , hypersonic type flow occurs at lower M than for small α (the familiar effect of shape on the existence of hypersonic flow). In fact, the behavior of the forces on a wing in stalled flight at subsonic speeds is somewhat like the behavior at hypersonic speeds. Part c shows the interaction of viscous effects and shock effects (including dissociation) which causes the forces to be altitude-dependent. Though the data shown in Figure 4.4 characterizes the behavior of $C_{z\alpha}$ in symmetrical flight, it also characterizes the behavior of most of the other small disturbance derivatives (e.g., $C_{m\alpha}$, $C_{n\alpha}$, $C_{l\beta}$) since they are either closely related to $C_{z\alpha}$ (e.g., $C_{l\beta}$ is proportional to $C_{z\alpha}$) or are an analogous derivative (e.g., $C_{y\beta}$ is the analogous lateral derivative).

To further characterize the behavior of the hypersonic forces and moments, we examine the normal force on a flat plate and a cone. For the flat plate, the normal force is given by

$$C_N = 2 \left(\frac{V_N}{V} \right)^2 \tag{4.26}$$

where V_N is the normal component of velocity. In terms of C_z as a function of α and β , Equation 4.26 becomes

$$-C_z = 2 \left(\frac{w}{V} \right) \left| \frac{w}{V} \right| = 2 \sin \alpha \cos \beta \left| \sin \alpha \cos \beta \right| \tag{4.27}$$

For a cone with half-cone angle δ_v , the normal force (with base area as reference area) is given for $\alpha < \delta_v$ as

$$C_N = \cos^2 \delta_v \sin 2\alpha \tag{4.28}$$

Then C_y and C_z are found from Equation 4.28 to be

$$-C_z = 2 \cos^2 \delta_v \left(\frac{u}{V} \right) \left(\frac{w}{V} \right) = 2 \cos^2 \delta_v \sin \alpha \cos \alpha \cos^2 \beta \tag{4.29}$$

$$C_y = 2 \cos^2 \delta_v \left(\frac{u}{V} \right) \left(\frac{v}{V} \right) = 2 \cos^2 \delta_v \sin \beta \cos \beta \cos \alpha \tag{4.30}$$

For small disturbances about $\alpha = \beta = 0$, the force derivatives are as follows:

Flat Plate:

$$-C_{z\alpha} = 0 \tag{4.31}$$

Cone:

$$-C_{z\alpha} = 2 \cos^2 \delta_v \tag{4.32}$$

$$C_{y\beta} = 2 \cos^2 \delta_v \tag{4.33}$$

Equations 4.26 through 4.33 demonstrate several interesting properties. Whereas at $\alpha = 0$ a flat plate will have $C_{L\alpha} = 0$, a slender body will have a

finite $C_{L\alpha}$. Furthermore, it is shown in Reference 4.8 (Chapter 3, page 82) that Equations 4.32 and 4.33 agree with the exact gas dynamic solutions for cone lift at small angles of attack. These results hold for $5^\circ < \delta_v < 30^\circ$ and $2 < M < 20$ (presumably also for $M > 20$). Thus, the supersonic small disturbance derivatives are shown to be asymptotic to the hypersonic values for both a cone and a flat plate. The gross behavior of wings and bodies for large α and β described by Equations 4.26 through 4.30; it is clear that the direction cosines u/V , v/V , and w/V are more natural coordinates than α and β for describing the forces and moments.

It is instructive to look at flap effectiveness from the Newtonian viewpoint. For a flat plate with a flap, the normal force on the flap is given as

$$\left. \begin{aligned} C_N' &= 2 \sin^2(\alpha + \delta), \text{ for } \delta > -\alpha \\ C_N' &= 0, \text{ for } \delta < -\alpha \end{aligned} \right\} \quad (4.34)$$

Equation 4.34 expresses the effect of wing shielding of the flap. The total normal force on the flat plate, where S_f is the flap area, is given by

$$\left. \begin{aligned} C_N &= 2 \sin^2 \alpha \left(\frac{S - S_f}{S} \right) + 2 \sin^2(\alpha + \delta) \cos \delta \frac{S_f}{S}, \text{ for } \delta > -\alpha \\ C_N &= 2 \sin^2 \alpha \left(\frac{S - S_f}{S} \right), \text{ for } \delta < -\alpha \end{aligned} \right\} \quad (4.35)$$

Equation 4.35 shows that both the lift curve slope and flap effectiveness are affected by flap deflection. The results can be extended readily (in the same manner as for previous equations) to determine control surface derivatives, and particularly to show the necessity for antisymmetric rudder deflection ($\delta_{R\delta}$) if a stable $C_{N\beta}$ is to be obtained.

4.4.2 Various Applications

In a flight simulator the objectives govern the degree of sophistication required in the aerodynamic representation. If only energy management is of interest - not the attitude control problem - then adequate simulation may be achieved by just representing C_L and C_D (or C_x and C_z) as a function of α , M and h . Some nominal transfer function could be used between the pilot's control sticks and α . If C_L and C_D are to correspond correctly with α , then the effect of trim should be included.

If only the attitude control problem is being simulated, two possible simulation techniques are suggested: one with constant speed and altitude (fixed flight condition), the other with a time programmed speed and altitude. In either event the forces and moments would have to be computed as functions of the attitude and control deflection (α , β , p , q , r , δ_e , δ_a , δ_r , etc.); but, in the first case no change in flight condition would be called for, in the second case the only additional variable would be t (i.e., the programmed $M(t)$, $\rho(t)$, $h(t)$, etc. could be used to eliminate any explicit dependence of the forces and moments on flight condition).

If complete simulation of both the attitude and trajectory control problem is required, then the full aerodynamic representation will be required. However, how complicated this has to be depends to a great extent on the leeway allowed the pilot. If he is required to follow a particular schedule of V , h , and α quite

closely and hold lateral perturbations to a minimum (β , ρ , and r small), then a linear representation (about a trim α) using just stability derivatives might be adequate. On the other hand, if large perturbations are required in the simulation (the ultimate might include no restrictions on attitude at all, so that tumbling or spinning could be simulated), then the non-linearities associated with these perturbations must be represented. It may be presumed that if the pilot is flying with direct manual control (probably only an emergency condition), then large motions will occur - mostly at the higher altitudes. In this case, accurate simulation will require the full non-linear representation of the aerodynamics.

4.5 VEHICLE CONTROL

Though the control problem in re-entry and landing involves both trajectory and attitude control, our concern here is only with the latter. It has been shown in Section 4.2 that the pilot's task is essentially to control α and ϕ , both through wide ranges. We may add β to the list; but the pilot will want $\beta \cong 0$. This is essentially the same task that the pilot of a conventional aircraft performs, but with different emphasis. For one, much larger α 's will be used in re-entry; two, the n_z/α in re-entry will be much smaller. In fact, normal acceleration - which is so important an input to the pilot in conventional flight - will be almost non-existent ($n_z/\alpha \cong 0$) in the initial part of the re-entry.

The details of the actual flight control systems that will be used in re-entry aircraft are not of real concern here - they depend too much on the specific configuration and hardware involved. But the aircraft response that the flight control system must produce, if the aircraft is to have satisfactory handling qualities, is not subject to radical variation (see Reference 4.5). Since our concern is with the piloting task, we need not consider regulatory control modes (i.e., attitude hold mode, altitude hold mode, etc.) but only actual responses to pilot inputs.

Two types of control systems can be envisioned: direct manual control and control through an automatic stabilization system. Two types of control actuators are involved: aerodynamic control surfaces and reaction controls. Direct manual control needs no further discussion, except perhaps to state that its implementation is straightforward, and to restate that it will probably present a severe control task for the pilot. With automatic stabilization, it will make little difference if aerodynamic or reaction controls are used if a desirable response is produced. Differences will arise from the failure to produce such a response, perhaps due to control limits, limit cycles, unforeseen problems, etc. Thus at this stage the question becomes what is a desirable response.

From the handling qualities research (summarized in Reference 4.5) there seems to be little doubt as to the formulation of a desirable response in angle of attack. Pilots like the following transfer function.

$$\frac{\alpha}{\delta_{s_0}} = \frac{K}{\omega_n^2 + \frac{2\zeta}{\omega_n} s + 1} \tag{4.36}$$

$\zeta \cong 0.7$ $\omega_n = 0.7 \text{ cps}$

The value of K is not well established and admits to considerable variation. There is every reason to expect the above criteria to hold for re-entry.

Much less is known about lateral handling qualities - perhaps because they

are more complicated than longitudinal ones. However, the response of β and r should be well damped. Two possibilities for ϕ are suggested:

$$\frac{\phi}{\delta_{s_a}} = \frac{K}{1 + \tau_2 s} \quad (4.37)$$

and

$$\frac{\phi}{\delta_{s_a}} = \frac{K}{\frac{s^2}{\omega_n^2} + \frac{2\zeta}{\omega_n} s + 1} \quad (4.38)$$

Equation 4.37 is the conventional response expected for a lateral stick (aileron) deflection; but for re-entry Equation 4.38 has much to recommend it. Perhaps some combination will prove best.

In the computer studies performed for this report, a perfectly adaptive automatic control system was assumed - one that would produce the desired response irrespective of the aerodynamic moments. Such a control system would be capable of producing the following moment equations.

$$\begin{aligned} L &= k_{L\phi} (\phi - \phi_c) + k_{L\dot{\phi}} \dot{\phi} \\ M &= k_{m\alpha} (\alpha - \alpha_c) + k_{m\dot{\alpha}} \dot{\alpha} \\ N &= k_{n\beta} (\beta - \beta_c) + k_{n\dot{\beta}} \dot{\beta} \end{aligned} \quad (4.39)$$

Then the transfer functions for command inputs and small disturbances from straight symmetric flight would be the following

$$\begin{aligned} \frac{\alpha}{\alpha_c} &= \frac{\omega_{n\alpha}^2}{s^2 + 2\zeta_\alpha \omega_{n\alpha} s + \omega_{n\alpha}^2} \\ \frac{\beta}{\beta_c} &= \frac{\omega_{n\beta}^2}{s^2 + 2\zeta_\beta \omega_{n\beta} s + \omega_{n\beta}^2} \\ \frac{\phi}{\phi_c} &= \frac{\omega_{n\phi}^2}{s^2 + 2\zeta_\phi \omega_{n\phi} s + \omega_{n\phi}^2} \end{aligned} \quad (4.40)$$

where

$$\begin{aligned} \omega_{n\alpha}^2 &= k_{m\alpha} / I_y = m\alpha \\ \omega_{n\beta}^2 &= k_{n\beta} / I_z = n\beta \\ \omega_{n\phi}^2 &= k_{L\phi} / I_x = l\phi \end{aligned} \quad (4.41)$$

and

$$\begin{aligned} 2\zeta_\alpha \omega_{n\alpha} &= -k_{m\dot{\alpha}} / I_y + \frac{\rho S V C_{L\dot{\alpha}}}{2m} = -m\dot{\alpha} - z_\alpha \\ 2\zeta_\beta \omega_{n\beta} &= k_{n\dot{\beta}} / I_z = n\dot{\beta} \\ 2\zeta_\phi \omega_{n\phi} &= -k_{L\dot{\phi}} / I_x = -l\dot{\phi} \end{aligned} \quad (4.42)$$

Equation 4.39 was used in the computer studies and provided adequate control. No attempt was made to adapt k_{m_i} to produce a constant ξ_a ; all gains were held fixed. Inertia coupling effects were encountered in rolling maneuvers (see Figure 5.8). Very small steady state errors persisted in α , β , and ϕ due to the accelerations and angular velocities associated with earth rotation and flying a curved flight path around the earth. Also, a surprisingly large transient effect was uncovered during rolling maneuvers which was associated with earth-rotation terms in the equations for α and β (see Figure 6.1 and discussion in Section 6.3.1); unfortunately, there was insufficient time to make a thorough study of the implications of the effect.

4.6 REFERENCES

- 4.1 Eggers, Alfred J., Jr.: "The Possibility of a Safe Landing." Chapter 13, Space Technology, Howard S. Seifert Editor, John Wiley and Sons, Inc., New York, 1959.
- 4.2 Metcalf, H.: Some Consideration of Shape and Control for Hypersonic Vehicles. IAS Paper No. 59-144, October 1959.
- 4.3 General Electric Company: Flight Control Study of a Manned Re-entry Vehicle. WADD Technical Report 60-695, July 1960.
- 4.4 Eggleston, John M. and John W. Young: Trajectory Control for Vehicles Entering the Earth's Atmosphere at Small Flight-Path Angles. NASA Memorandum 1-19-59L, February 1959.
- 4.5 Breuhaus, W.O., P.A. Reynolds, and E.A. Kidd: Handling Qualities Requirements for Hyper-Velocity Aircraft. (Title Unclassified). Cornell Aeronautical Laboratory, Inc., Report No. TC-1332-F-1, September 30, 1959, Revised January 28, 1960. CONFIDENTIAL.
- 4.6 Eggers: "Performance of Long Range Hypervelocity Vehicles".
 Hansen: "Some Characteristics of the Upper Atmosphere Pertaining to Hypervelocity Flight".
 Batdorf: "Structural Problems in Hypersonic Flight".
 Lees: "Recent Developments in Hypersonic Flow".
 Stalder: "A Survey of Heat Transfer Problems Encountered by Hypersonic Aircraft".

Reference 4.6 (continued)

- Ferri, Feldman, Daskin: "The Use of Lift for Re-Entry from Satellite Trajectories".
Hypervelocity Flight Issue, Jet Propulsion, November 1957.
- 4.7 Lees, Lester, Frederic W. Hartwig and Clarence B. Cohen: "Use of Aerodynamic Lift During Entry into Earth's Atmosphere". ARS Journal, September 1959.
- 4.8 Truitt, Robert W.: Hypersonic Aerodynamics. The Ronald Press Co., New York, 1959.
- 4.9 Hayes, Wallace D. and Ronald F. Probst: Hypersonic Flow Theory. Academic Press, New York, 1959.
- 4.10 Kuethe, A.M. and J.D. Schetzer: Foundations of Aerodynamics. John Wiley and Sons, Inc., New York, 1950 Chapter 11.
- 4.11 Hoerner, Sighard F.: Fluid-Dynamic Drag. Published by Author, 1958 Chapter 18.
- 4.12 Lees, Lester: "Recovery Dynamics - Heat Transfer at Hypersonic Speeds in a Planetary Atmosphere". Chapter 12, Space Technology, Howard S. Seifert Editor, John Wiley and Sons, Inc., New York, 1959.
- 4.13 Yoler, Yusuf A.: "Dyna-Soar: A Review of the Technology." Aerospace Engineering, August 1961.

ALL CURVES COMPUTED ASSUMING NONROTATING EARTH EXCEPT FOR ONE AS MARKED

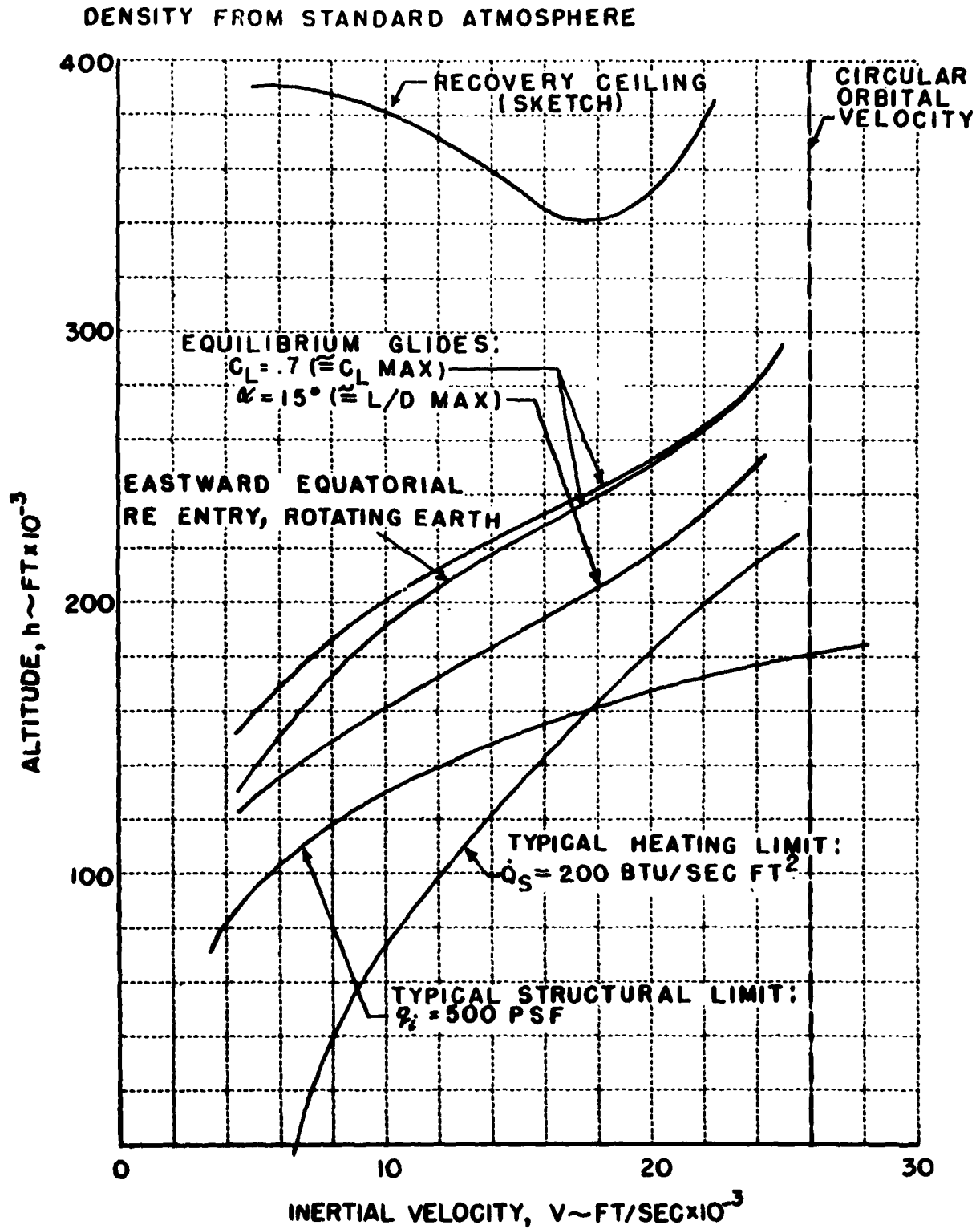


FIGURE 4.1 h - V DIAGRAM FOR THE STUDY VEHICLE

INITIAL CONDITIONS:

- $V = 24,000$ ft/sec
- $R = 300,000$ ft
- $\gamma = -1^\circ$
- $\psi = +120^\circ$
- $\lambda = 0^\circ$
- $\varphi = +30^\circ$

Projection Technique: Solutions plotted on rectangular $\lambda - \varphi$ grid - range computed using average value of 60 naut. mi/deg

— $\alpha = \text{constant } 15^\circ \cong \alpha_{L/D_{MAX}}$ for Case II and III
 - - - - - sketched

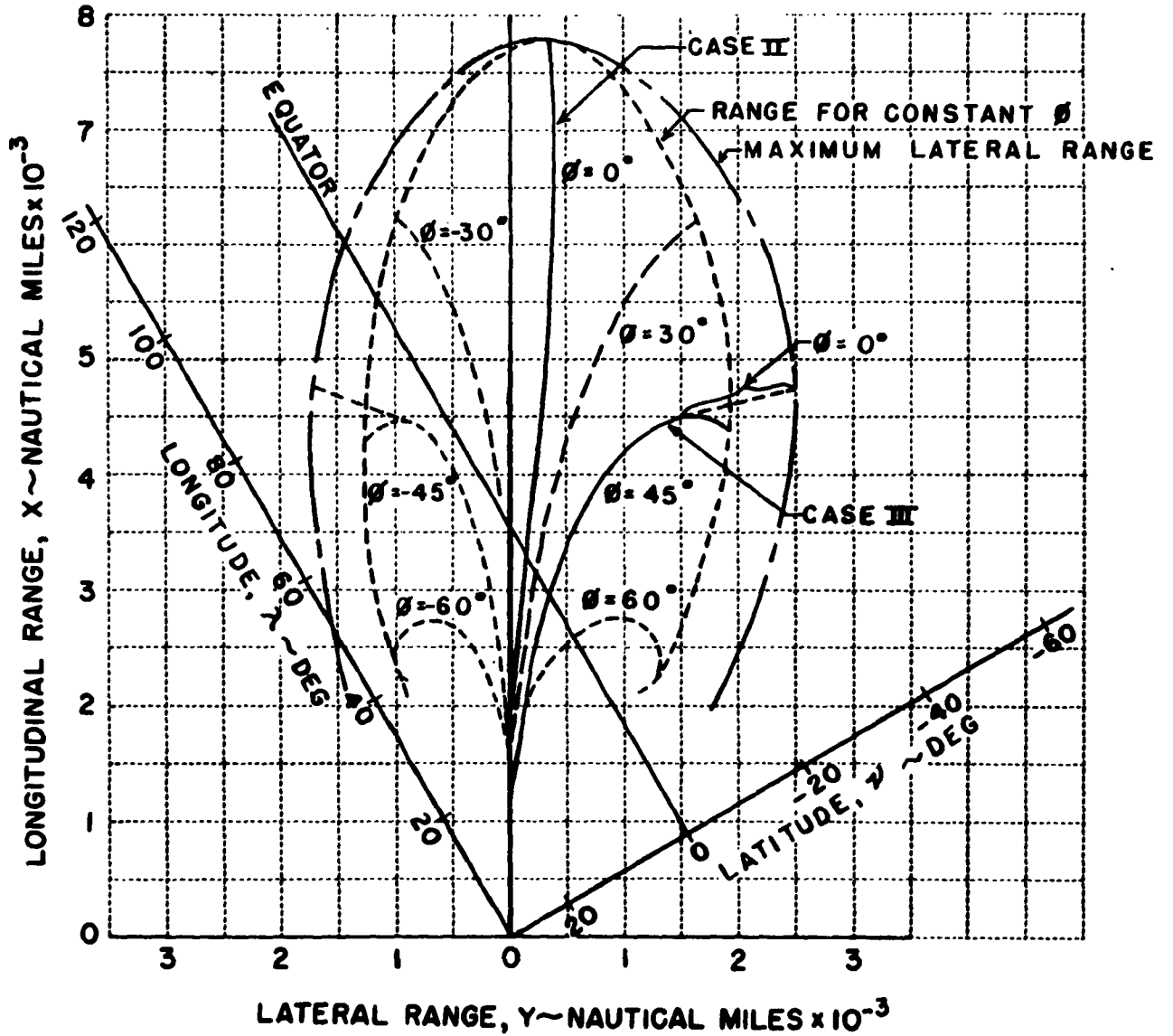


FIGURE 4.2 APPROXIMATE FOOTPRINT FOR THE STUDY VEHICLE

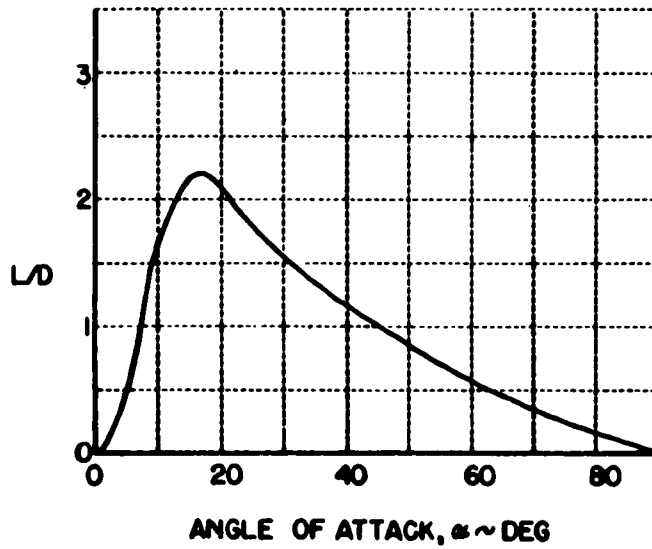
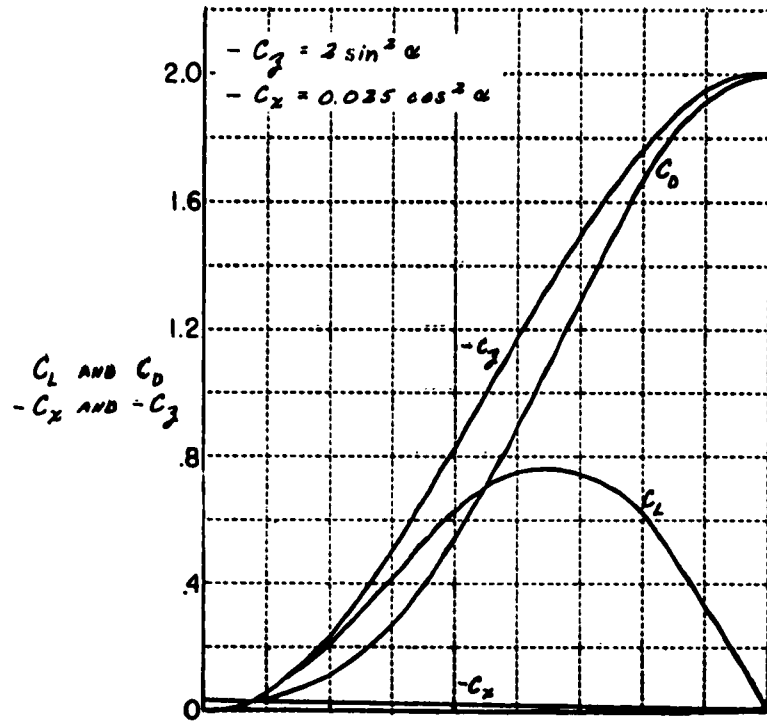


FIGURE 4.3 NEWTONIAN HYPERSONIC LIFT AND DRAG CHARACTERISTICS

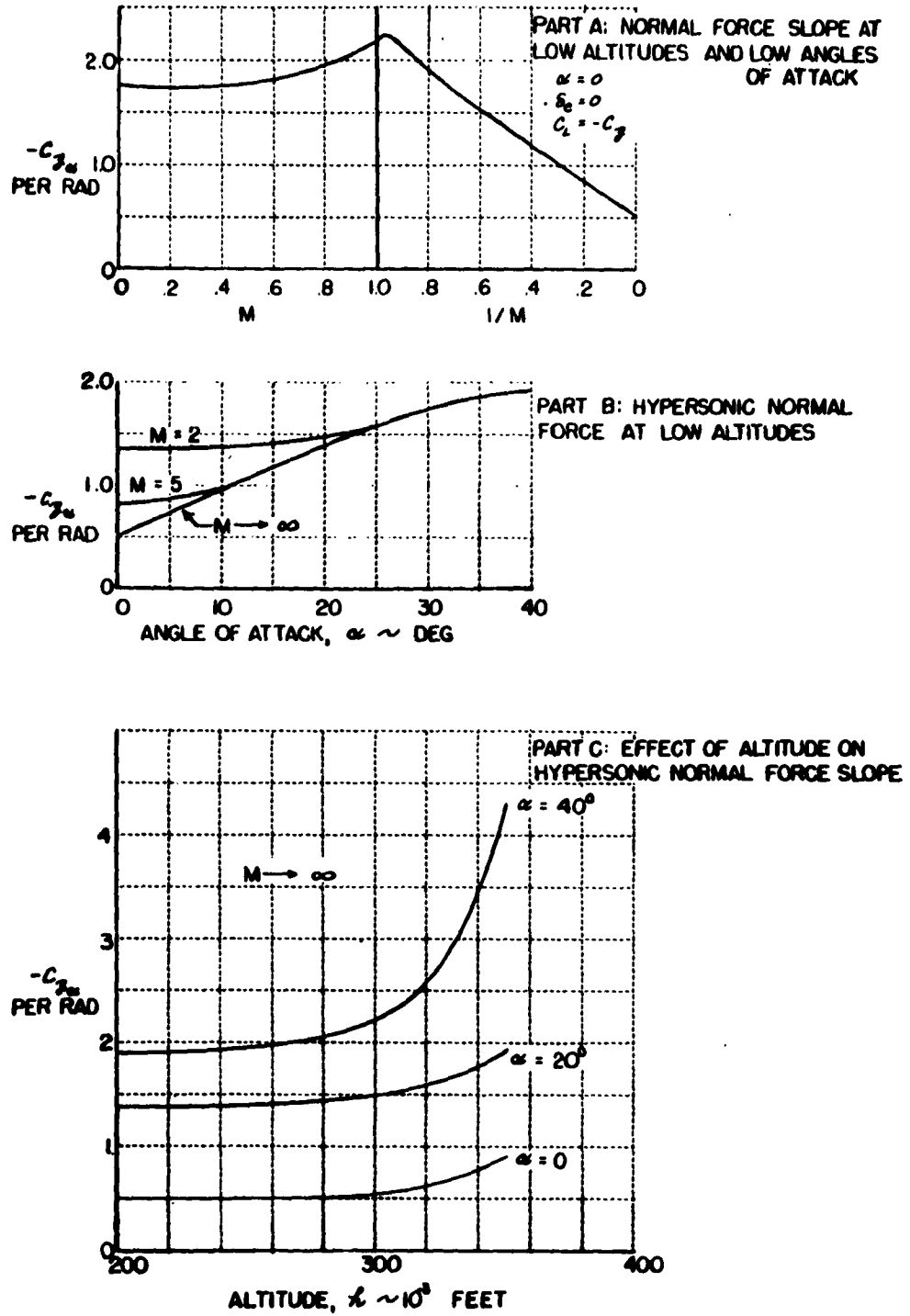


FIGURE 4.4 TYPICAL NORMAL FORCE CHARACTERISTICS FOR HYPERSONIC GLIDER

SECTION V
SOLUTIONS OF THE EQUATIONS OF MOTION

This section deals with solutions of the complete equations of motion as derived in Section III. Solutions described here represent: (1) three basic cases (Cases I, II, and III) depending upon the initial heading of the vehicle and the bank angle maintained during re-entry, and (2) solutions which represent perturbations in control input from the third basic case. Section 5.1 defines the general conditions used for solution of the equations of motion including vehicle, geophysical, aerodynamic, and control system characteristics. The solutions, themselves, including perturbations, are presented in Section 5.2. Case III involves a roll to a 45° bank angle early during the re-entry, and special attention is given to this maneuver in Section 5.3.

5.1 CONDITIONS FOR SOLUTION

The example vehicle and the specific data and equations used in computing the re-entry solution presented in this report are described below.

5.1.1 Vehicle Configuration

A typical configuration for a maneuvering re-entry glider was assumed for the study vehicle. The configuration is depicted in Figure 5.1, and the following physical characteristics were assumed for use in the equations of motion.

$$\begin{aligned} m g_0 / S &= 23.6 \text{ psf} & \frac{I_z - I_x}{I_y} &= .94 & I_{xz} &= 0 \\ \frac{I_y - I_z}{I_x} &= -.66 & \frac{I_x - I_y}{I_z} &= -.74 & & \end{aligned}$$

The principal axes, the body axes, and the reference line for measuring angle of attack, etc. are all assumed to be coincident.

5.1.2 Characteristics and Range of Solutions

Typical re-entry solutions were computed which included the following general characteristics:

- a. Flight path skewed to the equator,
- b. Skipping flight path,
- c. Turn to produce lateral range,
- d. Rapid maneuvers to produce large rotations about all three vehicle axes.

In order to appraise the validity of simplification in the equations, it is necessary to study their effect in the most general type of motion and not in a special case. Case III was just such a general solution, and provided a good medium for investigating simplifications.

The following initial conditions, typical for a near-orbital hypersonic glider starting re-entry, were common to the three basic cases.

$$\begin{aligned} h_0 &= 300,000 \text{ ft} \\ \gamma_0 &= -1^\circ \\ V_0 &= 24,000 \text{ ft/sec} \\ \alpha_0 &= 15^\circ \end{aligned}$$

The initial conditions for the three cases differed in the following characteristics.

$$\text{Case I: } \psi_0 = 0^\circ, \quad \nu_0 = 0^\circ; \quad \text{Case II and III: } \psi_0 = 120^\circ, \quad \nu = 30^\circ$$

The method of computing all the required initial variables is given in Appendix D.

The solutions were programmed so that they simulated tasks that might be asked of the pilot. This was done by commanding the control system to hold the following angle of attack (α), sideslip (β), and bank angle (ϕ) time histories.

$$\begin{array}{lll} \text{Case I and II:} & \alpha = 15^\circ, & \beta = 0^\circ, & \phi = 0^\circ \\ \text{Case III:} & \alpha = 15^\circ, & \beta = 0^\circ, & \phi = 0^\circ \text{ to } \tau = 185 \text{ sec} \\ & \alpha = 15^\circ, & \beta = 0^\circ, & \phi = 45^\circ \text{ for } \tau > 185 \text{ sec} \end{array}$$

In Case III at $\tau = 185$ sec a roll to $\phi = 45^\circ$ is commanded. This time corresponds to the bottom of the first skip, or the first occurrence of level flight in the re-entry. The roll maneuver produces large motions about all three vehicle axes (due to inertia coupling), and thus provides a good medium for studying the short-period or rapid modes of motion. The commanded angle of attack ($\alpha_c = 15^\circ$) was selected to correspond roughly to that for $(L/D)_{\max}$. Thus the three basic cases cover a wide range of re-entry tasks, and at the same time compare the effects of maneuvering, turning, skipping, and varying the flight path direction.

The solutions were terminated according to the criterion $h < 100,000$ ft. The Mach number at this point was roughly $M = 2.5$, so that the vehicle was now flying at a conventional altitude and supersonic speed. This point was also chosen as the terminating point because it is about the beginning of the landing approach.

5.1.3 Equations of Motion

The solutions appearing in this section (V) were obtained using the complete equations of motion as derived in Section III and shown in fully expanded algebraic form in Appendix A. The specific equations solved by the IBM 704 computer are all the equations listed in Appendix A, which are numbered to correspond with the same equation in matrix form in Section III. The computer program used the matrix form of the equations directly, and the following listed equations and associated scalar and matrix definitions form the complete set.

$$\begin{array}{l} \text{Equations: } 3.37 - 3.51, 3.55 - 3.57, 3.55s, 3.56s, \\ 3.59 - 3.64, 3.68 - 3.71, 3.73 - 3.81 \end{array}$$

Though it was intended to include wind and gust data in the equations, this was not actually done for lack of time. Also, the applied moments given by Equation 4.39 were inserted as $[M_\tau]$ in Equation 3.78. A three-axis flight control system was simulated, as defined by Equations 4.39, to provide vehicle path and attitude control. This flight control system, which because of the numbers used might be thought of as a combination of pilot and automatic control system, is described specifically in Section 5.1.6.

Numerical integration was performed using a fourth order Runge-Kutta method. The time interval or step size was 5 sec, except for 21 one-second steps which were used at $\tau = 185$ sec when the 45° right bank was commanded by the controller. This numerical integration method and other pertinent digital techniques are described in Appendix D.

For all but three time history solutions which were stopped at $t = 500$ sec, the digital program stopped computing on meeting the condition $h < 100,000$ ft.

5.1.4 Geophysical Characteristics

The geophysical characteristics of the earth used for solution of the equations of motion in this chapter have been described in Section 2.2 and 2.3. For convenience, however, the specific characteristics are included here also.

The earth is assumed to be spherical, to be rotating at a constant angular velocity, and to have an inverse-square gravitational field. The following constants are used:

- 1. Radius of the earth, $R_0 = 20,860,000$ ft
- 2. Angular velocity of rotation, $\omega = 0.004178$ deg/sec
- 3. Acceleration of gravity at the earth's surface, $g_0 = 32.17$ ft/sec²

The atmospheric properties used in the solutions are the density and temperature. The density is given by the equation:

$$\rho = \rho_0 e^{-\frac{h}{31,600-x}} \tag{5.1}$$

in which $x = 0$, $0 \leq h < 25,000$ ft
 $= 0.2 h - 5000$, $25,000 \text{ ft} \leq h \leq 65,000$ ft
 $= 8000$, $65,000 \text{ ft} < h$

and the sea level density is

$$\rho_0 = 0.002378 \text{ slugs/ft}^3$$

The atmospheric temperature variation with altitude is programmed as a table which is linearly interpolated by the computer:

$h \sim \text{Feet}$	$T \sim ^\circ R$
0	518.688
36,500	389.988
82,000	389.988
156,000	508.788
175,000	508.788
250,000	354.35

(5.2)

The wind velocity model was programmed, but it was not used. No gust velocity model was programmed.

5.1.5 Aerodynamic Characteristics

General aerodynamic characteristics of a re-entry vehicle are described in Section IV. It is obvious that a complete aerodynamic representation would be very complex; consequently, to facilitate solution of the equations of motion as presented in this section (V), a much simplified representation is used.

Trimmed lift and drag coefficients were used to represent the longitudinal forces. This expedient simplifies the force equations, eliminates the need for

considering elevator deflections as such, and gives good over-all values for lift and drag. Though errors result in some of the force derivatives, notably $C_{L\alpha}$ and $C_{D\alpha}$, these errors are not significant to the results of the study. The representation is given, then, in terms of x and z body axis trimmed force coefficients, C_{x_T} and C_{z_T} . Expressions for these coefficients are as follows:

$$C_{x_T} = 0.025 \quad (5.3)$$

$$C_{z_T} = -0.0325 + (0.401 + 2.063 \frac{1}{M}) \alpha + (1.166 - 2.298 \frac{1}{M}) |\alpha| \alpha \quad (5.4)$$

in which M is the Mach number, and α is the angle of attack in radians. These expressions are plotted Figure 5.2a for α in degrees. Aerodynamic forces are obtained by inserting Equation 5.3 and 5.4 in the matrix equation:

$$[F_a] = \frac{1}{2} \rho V_a^2 S [C_F] \quad (5.5)$$

in which

$$[C_F] = \begin{bmatrix} C_x \\ C_y \\ C_z \end{bmatrix} = \begin{bmatrix} C_{x_T} \\ 0 \\ C_{z_T} \end{bmatrix} \quad (5.6)$$

The aerodynamic moment coefficient matrix $[C_M]$ was set to zero, and all moments were handled through $[M_T]$ as described in the next section.

To provide a better visualization of the trimmed longitudinal aerodynamic representation, the trimmed lift and drag coefficients, C_{L_T} and C_{D_T} , and the trimmed lift-drag ratio, $(L/D)_T$, have been obtained and are plotted in Figures 5.2b and 5.2c respectively. The matrix equation

$$\begin{bmatrix} -C_{D_T} \\ 0 \\ -C_{L_T} \end{bmatrix} = [\alpha]^T \begin{bmatrix} C_{x_T} \\ 0 \\ C_{z_T} \end{bmatrix} \quad (5.7)$$

defines the transformation from body axes to wind axes when the sideslip, β , is zero.

5.1.6 Control System - Concept and Characteristics

In order to compute solutions of the equations of motion which are similar to what actual re-entry flights might be, some method for controlling vehicle attitude and path had to be devised. The normal process would have been to incorporate the complete aerodynamic characteristics for the vehicle into the equations, and then design and incorporate into the equations a flight control system for the vehicle which would control the aerodynamic surfaces (elevator, ailerons, and rudders) and reaction controls so as to provide the vehicle with a desirable response to pilot command inputs. The flight control system would have logically been an adaptive one, which would have provided a sensibly constant dynamic response throughout the re-entry. For this study, an expedient short cut was taken. A desired response in α , β , and ϕ was hypothesized, and then only the moments necessary to produce this response were applied to the vehicle. The selected control scheme, involving six feedback loops, was one that could be easily incorporated into the equations, had physically significant parameters, and simulated roughly what might be realized from a good adaptive control system.

The three-axis controller, described by Equations 4.39 - 4.42 in Section 4.5, provides several of the conventional stability derivatives, namely $C_{m\dot{\alpha}}$, $C_{m\dot{\beta}}$, $C_{n\dot{\alpha}}$, and $C_{n\dot{\beta}}$, and the derivative $C_{L\dot{\phi}}$ is similar to the conventional $C_{L\dot{\beta}}$. The $C_{L\dot{\phi}}$ derivative is not one that is inherently present, and would only be formed as an element of the flight control system. In addition to its primary function of attitude stabilization and control, the three-axis controller provides path control capability for the vehicle. Thus, the ϕ controller allows variation of the lift-drag ratio with the consequent variations of range, maximum heating rate, total heat input, deceleration, etc. The ϕ controller can be used to rotate the total lift vector about the X body axis, thus providing capability for lateral or cross range movement of the vehicle. Most solutions presented in this section (V) makes use of the ϕ controller to maintain a nearly constant 15° angle of attack corresponding roughly to $(L/D)_{max}$ for the programmed C_x and C_y . Case III solutions include a banking right turn which is accomplished by rolling the vehicle to $\phi = +45^\circ$ by commanding a step in ϕ_c , and perturbations from the basic Case III solution involve step commands in α_c , β_c , and ϕ_c .

The three-axis controller is described by the following matrix equation (from Equation 4.39):

$$\begin{bmatrix} L \\ M \\ N \end{bmatrix} = \begin{bmatrix} k_{L\phi} (\phi - \phi_c) + k_{L\dot{\phi}} \dot{\phi} \\ k_{m\alpha} (\alpha - \alpha_c) + k_{m\dot{\alpha}} \dot{\alpha} \\ k_{n\beta} (\beta - \beta_c) + k_{n\dot{\beta}} \dot{\beta} \end{bmatrix} \quad (5.8)$$

In this equation, the various k 's are gain constants; ϕ_c , α_c , and β_c are command inputs to the controller; the three variables (ϕ , α , and β) and their rates are available in the computing program. The gain constants were selected to produce desirable natural frequencies and damping ratios for the equivalent linearized equations of motion. In this study, the natural frequencies and damping ratios were made respectively equal for all three control modes.

In order to shorten computation time for the solutions, the highest frequencies present in the equations of motion (those due to the controller) were set at $\omega_n = 0.3$ rad/sec, giving a period of about 21 seconds. This allowed an integration step size or time interval of 5 seconds. The frequency, ($\omega_n = 0.3$ rad/sec) is approximately that of the longitudinal "short" period mode given by Etkin (in Reference 1.6, Figure 8) for an altitude of 250,000 ft. The controller gains were selected to give a damping ratio $\zeta = .7$. The gain constant follows.

$$\begin{aligned} k_{\phi} &= \frac{k_{L\phi}}{I_y} = -0.09, & k_{\dot{\phi}} &= \frac{k_{L\dot{\phi}}}{I_y} = -0.42 \\ k_{\alpha} &= \frac{k_{m\alpha}}{I_y} = -0.09, & k_{\dot{\alpha}} &= \frac{k_{m\dot{\alpha}}}{I_y} = -0.42 \\ k_{\beta} &= \frac{k_{n\beta}}{I_y} = +0.09, & k_{\dot{\beta}} &= \frac{k_{n\dot{\beta}}}{I_y} = +0.42 \end{aligned} \quad (5.9)$$

5.2 RE-ENTRY SOLUTIONS

The intent of this project was to develop equations of motion for use with a simulator and then to compute re-entries to check the equations, to determine the effect of small changes in flight conditions (perturbations), and to determine what mathematical or geophysical simplifications, if any, could be made in the equations of motion (simplifications). Because of unavoidable delays in checking out the computer program, the number of re-entry solutions for perturbations and simplifications was extensively

curtailed. Nevertheless, this section (V) and Section VI clearly demonstrate the capability of obtaining excellent re-entry solutions with the complete equations of motion, and the two sections (V and VI) present a number of solutions indicating effects of the more important perturbations (from the piloting task point of view) and simplifications.

Section 5.2.1 introduces the three basic cases (I, II, and III) chosen for analysis and describes perturbations made on Case III. Section 5.2.2 presents the solutions for Cases I, II, and III, and Section 5.2.3 presents the perturbations of Case III.

5.2.1 Introduction

Three basic solutions were computed during the course of this program: Case I, a re-entry in the equatorial plane, was chosen as the simplest to check and analyze and to provide a comparison with Case II, a re-entry whose initial heading is roughly along the Atlantic Missile Range. Cases I and II have identical initial conditions except for the heading angle. Case III may be compared with Case II to show the effect of a banking turn upon the re-entry trajectory. It is probably a more meaningful re-entry solution insofar as pilot and control system tasks are concerned because of the banking turn and because deceleration, heating rate and dynamic pressure are greater. In addition, Case III illustrates inertia coupling during the bank angle transient response and the lateral or cross range capability of the winged re-entry glider.

As far as initial conditions are concerned, the three basic cases are nearly identical. For all solutions, the geophysical representation of the earth, the controller parameters and the vehicle's aerodynamic representation are identical. These are described in Section 5.1. Initial angular velocity of the vehicle in inertial space is zero. Angle of attack is initially set at $+15^\circ$; the control system attempts to maintain this value throughout the re-entry except, of course, during α perturbation solutions. Large deviations from the commanded α , ϕ , and β occurred only during the roll maneuver, caused by inertia coupling. The initial sideslip is zero; therefore, the condition $\theta = \alpha + \gamma$ holds and yields an initial pitch angle of $+14^\circ$. Initial sideslip is zero; therefore, the Euler angle ψ is initially equal to the heading angle ψ_r . In every solution the initial bank or roll angle is zero. Since it makes no difference to the solutions, the initial longitude in every case is zero. These are the initial conditions which are identical in every solution.

The differences among the three basic cases are best shown in tabular form with some initial trajectory parameters—altitude, inertial velocity and flight path angle— included for completeness.

NAVTRADEVGEN 801A

RE-ENTRY CLASSIFICATION	INITIAL CONDITIONS					CONTROL INPUTS DURING RE-ENTRY
	h ft	V ft/sec	γ deg	ψ deg	ψ_T deg	
Case I "Equatorial"	300,000	24,000	-1	0	+90	$\alpha_c = +15^\circ$ $\beta_c = 0^\circ$ $\phi_c = 0^\circ$
Case II "Atlantic Missile Range"	300,000	24,000	-1	+30	+120	$\alpha_c = +15^\circ$ $\beta_c = 0^\circ$ $\phi_c = 0^\circ$
Case III "Atlantic Missile Range" with Banked Turn	300,000	24,000	-1	+30	+120	$\alpha_c = +15^\circ$ $\beta_c = 0^\circ$ For $t < 185$ sec $\phi_c = 0^\circ$ For $t \geq 185$ sec $\phi_c = +45^\circ$ (Step input in ϕ_c)

The table shows that the basic differences in the three cases are initial values of latitude and heading angle, and a banking maneuver during the solution.

Since the computer program input routine requires the initial values of those twelve variables whose rates are integrated during solution ($u, v, w; p, q, r; \dot{\psi}, \dot{\theta}, \dot{\phi}; \dot{\lambda}, \dot{\nu}, \dot{\lambda}$), specifying parameters such as $V, \gamma, \psi_T, \alpha$, etc. is not sufficient. Appendix D shows a sample calculation for the required values of the computer variables for Case III. In the general case, the computation of initial conditions is not so easy as shown for Case III, a case which had no initial angular rates, bank angle or sideslip.

A re-entry trajectory is fraught with limits pertaining to maximum heat input, maximum heating rate, maximum dynamic pressure, maximum decelerations, maximum lift, etc. These limits define a re-entry corridor which is usually narrow; therefore, it is of interest to present trajectory solutions in a form which can be related to the re-entry corridor. To this end, the data is presented in graphical and tabular forms; each is necessary to illustrate certain aspects of the re-entry solutions. Especially important from the re-entry corridor point of view are the altitude (h) versus relative velocity (V_E) plots. In general, the re-entry solutions presented here stay within reasonable limits for a gliding re-entry vehicle. This is not surprising since the vehicle has a high lift-drag ratio (≈ 2.4), the initial inertial velocity (24,000 ft/sec) is lower than the circular orbital velocity (25,721 ft/sec at the same altitude with the same sea level gravity), and the initial flight path angle is small (-1°).

Small changes in the commanded attitude provide perturbations of the basic trajectory, Case III. These solutions are designed to show how carefully a given attitude must be held to result in desired range, cross or lateral range, heat input, deceleration, etc. The results are presented in tabular form; however, where the perturbations produce significant differences in certain variables, a graphical presentation is also used.

5.2.2 Presentation and Comparison of Three Basic Cases

The major trajectory parameters for the three basic solutions are presented as follows:

Case I	Figure 5.3
Case II	Figure 5.4
Case III	Figure 5.5

Each figure presents time histories of altitude h , relative velocity V_r , and flight path angle γ , and a plot of vehicle altitude versus its relative velocity. Since the coordinates of the h and V_r plot are closely associated with potential and kinetic energy respectively, this plot is useful from the energy management point of view. In fact, altitude versus relative velocity would be a desirable display for the pilot of a re-entry vehicle especially if the instrument had a re-entry corridor overlay. The important Case III presented in Figure 5.5 also includes a map-like plot of latitude (ψ) versus longitude (λ) which is the vehicle's track over the surface of the earth during re-entry.

Comparison of the three basic cases is made using Figure 5.6 and Table 5.1. The figure contains the same data as in Figures 5.3 through 5.5, but each plot contains three curves, one for each case. The table presents trajectory data for three distinct conditions during the re-entry:

1. The bottom of the first skip; that is, the first point on the altitude versus time plot at which altitude reaches a minimum point.
2. The "top" of the first skip; that is, the first point at which altitude reaches a maximum.
3. The point at which the vehicle reaches an altitude of 100,000 ft. This is the condition for stopping the particular solutions.

None of these conditions is met exactly because of the discrete-time nature of the solutions, a five second time interval being used for numerical integration. Certain key variables are tabulated which show the variation from the exact desired conditions. For conditions (1) and (2) above, the flight path angle γ is the tabulated key variable. Whenever altitude is at a maximum or minimum, the flight path angle should be exactly zero. Similarly, altitude is the tabulated key variable for condition (3) for which h should be always exactly 100,000 ft. In view of these considerations, perfect comparisons using the tabulated data cannot be made; however, as the indicators (h and γ) show, the conditions are met closely enough so that valid comparisons can be made.

The values of range and stagnation-point heat-transfer rate tabulated in Table 5.1 were hand calculated using computer print-out results. Range, in nautical miles, was calculated from the initial and final values of latitude and longitude using the equation

$$RANGE = R_0 \cos^{-1} [\sin \psi_i \sin \psi_f + \cos \psi_i \cos \psi_f \cos (\lambda_f - \lambda_i)] \quad (5.10)$$

where R_0 is in nautical miles. Care must be exercised in evaluating the arc-cosine. The stagnation point heat transfer rate was calculated using the equation

$$\dot{Q} = 22 \times 10^{-9} \sqrt{\frac{\rho}{R}} V_a^3 \frac{BTU/ft^2}{sec} \quad (5.11)$$

in which ρ and V_a are expressed in slugs/ft³ and ft/sec respectively. R is the nose radius of the body in ft, and $R = .5$ ft was assumed for the nose of the study vehicle.

5.2.3 Perturbations - Case III

Table 5.2 presents the results of introducing small attitude perturbations in Case III at 185 seconds* of the time history. These perturbations in the attitude command were held throughout the rest of the solution. To focus attention upon the linearity (or non-linearity, as the case may be) of the perturbational effects on trajectory parameters, the changes in the parameters rather than the parameters themselves are tabulated in Table 5.2. Since the commanded changes in α , β , and ϕ were small ($\pm 1^\circ$ from conditions of Case III), the differences in the trajectory are generally too small to be presented in time history plots. This is another reason for presenting tabulated differences between the perturbation solution and the basic Case III.

The perturbation solutions are six in number: three, those with increased α , β , and ϕ , were stopped when the altitude became 100,000 ft; and three, those with decreased α , β , and ϕ , were stopped after 500 seconds of the time history had elapsed. Inadvertently, the latter three solutions were obtained as perturbations of Simplification Solution III-S1 (III-S1 is described in detail in Section VI). Since this simplification solution closely approximates the complete solution, it is possible to consider all six perturbation solutions as perturbations of the basic Case III. Nevertheless, in Table 5.2 the differences listed for Solutions III-P4, III-P5, and III-P6 were obtained by using Solution III-S1. This is a third reason for presenting tabular differences.

One result has been presented graphically in Figure 5.7; it is an altitude time history comparison of Solutions III, III-P1, and III-P4. This figure shows the angle of attack perturbations for the first 700 seconds of time history. The $\alpha = 14^\circ$ case (Solution III-P4) ends at 500 seconds, the program stop for that solution.

So far as conditions at solution termination are concerned, the ϕ and β perturbations have a larger effect than the α perturbation. This is probably because near α for $(L/D)_{max}$, small changes in α have no effect on L/D. Table 5.2 contains data which compares the perturbation solutions III-P1, III-P2, and III-P3 with III when $h \approx 100,000$ ft, at which condition the small attitude perturbations have had sufficient time to produce noticeable changes in the trajectory.

A principal reason for computing the perturbation solutions was to obtain a measure of the trajectory controllability, and hence to provide a yardstick for measuring the significance of errors introduced by simplifications in the equations of motion.

* The same time that the banking turn is introduced during each solution.

5.3 ROLL MANEUVER AND TURN DURING RE-ENTRY

5.3.1 Introduction

The turn in the Case III solutions is important in this study because it allows evaluation of the maneuverability of the vehicle. The roll entry into the turn is especially important because, due to inertia coupling, dynamic responses in all three of the attitude modes of motion are excited, and this represents a very general type of short-period response.

5.3.2 Case III - The Turning Re-Entry

Trajectory parameters of the basic Case III solution are presented in Figure 5.5 and Table 5.1 in sufficient detail that discussion here can be brief. Figure 5.6 provides a graphical comparison of Cases II and III which differ only in the commanded bank angle. The one quantity of interest that is not numerically specified in Figure 5.6 is the lateral or cross range achieved by the turn of Case III with respect to the straight-in solution of Case II. Roughly, the cross range achieved is 1600 nautical miles, certainly a significant capability. This information was obtained from the map-like Figure 5.6c which compares the latitude versus longitude plots for the three basic cases.

It is readily apparent that cross range obtained by rotation of the lift vector is costly from other points of view. The effective (vertical) lift-drag ratio is considerably smaller by some 30% for the 45° bank angle, resulting in increased deceleration, heating rate, and dynamic pressure; for as Figure 5.6b shows, at any given altitude (consequently, air density) after the roll angle input, the turning re-entry of Case III has a greater relative velocity than Case II.

The roll input command ($\phi_c = +45^\circ$) at $t = 185$ seconds produces a dynamic response of the vehicle in roll which is governed essentially by the ϕ and $\dot{\phi}$ derivatives of the three-axis controller described in Section 5.1.6. Equally significant is the transient in α and β caused by inertia coupling. Figure 5.8 presents time histories of α , β , and ϕ for the period of time which includes the response transient.

5.3.3 Perturbations

From the piloting-task point of view, the perturbations of Case III, presented in Table 5.2, shed some light on the care with which the vehicle's altitude must be controlled to produce a desired trajectory. Suppose that a given angle of attack must be held to achieve a desired cross range. Does a one degree change in a specific attitude angle seriously affect energy management? Will the pilot's instruments have to be accurate enough to indicate an angle within a few tenths of a degree or will less precise instruments suffice? How much steady-state error can be tolerated in an attitude control system before the system ceases to be adequate? A rough answer to such questions can be made based on the perturbation solutions.

NAVTRADEVGEN 801A

CONDITION	VARIABLE	I	II	III
		Equatorial Re-Entry	Atlantic Missile Range Re-Entry	Turning Re-Entry
First Minimum Altitude Point, "Bottom" of First Skip	h ft	206,677	207,337	207,337
	V_E ft/sec	22,082	22,385	22,385
	γ deg	-0.0034	+0.0597	+0.0597
	t sec	185	185	185
	\dot{Q} $\frac{\text{BTU}}{\text{ft}^2 \text{ sec}}$	228	240	240
	q_i^* lb/ft ²	91.2	91.1	91.1
First Maximum Altitude Point, "Top" of First Skip	h ft	276,236	276,312	252,278
	V_E ft/sec	21,442	21,442	21,635
	γ deg	+0.0046	-0.0213	+0.0083
	t sec	390	390	366
	q_i^* lb/ft ²	4.5	4.5	12.7
End of Solution $h \approx 100,000$ ft	h ft	100,184	100,148	100,032
	V_E ft/sec	2,033	2,005	2,464
	γ deg	-3.86	-3.65	-4.03
	λ deg	+122.53	+113.66	+49.17
	ψ deg	0	-33.66	-31.11
	ψ_T deg	+90.00	+117.00	+350.29
	t sec	3,035	3,065	2,146
	Range naut. mile	7,330	7,450	4,607

* $q_i = \frac{1}{2} \rho V_a^2$, the incompressible dynamic pressure.

TABLE 5.1 COMPARISON OF THREE BASIC CASES

CONDITION	VARIABLE	III-P1	III-P4	III-P2	III-P5	III-P3	III-P6
		$\alpha = 16^\circ$	$\alpha = 14^\circ$	$\phi = 46^\circ$	$\phi = 44^\circ$	$\beta = +1^\circ$	$\beta = -1^\circ$
First Maximum Altitude Point, "Top" of First Skip	Δh ft	+5920	-6125	-1115	1085	-403	398
	ΔV_E ft/sec	-36	53	-6	6	-2	2
	Δt sec	+5	-5	0	0	0	0
	Δq_i lb/ft ²	-2.9	3.8	.6	-.6	.2	-.2
End of Solution $h \approx 100,000$ ft	ΔV_E ft/sec	-105		80		70	
	$\Delta \gamma$ deg	-.20		.48		.35	
	$\Delta \lambda$ deg	.10		-1.06		-.32	
	$\Delta \psi$ deg	.47		1.01		.26	
	$\Delta \psi_T$ deg	.45		.22		-2.54	
	Δt sec	-15		-40		-15	
	Δ Range naut. mile	-17		-81		-64	

TABLE 5.2 EFFECT OF ATTITUDE PERTURBATIONS ON TRAJECTORY PARAMETERS

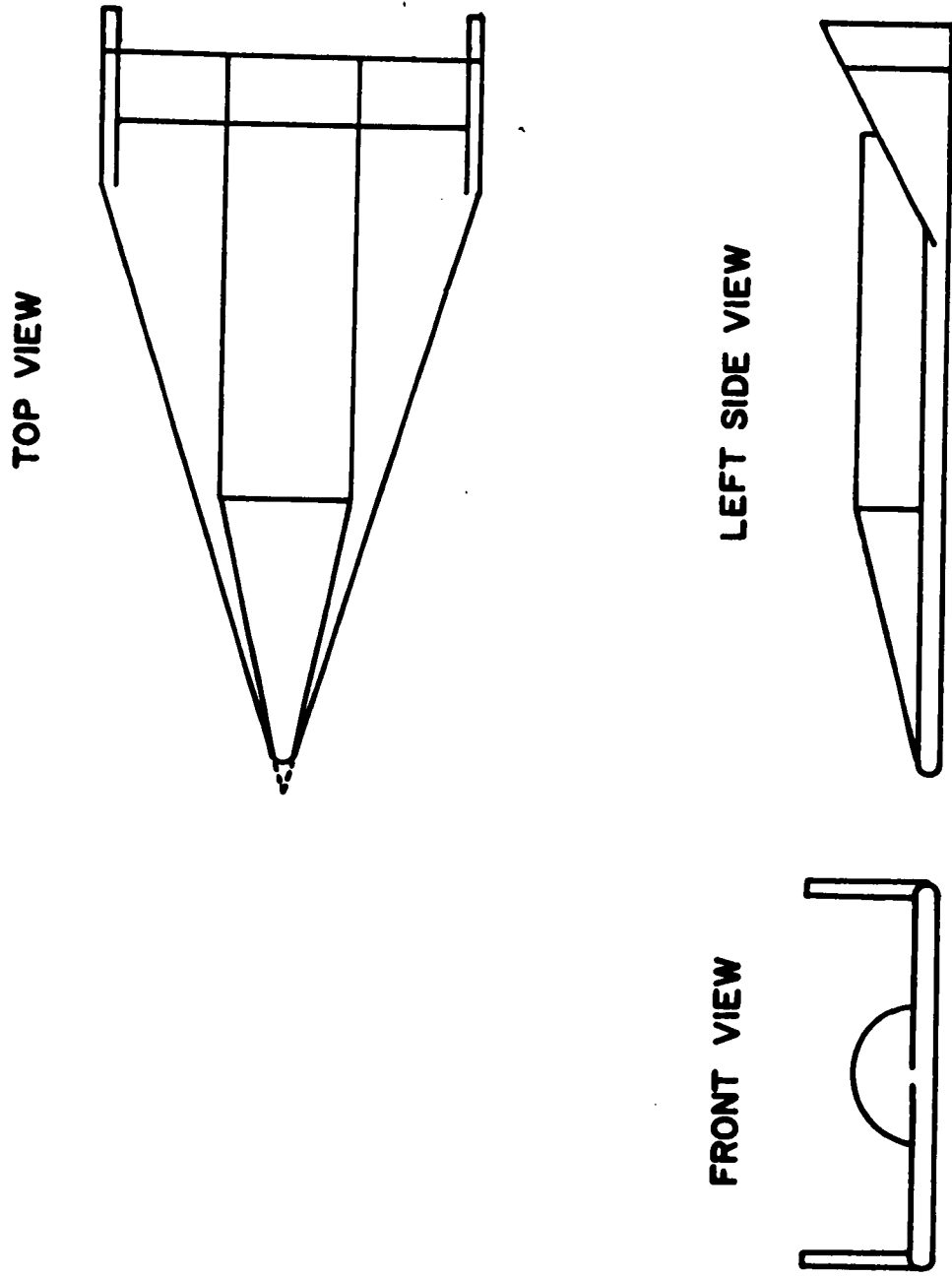
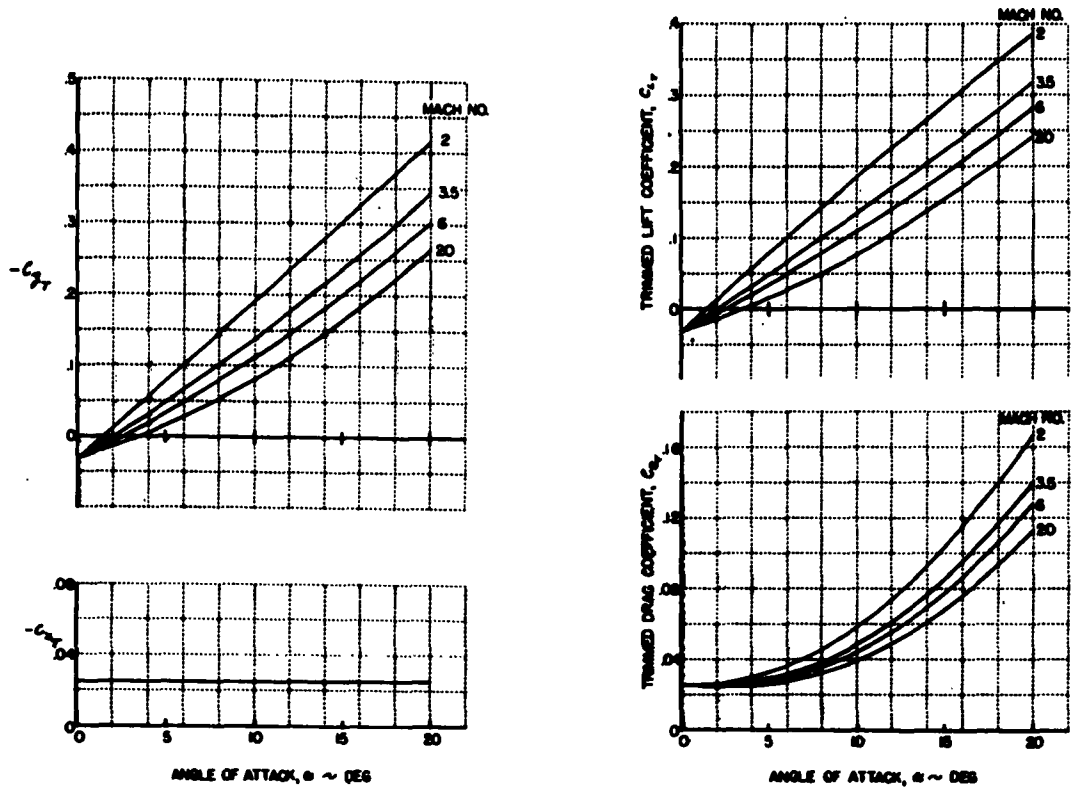
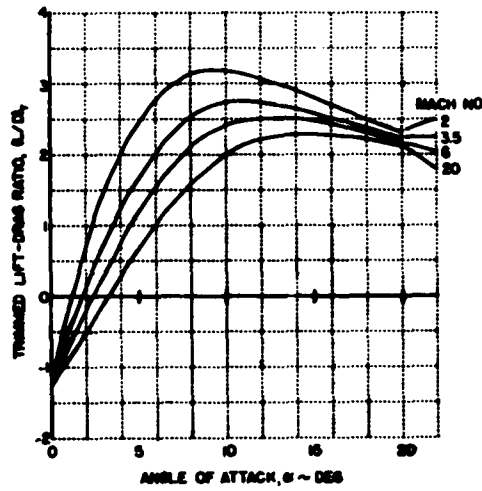


FIGURE 5.1 THREE VIEW OF TYPICAL RE-ENTRY VEHICLE



a. Body Axes Force Coefficients

b. Lift and Drag Coefficients



c. Lift-Drag Ratio

FIGURE 5.2 LONGITUDINAL AERODYNAMICS - TRIMMED CONDITION

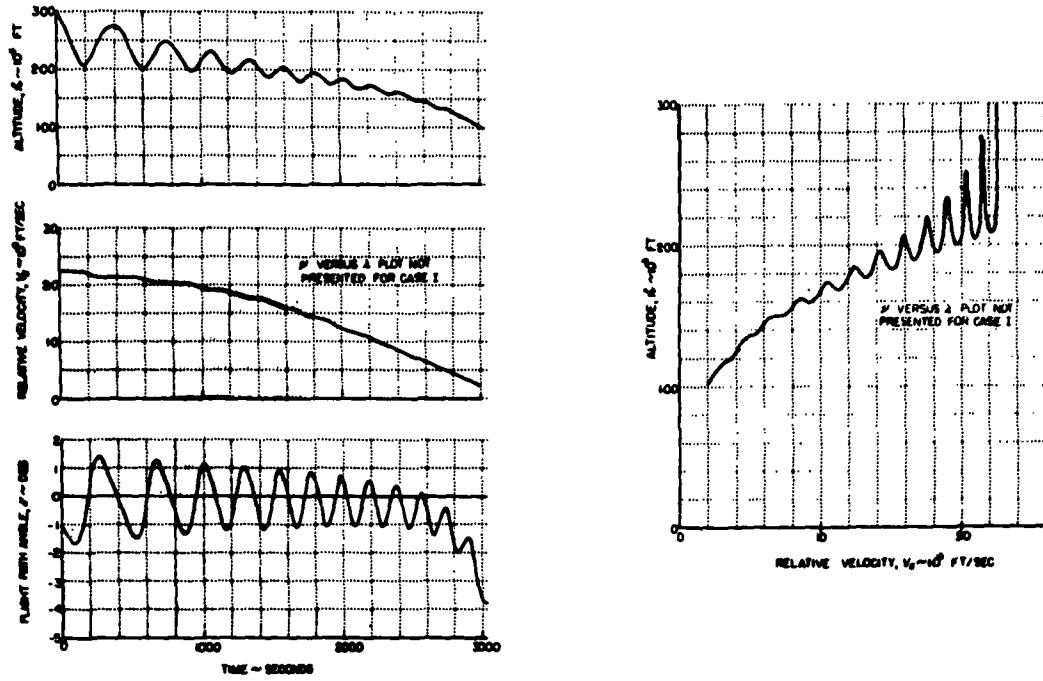


FIGURE 5.3 EQUATORIAL RE-ENTRY SOLUTION - CASE I

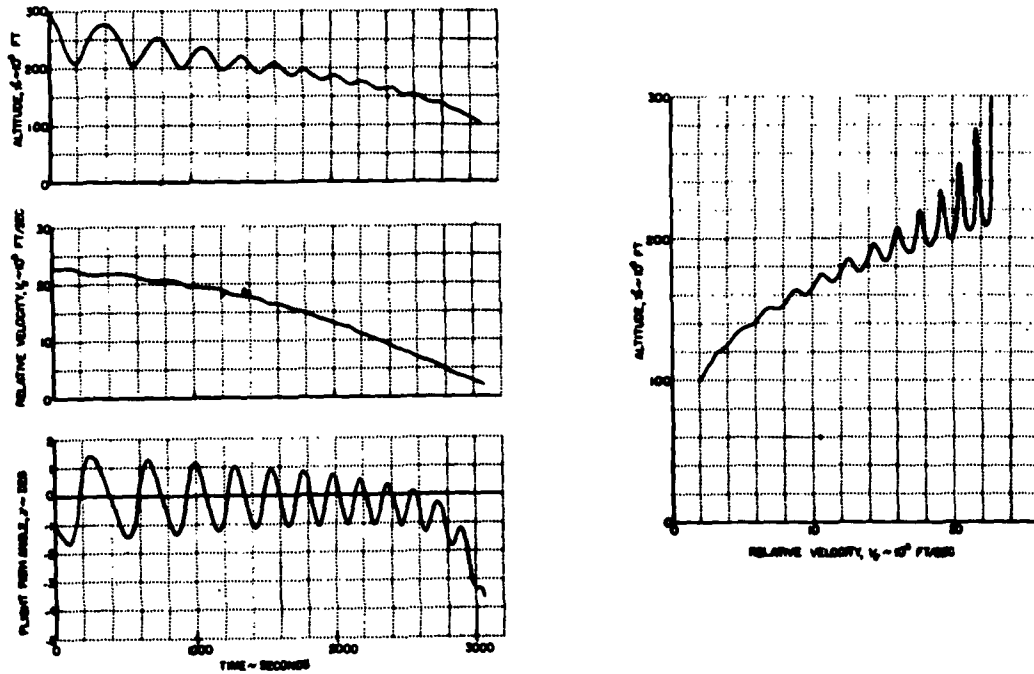


FIGURE 5.4 ATLANTIC MISSILE RANGE RE-ENTRY SOLUTION - CASE II

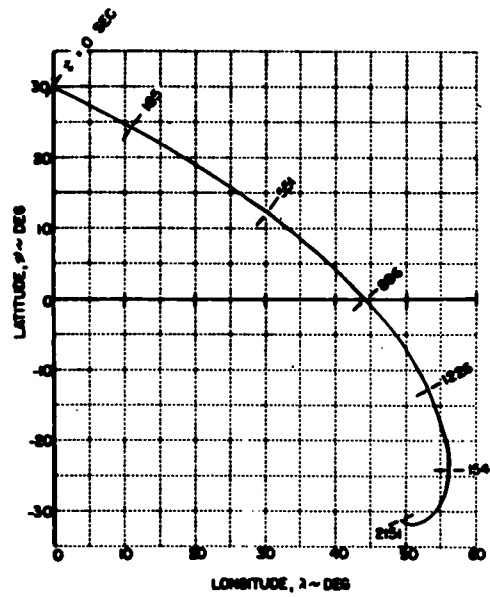
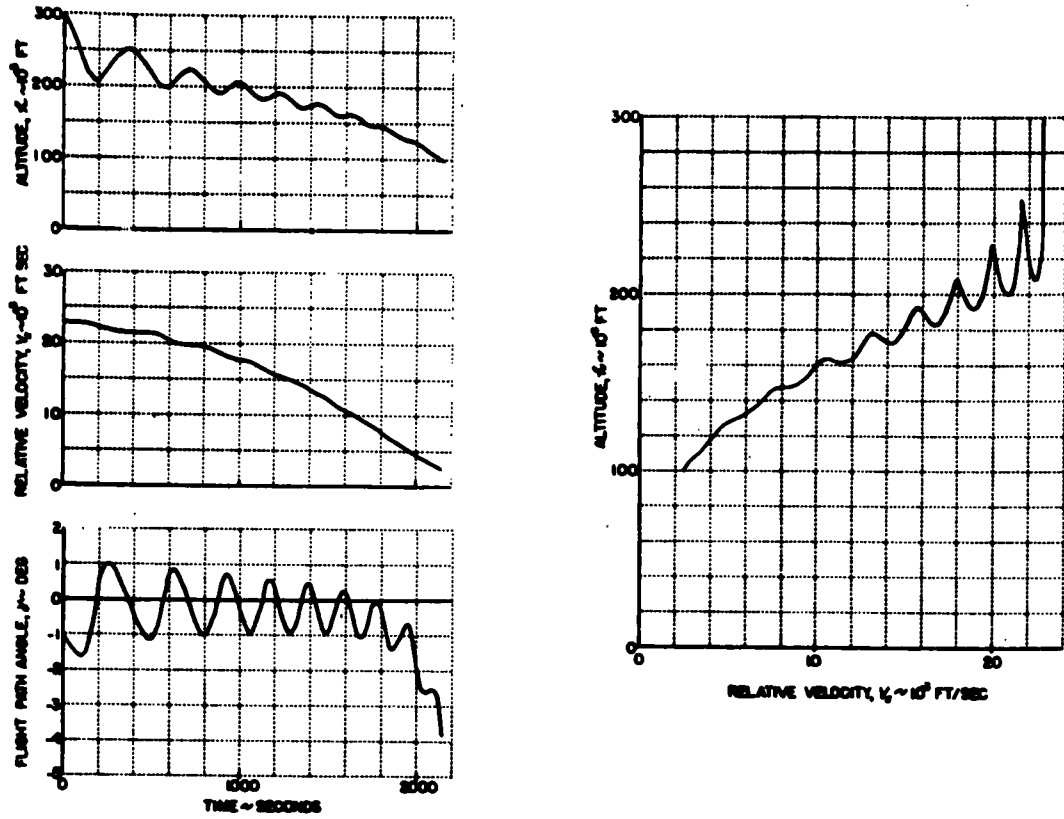


FIGURE 5.5 TURNING RE-ENTRY SOLUTION - CASE III

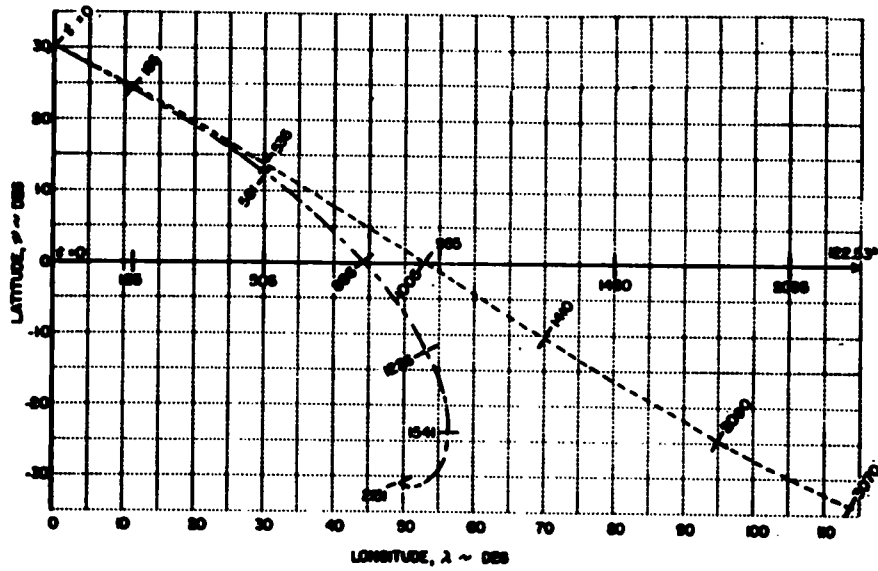
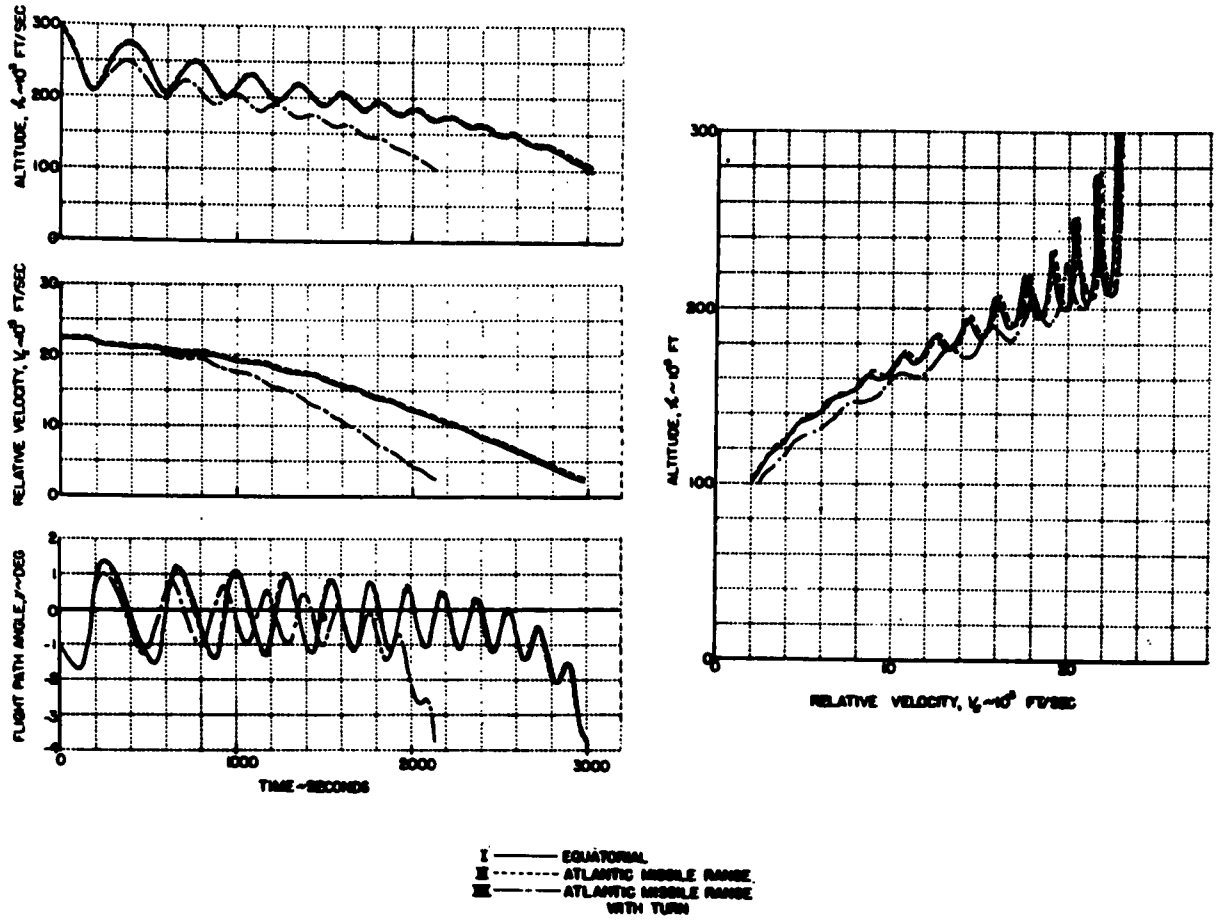


FIGURE 5.6 COMPARISON OF THREE BASIC CASES

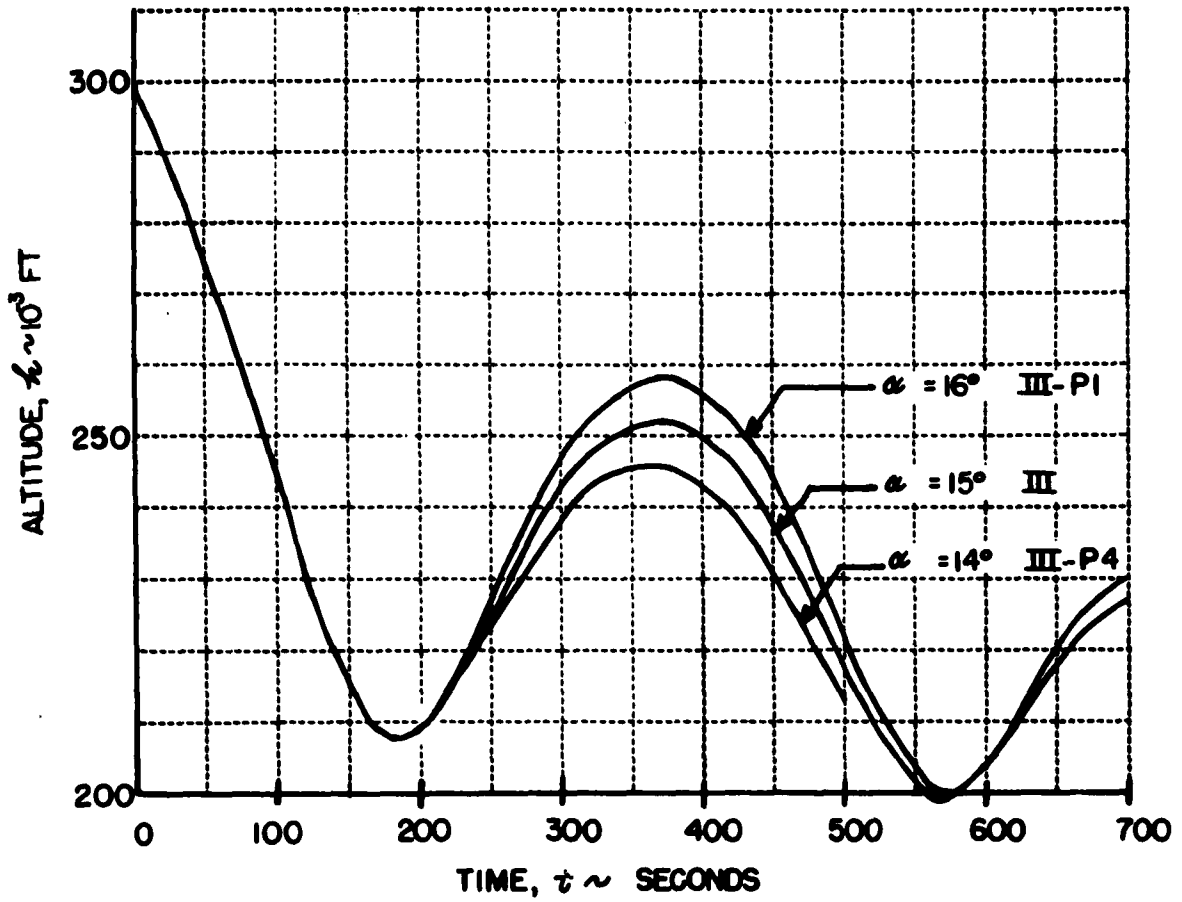


FIGURE 5.7 ANGLE OF ATTACK PERTURBATIONS

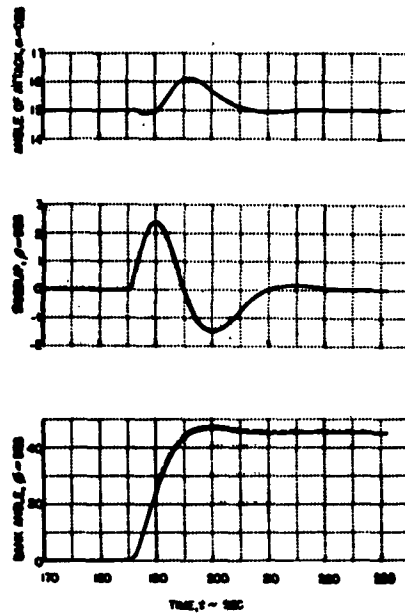


FIGURE 5.8 SHORT PERIOD TRANSIENT, ROLL ANGLE INPUT - CASE III

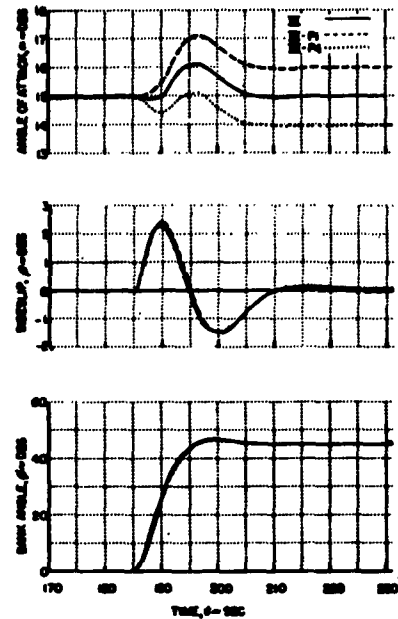


FIGURE 5.9 SHORT PERIOD TRANSIENT, ANGLE OF ATTACK PERTURBATION

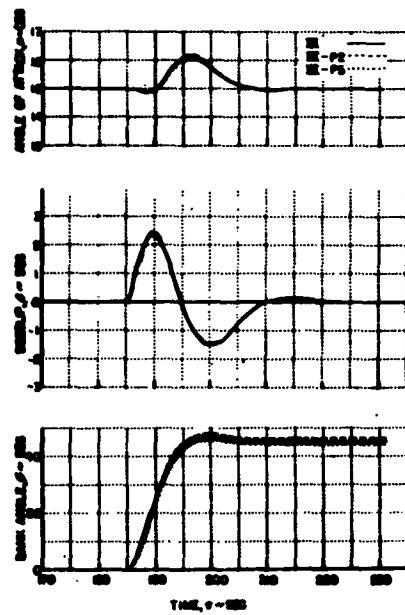


FIGURE 5.10 SHORT PERIOD TRANSIENT, BANK ANGLE PERTURBATION

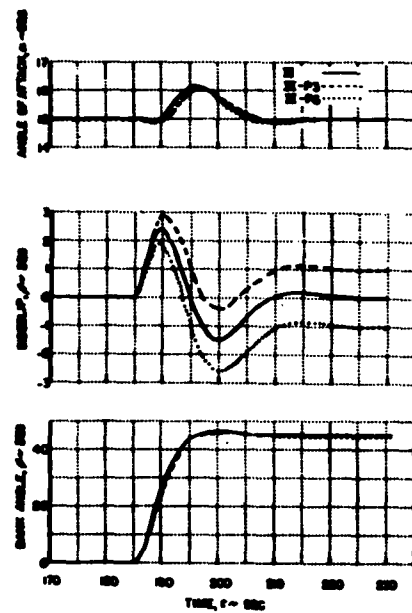


FIGURE 5.11 SHORT PERIOD TRANSIENT, SIDESLIP PERTURBATION

NAVTRADEVGEN 801A
SECTION VI
SIMPLIFICATION OF EQUATIONS OF MOTION

6.1 INTRODUCTION

This section (VI) is important to the successful use of the equations of motion for a hypersonic re-entry vehicle in a simulator with a real-time digital computer. The very concept of a piloted simulator implies precision of a low order relative to the precision required for pre-programmed satellite launchings, etc. The simulated short period dynamic motions must simply satisfy the pertinent senses of the pilot "flying" the simulator. Trajectory parameters which are observed over long periods of time by the simulator pilot must be accurate, but not so accurate as calculation of orbital ephemeris, etc. Consequently, the equations of motion were investigated for possible simplification to facilitate real-time computation and integration of the equations, while providing adequate simulation in all long and short period aspects of re-entry.

The following sections (6.2 and 6.3) will respectively deal with assumptions made to simplify initial derivation of the equations, and subsequent mathematical and geophysical simplification of the derived equations. The latter simplifications will be treated much more thoroughly in the following discussion because they involve solutions of the equations of motion and because the simplifications used to derive the equations are discussed in Section III and Appendices B and C.

6.2 SIMPLIFYING ASSUMPTIONS FOR DERIVATION OF EQUATIONS OF MOTION

There are three basic simplifying assumptions which were made to facilitate the initial derivation: one is geophysical in nature and the other two concern the vehicle configuration. It should be noted, of course, that there are other assumptions made during the derivation of Section III, but they result in neglecting relatively minor effects which are not at all well known or which do not pertain to the objectives of the derivation. The basic assumptions are listed:

1. Earth oblateness is neglected,
2. The vehicle's mass is constant, and
3. Large thrust forces are not considered.

6.2.1 Earth Oblateness

A spherical earth is the basis for the derivation of equations in Section III. This is a reasonable simplification of the more nearly correct oblate spheroidal character of the earth which greatly facilitates the derivation and which results in a computation scheme economical of time. Parameters, needed to locate a vehicle relative to the spherical earth (θ , λ , and ψ), comprise a set of pseudo-spherical* coordinates whose rates are integrated during the computation process. Aside from the purely mathematical convenience afforded, the spherical earth assumption appears to be adequate for use with a simulator when one considers some reasons for using the simulator. For example, familiarization with vehicle controls, instruments and handling qualities is not affected, crisis procedural

* The description pseudo-spherical is used because the actual spherical coordinates would be the quantities $R_0 + h$, λ and $90^\circ - \psi$ respectively.

training is not affected, and vehicle dynamic response (as indicated by instrument panel displays) is not affected. These are among the most important considerations for good simulation.

Flight time of a gliding re-entry vehicle can be substantial, especially if the vehicle is required to orbit the earth once, twice, or more often. Under these conditions it may be important that the pilot perform navigational tasks, thus requiring that consideration be given to navigation during pilot training. To obtain accurate computation of the trajectory or path of the vehicle for long duration flights, earth oblateness and related effects should be included in the equations; however, this addition is necessary only to obtain trajectories which are to match real trajectories. Navigational techniques used in a simulator would be identical with either earth model, although the paths realized would be different; therefore, there is no justification for the added complication of earth oblateness as far as navigation training is concerned. Another reason for neglecting oblateness is that the equations are developed basically for re-entry which is a short duration, short range phase of flight relative to the orbital phase.

The most difficult objection to overcome, with regard to neglecting earth oblateness, is the effect of oblateness on large-scale maneuvers. For example, if a control input had been computed to provide a specific resulting location for the real vehicle based on the oblate shape of the earth, to obtain the desired result with a simulator would require equivalent modelling of earth oblateness, all else being equal. Thus, where accurate simulation of the trajectory over a large range is required, earth oblateness will need to be included in the equation. The required equations are derived in Appendix C to fill this need. Nielsen, Goodwin, and Mersman (Reference C. 4) give solutions from which a measure of the effect of oblateness can be obtained.

6.2.2 Thrust and Variable Mass

While earth oblateness is a geophysical aspect of the simplification problem, consideration of variable mass and thrust are strictly aspects of the vehicle itself. The equations of motion developed in Section III are capable of handling the near-orbital phase of a boost-orbit-re-entry flight as well as the re-entry phase, but main emphasis for the derivation was placed on the re-entry phase. Since for re-entry only the glide vehicle is involved, the mass is very nearly constant (the small loss being due only to reaction controls). It is likely that the glider may use a landing engine, but this has not been specifically considered in the derivation since methods for handling such engines are well known. Consequently, the vehicle has a constant mass and no thrust, assumptions founded in the ground rules of the study.

If the desired configuration is composed of booster and glider, variable mass and large thrust forces certainly must be considered. The allied problems of variable moments of inertia, inclusion of products of inertia which vary, and moments due to the thrust also require attention. These problems are treated in Appendix B.

6.2.3 Less Significant Assumptions

It should be mentioned for completeness that other, less significant, assumptions are made for the derivation of Section III. Most of these are made

because of lack of knowledge of a particular phenomenon, a situation apparent in mathematical representation of the geophysical environment, especially winds and gusts. Other assumptions, such as considering a non-rotating reference frame fixed at the earth's center as an inertial frame for the motion of the vehicle relative to the earth, are made because they have completely negligible effect on solutions of the equations of motion.

6.3 EFFECT OF SIMPLIFICATIONS IN THE EQUATIONS OF MOTION

Two types of simplifications are dealt with in this section. Although both types are accomplished in essentially the same manner, by adjusting the computer program, they are basically different in effect. The simplifications are:

1. geophysical, or
2. mathematical

in nature. Presumably, simplifications of complete six-degree-of-freedom equations of motion can be made in many ways. The simplifications described in this section were made: first, by eliminating terms in certain equations; secondly, by forcing certain constants to zero; and thirdly, by making certain variable quantities constant. Linearization, a widely used technique for simplification of mathematical equations, was not explicitly attempted in this study although it could for special cases be advantageous. An example of the sort of linearization which might be used is the replacing of sines and cosines by their small angle approximations.

6.3.1 Mathematical Simplifications

There are three basic mathematical simplifications described in this section. They involve two successive approximations of a lengthy equation, an approximation for the vehicle's angular velocity with respect to the earth, and simplification of the equation for the rate of change of the vehicle's orientation angles. It is not implied that these exhaust the possible mathematical simplifications. The simplifications examined were those thought to be most desirable for facilitating real-time digital computation.

The most lengthy equation derived in Section III is that for the rate of change of the vehicle's velocity with respect to the air (see Equation 3.73 and Equation A.73). Equation 3.20^{*}, with wind and gust terms omitted, is used to explain the first two simplifications:

$$(\dot{\bar{V}}_a)_B = (\dot{\bar{V}})_B - (\dot{\bar{V}}_{er})_E + \bar{\omega}_E \times \bar{V}_{er} \quad (6.1)$$

Solution III-S1 shows the effect of neglecting the $(\dot{\bar{V}}_{er})_E$ term in Equation 6.1. Trajectory data is presented in Table 6.1 so that parameters may be compared with Case III. Table 6.2 must be used to determine the effects of the simplification upon the short period dynamic response because the differences between III-S1 and III are too small to illustrate graphically.

A further and final simplification which can be provided for Equation 6.1 is to eliminate the $\bar{\omega}_E \times \bar{V}_{er}$ term in addition to the $(\dot{\bar{V}}_{er})_E$ term. This simplification, demonstrated by Solution III-S2, is presented in Tables 6.1 and 6.2 and Figure 6.1. Comparison of III, III-S1, and III-S2 shows that all three solutions are nearly identical as far as trajectory parameters are concerned. Figure 6.1 shows that in

* see page 47

attitude dynamics III-S2 is considerably different from III. Solution III-S1 was not plotted on Figure 6.1 because no difference between it and III could be shown.

The results of these first two mathematical simplifications indicate that they are both good for trajectory purposes; but, whereas neglecting $(\dot{V}_{er})_E$ provides a good approximation for the short period response, neglecting $\bar{\omega}_E \times \dot{V}_{er}$ is definitely not allowable. On this basis, we can conclude that $[(\dot{V}_{er})_E]$ and $[\dot{W}]$ may be neglected in Equation 3.73.

Equation 3.15 gives the vehicle's angular velocity relative to the earth. It is repeated here:

$$\bar{\omega}_E = \bar{\omega} - \bar{\Omega} \quad (6.2)$$

Solution III-S5 indicates that neglecting $\bar{\Omega}$ in Equation 6.2 provides totally unacceptable results in both the trajectory and short period responses (Figure 6.2 and Tables 6.1 and 6.2). Neglecting the earth's angular velocity in Equation 6.2 is an example of an inconsistent geophysical simplification; it essentially removes earth rotation from the vehicle's rotational or angular equations while not removing it from translational or position equations. There are two specific effects of this situation which bear mentioning. First, the $\bar{\omega}_E = \bar{\omega}$ simplification, like that of $\bar{\Omega} = 0$, produces a negligible effect on short period response (Table 6.2). Secondly, for the solution termination condition ($h \approx 100,000$ ft), $\bar{\omega}_E = \bar{\omega}$ produces effects of opposite sense from those of $\bar{\Omega} = 0$ in altitude h , relative velocity V_E , flight path angle γ , as well as the vehicle's track (compare Figures 6.2a and 6.2b with 6.4a and 6.4b respectively for details). Since the $\bar{\omega}_E = \bar{\omega}$ simplification affects the vehicle's orientation directly through Equation 3.55 and indirectly through Equation 3.73 and the control system, it is not difficult to see why γ for III-S5 is so much different from γ for III (Figure 6.2a).

The final mathematical simplification involves the Euler angle calculation given vectorially by Equation 3.52:

$$\bar{\psi} + \bar{\theta} + \bar{\phi} = \bar{\omega} - \bar{\Omega} - (\bar{\lambda} + \bar{\nu}) \quad (6.3)$$

Solution III-S6 was obtained for the condition that

$$\bar{\psi} + \bar{\theta} + \bar{\phi} = \bar{\omega} \quad (6.4)$$

Table 6.2 shows that there is very little difference between the short period responses of III-S6 and III. This situation, like that of the $\bar{\omega}_E = \bar{\omega}$ simplification, is a result of the fact that the short period response is primarily dependent upon the vehicle's physical characteristics and the three-axis controller. Table 6.1 indicates that the trajectory is very poorly computed with the condition of Equation 6.4. It is a completely worthless simplification, so poor in fact that the solution has not been plotted. If only $\bar{\Omega}$ had been neglected in Equation 6.3, a more valid simplification might have been obtained.

6.3.2 Geophysical Simplifications

Two geophysical simplifications were investigated—constant gravitational acceleration and non-rotating earth. It would seem that these are rather drastic simplifications of the vehicle's complex geophysical environment; however, they are the basic assumptions made for analytical solution of re-entry trajectory equations. How reasonable are these geophysical simplifications from the

simulator point of view? The tabular and graphical results presented in this section should satisfactorily answer the question.

An inverse-square gravitational field is programmed with the equations of motion (see Equation 3.81). At an altitude of 300,000 ft, the initial altitude for all re-entry solutions, the acceleration of gravity is

$$g_{t=0 \text{ sec}} = 32.17 \frac{(20.86 \times 10^6)^2}{(21.16 \times 10^6)^2} = 31.2643 \text{ ft/sec}^2 \quad (6.5)$$

It is this value of gravitational acceleration that is used in Solution III-S3 so that III-S3 will have initial conditions matching all other solutions. Solution III-S3 is actually a simplification of Solution III-S2 since $(\vec{V}_a)_B = (\vec{V})_B$ in both; thus the two are compared for trajectory parameters in Figure 6.3 and may also be compared in Table 6.1. Constant gravity has too small an effect on the vehicle's short period response to be plotted; in fact, the little difference that might exist between Solutions III-S2 and III-S3 is not perceptible in Table 6.2 which contains data to just two decimal places.

The graphical data shows that a constant g equal to the value at 300,000 ft results in a small drift of the trajectory parameters from those of III-S2. The maximum difference between the two solutions could be lessened if some mean value of gravitational acceleration were used. Such a mean value can probably be determined for any desired re-entry simulation. However, in a digital computer program the calculation saved hardly seems worthwhile.

The motions relative to the earth are described in terms of the vehicle's inertial linear and angular velocities and the rotation of the earth. In many situations it is not necessary to consider earth rotation; however, this convenience cannot be justified in the equations of motion considered here because the duration of each solution is long enough for the earth to rotate through several degrees (corresponding to several hundred miles on the earth's surface) and because the vehicle's velocity relative to the air would be different, resulting in different aerodynamic forces and moments.

To be able to assess the effects of a non-rotating earth, Solution III-S4 was obtained. Trajectory parameters are plotted in the two parts of Figure 6.4 along with the corresponding data for basic Case III solution. It is important to note (Figure 6.4b) that earth rotation cannot be accounted for just by a correction in longitude (λ). A numerical comparison of the trajectory can be made by using Table 6.1. Like the constant g solution, Solution III-S4 shows that effects of the $\vec{\omega} = 0$ simplification on short period dynamic response are completely negligible. Table 6.2 tabulates various short period dynamic response parameters for Solutions III and III-S4.

Of the two simplifications described in this section, constant g is by far the better. Both simplifications are equally good in short period dynamic response characteristics, but comparison of Figures 6.3 and 6.4 shows that constant g is better for trajectory computation. This is not an unexpected result since the variation of g from zero to 300,000 ft of altitude is small, less than 3%.

NAVTRADEVGEN 801A

Geophysical simplifications are discussed in Section VII and recommendations are made regarding whether the simplifications should be adopted or whether, in fact, more accurate geophysical representations are needed such as described in Appendix C.

NAVTRADEVGEN 801A

CONDITION	VARIABLE	III	III-S1	III-S2	III-S3	III-S4	III-S5	III-S6
		Basic Solution	$(\dot{V}_a)_0 = (\dot{V})_0$ $+ \dot{w}_x \times \dot{V}_{op}$	$(\dot{V}_a)_0 = (\dot{V})_0$	$(\dot{V}_a)_0 = (\dot{V})_0$ $g = 31.266 \frac{ft}{sec^2}$	$\dot{A} = 0$	$\dot{w}_x = \dot{w}$	$\dot{F} + \dot{D} + \dot{D}$ $= \dot{w}$
First Minimum Altitude Point, "Bottom" of First Skip	λ ft	207,337	207,291	207,326	208,140	209,632	200,283	153,169
	V_g ft/sec	22,385	22,385	22,385	22,396	23,592	22,356	21,494
	γ deg	+0.0597	+0.0583	+0.0584	+0.0540	+0.0803	-0.1256	+0.1574
	t sec	185	185	185	185	180	170	100
	q_i lb/ft ²	91.1	91.3	91.2	88.2	91.8	122.5	834.0
	\dot{Q} $\frac{BTU}{ft^2 \cdot sec}$	240	239	239	234	267	269	547
First Maximum Altitude Point "Top" of First Skip	λ ft	252,278	252,236	251,912	251,246	256,923	253,049	274,648
	V_g ft/sec	21,635	21,635	21,634	21,655	22,913	21,516	19,859
	γ deg	+0.0083	+0.0090	+0.0167	-0.0057	+0.0065	+0.0083	+0.0059
	t sec	366	366	366	371	361	336	203
	q_i lb/ft ²	12.7	12.7	12.9	12.2	11.7	12.1	4.1
End of Solution $\lambda \approx 100,000$ ft	λ ft	100,032	100,039	100,559	100,065	100,219	100,526	100,679
	V_g ft/sec	2,464	2,463	2,440	2,398	2,576	2,585	2,853
	γ deg	-4.03	-4.04	-4.50	-4.94	-4.09	-3.35	-8.31
	t sec	2,146	2,146	2,146	2,196	2,281	2,001	1,191
	\dot{V}_r deg	350.29	350.27	350.05	352.32	352.15	344.6	325.13
	λ deg	49.17	49.17	49.18	50.33	54.72	44.70	19.74
	ψ deg	-31.11	-31.11	-31.12	-32.51	-37.29	-25.30	2.80
	Range naut. mile	4.607	4.607	4.607	4.690	5.060	4.190	2.260

TABLE 6.1 COMPARISON OF SIMPLIFICATION SOLUTIONS

VARIABLE		III	III-S1	III-S2	III-S3	III-S4	III-S5	III-S6
		Basic Solution	$(\dot{V}_a)_0 = (\dot{V})_0$ $+ \dot{w}_x \times \dot{V}_{op}$	$(\dot{V}_a)_0 = (\dot{V})_0$	$(\dot{V}_a)_0 = (\dot{V})_0$ $g = 31.266 \frac{ft}{sec^2}$	$\dot{A} = 0$	$\dot{w}_x = \dot{w}$	$\dot{F} + \dot{D} + \dot{D}$ $= \dot{w}$
α min	deg	14.89	14.87	14.67	14.67	14.90	14.90	14.91
t_{α} min	sec	189	189	190	190	189	189	189
α max	deg	16.13	16.11	15.56	15.56	16.13	16.13	16.15
t_{α} max	sec	196	196	197	197	196	196	196
β max	deg	2.36	2.36	2.19	2.19	2.37	2.36	2.35
t_{β} max	sec	190	190	190	190	190	190	190
β min	deg	-1.50	-1.50	-1.58	-1.58	-1.50	-1.50	-1.49
t_{β} min	sec	200	200	200	200	200	200	200
$\dot{\beta}$ max	deg/sec	5.96	5.95	5.96	5.96	5.96	5.95	5.95
$t_{\dot{\beta}}$ max	sec	189	189	189	189	189	189	189

TABLE 6.2 EFFECT OF SIMPLIFICATIONS ON SHORT PERIOD DYNAMIC RESPONSE

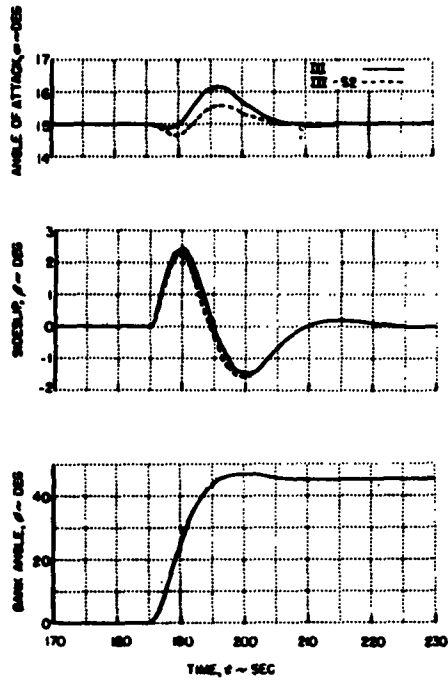
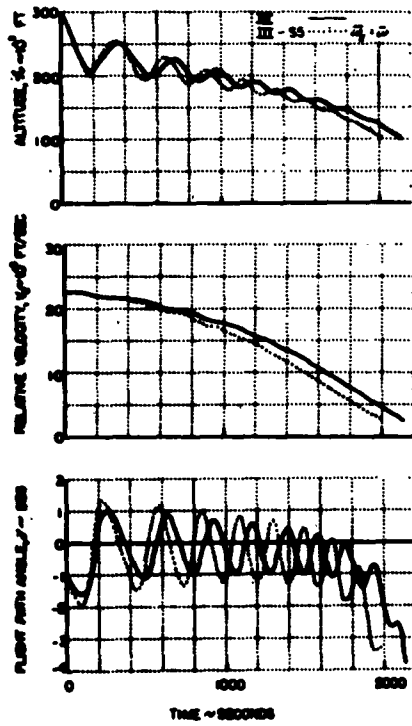
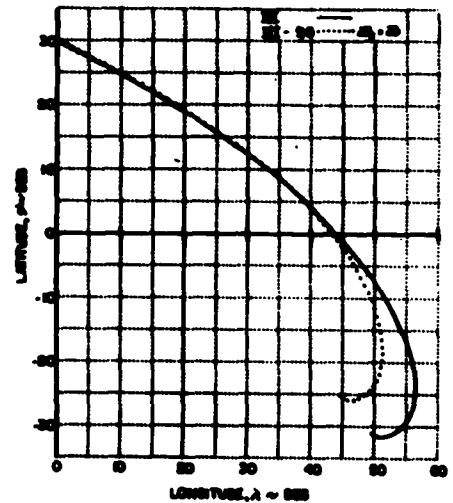


FIGURE 6.1 EFFECT OF $(\dot{V}_{A_0}) = (\dot{V})_0$ SIMPLIFICATION ON SHORT PERIOD TRANSIENT

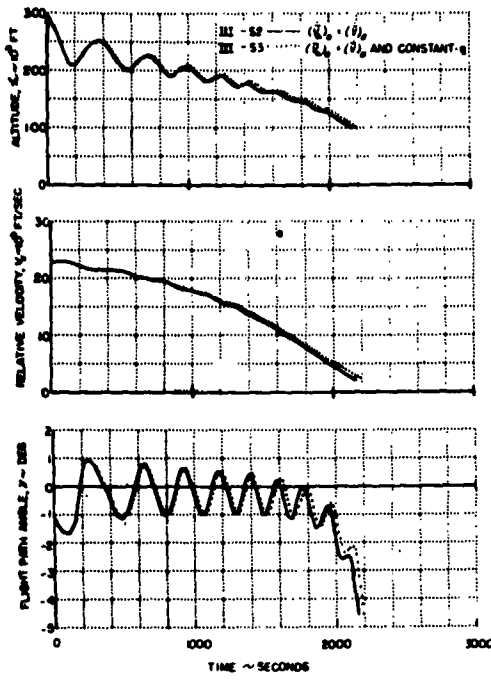


(a)

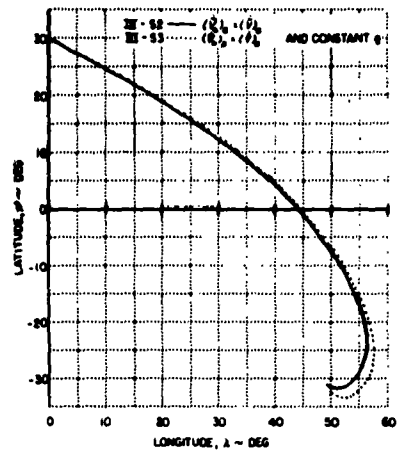


(b)

FIGURE 6.2 EFFECT OF ANGULAR VELOCITY SIMPLIFICATION ON TRAJECTORY PARAMETERS

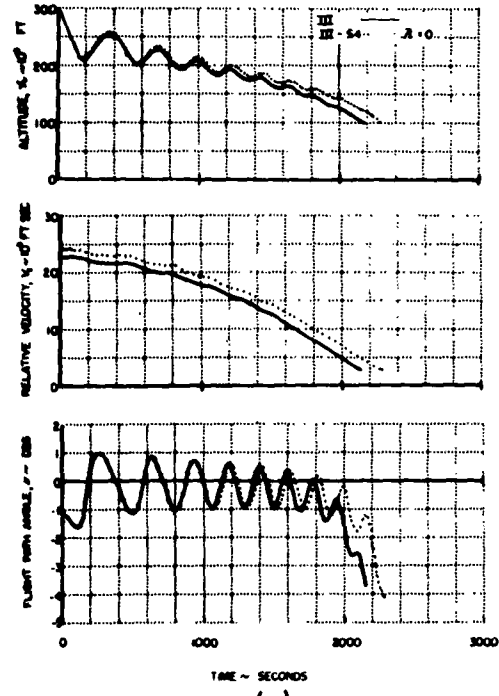


(a)

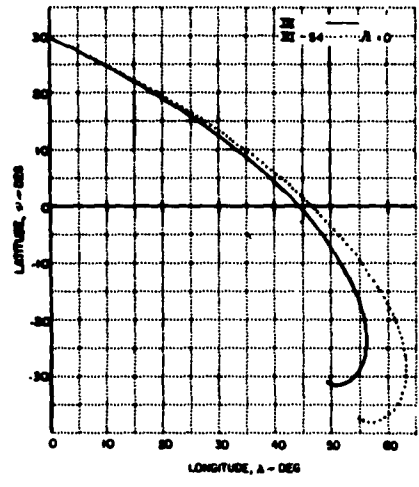


(b)

FIGURE 6.3 EFFECT OF CONSTANT GRAVITATIONAL ACCELERATION ON TRAJECTORY PARAMETERS



(a)



(b)

FIGURE 6.4 EFFECT OF EARTH ROTATION ON TRAJECTORY PARAMETERS

SECTION VII
CONCLUSION

7.1 INTRODUCTION

The purpose of this concluding section is to summarize the requirements for simulating the re-entry and landing of hypervelocity aircraft as determined from the study described in this report. Although the study emphasized those aspects of the problem associated with re-entry, consideration was given to the requirements for simulating final approach and landing. In addition, information was obtained relative to boost and en-route cruise or orbital flight. Basically, this study concerned only the requirements for the equations of motion, but the rest of the simulation had to be considered in order to perform this task. Special importance was attached to the required piloting task, since the accuracy required in the equations of motion is directly a function of the combined response of the pilot and the aircraft--of how tight the loop is closed.

The development in this section for the recommended equations follows the outline of the report: geophysics, axis systems and coordinates, aerodynamics and control, and numerical methods and allowable simplifications. The accuracy required depends on the piloting task and the purpose of the simulator. Is it enough to simulate just the trajectory (energy management) problem or just attitude dynamics, or is complete simulation of the control problem required? Is accurate navigation important? Or is it enough to let the pilot just re-enter and land the aircraft anywhere? In this section an attempt has been made to indicate what is required in the equations for each of these types of simulation.

Computational accuracy is an important factor in solving the equations. No problem was encountered with obtaining sufficient accuracy in this study using the recommended equations and an IBM 704 to solve them. However, if the accuracy of the computer used in a specific simulator (such as UDQFTT) is less than that of the usual general-purpose digital computer (i. e., IBM 704, etc.), then ways of improving the accuracy of the computation are described, especially through the use of special coordinates for integrating the equations.

Although considerable effort has been spent in this study trying to develop the best equations for the task, there are many areas where further study is obviously needed. Some of these are: numerical integration techniques, coordinates for improving the inherent accuracy, simplifications in the kinematics and dynamics, representation and effects of aerodynamic forces and moments, stability and control requirements, and expected dynamic characteristics particularly at high angles of attack.

7.2 GEOPHYSICAL DATA

Recommendations for geophysical representation of the earth are made in four parts:

1. Earth motions,
2. Earth shape,
3. Gravitational field, and
4. Atmosphere.

If a detailed specification of a simulation task is presented, specific recommendations can be made. Here the discussion is based upon the premise of complete simulation with additional comments being made when necessary to describe less accurate simulation.

7.2.1 Earth Motions

As mentioned in Section 2.2.1, the earth has numerous motions in inertial space—the most important being translation in its orbit and rotation about its axis. Mathematical justification has been given in Section 2.2.1 and 3.2.1 for neglecting the earth's translation; therefore, the rotation remains as an important motion. Results presented in Section VI, especially in Figure 6.4, indicate that accurate trajectory simulation requires the presence of earth rotation.

It is recommended that constant earth rotation be included for proper simulation of re-entry flight under all conditions.

7.2.2 Earth Shape

There are many possible approximations for the shape of the earth; notably, flat, spherical and oblate. For re-entry simulation the flat earth is ruled out entirely (with one qualification; see Section 7.5.2). A spherical earth, used for obtaining the solutions of Sections V and VI, is adequate for short range re-entries (e.g., small L/D); but, in fact, the re-entry solutions obtained during this program have ranges too long for the spherical approximation. An oblate representation of earth shape should be considered the minimum for re-entry simulation though the full representation needed for predicting a satellite ephemeris is certainly not needed.

A first-order approximation of the oblateness effect, as described in Appendix C, is recommended. This extension, of equations developed in Section III, is easy to incorporate and will result in significant improvement in a general simulation of re-entry. It provides not only oblate shape for the earth, but also the corresponding oblate shape of the atmosphere.

7.2.3 Gravitational Field

It has been shown in Reference 1.6 and elsewhere that an inverse-square gravitational force field is necessary for the accurate description of the skipping (phugoid) motions of a re-entry vehicle. Except for the constant gravitational acceleration solution, the solutions of Sections V and VI were obtained using the inverse-square approximation. It appears that nothing less accurate than this should be used with the equations of motion. Two comments can be made concerning this statement, however:

1. The constant gravity solution (see Figure 6.3) is surprisingly good and it could have been better had some mean value of the constant acceleration been used instead of the value for $g = 300,000$ ft.
2. For simulation of long-range re-entries or flights involving one or two orbits of the earth, the oblate gravitational field is required.

Since the discussion concerns a general simulation, it is recommended that the gravitational field be represented by the gradient of the potential function (Appendix C, Equation C.12; zero and second harmonic terms only).

7.2.4 Atmosphere

Physical properties of the atmosphere are not well defined at this time. In fact, mathematical description of these properties under all conditions is a seemingly hopeless task. Thus, someone intending to make use of these properties must turn to mean data such as contained in Reference 2.6, the ICAO Standard Atmosphere; although one recognizes that complete correspondence between this mean and the actual conditions in the atmosphere is unlikely.

This study dealt with re-entries using atmospheric temperature, density and pressure models for altitudes below 300,000 ft, a region in which the properties are relatively well defined in the mean. However, the properties exhibit large percentage variations from the mean which depend upon season, time of day, large scale surface weather conditions, etc. Above 300,000 ft even the mean is not well defined and again variations are large depending on the conditions mentioned above, with added dependency on solar activity and other extra-terrestrial phenomena.

Figures 2.1 and 2.2 compare the models of temperature and density developed in this study with the ICAO Standard Atmosphere. The temperature model is an exact match; the density model is only an approximate match but, in view of the discussion in the preceding paragraph, it is certainly adequate.

It is impossible to fit a single unchanging exponential function to the standard atmosphere density data if adequate density description is required for the entire altitude range of interest. Without going to undue complexity, very little improvement can be obtained over the density model given by Equation 2.1.2.

The temperature and density models described in Section 2.3.2 are therefore recommended.

Atmospheric motions are, like density, temperature, etc., poorly defined except at low altitudes where mean data on winds and gusts is available. Weather, time of day, season, etc. affect intensity, direction and gradients of the motions, thus making mathematical description of winds and gusts difficult. This is unfortunate, for wind gradients have been found to significantly affect short period motions of aircraft.

Typical averaged mean wind data, modelled for use with the equations of motion (Equation 2.14), can be useful, but good simulation should possibly have a wind velocity vector model which is more accurately defined relative to geographical location and altitude and which more accurately depicts jet stream location.

No gust model was devised during this study, but certainly a model can be used to advantage to provide good simulation of short period response and handling problems especially at low altitudes during approach and landing.

Mathematical application of gust data to equations of motion can be handled in many ways; it is felt, however, that the method described in Section III (using $[\mu]$) is entirely adequate for general simulation of re-entry flight.

Atmospheric Oblateness: All properties of the atmosphere are presented as functions of altitude so that if altitude is measured above the oblate earth and is used for determination of these properties, the atmosphere will be similarly oblate. Atmospheric oblateness would be, therefore, one of the geometric effects of earth oblateness.

7.3 COORDINATES AND AXES FOR INTEGRATION

The coordinates and axis systems derived in this report are believed to be best for the simulation problem. Some comments will be made, however, to justify this statement and to indicate that one system can actually be better than another as far as accuracy of numerical integration is concerned.

The three primary sets of axes developed in the study are listed here:

1. **Earth axes.** This is a frame whose origin is fixed at the earth center and which rotates at angular velocity Ω with the earth. The location of the vehicle's center of gravity with respect to the earth is given in terms of spherical coordinates of this frame (r_{EB}, λ, ψ).
2. **Earth-surface axes.** This is a frame whose $x_{ES} - y_{ES}$ plane is parallel to the local surface of the earth, whose z_{ES} is directed toward the center of the earth, and whose origin is positioned at and moves with the vehicle's center of gravity. Since the position of the earth-surface frame is given in terms of r_{EB}, λ , and ψ , it is an ideal frame with which to reference geophysical parameters of the earth, especially gravitational acceleration, winds, etc.
3. **Body axes.** The origin of this frame is located at the vehicle's center of gravity. Its x axis is directed forward; its y axis, to the right; and its z axis down (as viewed by the pilot). This frame is of prime importance in the equations of motion because the vehicle's force and moment equations are integrated in this frame. The vehicle's orientation is given by the orientation of the body frame relative to the earth surface frame. These axes are the natural coordinates of the vehicle, for instrumentation, for accelerations, for defining physical characteristics of the vehicle; and they are also convenient for representing aerodynamic forces and moments particularly at hypersonic speeds.

There are other reference frames used which are of less importance to the mathematical development of the equations of motion. Two of them, the wind and stability axis frames, are used in obtaining and handling aerodynamic data. These frames have been adequately described in the Symbols and Definitions at the front of this report. The so-called trajectory (τ) axis frame was not specifically used in the study but is, nevertheless, defined by the vehicle's center of gravity and the tangential velocity vector (V_τ) which is directed along the x_τ axis. Since it is conveniently present in the development of the equations, it was considered as a possible frame in which to integrate the force and moment equations rather than the body axis frame.

It is important that the proper variables and reference axes be used for integration. To illustrate simply, V_p should be integrated to obtain \mathcal{A} and then $V_{EB} = \mathcal{A} + R_0$; if V_p is integrated to yield V_{EB} directly, then \mathcal{A} becomes the difference of two large numbers and its accuracy may be reduced by several orders of magnitude. The above case is trivial, but the computation of the aircraft's translational velocity from the accelerations presents significant problems. If body axes are used, then during re-entry where the velocity (V) is large, rigid body rotations will cause large changes in the components of velocity which consequently may cause substantial errors in the actual accelerations (i.e., $a_x \ll \dot{u}$). Howe* has suggested the use of the "H-frame" - \mathcal{Z}_H directed along the projection of the inertial velocity on the plane normal to the earth radius vector, \mathcal{Z}_H along this vector - for integration of the accelerations to obtain accurate velocities. The H-frame serves admirably for computing near-orbital velocities, but it is subject to difficulties at low speeds such as in landing. Here the inertial velocity is large compared to the aircraft's relative velocity ($V_{er} \cong 1500$ fps as compared to $V_E \cong 200$ fps) and could cause errors. It appears that the best frame would be the T-frame - \mathcal{Z}_T along V_T and \mathcal{Z}_T coincident with \mathcal{Z}_{Es} - so that the relative motion with respect to the earth would be computed with maximum accuracy. The use of either the H-frame or the T-frame requires extra transformation (as compared with body axes), but where computational accuracy is limited (such as on an analog computer, and perhaps also for UDOFTT which has only 20 bit words as compared with the 32 bit words of the IBM 704) the use of such frame may be mandatory. No difficulty was encountered from this source in the present studies which employed an IBM 704 for solving the equations. For example, in the computation of the path of a highly eccentric orbit with rigid body rotations, the total error in position was found to be only 30 ft in roughly a quarter of an orbit (30 ft out of 3,000,000 ft).

7.4 AERODYNAMIC REPRESENTATION

Present knowledge of the aerodynamics of re-entry aircraft is not adequate to formulate an accurate description at this time. The best that can be done is to base the formulation on present estimation methods, but with the recognition that this formulation may be substantially in error and may neglect important variations which may not be uncovered until such aircraft are actually flight tested. However, it may be stated with confidence that for normal re-entry flight, an automatic control system will be needed and that direct manual control will pose a serious piloting problem and will only be used as an emergency measure.

Several possible simulations can be considered: simulation of the trajectory only, simulation of the attitude control problem only, and complete simulation. How each of these can be handled is described in Section 4.4.2, but the results can be summarized: trajectory simulation requires lift and drag data only, attitude simulation requires full description of the forces and moments but not necessarily as a function of flight condition, and the complete simulation requires including the dependence of forces and moments on the flight condition.

* Fogarty, L. E. and R. M. Howe: Analog Computer Solutions of the Orbital Flight Equations. University of Michigan, College of Engineering, sponsored by Air Force Contract No. AF33(616)-5864, to be published.

A recommended procedure for handling the aerodynamic data and arriving at suitable equations is presented in Section 4.4. The general equations for representing the forces and moments in terms of aerodynamic coefficients are given by Equation 4.12. As for the coefficients: basically, the longitudinal forces and moments (C_L , C_D , C_m) require nonlinear representation as functions of attitude and flight condition (α , β , δ , M , V_a , h); the lateral forces and moments (C_Y , C_l , C_n) can be represented by linear stability derivatives with nonlinear corrections added at hypersonic speeds. These concepts are summarized by Equations 4.16, 4.17, 4.22 and 4.23, and an illustration of the techniques required is presented in Figure 4.4.

Normally, the force and moment coefficients are represented as function of α and β . However, the data discussed and equations presented in Section 4.4.1 show that the direction cosines u_a/V_a , v_a/V_a , w_a/V_a could be used to much better advantage in hypersonic flight.

7.5 REQUIRED EQUATIONS

In the preceding sections recommendations have been made concerning the geophysical and aerodynamic characteristics that should be included in the equations of motion, and the coordinates and axis systems that should be used for the equations of motion. Here recommendations are made concerning the equations that are needed for the simulation. Since the degree of sophistication needed in the equations depends on the extent of the simulation involved and the task that is required of the pilot, three general types of re-entry simulation are considered: trajectory and energy management simulation, short-period dynamics and handling qualities simulation, and complete simulation.

7.5.1 Re-Entry Simulation

Because trajectory and energy management simulation requires accurate geophysical models even when the navigational aspects are not considered, the least accurate representation that can be used must include a spherical rotating earth with an inverse-square gravitational force. If accurate navigation is required, then the oblate shape of the earth and its atmosphere, as described in Appendix C, must be included. The lift and drag (C_L and C_D) of the vehicle must be accurately represented, and also the side force (C_Y) unless it can be presumed zero. However, the attitude dynamics of the vehicle may be greatly simplified. In fact, if positive attitude control is provided the pilot, that is, if α and β are made functions of control position only ($\delta = 0$ is presumed), then the equations of motion can be reduced to the three degrees of freedom required to solve for the vehicle's trajectory. In this case the T-axis frame described in Section 7.3 would probably be the best frame to use for the equations of motion. The body axes would only be used to define the attitude of the vehicle, for the pilot's attitude displays and for resolving lift and drag. The vehicle attitude angles can be resolved directly given α and β .

Short period and handling qualities simulation requires accurate representation of the aerodynamic forces and moments with respect to all three axes to handle the lateral and longitudinal motions of the aircraft. In addition control system simulation should be accurate. Since the emphasis here is on short period, the geophysical simplifications $\bar{N} = 0$ and constant g as described in

Section VI may be conveniently used. Table 6.2 shows their negligible effect, if any, on the short period dynamics. Also, the mathematical simplifications, described in the next paragraph, may be used (though $\bar{V}_{er} = 0$ already if $\bar{\lambda} = 0$).

Complete re-entry simulation requires the complete equations derived in Section III except for the following modifications. The oblate shape for the earth and its atmosphere, described in Appendix C, must be included in the equations if accurate navigation is a requirement. The $(\bar{V}_{er})_E$ term in Equation 3.20a (follows Equation 3.72; term also found in Equation 6.1) may be omitted. Furthermore, based on the study of the effects of this term, it can be concluded that $(\bar{W})_E = (\bar{W})_{ES} + \bar{\omega}_{ES-E} \times \bar{W}$ can also be omitted in Equation 3.20a. Therefore, the matrix equation 3.73 may be simplified to

$$[\dot{V}_a] = [\dot{V}] + [\omega_E \times] [L_{\theta-ES}] \left\{ [V_{ar}] + [W] \right\} - [\mu] \quad (7.1)$$

thus affecting a considerable economy in the solution for $\dot{\alpha}$ and $\dot{\beta}$. These conclusions assert the validity of the fourth assumption in Section 3.2.3 concerning relative air motion. However, these simplifications have been shown to be valid if $[V_a]$, α , and β are computed from Equations 3.68 through 3.71. If $[V_a]$, α , and β are computed by integrating $[V_a]$, α , or β directly, then these simplifications may not be valid. Since Equations 3.73 through 3.75 add considerable complexity to the over-all equations, their elimination is worth considering. They could be dispensed with by numerically differentiating α and β in the computer to obtain $\dot{\alpha}$ and $\dot{\beta}$. Also, if $\dot{\alpha}$ and $\dot{\beta}$ are needed only for the aerodynamic representation, it may be acceptable in some cases to neglect their effect entirely.

7.5.2 Landing Problem

When the vehicle reaches its approximate landing location, it would be desirable to refer its position to some axis system fixed with respect to the landing field and to consider the earth flat. Longitude and latitude are no longer significant to the flight problem, and V_μ , V_λ , and V_r can be integrated directly to obtain the position of the vehicle in rectangular coordinates. For simulating the approach and landing problem, the equations of motion can be greatly simplified by neglecting earth rotation, considering the earth flat, and assuming the gravitational force constant both in magnitude and direction. With these simplifications, the equations of motion revert back to the equations normally used for conventional airplanes.

7.5.3 Computer Requirements

It may prove of value to know how the IBM 704 storage capacity was allotted in the computer program used in this study. Of the total 3310 words used for the basic program, the breakdown is as follows:

1. The input, including initial storage of all data, requires about 710 words.
2. The program itself requires about 2150 words of which standard subroutines comprise 1030 words.
3. The output requires 450 words.

Included in the 2150 words of storage used for the program itself are an estimated 550 words needed for the aerodynamic representation given by Equations 4.16 and 4.17.

The time required for the time history solutions of Sections V and VI averaged about 40 computation cycles (time history points) per minute.

7.6 CONCLUSIONS

In conclusion, the results of this study show that significant simplification of the equations of motion can be allowed in their application to flight simulators, particularly in the calculation of the accelerations of the vehicle with respect to the air. Additional simplifications can be made if accurate trajectories are not required, and certainly in some cases still other simplifications, such as small angle ones, can be made which have not even been considered in the present study.

Because of the wide range of frequencies involved in simulating the full flight dynamics of piloted hypersonic or near-orbital vehicles, and because of the difficulties caused by such a frequency spread (Appendix D), it appears that new mathematical techniques for numerical integration, of adequate accuracy and favorable properties, need to be developed. If such new techniques are not forthcoming, it appears that considerably faster digital computers than are now presently available will be needed if the full flight equations are to be solved in real time. Several expedients can be adopted to solve the equations on present computers such as UDOFTT. The full flight of the vehicle can be subdivided, say into boost, orbital, re-entry, and landing phases, so that much simpler equations can be used in each phase than would be needed for the full flight. Also high frequencies associated with control systems, structural dynamics, etc., can be neglected so that a long time interval can be used in the numerical integration. Analog computers do not offer a good answer to the problem because of the difficulty in obtaining adequate accuracy, and the very complex functions that must be generated to adequately represent the aerodynamics. Perhaps a solution can be arrived at by combining analog and digital techniques, using digital simulation where accuracy, complex function generation and logic are required, while using analog simulation for the high frequency elements of the problem.

APPENDIX A
SUMMARY OF EQUATIONS OF MOTION IN ALGEBRAIC FORM

This appendix presents the equations of motion as developed in Section 3.4 but, unlike that section, the equations are presented here in fully expanded algebraic form. Also, certain transformation matrices are included which are used frequently in the equations. Each equation is given the same number which appears with its matrix form in Section 3.4.

A.1 EQUATIONS OF MOTION

A.1.1 Equations of Motion

$$\begin{aligned}\dot{u} &= \frac{F_x}{m} + r\nu - q\omega \\ \dot{\nu} &= \frac{F_y}{m} - r u + p\omega \\ \dot{\omega} &= \frac{F_z}{m} + q u - p\nu\end{aligned}\tag{A.37}$$

$$\begin{aligned}\dot{\phi} &= \frac{I_z}{I_x I_y - I_{xz}^2} M_x + \frac{I_{xz}}{I_x I_y - I_{xz}^2} M_y + \frac{I_z}{I_x I_y - I_{xz}^2} [(I_y - I_z) r q + I_{xz} p q] \\ &+ \frac{I_{xz}}{I_x I_y - I_{xz}^2} [(I_x - I_y) p q - I_{xz} r q]\end{aligned}$$

$$\dot{\psi} = \frac{1}{I_y} M_y + \frac{1}{I_y} [(I_z - I_x) p r + I_{xz} (r^2 - p^2)]\tag{A.38}$$

$$\begin{aligned}\dot{\eta} &= \frac{I_x}{I_x I_y - I_{xz}^2} M_y + \frac{I_{xz}}{I_x I_y - I_{xz}^2} M_x + \frac{I_{xz}}{I_x I_y - I_{xz}^2} [(I_y - I_z) r q + I_{xz} p q] \\ &+ \frac{I_x}{I_x I_y - I_{xz}^2} [(I_x - I_y) p q - I_{xz} r q]\end{aligned}$$

A.1.2 Trajectory Kinematics

$$\begin{aligned}V_\phi &= u (\cos \Theta \cos \Psi) + \nu (\sin \phi \sin \Theta \cos \Psi - \sin \Psi \cos \phi) \\ &+ \omega (\cos \Psi \cos \phi \sin \Theta + \sin \Psi \sin \phi)\end{aligned}$$

$$\begin{aligned}V_\lambda &= u (\cos \Theta \sin \Psi) + \nu (\sin \Psi \sin \Theta \sin \phi + \cos \Psi \cos \phi) \\ &+ \omega (\sin \Psi \cos \phi \sin \Theta - \cos \Psi \sin \phi) - V_{\Theta r}\end{aligned}\tag{A.41}$$

$$-V_r = u (-\sin \Theta) + \nu (\sin \phi \cos \Theta) + \omega (\cos \phi \cos \Theta)$$

$$V_{or} = \Omega r_{EB} \cos \nu \quad (\text{A.42})$$

$$V_T = \sqrt{V_\lambda^2 + V_\nu^2}; V_T > 0 \quad (\text{A.43})$$

$$V_E = \sqrt{V_r^2 + V_T^2}; V_E > 0 \quad (\text{A.44})$$

$$\nu_T = \sin^{-1} \frac{V_\lambda}{V_T}; \left\{ \begin{array}{l} \text{QUAD.} \\ V_\nu \\ V_\lambda \end{array} \begin{array}{cccc} \text{I} & \text{II} & \text{III} & \text{IV} \\ + & - & - & + \\ + & + & - & - \end{array} \right\} \quad (\text{A.45})$$

$$\nu = \sin^{-1} \frac{V_r}{V_E}; \begin{array}{l} 0 \leq \nu < 90^\circ \text{ for } V_r > 0 \\ 0 \geq \nu > -90^\circ \text{ for } V_r < 0 \end{array} \quad (\text{A.46})$$

$$\dot{\lambda} = V_r \quad (\text{A.48})$$

$$\dot{\nu} = \frac{V_\nu}{r_{EB}} \quad (\text{A.49})$$

$$\dot{\lambda} = \frac{V_\lambda}{r_{EB} \cos \nu} \quad (\text{A.50})$$

$$r_{EB} = R_o + \lambda \quad (\text{A.51})$$

A.1.3 Vehicle Orientation

$$\begin{aligned} \dot{\theta} &= \rho_E + \left(\frac{\sin \theta \sin \Theta}{\cos \Theta} \right) \rho_E + \left(\frac{\cos \theta \sin \Theta}{\cos \Theta} \right) \rho_E - \frac{\dot{\lambda} \cos \nu \cos \nu_T - \dot{\nu} \sin \nu_T}{\cos \Theta} \\ \dot{\theta} &= (\cos \theta) \rho_E - (\sin \theta) \rho_E + \dot{\lambda} \cos \nu \sin \nu_T + \dot{\nu} \cos \nu_T \\ \dot{\nu} &= \left(\frac{\sin^2 \theta \sin \theta}{\cos \Theta} + \cos \theta \sin \theta \right) \rho_E + \left(\frac{\sin^2 \theta \cos \theta}{\cos \Theta} + \cos \theta \cos \theta \right) \rho_E \\ &\quad - \frac{\dot{\lambda} \cos \nu \cos \nu_T \sin \Theta - \dot{\nu} \sin \nu_T \sin \Theta}{\cos \Theta} + \dot{\lambda} \sin \nu \end{aligned} \quad (\text{A.55})$$

$$\begin{aligned}
 p_E &= p - \Omega (\cos \psi \cos \gamma \cos \Theta + \sin \psi \sin \Theta) \\
 q_E &= q + \Omega (\cos \psi \sin \gamma \cos \Theta - \cos \psi \cos \gamma \sin \Theta \sin \phi + \sin \psi \cos \Theta \sin \phi) \\
 r_E &= r - \Omega (\cos \psi \sin \gamma \sin \phi + \cos \psi \cos \gamma \sin \Theta \cos \phi - \sin \psi \cos \Theta \cos \phi)
 \end{aligned}
 \tag{A.57}$$

Details of the vehicle orientation angle switching mechanism are given in Section 3.4.3.

$$\begin{aligned}
 \dot{\phi}_s &= -r_E + \left(\frac{\sin \Theta_s \sin \phi_s}{\cos \Theta_s} \right) q_E + \left(\frac{\sin \Theta_s \cos \phi_s}{\cos \Theta_s} \right) p_E - \frac{\lambda \cos \gamma_s \cos \gamma_s - \dot{\psi} \sin \gamma_s}{\cos \Theta_s} \\
 \dot{\Theta}_s &= (\cos \phi_s) q_E - (\sin \phi_s) p_E + \lambda \cos \gamma_s \sin \gamma_s + \dot{\psi} \cos \gamma_s \\
 \dot{\gamma}_s &= \left(\frac{\sin^2 \Theta_s \sin \phi_s}{\cos \Theta_s} + \cos \Theta_s \sin \phi_s \right) q_E + \left(\frac{\sin^2 \Theta_s \cos \phi_s}{\cos \Theta_s} + \cos \Theta_s \cos \phi_s \right) p_E \\
 &\quad - \frac{\lambda \cos \gamma_s \cos \gamma_s \sin \Theta_s - \dot{\psi} \sin \gamma_s \sin \Theta_s}{\cos \Theta_s} + \lambda \sin \gamma_s
 \end{aligned}
 \tag{A.55a}$$

A.1.4 Relative Wind Kinematics

$$\begin{aligned}
 u_a &= u - W_p (\cos \Theta \cos \gamma) - (V_{or} + W_\lambda) \cos \Theta \sin \gamma - W_r \sin \Theta - u_x \\
 v_a &= v - W_p (\sin \phi \sin \Theta \cos \gamma - \sin \gamma \cos \phi) \\
 &\quad - (V_{or} + W_\lambda) (\sin \gamma \sin \Theta \sin \phi + \cos \gamma \cos \phi) + W_r \sin \phi \cos \Theta - u_y \tag{A.68} \\
 w_a &= w - W_p (\cos \gamma \cos \phi \sin \Theta + \sin \gamma \sin \phi) \\
 &\quad - (V_{or} + W_\lambda) (\sin \gamma \cos \phi \sin \Theta - \cos \gamma \sin \phi) + W_r \cos \phi \cos \Theta - u_z
 \end{aligned}$$

$$V_a = \sqrt{u_a^2 + v_a^2 + w_a^2} ; V_a > 0 \tag{A.69}$$

$$\beta = \sin^{-1} \frac{v_a}{V_a} ; \left\{ \begin{array}{c} \text{QUAD. I II III IV} \\ u_a \quad + \quad - \quad + \\ v_a \quad + \quad + \quad - \quad - \end{array} \right\} \tag{A.70}$$

$$\alpha = \sin^{-1} \frac{w_a}{V_a \cos \beta} ; \begin{array}{l} 0 < \alpha \leq 90^\circ \text{ for } w_a > 0 \\ 0 > \alpha \geq -90^\circ \text{ for } w_a < 0 \\ \alpha = 0 \text{ for } \beta = \pm 90^\circ \end{array} \tag{A.71}$$

$$\begin{aligned} \dot{\omega}_z = & \dot{\omega} + V_{0n} [g_E (\sin \psi \cos \phi \sin \theta - \cos \psi \sin \phi) - r_E (\sin \psi \sin \theta \sin \phi + \cos \psi \cos \phi)] \\ & + \Omega [V_\nu \sin \nu \cos \theta \sin \psi + V_\lambda (\cos \nu \sin \theta - \sin \nu \cos \theta \cos \psi) - V_\mu \cos \nu \cos \theta \sin \psi] \\ & + W_y [g_E (\cos \psi \cos \phi \sin \theta + \sin \psi \sin \phi) - r_E (\sin \phi \sin \theta \cos \psi - \sin \psi \cos \phi) + (\dot{\lambda} \sin \nu \cos \theta \sin \psi + \dot{\nu} \sin \theta)] \\ & + W_x [g_E (\sin \psi \cos \phi \sin \theta - \cos \psi \sin \phi) - r_E (\sin \psi \sin \theta \sin \phi + \cos \psi \cos \phi) + (\dot{\lambda} \cos \nu \sin \theta - \dot{\lambda} \sin \nu \cos \theta \cos \psi)] \\ & + W_n [r_E \sin \theta \cos \theta - g_E \cos \phi \cos \theta - \dot{\nu} \cos \theta \cos \psi - \dot{\lambda} \cos \nu \cos \theta \sin \psi] - \dot{W}_y \cos \theta \cos \psi - \dot{W}_x \cos \theta \sin \psi \\ & - \dot{W}_n \sin \theta - \mu_z \end{aligned}$$

$$\begin{aligned} \dot{\omega}_y = & -\dot{\nu} + V_{0n} [r_E (\cos \psi \sin \theta - \sin \psi \cos \phi \sin \theta) + r_E \cos \theta \sin \psi] + \Omega [V_\nu \sin \nu (\sin \psi \sin \theta \sin \phi + \cos \psi \cos \phi) \\ & - V_\lambda (\cos \nu \sin \theta \cos \theta + \sin \nu \sin \theta \sin \theta \cos \psi - \sin \nu \sin \psi \cos \phi) - V_\mu \cos \nu (\sin \psi \sin \theta \sin \phi + \cos \psi \cos \phi)] \\ & W_y [-r_E (\cos \psi \cos \phi \sin \theta + \sin \psi \sin \phi) + r_E \cos \theta \cos \psi + \dot{\lambda} \sin \nu (\sin \psi \sin \theta \sin \phi + \cos \psi \cos \phi) - \dot{\nu} \sin \theta \cos \theta] \\ & W_x [-r_E (\sin \psi \cos \phi \sin \theta - \cos \psi \sin \phi) + r_E \cos \theta \sin \psi - \dot{\lambda} \sin \nu (\sin \phi \sin \theta \cos \psi - \sin \psi \cos \phi) - \dot{\lambda} \cos \nu \sin \theta \cos \theta] \\ & W_n [r_E (\cos \phi \cos \theta) + r_E \sin \theta - \dot{\nu} (\sin \phi \sin \theta \cos \psi - \sin \psi \cos \phi) - \dot{\lambda} \cos \nu (\sin \psi \sin \theta \sin \phi + \cos \psi \cos \phi)] \\ & - \dot{W}_y (\sin \phi \sin \theta \cos \psi - \sin \psi \cos \phi) - \dot{W}_x (\sin \psi \sin \theta \sin \phi + \cos \psi \cos \phi) + \dot{W}_n \sin \phi \cos \theta - \mu_y \end{aligned}$$

$$\begin{aligned} \dot{\omega}_x = & \dot{\omega} + V_{0n} [-g_E (\cos \theta \sin \psi) + r_E (\sin \psi \sin \theta \sin \phi + \cos \psi \cos \phi)] \\ & - \Omega [V_\nu \sin \nu (\sin \psi \cos \phi \sin \theta - \cos \psi \sin \phi) - V_\lambda [(\sin \nu) (\cos \psi \cos \phi \sin \theta + \sin \psi \sin \phi) + \cos \nu \cos \phi \cos \theta] \\ & - V_\mu \cos \nu (\sin \psi \cos \phi \sin \theta - \cos \psi \sin \phi)] \\ & W_y [-g_E \cos \theta \cos \psi + r_E (\sin \phi \sin \theta \cos \psi - \sin \psi \cos \phi) + \dot{\lambda} \sin \nu (\sin \psi \cos \phi \sin \theta - \cos \psi \sin \phi) - \dot{\nu} \cos \theta \cos \theta] \\ & W_x [-g_E \cos \theta \sin \psi + r_E (\sin \psi \sin \theta \sin \phi + \cos \psi \cos \phi) - \dot{\lambda} \sin \nu (\cos \psi \cos \phi \sin \theta + \sin \psi \sin \phi) - \dot{\lambda} \cos \nu \cos \phi \cos \theta] \\ & - W_n [g_E \sin \theta + r_E \sin \phi \cos \theta + \dot{\nu} (\cos \psi \cos \phi \sin \theta + \sin \psi \sin \phi) + \dot{\lambda} \cos \nu (\sin \psi \cos \phi \sin \theta - \cos \psi \sin \phi)] \\ & - \dot{W}_y (\cos \psi \cos \phi \sin \theta + \sin \psi \sin \phi) - \dot{W}_x (\sin \psi \cos \phi \sin \theta - \cos \psi \sin \phi) + \dot{W}_n \cos \phi \cos \theta - \mu_x \end{aligned}$$

(A.73)

$$\dot{\beta} = \frac{1}{V_a} (-\dot{u}_a \sin \beta \cos \alpha + \dot{w}_a \cos \beta - \dot{v}_a \sin \beta \sin \alpha) \quad (\text{A. 74})$$

$$\dot{\alpha} \cos \beta = \frac{1}{V_a} (-\dot{u}_a \sin \alpha + \dot{w}_a \cos \alpha) \quad (\text{A. 75})$$

$$\begin{aligned} p_a &= p_E = p - \Omega (\cos \nu \cos \psi \cos \theta + \sin \nu \sin \theta) \\ q_a &= q_E = q + \Omega (\cos \nu \sin \psi \cos \theta - \cos \nu \cos \psi \sin \theta \sin \phi + \sin \nu \cos \theta \sin \phi) \\ r_a &= r_E = r - \Omega (\cos \nu \sin \psi \sin \theta + \cos \nu \cos \psi \sin \theta \cos \phi - \sin \nu \cos \theta \cos \phi) \end{aligned} \quad (\text{A. 76})$$

A.1.5 Forces and Moments

$$\begin{aligned} F_{a_x} &= \frac{1}{2} \rho V_a^2 S C_x \\ F_{a_y} &= \frac{1}{2} \rho V_a^2 S C_y \\ F_{a_z} &= \frac{1}{2} \rho V_a^2 S C_z \end{aligned} \quad (\text{A. 79})$$

$$\begin{aligned} M_{a_x} &= \frac{1}{2} \rho V_a^2 S b C_x \\ M_{a_y} &= \frac{1}{2} \rho V_a^2 S c C_y \\ M_{a_z} &= \frac{1}{2} \rho V_a^2 S b C_z \end{aligned} \quad (\text{A. 80})$$

$$\begin{aligned} F_{g_x} &= -m g_0 \left(\frac{R_0}{r_{EB}} \right)^2 \sin \theta \\ F_{g_y} &= m g_0 \left(\frac{R_0}{r_{EB}} \right)^2 \sin \phi \cos \theta \\ F_{g_z} &= m g_0 \left(\frac{R_0}{r_{EB}} \right)^2 \cos \phi \cos \theta \end{aligned} \quad (\text{A. 81})$$

Equations A. 37, A. 38, A. 48, A. 49, A. 50, and A. 55 or A. 55s are simultaneously integrated using numerical methods.

A.2 TRANSFORMATION MATRICES

$$[L_{E3-E}] = [I^N] [\mathcal{V}] [\lambda] = \begin{bmatrix} -\sin \mathcal{V} \cos \lambda & -\sin \mathcal{V} \sin \lambda & \cos \mathcal{V} \\ -\sin \lambda & \cos \lambda & 0 \\ -\cos \mathcal{V} \cos \lambda & -\cos \mathcal{V} \sin \lambda & -\sin \mathcal{V} \end{bmatrix}$$

$$[L_{B-W}] = [\alpha] [\beta] = \begin{bmatrix} \cos \alpha \cos \beta & -\cos \alpha \sin \beta & -\sin \alpha \\ \sin \beta & \cos \beta & 0 \\ \sin \alpha \cos \beta & -\sin \alpha \sin \beta & \cos \alpha \end{bmatrix}$$

$$[L_{B-E3}] = [\phi] [\theta] [\mathcal{V}] = \begin{bmatrix} \cos \theta \cos \mathcal{V} & \cos \theta \sin \mathcal{V} & -\sin \theta \\ (\sin \phi \sin \theta \cos \mathcal{V}) & (\sin \mathcal{V} \sin \theta \sin \phi) & \sin \phi \cos \theta \\ -\sin \mathcal{V} \cos \phi & +\cos \mathcal{V} \cos \phi & \\ (\cos \mathcal{V} \cos \phi \sin \theta) & (\sin \mathcal{V} \cos \phi \sin \theta) & \cos \theta \cos \phi \\ +\sin \mathcal{V} \sin \phi & -\cos \mathcal{V} \sin \phi & \end{bmatrix}$$

$$[L_3] = [I^N] [\phi_s] [\theta_s] [\mathcal{V}_s] = \begin{bmatrix} (\cos \mathcal{V}_s \cos \theta_s \sin \phi_s) & (\sin \mathcal{V}_s \cos \theta_s \sin \phi_s) & \cos \theta_s \cos \phi_s \\ +\sin \mathcal{V}_s \sin \phi_s & -\cos \mathcal{V}_s \sin \phi_s & \\ (\sin \phi_s \sin \theta_s \cos \mathcal{V}_s) & (\sin \mathcal{V}_s \sin \theta_s \sin \phi_s) & \sin \theta_s \cos \phi_s \\ -\sin \mathcal{V}_s \cos \phi_s & +\cos \mathcal{V}_s \cos \phi_s & \\ -\cos \theta_s \cos \mathcal{V}_s & -\cos \theta_s \sin \mathcal{V}_s & \sin \theta_s \end{bmatrix}$$

$ \begin{aligned} & -\sin \psi \cos \lambda (\cos \theta \cos \psi) \\ & -\sin \lambda (\cos \theta \sin \psi) \\ & +\cos \psi \cos \lambda (\sin \theta) \end{aligned} $	$ \begin{aligned} & -\sin \psi \sin \lambda (\cos \theta \cos \psi) \\ & +\cos \lambda (\cos \theta \sin \psi) \\ & +\cos \psi \sin \lambda (\sin \theta) \end{aligned} $	$ \begin{aligned} & -\sin \psi \cos \lambda (\sin \theta \sin \psi) \\ & -\sin \lambda (\cos \theta \sin \psi) \\ & +\cos \psi \cos \lambda (\sin \theta) \end{aligned} $	$ \begin{aligned} & \cos \psi (\cos \theta \cos \psi) \\ & +\sin \psi (\sin \theta) \end{aligned} $
$ \begin{aligned} & -\sin \psi \cos \lambda (\sin \theta \sin \psi) \\ & -\sin \lambda (\cos \theta \sin \psi) \\ & +\cos \psi \cos \lambda (\sin \theta) \end{aligned} $	$ \begin{aligned} & -\sin \psi \sin \lambda (\sin \theta \sin \psi) \\ & +\cos \lambda (\sin \psi \sin \theta \sin \psi) \\ & +\cos \psi \cos \lambda (\sin \theta) \end{aligned} $	$ \begin{aligned} & -\sin \psi \cos \lambda (\sin \theta \sin \psi) \\ & -\sin \lambda (\cos \theta \sin \psi) \\ & +\cos \psi \cos \lambda (\sin \theta) \end{aligned} $	$ \begin{aligned} & \cos \psi (\sin \theta \sin \psi) \\ & -\sin \psi (\cos \theta \sin \psi) \\ & -\sin \psi (\sin \theta \cos \psi) \end{aligned} $
$ \begin{aligned} & -\sin \psi \cos \lambda (\cos \psi \cos \theta \sin \theta) \\ & +\sin \psi \sin \theta \\ & -\cos \psi \cos \lambda (\cos \theta \cos \psi) \end{aligned} $	$ \begin{aligned} & -\sin \psi \sin \lambda (\cos \psi \cos \theta \sin \theta) \\ & +\cos \lambda (\sin \psi \cos \theta \sin \theta) \\ & -\cos \psi \sin \lambda (\cos \theta \cos \psi) \end{aligned} $	$ \begin{aligned} & -\sin \psi \cos \lambda (\cos \psi \cos \theta \sin \theta) \\ & +\sin \psi \sin \theta \\ & -\cos \psi \cos \lambda (\cos \theta \cos \psi) \end{aligned} $	$ \begin{aligned} & \cos \psi (\cos \psi \cos \theta \sin \theta) \\ & +\sin \psi \sin \theta \\ & -\sin \psi (\cos \theta \cos \psi) \end{aligned} $

$$[L_{B-C}] = [Y][\theta][\psi][\lambda][\chi]$$

APPENDIX B
EXTENSION OF THE EQUATIONS TO LARGE
THRUST AND VARIABLE MASS

Equations of motion derived in Section III of this report are restricted to a rigid, constant-mass, re-entry glider. In this appendix equations are developed to describe the motion of a booster-glider combination. The general vector equations of motion for a jet-propelled body of varying mass are presented in integral form in Section B.1. Application of the general equations is outlined in Section B.2, where the various integrals are evaluated by making use of reasonable approximations, and a variety of problems related to use of the equations are discussed.

B.1 THE GENERAL VECTOR EQUATIONS

In Reference B.1* there are presented the full details of a derivation of the general equations of motion for a jet-propelled body of varying mass. Here in this appendix only pertinent assumptions, final results, and a minimum of detail are presented.

A body of constant volume T whose surface area S has fixed size and shape is assumed**. Mass density ρ is variable within the body, a function of time and location. Associated with the body is a reference frame x, y, z which is fixed relative to the body and with origin at some arbitrary point O . This frame will later be identified as the body axis frame of Section III.

The linear and angular momentum equations of fluid mechanics can be applied by considering the surface of the body to be a control surface encompassing a region of space, the body itself:

$$\sum \bar{F} = \frac{d}{dt} \int_T \rho (\bar{V} + \bar{\omega} \times \bar{R} + \bar{v}_R) d\tau + \oint_S \rho (\bar{V} + \bar{\omega} \times \bar{R} + \bar{v}_R) (\bar{v}_R \cdot \bar{n}) d\sigma \quad (B.1)$$

$$\begin{aligned} \sum \bar{M}_T = \frac{d}{dt} \int_T \rho [\bar{r}_{i0} \times (\bar{V} + \bar{\omega} \times \bar{R} + \bar{v}_R)] d\tau \\ + \oint_S \rho [\bar{r}_{i0} \times (\bar{V} + \bar{\omega} \times \bar{R} + \bar{v}_R)] (\bar{v}_R \cdot \bar{n}) d\sigma \end{aligned} \quad (B.2)$$

With the exception of definitions given below, the notation is consistent with that elsewhere in the report:

- \bar{R} position vector of any particle relative to body axes,
- $\bar{v}_R = (\dot{\bar{R}})_0$ velocity vector of any particle relative to body axes,
- \bar{n} unit normal vector to surface S , directed outward,

* Other sources of similar, but not so general, derivations are listed in Reference B.1.

** Although these assumptions are not strictly essential, they afford considerable simplification in the derivation.

- $\sum \bar{F}$ summation of all external surface and volume forces acting on the body,
- $\sum \bar{M}_I$ summation of all external moments on the body about the origin of the inertial frame,
- $\frac{d}{dt}$ differentiation relative to the inertial frame,
- $\left(\frac{d}{dt}\right)_B = (\dot{})_B$ time differentiation relative to body axes,
- $\int_V () d\tau$ volume integral over the volume contained by S ,
- $\oint_S () d\sigma$ surface integral over closed surface S .

In the terminology of fluid mechanics, the volume integral in each equation is called the "nonstationary" term and the surface integral is called the "convective" term.

By using the definition of the mass of the body

$$m \triangleq \int_V \rho d\tau \tag{B.3}$$

and the definition of net mass efflux

$$Q \triangleq \oint_S \rho (\bar{v}_R \cdot \bar{n}) d\sigma \tag{B.4}$$

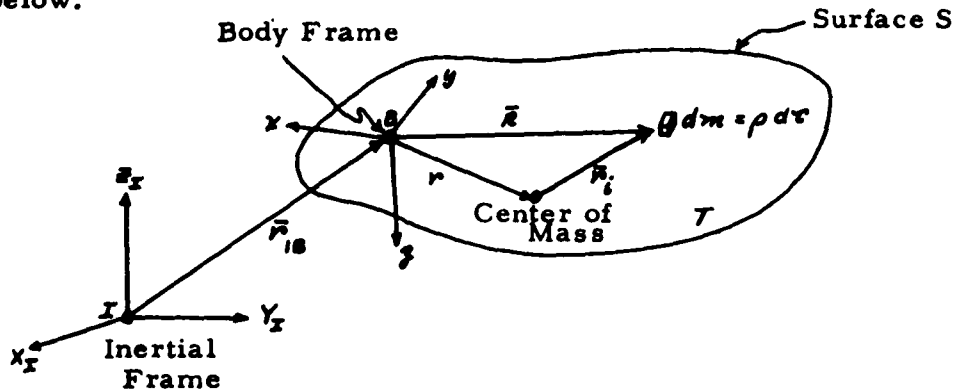
Equation B.1 can be simplified somewhat to read:

$$\begin{aligned} \sum \bar{F} = m \frac{d\bar{v}}{dt} + m \frac{d^2 \bar{r}_c}{dt^2} + (\dot{\bar{r}}_c)_B \dot{m} + \oint_S \rho \bar{v}_R (\bar{v}_R \cdot \bar{n}) d\sigma \\ + \left(\frac{d}{dt} \oint_S \rho \bar{r}_i (\bar{v}_R \cdot \bar{n}) d\sigma \right)_B + 2 \bar{\omega} \times \oint_S \rho \bar{r}_i (\bar{v}_R \cdot \bar{n}) d\sigma \end{aligned} \tag{B.5}$$

In this equation, the following new notation is used:

- \bar{r}_c position vector of center of mass relative to body axes
- \bar{r}_i position vector of any particle in the body relative to the center of mass

These vectors and some of those defined previously are depicted in the sketch below.



The summation of forces on the left-hand side of Equation B.1 includes many surface and volume (body) forces of which only gravity and surface pressures are considered here. The forces can be written as

$$\int_V \rho \bar{g} d\tau + \oint_S -p \bar{n} d\sigma = \sum \bar{F} \quad (\text{B.6})$$

in which these definitions apply:

- \bar{g} gravitational force per unit mass (acceleration of gravity) which is assumed to be uniform throughout the body
- p pressure acting on outside of surface S .

The pressure, p , can be broken down into two parts:

$$p = p_A + (p - p_A) \triangleq p_A + \Delta p \quad (\text{B.7})$$

in which p_A is the ambient (atmospheric) pressure assumed uniform everywhere in the immediate vicinity of the body. Thus, since p_A is uniform over S , the surface integral over S of p_A is zero, and Equation B.6 becomes

$$m \bar{g} + \oint_S -\Delta p \bar{n} d\sigma \triangleq \sum \bar{F} \quad (\text{B.8})$$

In Equation B.8 it is possible to identify the integral of Δp over S as the aerodynamic force on the body provided other surface forces, which are implicit in the integral, are zero. Further evaluation of the pressure integral requires specific information regarding the vehicle to which the integral is applied.

The result of the evaluation of Equation B.1 is

$$\begin{aligned} m \bar{g} + \oint_S -\Delta p \bar{n} d\sigma &= m \left[\frac{d\bar{V}}{dt} + \frac{d^2 \bar{r}_c}{dt^2} \right] + \dot{m} (\dot{\bar{r}}_c)_B + \oint_S \rho \bar{v}_R (\bar{v}_R \cdot \bar{n}) d\sigma \\ &+ \left(\frac{d}{dt} \oint_S \rho \bar{r}_i (\bar{v}_R \cdot \bar{n}) d\sigma \right)_B + 2 \bar{\omega} \times \oint_S \rho \bar{r}_i (\bar{v}_R \cdot \bar{n}) d\sigma \end{aligned} \quad (\text{B.9})$$

Equation B.2, the moment equation, can be made more meaningful by modifying it so that the summation of moments is about the body axes origin, $\sum \bar{M}_B$:

$$\begin{aligned} \sum \bar{M}_B &= \sum \bar{M}_I - \bar{r}_{i0} \times \sum \bar{F} , \\ \sum \bar{M}_B &= \frac{d}{dt} \int_V \rho \left[\bar{R} \times (\bar{V} + \bar{\omega} \times \bar{R} + \bar{v}_R) \right] d\tau + \bar{V} \times \int_V \rho (\bar{V} + \bar{\omega} \times \bar{R} + \bar{v}_R) d\tau \\ &+ \oint_S \rho \left[\bar{R} \times (\bar{V} + \bar{\omega} \times \bar{R} + \bar{v}_R) \right] (\bar{v}_R \cdot \bar{n}) d\sigma \end{aligned} \quad (\text{B.10})$$

Following techniques analogous to those used with the force equation and using Definitions B.3 and B.4, Equation B.10 can be simplified:

$$\begin{aligned} \sum \bar{M}_B &= \bar{r}_i \times m \frac{d\bar{V}}{dt} + \frac{d}{dt} \int_T \rho [\bar{R} \times (\bar{\omega} \times \bar{R})] d\tau + \frac{d}{dt} \int_T \rho \bar{R} \times \bar{v}_R d\tau \\ &+ \oint_S \rho [\bar{R} \times (\bar{\omega} \times \bar{R})] (\bar{v}_R \cdot \bar{n}) d\sigma + \oint_S \rho (\bar{R} \times \bar{v}_R) (\bar{v}_R \cdot \bar{n}) d\sigma \end{aligned} \quad (B.11)$$

Except for the fact that ρ is not constant, the first two terms are those which apply to a rigid body whose moment equation is evaluated relative to an arbitrary point (Reference 3.1). The last three integrals, due entirely to internal mass motion and mass-efflux, would vanish for a rigid body.

The left-hand side of Equation B.2 consists of the summation of moments due to all surface and volume forces acting on the body. As before, only the forces due to gravity and surface pressures are considered; in addition, it should be noted that ambient pressure produces no moment:

$$\bar{r}_i \times m \bar{g} + \bar{r}_i \times \oint_S -\Delta p \bar{n} d\sigma + \oint_S -\bar{r}_i \times \Delta p \bar{n} d\sigma \hat{=} \sum \bar{M}_B \quad (B.12)$$

Then, after combining Equations B.11 and B.12, the resulting moment equation is

$$\begin{aligned} \bar{r}_i \times m \bar{g} + \bar{r}_i \times \oint_S -\Delta p \bar{n} d\sigma + \oint_S -\bar{r}_i \times \Delta p \bar{n} d\sigma &= \bar{r}_i \times m \frac{d\bar{V}}{dt} \\ &+ \frac{d}{dt} \int_T \rho [\bar{R} \times (\bar{\omega} \times \bar{R})] d\tau + \frac{d}{dt} \int_T \rho \bar{R} \times \bar{v}_R d\tau \\ &+ \oint_S \rho [\bar{R} \times (\bar{\omega} \times \bar{R})] (\bar{v}_R \cdot \bar{n}) d\sigma + \oint_S \rho (\bar{R} \times \bar{v}_R) (\bar{v}_R \cdot \bar{n}) d\sigma \end{aligned} \quad (B.13)$$

The first term on the left-hand side of the equation is the gravitational moment about point B. The two surface integrals on the left-hand side would be the moment about B due to aerodynamic pressure if there were no other pressures (distributed or concentrated forces) acting on the surface of the body.

B.2 APPLICATION OF EQUATIONS TO ROCKET VEHICLES

In this section, a short discussion is presented to facilitate application of the equations of motion developed in the preceding section. A rocket vehicle is chosen as the vehicle of interest. It consists of a glider attached to two booster stages which eventually separate away from the glider during the initial phase of flight.

The development of equations throughout this report has been directed toward a description of the glider's motion; the objective is the same here. Equations B.9 and B.13 are written for the motion of the reference frame whose origin is B and which is fixed relative to a body of varying mass. If this

reference frame is identified as the body axes frame of Section III, the equations of motion developed in this appendix describe the motion of the glider in terms of translation of its center of mass (B) and rotation about its center of mass. In addition to interest in the glider's motion, it is desirable to use a reference frame which is fixed relative to a body because forces and moments are more easily described. Specifically, the origin of the body axes frame is the glider's center of mass (assumed fixed); the x axis is directed toward the nose of the vehicle, the z axis is directed downward, and the y axis is directed toward the right.

B.2.1 Evaluation of the Remaining Surface and Volume Integrals

Equations B.9 and B.13 contain surface and volume integrals which must be evaluated; otherwise, the equations are not very useful as equations of motion. Evaluation is made for a rocket-propelled vehicle.

The assumed planar and circular cross-sectional area (A_e) of the exit end of a rocket motor is the only area which need be considered in the surface integrals. No mass enters or leaves the vehicle elsewhere. It is assumed that \bar{n}_e over the exit plane can be replaced with an effective value \bar{n}_e which is uniform in magnitude and direction. The vector \bar{r}_i over the exit plane can be replaced with a vector \bar{r}_e directed to the effective "center" of the exit plane and a vector $\Delta\bar{r}$ directed from the effective "center" to any other location in the exit plane:

$$\bar{r}_i \text{ EXIT PLANE} = \bar{r}_e + \Delta\bar{r} \tag{B.14}$$

The effective "center" is defined such that

$$\int_{A_e} \rho \bar{r}_i (\bar{n}_e \cdot \bar{n}) d\sigma = \bar{r}_e Q + \int_{A_e} \rho \Delta\bar{r} (\bar{n}_e \cdot \bar{n}) d\sigma = \bar{r}_e Q \tag{B.15}$$

However, when $\Delta\bar{r}$ appears twice in a triple vector product (see Equation B.13, first surface integral on right-hand side), the integral containing this product does not vanish. Reference B.1 shows details of the evaluation for this case in terms of the radius of gyration of the exit plane.

Equation B.13 contains the volume integral, $\frac{d}{dt} \int_V \rho \bar{r} \times \bar{n}_e d\tau$ which can be separated into two parts using \bar{r}_e and \bar{r}_i , but this process leads to many small terms involving \bar{r}_e and its derivatives in addition to the integral $\frac{d}{dt} \int_V \rho \bar{r}_i \times \bar{n}_e d\tau$ which is really just as bad as the original integral involving \bar{r} . The original integral cannot be considered always unimportant because it includes the effects of internal rotating parts, fuel sloshing, etc. Without any knowledge of the internal motion in the rocket vehicle, nothing can be said about the value of the integral; therefore, it will be carried along as it is.

The exit-plane portion of each pressure integral in Equations B.9 and B.13 is usually considered part of the total thrust force or moment due to the rocket motor. It is assumed that the exit pressure (p_e) of the rocket motor is effectively uniform over the exit plane; thus

$$\int_{A_e} -(p_e - p_a) \bar{n} d\sigma = (p_a - p_e) \bar{n} A_e \tag{B.16}$$

The remainder of each pressure integral is now defined as an aerodynamic force or moment, as the case may be. Evaluation is usually made in terms of experimentally or theoretically derived aerodynamic coefficients (e.g., see Section 4.3).

Making use of the assumptions described in the three paragraphs above, Equations B.9 and B.13 can be written in more meaningful forms. The force equation is:

$$\begin{aligned} \bar{F}_g + \bar{F}_a + \bar{F}_T = & \kappa [(\dot{V})_B + \bar{\omega} \times \bar{V}] \\ & + \kappa [(\dot{\bar{r}}_c)_B + \dot{\bar{\omega}} \times \bar{r}_c + 2\bar{\omega} \times (\dot{\bar{r}}_c)_B + \bar{\omega} \times (\bar{\omega} \times \bar{r}_c)] + \kappa (\dot{\bar{r}}_c)_B \end{aligned} \quad (B.17)$$

in which $\bar{F}_g = \kappa \bar{g}$

$$\bar{F}_a = \int_{S-A_0} -\Delta p \bar{n} d\sigma \quad (B.18)$$

$$\bar{F}_T = -Q [\bar{r}_c + 2\bar{\omega} \times \bar{r}_c + (\dot{\bar{r}}_c)_B] - \bar{r}_c \dot{Q} + (p_A - p_B) \bar{n}_e A_0 \quad (B.19)$$

The moment equation becomes:

$$\begin{aligned} \bar{M}_g + \bar{M}_a + \bar{M}_T = & \kappa \bar{r}_c \times [(\dot{V})_B + \bar{\omega} \times \bar{V}] + \frac{d}{dt} \int_V \rho \bar{R} \times \bar{r}_R d\tau \\ & + (\dot{\bar{I}})_B \bar{\omega} + \bar{\omega} \times \bar{I}' \bar{\omega} + \bar{I}' \dot{\bar{\omega}} \end{aligned} \quad (B.20)$$

in which $\bar{M}_g = \kappa \bar{r}_c \times \bar{g}$

$$\bar{M}_a = \bar{r}_c \times \int_{S-A_0} -\Delta p \bar{n} d\sigma + \int_{S-A_0} \bar{r}_i \times \Delta p \bar{n} d\sigma \quad (B.21)$$

$$\begin{aligned} \bar{M}_T = & -Q [\bar{r}_{B_0} \times (\bar{\omega} \times \bar{r}_{B_0}) + \frac{1}{2} k_e^2 (\bar{\omega} + \omega_x \bar{e}_x) + \bar{r}_{B_0} \times \bar{v}_e] \\ & + \bar{r}_{B_0} \times (p_A - p_B) \bar{n}_e A_0 \end{aligned} \quad (B.22)$$

Certain symbols and notation used in these equations must be defined:

- \bar{r}_c position vector from center of mass to effective center of exit area
- \bar{n}_e unit normal to exit plane; positive outward
- \bar{v}_e effective value of \bar{v}_R over exit plane, or exit velocity; positive outward
- \bar{r}_{B_0} position vector of effective center of exit plane relative to point B ($\bar{r}_{B_0} = \bar{r}_c + \bar{r}_e$)

- \bar{I}' moment of inertia tensor of the entire vehicle (booster and glider) relative to point B
- k_e radius of gyration of exit area ($k_e = \frac{1}{\sqrt{A_e}}$ radius of exit area)
- $\omega_x \bar{e}_x$ component of $\bar{\omega}$ in x body axis direction; \bar{e}_x is unit vector and $\omega_x \equiv \dot{\phi}$, the rolling velocity
- $\int_{S-A_e} () d\phi$ surface integral over entire surface of vehicle except the exit area A_e

B.2.2 Obtaining the Desired Accelerations

At this point, the force equations would be solved for $(\dot{V})_B$ and the moment equation for $\bar{\omega}$ as is done with Equations 3.35 and 3.36; however, inspection shows that both $(\dot{V})_B$ and $\bar{\omega}$ appear in both Equations B.17 and B.20. Therefore, Equations B.17 and B.20 must be solved simultaneously for $(\dot{V})_B$ and $\bar{\omega}$.

Simultaneous solution of Equations B.17 and B.20 results in both \bar{F} and \bar{M} appearing in each of the equations for $(\dot{V})_B$ and $\bar{\omega}$, which precludes the use of aerodynamic derivatives such as $C_{L\dot{\alpha}}$, $C_{y\dot{\beta}}$, $C_{m\dot{\alpha}}$, or any other derivative whose application depends somehow on the linear and angular accelerations ($(\dot{V})_B$ and $\bar{\omega}$). If the affected derivatives are modified to be used with the linear and angular accelerations explicitly (e.g., components \dot{w}_a , \dot{v}_a , etc. instead of $\dot{\alpha}$, $\dot{\beta}$, etc. respectively), then again Equations B.17 and B.20 can be solved for $(\dot{V})_B$ and $\bar{\omega}$. This is, however, easier said than done: Vectors $(\dot{V})_B$ and $\bar{\omega}$ are rates of change of inertial velocities relative to the body axis frame whereas the pertinent aerodynamic derivatives are with respect to the rates of change of the vehicle's linear and angular velocities relative to the air, vectors $(\dot{V})_a$ and $\bar{\omega}_a$. It may prove more reasonable, if not necessary, to neglect all aerodynamic derivatives such as those mentioned above. In Section III of this report, it is shown that without special treatment such as an iteration, the equation for $[\dot{V}]$ (Equation 3.37) cannot contain derivatives with respect to $\dot{\alpha}$ and $\dot{\beta}$ but, because of $\dot{\alpha}$ and $\dot{\beta}$ do not depend on $[\dot{\omega}]$, derivatives involving $\dot{\alpha}$ and $\dot{\beta}$ can be used in Equation 3.38 for $[\dot{\omega}]$. The situation is worse in Equations B.17 and B.20. These equations must be solved for $[\dot{V}]$ and $[\dot{\omega}]$ and, since both $[F]$ and $[M]$ appear in the equation for $[\dot{V}]$, even the moment derivatives with respect to $\dot{\alpha}$ and $\dot{\beta}$ (which are more important than the analogous force derivatives) cannot be used without special treatment.

B.2.3 Data for the Combined Booster-Glider Vehicle

In Equations B.17 and B.20, center of mass location (\bar{r}_c) and the moment of inertia tensor (\bar{I}') are required in terms of instantaneous mass:

$$\begin{aligned} \bar{r}_c &= \bar{r}_c(m) \\ \bar{I}' &= \bar{I}'(m) \end{aligned} \tag{B.23}$$

The specific form of Equations B.23 may be either functional or tabular and, in fact, reasonably smooth tabular data can be curve fit if desired. At any instant, mass is given by numerically integrating $\dot{m} = -Q$:

$$m = m_0 - \int_0^t Q dt \quad (\text{B.24})$$

Equations B.17 and B.20 also contain first derivatives of \bar{r}_c and \dot{I}' which can be obtained directly by numerical differentiation with respect to time, or indirectly by either functional or numerical differentiation with respect to mass (depending upon the form of Equations B.23) according to the scheme:

$$\begin{aligned} (\dot{\bar{r}}_c)_B &= \left(\frac{d\bar{r}_c}{dm} \right) \dot{m} \\ (\dot{I}')_B &= \left(\frac{dI'}{dm} \right) \dot{m} \end{aligned} \quad (\text{B.25})$$

The second derivative of center of mass location, $(\ddot{\bar{r}}_c)_B$, can be easily found by numerically differentiating $(\dot{\bar{r}}_c)_B$, whereas a scheme similar to that shown in Equations B.25 is more difficult because $(\ddot{\bar{r}}_c)_B$, unlike $\ddot{\bar{r}}_c$, is a function of both m and \dot{m} . Fortunately, the velocity and acceleration of the center of mass relative to the body are small; therefore, inaccuracy in the numerical differentiation is of little consequence.

The quantities pertaining to rocket motor operation ($Q = -\dot{m}$, \dot{Q} , \bar{r}_e , ρ_e , etc.) can be related using equations governing the injection, combustion, and expansion of the propellant gases. However, a useful expedient for situations not requiring utmost accuracy is to treat the mass flow rate as a function of throttle position.

$$Q = Q(S_T)$$

Such dependency is useful if the rocket thrust magnitude is controlled by a pilot or, lacking a pilot, S_T can be made a function of time or some other variable. The quantity \dot{Q} may then be obtained by numerical differentiation of Q with respect to time.

Equations B.18 and B.21 represent integral forms of the aerodynamic force and moment respectively which, as stated previously, may be evaluated in any desirable manner, but most probably by using the method described in Section 4.3. It must be remembered that during the boost phase of the flight each separation of a stage changes radically the over-all aerodynamic representation of remaining portions of the vehicle; therefore, effects of separation must be considered in the evaluation of Equations B.18 and B.21.

B.3 REFERENCES

- B.1 Pritchard, Francis E.: General Vector Equations of Motion for a Jet-Propelled Body of Varying Mass. Cornell Aeronautical Laboratory FDM No. 322, October 1961.

APPENDIX C
EXTENSION OF EQUATIONS FOR EARTH OBLATENESS
AND SURFACE ABERRATIONS

C.1 EXTENSION FOR FIRST-ORDER OBLATENESS

It is assumed in Section III that a spherical representation of the earth is entirely adequate for purposes of re-entry flight simulation. This implies that both the geometric and gravitational effects of oblateness are negligible. Consequently, the simulation equations for earth size, shape, and gravitational field are fewer and simpler providing a substantial saving of digital computation time. This saving is certainly a desirable feature of the spherical earth representation.

The models which constitute adequate representation of the earth's size, shape, and gravitational field are determined by the scope and purpose of the flight simulation. Simulation of the boost and orbital phases of a vehicle such as Dyna-Soar probably requires an oblate representation of the earth, while the re-entry phase can be adequately represented using a spherical-earth model. In the event that the more precise representation may be needed, the process for inclusion of earth oblateness with the equations of motion is developed here to first-order accuracy.

Inclusion of earth oblateness should generally result in both geometric and gravitational effects although it is not really necessary to include both. The development in Section C.1.1 and C.1.2 implies that the two effects can be separated for simulation purposes if desired. The geometric effects are, roughly speaking, larger than the gravitational effects so that it might be desirable to include the former but not the latter.

Geometric effects can be arbitrarily divided into three groups:

1. Location of vehicle—latitude, longitude and altitude
2. Atmospheric models—density, temperature, etc.
3. Vehicle orientation—the Euler angles

Longitude is unaffected because the oblate shape of the earth is axially symmetric. Latitude is different by no more than about 0.2° , a small angle; but in terms of distance on the earth's surface, this corresponds to about 12 nautical miles. Altitude is much different from that of the mean spherical earth. For a given constant distance from the center of the earth the oblate earth causes the altitude to be greater by about 47,000 ft at the poles and smaller by about 26,000 ft at the equator when the spherical-earth radius of Equation 2.3 is used for comparison. If altitude above the oblate earth is used with the models of atmospheric properties given in Section II, these properties become "oblate" to conform with the earth's shape. The Euler angles are affected only slightly, the largest effect being less than 0.2° for any of the angles; but, since these angles are used in coordinate transformations, the slight effect should be considered important. There are numerous sources for further information on the effects of oblateness; References C.4, C.5, and C.6 are examples.

C.1.1 Earth Size and Shape

The earth is assumed to be oblate spheroidal; that is, it is an ellipsoid of revolution whose radius ($R_{\theta\theta}$) at any geocentric latitude (ψ) is (an alternate form of Equation 2.2)

$$R_{\theta\theta} = \frac{a(1-\epsilon)}{\sqrt{1-(2\epsilon-\epsilon^2)\cos^2\psi}} \quad (C.1)$$

For this equation: (data from Reference 2.3)

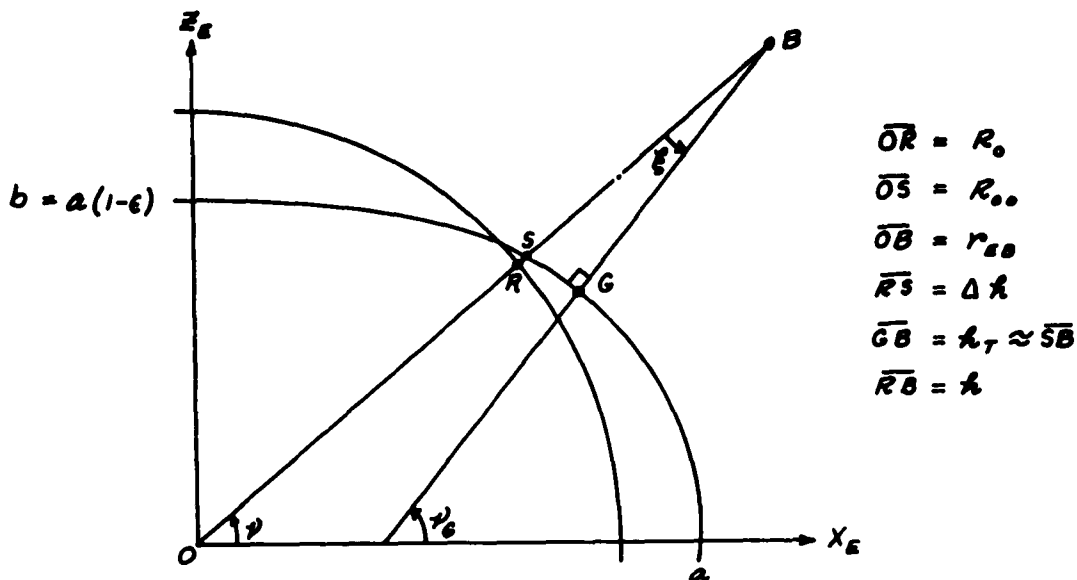
a , the equatorial radius = 6,378,163 meters = 20,925,732 ft

ϵ , the flattening = $\frac{a-b}{a} = \frac{1}{298.24}$

A first-order approximation in ϵ for $R_{\theta\theta}$ can be obtained in the form:

$$R_{\theta\theta} \approx a(1-\epsilon \sin^2 \psi) \quad (C.2)$$

Geocentric latitude (ψ), geodetic latitude (ψ_G), and the true altitude (h_T) are defined by the sketch below.



The quantities to be obtained are ψ_G and line $GB = h_T$ in terms of ψ , a , and ϵ which are known. This is done by developing corrections for ψ and h , the variables ordinarily computed. Reference C.2 supplies expressions for $\psi_G - \psi \equiv \xi$ and h_T but using notation different from this appendix. Equation 4 of Reference C.2 is a series expansion for ξ which is modified and simplified to result in the equation:

$$\xi = a\epsilon \frac{\sin 2\psi}{r_{\theta\theta}} \quad (C.3)$$

This expression has an error of less than $\pm 0.5\%$ when compared with the more precise expression in Reference C.4 and should, therefore, be adequate for simulator use.

Refer to the sketch above. Line \overline{CB} is the true altitude, h_T . The radius of the oblate earth at geocentric latitude, ψ , is $\overline{OS} = R_o$. Altitude, $\overline{RB} = h$, is computed from the equations of motion of Section III. The altitude along the position vector \overline{OB} is $\overline{SB} = \overline{RB} - \overline{RS}$. It can be shown, by comparison with the altitude computed from Equation 6 of Reference C.2, that $\overline{SB} \approx h_T$ with an error less than $\pm 0.1\%$. Now, this means that a correction, $\overline{RS} = \Delta h$, which is the difference between the oblate-earth radius and the mean spherical-earth radius (as used in Section III) can be added to the altitude, h , to obtain the altitude, h_T , above the local surface of the oblate earth. The following equations define this process:

$$\Delta h = R_{o0} - R_o \quad (C.4)$$

$$\Delta h = (a - R_o) - a_6 \sin^2 \psi \quad (C.5)$$

$$h_T = h + \Delta h \quad (C.6)$$

The mean spherical-earth radius is given by Equation 2.3.

Methods for correcting spherical-earth latitude and altitude for oblateness are discussed in Section C.1.3. Further information on the problem of vehicle position relative to the oblate earth is presented by Reference C.1 in a development similar to that given here.

C.1.2 Gravitational Acceleration and Force

The gravitational potential function is given by Equation 2.5, but is repeated here for convenience:

$$U = \frac{Gm_o}{r_{EB}} \sum_{n=0}^{\infty} J_n \left(\frac{a}{r_{EB}} \right)^n P_n \quad (C.7)$$

in which P_n is the n^{th} degree Legendre polynomial in $\sin \psi$.

$$a = 6,378,163 \text{ meters} = 20,925,732 \text{ ft}$$

$$J_0 = 1$$

$$J_1 = 0$$

$$J_2 = -1082.61 \times 10^{-6}$$

$$J_3 = +2.05 \times 10^{-6}$$

$$J_4 = +1.43 \times 10^{-6}$$

$$Gm_o = 3.98602 \times 10^{14} \frac{\text{meters}^3}{\text{sec}^2} = 1.40765 \times 10^{16} \text{ ft}^3/\text{sec}^2$$

The second degree Legendre polynomial will be used later; it is:

$$P_2 = \frac{1}{2} (3 \sin^2 \nu - 1) \quad (\text{C. 8})$$

A listing of Legendre polynomials and their properties is given by Jahnke and Emde, Reference C.3.

The gradient of the scalar potential function is the vector acceleration of gravity, thence the force is given by the product of mass and acceleration:

$$\bar{g} = \bar{\nabla} U \quad (\text{C. 9})$$

$$\bar{F}_g = m \bar{\nabla} U \quad (\text{C. 10})$$

The operator $\bar{\nabla}$ must be expressed in terms of a particular coordinate frame, here the spherical* coordinate frame is chosen:

$$\bar{\nabla} = \frac{1}{r_{EB}} \frac{\partial}{\partial \nu} \bar{e}_\nu + \frac{1}{r_{EB} \cos \nu} \frac{\partial}{\partial \lambda} \bar{e}_\lambda - \frac{\partial}{\partial r_{EB}} \bar{e}_r \quad (\text{C. 11})$$

in which \bar{e}_ν , \bar{e}_λ , and \bar{e}_r are unit vectors in that reference frame. The components of \bar{g} are then obtained in the same frame.

Using only the second harmonic which is adequate for simulation, the following matrix equation for components of \bar{F}_g in spherical axes results from Equation C.10:

$$[(F_g)_{sph}] = m [\nabla U] = m \begin{bmatrix} \frac{3}{2} \frac{G m_\oplus}{r_{EB}^2} J_2 \left(\frac{a}{r_{EB}} \right)^2 \sin 2\nu \\ 0 \\ \frac{G m_\oplus}{r_{EB}^2} \left\{ 1 + \frac{3}{2} J_2 \left(\frac{a}{r_{EB}} \right)^2 (3 \sin^2 \nu - 1) \right\} \end{bmatrix} \quad (\text{C. 12})$$

Here the matrix $[\nabla U]$ represents the components of the vector $\bar{\nabla} U$ in the spherical coordinate frame. Equation C.12 should be used to replace the corresponding equation of Section III.

* In this appendix, the term "spherical" denotes the frame previously called "earth-surface" in Section III. This usage is explained in the fourth paragraph of Section C.1.3 which follows.

C. 1. 3 Modification of Equations of Motion to Include Oblateness

This section discusses ways to incorporate earth oblateness corrections to the equations of motion developed in Section III. Certain concepts presented in Sections C. 1. 1 and C. 1. 2 are used in addition to, or to modify, the equations of Section III. The result is an adequate first-order representation of oblateness.

What variables are used? The vehicle's six inertial velocities ($u, v, w; p, q, r$) are retained. The variables $\mathcal{R}, \lambda, \nu$ are essentially spherical position coordinates which, of necessity, are retained. Relative to the local surface of the oblate earth, the vehicle's angular position is given by the new Euler angles (ψ_e, θ_e, ϕ_e). These twelve are the variables chosen for simultaneous numerical integration.

Position of the vehicle relative to the oblate earth is described by the pseudo-spherical coordinates ($\mathcal{R}, \lambda, \nu$) appropriately modified. True altitude (\mathcal{R}_T) is obtained by adding the correction ($\Delta\mathcal{R}$) of Equation C. 5 to the given altitude (\mathcal{R}). In like manner, geodetic latitude (ν_e) is obtained by adding the correction (ξ) calculated using Equation C. 3 to the geocentric latitude (ν). Longitude (λ) is unaffected by oblateness. Thus, vehicle position is simply handled.

The earth-surface (ES) reference frame has been previously defined as the frame whose z_{ES} axis is directed downward and normal to local (smoothed) surface of the earth; x_{ES} axis is directed northward; y_{ES} axis is directed eastward. The $x_{ES} - y_{ES}$ plane is then parallel to the local earth's surface. In Section III the earth-surface axes were associated with a spherical model of the earth, while in this appendix the earth-surface axes are associated with an oblate-earth model. Consequently, the earth-surface frame here is not the same as that of Section III. Since certain variables in this appendix must be expressed in spherical coordinates, the earth-surface (ES) frame of Section III is retained, but denoted differently as the spherical (SPH) frame. Then, the frame associated with the oblate earth is denoted as the earth-surface (ES) frame to be consistent with the definition of that frame given above. The origin of each frame is the same point (B), the center of mass of the vehicle, and the y_{SPH} axis is collinear with the y_{ES} axis. This new notation should be carefully observed throughout the remainder of this appendix.

Transformation from the spherical (SPH) axes to the earth-surface (ES) axes is obtained by using

$$[\xi] = \begin{bmatrix} 1 & 0 & \xi \\ 0 & 1 & 0 \\ -\xi & 0 & 1 \end{bmatrix} \quad (C. 13)$$

Here the small angle approximation for sines and cosines is valid because ξ is always less than 0.2° . The complete transformation from earth (E) axes to body (B) axes is

$$[L_{B-E}] = [L_{B-SPN}] [L_{SPN-E}] = [\phi_0] [\theta_0] [\gamma_0] [\xi] [I''] [\mathcal{V}] [\lambda] \quad (C. 14)$$

where

$$[L_{B-SPN}] = [\phi_0] [\theta_0] [\gamma_0] [\xi] \quad (C. 15)$$

The transformation $[L_{B-SPN}]$ here defined is identically the $[L_{B-ES}]$ transformation of Section III except that here it is denoted differently and consists of four consecutive rotations. A further definition is made for convenience.

$$[L_{B-ES}] = [\phi_0] [\theta_0] [\gamma_0] \quad (C. 16)$$

This new $[L_{B-ES}]$ matrix transforms vector components from the earth-surface frame to the body frame.

The velocity of the vehicle relative to the earth must be calculated in two ways. First, in order that the pseudo-spherical coordinates may be obtained, the vector $[V_E]$ is calculated in spherical (SPN) axes. The components of this vector, $[(V_E)_{SPN}]$, are required for computation of $\dot{\lambda}$, $\dot{\lambda}$, and $\dot{\mathcal{V}}$ from Equations 3.48, 3.49 and 3.50 respectively. The magnitude (r_{EB}) of the position vector, needed for Equations 3.49 and 3.50, is computed by adding altitude (\mathcal{H}) to the mean radius (R_0) of the spherical earth. Second, the relative velocity $[(V_E)_{ES}]$ in earth-surface axes is obtained as

$$[(V_E)_{ES}] = [\xi] [(V_E)_{SPN}] \quad (C. 17)$$

The Euler angles ($\dot{\phi}_0$, $\dot{\theta}_0$, $\dot{\gamma}_0$) are obtained by integrating an equation identical in form with Equation 3.55:

$$[\dot{E}_{B-ES}] = \begin{bmatrix} \dot{\phi}_0 \\ \dot{\theta}_0 \\ \dot{\gamma}_0 \end{bmatrix} = [A_0] [\omega_E] - [B_0] \begin{bmatrix} 0 \\ -\dot{\mathcal{V}} \\ \dot{\lambda} \end{bmatrix} \quad (C. 18)$$

in which

$$[A_0] = \begin{bmatrix} 1/\cos \theta_0 & 0 & 0 \\ 0 & 1 & 0 \\ \sin \theta_0 / \cos \theta_0 & 0 & 1 \end{bmatrix} [\theta_0]' [\phi_0]'$$

$$[B_0] = \begin{bmatrix} 1/\cos \theta_0 & 0 & 0 \\ 0 & 1 & 0 \\ \sin \theta_0 / \cos \theta_0 & 0 & 1 \end{bmatrix} [\gamma_0] [\xi] [I''] [\mathcal{V}]$$

The rate of change of geodetic latitude ($\dot{\psi}_G$) is obtained by directly adding two collinear angular velocities:

$$\dot{\psi}_G = \dot{\psi} + \dot{\xi} \quad (C.19)$$

for which differentiation of Equation C.3 gives $\dot{\xi}$:

$$\dot{\xi} = a \epsilon \left(\frac{2 \dot{\psi} \cos 2 \psi}{r_{EO}} - \frac{\dot{h} \sin 2 \psi}{r_{EO}^2} \right) \quad (C.20)$$

The vector $[\omega_E]$ is given by Equation 3.57 except that $[L_{\theta-E}]$ is now defined as in Equation C.14.

Velocity of the vehicle relative to the air is calculated in essentially the same manner as in Section III:

$$[V_a] = [V] - [L_{\theta-ES}] \left\{ [V_{er}] + [W] \right\} - [\mu] \quad (C.21)$$

Here, the wind velocity vector $[W]$ has components in the new earth-surface frame which are calculated using geodetic position variables such as h_r and ψ_G . It should be noted that $[V_{er}]$ is the same in either earth-surface or spherical frames. If the gust velocity vector $[\mu]$ should depend on the vehicle's position, it must also be calculated using geodetic position coordinates. The components of $[V_a]$ are used to calculate its magnitude V_a , and α and β .

To obtain $[\dot{V}_a]$, Equation 3.73 is written in terms of the oblate-earth quantities already defined in this appendix:

$$\begin{aligned} [\dot{V}_a] = & [\dot{V}] + [\omega_E \times] [L_{\theta-ES}] \left\{ [V_{er}] + [W] \right\} - [\dot{\mu}] \\ & - [L_{\theta-SPH}] \left[(\omega_{SPH-E})_{SPH} \times \right] \left[\frac{h}{r} \right]' [W] - [L_{\theta-SPH}] \left\{ [L_{SPH-E}] [(\dot{V}_{er})_E] + \left[\frac{h}{r} \right]' [W] \right\} \end{aligned} \quad (C.22)$$

Then $\dot{\alpha}$ and $\dot{\beta}$ are calculated by using Equations 3.74 and 3.75 with the components of $[\dot{V}_a]$ and other quantities associated with the oblate earth.

In addition to the wind and gust velocities, other geophysical quantities are calculated as functions of geodetic position variables. Specifically, atmospheric properties, such as density, temperature, and pressure, are functions of h_r , the true altitude above the oblate earth.

Gravitational force for an oblate earth is given in terms to the second zonal harmonic by Equation C.7. This force, in terms of spherical (SPH) coordinates, must be transformed to the body axes coordinates:

$$[F_g] = [L_{\theta-SPH}] \left[(F_g)_{SPH} \right] \quad (C.23)$$

where again $[L_{\theta-\phi}]$ is defined by Equation C.15. Aerodynamic forces and moments are calculated using oblate earth quantities V_a and $\rho(h_T)$.

C.2 SPECIAL SURFACE ABERRATIONS

Certain small-scale geometric aberrations of the earth's surface such as mountains or mountain ranges, etc. which would comprise obstacles to low altitude flight, near landing for example, can be simulated. One possible method for providing such obstacles is given here and another more precise method is mentioned.

The equation

$$\Delta h_m = H \cos \frac{\pi}{2L_\mu} (\mu_m - \mu_0) \cos \frac{\pi}{2L_\lambda} (\lambda_m - \lambda) \quad (C.24)$$

with the conditions

$$\begin{aligned} |\mu_m - \mu_0| &< L_\mu \\ |\lambda_m - \lambda| &< L_\lambda \end{aligned}$$

defines what can be called a "cosine ridge" because it can be longer than wide or vice versa depending on choice of L_μ and L_λ . Here:

- L_μ is the west-to-east dimension of the ridge in radians on the earth's surface,
- L_λ is the south-to-north dimension of the ridge in radians on the earth's surface,
- H is the height of the ridge in feet,
- μ_m, λ_m are latitude and longitude of pole or center of ridge,
- Δh_m is the correction to the vehicle height in feet.

There are no restrictions on the magnitudes of L_μ , L_λ , or H . Also, geocentric latitude (μ) can be used in place of geodetic latitude (μ_g) if the earth is assumed spherical as in Section III.

If a number of separate ridges are placed near one another, they combine to produce a "mountain range". At any particular location, the total height correction for the vehicle is obtained by summing the cosine ridges, including the conditions on each Δh_m as shown above. The true height of the vehicle above this obstacle is given, then, by the addition of the summation to Equation C.6.

$$h_T = h + \Delta h - \sum_m \Delta h_m \quad (C.25)$$

It must be remembered that the true altitude to be used with the air density, air temperature, wind function, etc. is that given by Equation C.6 without the correction due to the obstacle. The altitude, h_r , as obtained from Equation C.25 should be used only as a cockpit display or as a program stop if it should become negative, indicating a crash.

The computation of Δh_m from Equation C.24 can be facilitated by using the first two terms of the power series expansion for the cosines. This is allowable because the obstacles need not have any particular representation. In fact, the cosine representation was used only because it resulted in an obstacle with roughly the appearance of a "mountain" or "ridge".

There are methods for obtaining a more precise simulation of a portion of the earth's surface, if such is desired. For example, a two-dimensional array representing elevation (E) of terrain at intersection points of grid lines of longitude (λ) and geodetic latitude (ν_g), or equivalent coordinates on the earth's surface, can be stored in the memory of a simulator such as UDOFTT. For a given position of the vehicle, the computer interpolates the data of the array to obtain elevation, $E(\lambda, \nu_g)$, which modifies the vehicle's altitude. Using an oblate earth model, within the region covered by the array, the true altitude of the vehicle is:

$$h_r = h + \Delta h - E(\lambda, \nu_g) \quad (C.26)$$

It is possible to use orthogonal functions in two independent variables to curve-fit elevation contour data and then use the orthogonal functions in the simulator computer. However, this method is probably more costly in storage and computation time than the interpolation method above for equivalent accuracy of simulation.

C.3 REFERENCES

- C.1 Purcell, E. W. and W. B. Cowan: "Relating Geodetic Latitude and Altitude to Geocentric Latitude and Radius Vector". ARS Journal, Vol. 31, No. 7, July 1961, P. 932.
- C.2 Berger, W. J. and R. J. Ricupito: "Geodetic Latitude and Altitude of a Satellite". ARS Journal, Vol. 30, No. 9, P. 901.
- C.3 Jahnke, E. and F. Emde: Tables of Functions with Formulae and Curves. Fourth Edition, Dover Publications, Inc.
- C.4 Nielsen, J. N.; F. K. Goodwin; and W. A. Mersman: Three-Dimensional Orbits of Earth Satellites, Including Effects of Earth Oblateness and Atmospheric Rotation. NASA Technical Memorandum 12-4-58A, December 1958.

- C.5 Allen, W. A.: "Effect on a Rocket of the Oblateness of a Planet".
ARS Journal, Vol. 30, No. 7, P. 623.
- C.6 Wu, Ching-Sheng: "Effect of Earth's Oblateness on the Calculation of
the Impact Point of Ballistic Missiles". ARS Journal, Vol. 30,
No. 12, P. 1172.

APPENDIX D
SUMMARY OF DIGITAL TECHNIQUES USED IN PROGRAM

In the sections which follow, the important digital techniques used during programming and solution of the equations of motion are discussed. Needless repetition is eliminated, however, so that only topics not covered elsewhere are treated in detail here. The three main sections are devoted respectively to general mathematical techniques, numerical integration, and obtaining solutions of the equations. A simplified diagram of the computer program (Figure D. 1) is included to illustrate the computation scheme.

D. 1 GENERAL MATHEMATICAL TECHNIQUES

Many of the digital techniques mentioned in this section are discussed in Reference D. 1 which is a general description of the IBM 704 program evolved in this study. The reference contains a description of the characteristics of the problem, a mathematical statement of the problem, the method of solution, a series of flow diagrams of the computer program, and instructions in the use of the program. Because they are treated in Reference D. 1, the computer routines are discussed only briefly in Section D. 1. 1.

The remaining sections, D. 1. 2 and D. 1. 3, deal with axis switching and the control system respectively, both of which are described in detail elsewhere in the report; therefore, the two sections will be short.

D. 1. 1 Routines for the Computer

Of the digital routines which facilitate use of the program, the input and output routines are among the most important. The input routine provides for loading of any storage location in the program, consequently it facilitates changing of conditions for different solutions. Input and output routines both use floating-point decimal notation. Specifically, the output routine prints floating-point numbers which at any given time may be used directly as initial condition inputs for a continuation of the same solution or a different solution. A time history solution may be halted upon reaching some condition of a computed parameter, or upon reaching a preselected time. To increase the computing speed, 900 core storage locations for each output variable are used to store results so that mechanical operations (of tape feed mechanism) are not performed after each computation cycle. The print-out from core storage to tape is made at one time when the entire 900 locations become filled or sooner if desired. An option exists for storing only the solution of each n^{th} computation cycle. The input routine code number is RS 0046, and the output is GL OUT 2. These are SHARE sub-routines.

Program outputs require three magnetic tapes, each handling about one third of the total number of variables. Arranged according to the tapes in which they appear, the variables are:

1. $u, v, w; p, q, r; q_i$
2. $\phi, \theta, \psi; h, \nu, \lambda; M_T$
3. $\alpha, \beta, \gamma, V_a, V_T, V_E, \mathcal{W}_T$

where $q_i = \frac{1}{2} \rho V_a^2$ and M_T is the moment about the y body axis due to the controller described in Section 5.1.6.

Other standard SHARE sub-routines are used for square root, sine, cosine, exponential and natural logarithm. These are listed with their code numbers in Reference D.1. Because of errors arising from truncation of numbers by the computer, a SHARE sub-routine for arcsine (CL ASC 1) was modified so that the program would error stop if the argument of the arcsine were greater than 1.001, or the argument would be used as unity if it actually were less than 1.001.

Three matrix sub-routines were developed especially for this IBM 704 program. They are routines which:

1. premultiply a 3 x 3 matrix by another 3 x 3 matrix,
2. premultiply a 3 x 1 (column) matrix by a 3 x 3 matrix, and
3. obtain the transpose of a 3 x 3 square matrix.

A diagnostic routine called FIDØ was used extensively during checkout of the program. This routine enables one to obtain a print-out of the content of any storage location used during the computation cycle.

D.1.2 Axis Switching

Vehicle orientation may be approached from two points of view: the use of direction cosines and the use of Euler angles. The latter have been chosen here because they provide a more meaningful physical picture of orientation. The Equations A.55 for ϕ and ψ contain a $(\cos \Theta)^{-1}$ factor which becomes zero as Θ approaches $\pm 90^\circ$. An actual re-entry vehicle can possibly operate at this condition; therefore, the program would be severely limited if it could not adequately handle the $\Theta \rightarrow \pm 90^\circ$ case. This is the purpose for the axis switching mechanism described in Sections 3.3.2 and 3.4.3 and in Reference D.1.

A present restriction on use of the program is that the vehicle not be allowed to pass directly over either pole of the earth. This is a result of using latitude as a position variable for the vehicle. Note that Equation A.50 is not defined when $\cos \psi$ approaches zero; that is, when $\psi \rightarrow \pm 90^\circ$. A switching mechanism similar to that used for the Euler angles could be developed to overcome the polar flight restriction.

D.1.3 Control System

The basic digital technique use of the controller described in Section 5.1.6 is that the natural frequency and damping of the controller were adjusted to allow reasonable computing times per re-entry solution. The numerical integration time interval required to produce an accurate solution is a function of the latent roots of the equations of motion. Neither aerodynamic characteristics of the vehicle nor the vehicle's mode of motion (as programmed) results in frequencies greater than about 0.1 radians per second; therefore, the highest frequencies would be contributed by the controller dynamics. After this condition was recognized, the controller characteristics were changed from the "ideal" $\omega_n = 3$ rad/sec and $\zeta = 0.7$ to a more reasonable $\omega_n = 0.3$ rad/sec and $\zeta = 0.7$. With this lower frequency, the Runge-Kutta integration method produced accurate results using a time interval of five seconds.

D.2 NUMERICAL INTEGRATION

D.2.1 Introduction

Twelve time rates of change of both linear and angular position and velocity parameters of the vehicle are simultaneously integrated once each computation cycle using some numerical method. These parameters are given by Equations A.37, A.38, A.48, A.49, A.50, and A.55 or A.55s. The equations are evaluated using position and velocity variables assumed given at some time (t) and thence numerically integrated with a time interval or step size (Δt) to obtain the position and velocity variables at the later time $t + \Delta t$. This cycle of operations, with the auxiliary computations that may be necessary during each cycle, is repeated as long as desired.

The above comments are applicable to the use of any numerical integration method (though specifically referred to the problem of this report). However, there is no mention above that a number of numerical integration methods are available, each of whose application in a specific situation is different from the others. Taylor's Series, the fourth order Runge-Kutta equations, an open equation, a closed equation, and an open-closed combination are examples of methods which require different mechanics of application although in some cases, the differences may be small. Similarly, there is no mention of characteristics of a method (per-step error*, propagation of per-step error**, and stable convergence***). From the user's point of view, the concept of stable convergence is not of prime importance, for if he knows the method is convergent, he need not further concern himself with it. Per-step error and its propagation are, however, very important. In fact, these concepts have direct bearing upon whether the integration method may be satisfactorily used for real time operations. The studies performed by various workers (notably H. J. Gray, Jr.) at the Moore School of Electrical Engineering at the University of Pennsylvania were directed at obtaining suitably convergent integration formulas with favorable propagation characteristics. A useful result of these studies is the so-called stability chart (see Reference D.3) which provides a graphical determination of propagation characteristics.

* Per-step error as used here includes error from two sources:

1. Truncation error of the numerical integration formula; that is, the formula results in a value which is slightly different from the true value. The numerical formulas are generally based upon a finite number of terms of a Taylor's or Maclaurin's series; thus the infinite series has been "truncated".
2. Round-off error due to the limited number of digits carried by the computer.

Both errors occur each time the formula is used.

** Propagation of per-step error concerns how the error obtained at one step affects the solution in subsequent steps.

*** Stable convergence is obtained if, for $\Delta t \rightarrow 0$ at a point, the value of the solution at that point converges to the true solution, providing of course that the given data is true.

If a method is stably convergent, by the precise definition of Reference D. 2, the propagation of per-step error is a function of the characteristics of the given differential equations and the time interval. The characteristics of the equations do, in fact, change with time and, since little control can be had over the equations without restricting their solution, the only real freedom lies in choosing some optimum time interval.

Per-step error has been defined previously as the sum of the integration formula truncation error and the number round-off error. For the Runge-Kutta formula discussed in Section D. 2. 2, the per-step truncation error is

$$\epsilon_T \approx k_1 (\Delta t)^5 \tag{D. 1}$$

where Δt is the integration step-size or time interval and k_1 is a constant (assumed) which is proportional to the fifth derivative of the solution. The per-step round-off error can be represented simply as a constant, k_2 , which is an average of the possible values of the round-off error and is independent of the characteristics of the equations to be solved:

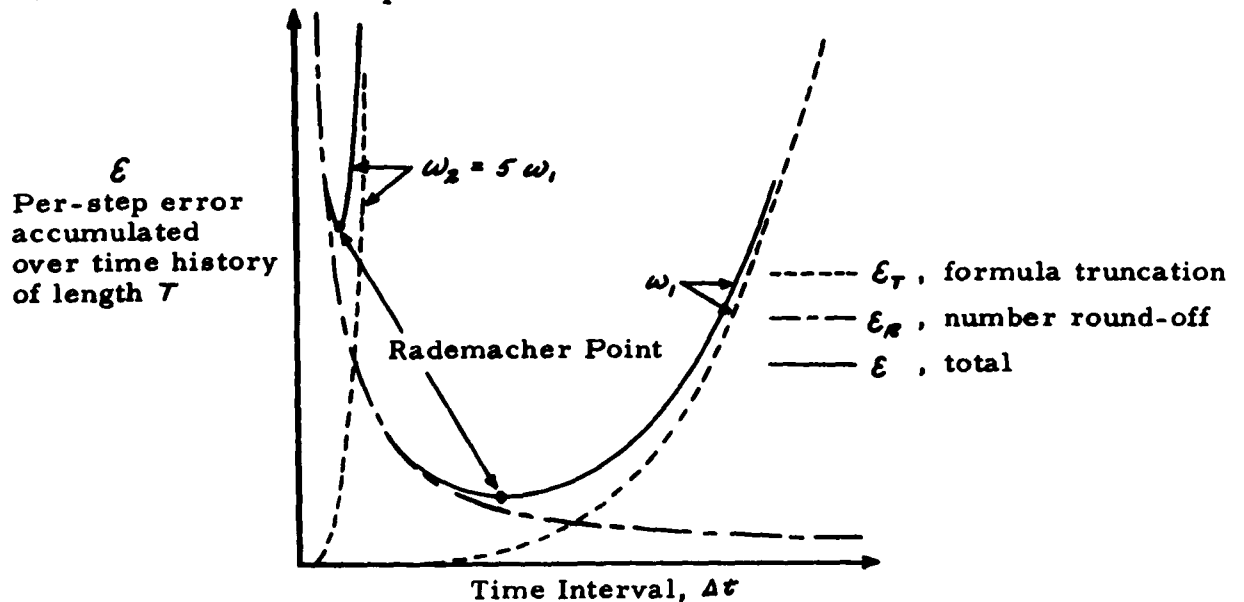
$$\epsilon_R \approx k_2 \tag{D. 2}$$

Equation D. 1 shows that per-step truncation error, ϵ_T , depends heavily on time interval, while Equation D. 2 shows that per-step round-off error, ϵ_R , is independent of time interval.

Now, over a given length of time history, T , the total accumulated per-step error is the sum of accumulated truncation and round-off errors:

$$\epsilon \approx k_1 T (\Delta t)^5 + k_2 \frac{T}{\Delta t} \tag{D. 3}$$

where $T/\Delta t$ is the number of integration steps. The sketch below depicts ϵ , ϵ_R , and ϵ_T for two frequencies, ω_1 and $\omega_2 = 5\omega_1$. The one ϵ_R curve holds for both frequencies.



Ideally, a solution should be obtained by using the time interval resulting in minimum accumulated per-step error: this is the time interval at the so-called Rademacher point. However, numerical solution of differential equations must be accomplished so that requirements of the highest frequency in the equations (ω_2 in the sketch) are met. As a consequence, the error in the lower frequency (ω_1) portions of the solution is considerably greater than optimum.

In addition, the Rademacher point is not fixed; it depends on the characteristics of the differential equations, specifically the latent roots, which in general change during the time history. Thus, the equations themselves can thwart effort to locate the optimum time interval.

To obtain solutions of the equations of motion during the present study, two numerical integration methods were studied: a fourth order Runge-Kutta method and a fourth order open-closed method*. The original plan was to modify the open-closed method so that it would automatically change its own time interval (to that value which allows the estimated per-step error to meet desired limits) thus optimizing computation time with respect to the pre-selected limits. This method is workable but, because of various complications, its development was never completed. As a result, integration was performed using the Runge-Kutta method with a fixed-step size (except when changed by an independent computer instruction based on considerations other than per-step error). The computation time was made acceptable by employing special controller characteristics as described in Section 5.1.6. It became possible, therefore, to use a time interval of 5 sec for the time history solutions.

Certainly $\Delta t = 5$ sec is not capable of correctly computing solutions if the normal aircraft high frequency dynamics are to be described. The solutions presented in Sections V and VI of this report are intended to be basically trajectory time histories; nevertheless, conditions have been selected so that some information on high frequency dynamics is available.

D.2.2 Runge-Kutta Method

Of the many similar formulas called "Runge-Kutta", a particular fourth order formula (the most commonly known) was used to obtain the solutions presented in Sections V and VI. The formula is given for a single first order differential equation:

$$y_{n+1} = y_n + \frac{1}{6} (k_1 + 2k_2 + 2k_3 + k_4) \quad (D.4)$$

where:

$$\begin{aligned} k_1 &= \Delta t \dot{y}(t_n, y_n) \\ k_2 &= \Delta t \dot{y}(t_n + \frac{1}{2} \Delta t, y_n + \frac{1}{2} k_1) \\ k_3 &= \Delta t \dot{y}(t_n + \frac{1}{2} \Delta t, y_n + \frac{1}{2} k_2) \\ k_4 &= \Delta t \dot{y}(t_n + \Delta t, y_n + k_3) \end{aligned}$$

and where:

$$\dot{y} \equiv \frac{dy}{dt} \equiv f(t, y)$$

* The open-closed method, also called predictor-corrector, provides an estimate of per-step error in terms of the predictor solution and the corrector solution.

The Runge-Kutta method was chosen as one of two methods to be used with the IBM 704 program because of its excellent propagation and truncation error properties and because it is always stably convergent and self-starting when properly used. Thus it provided reliable solutions with which the modified open-closed method could be compared during its development. A drawback of the Runge-Kutta method, however, is the necessity for four evaluations of the differential equations for each step to obtain the four k's.

D.2.3 Open-Closed Method

The open-closed method was selected because it held promise of automatically choosing its own optimum time interval, thus providing minimum time history computation time. The method is stably convergent and has truncation error of about the same order as Runge-Kutta. The open-closed method has generally worse propagation properties, however, and it must be started by using some process such as Taylor's series or the Runge-Kutta method. The formulas investigated during the study are given in Reference D.4:

$$\text{OPEN: } y_{\pi+1}^o = y_{\pi} + \frac{\Delta t}{24} [55\dot{y}_{\pi} - 59\dot{y}_{\pi-1} + 37\dot{y}_{\pi-2} - 9\dot{y}_{\pi-3}] \quad (\text{D.5})$$

$$\text{CLOSED: } y_{\pi+1}^c = y_{\pi} + \frac{\Delta t}{24} [9\dot{y}_{\pi+1}^o + 19\dot{y}_{\pi} - 5\dot{y}_{\pi-1} + \dot{y}_{\pi-2}] \quad (\text{D.6})$$

with the corresponding error formulas:

$$\text{OPEN: } \epsilon^o = \frac{251}{720} \frac{d^4 y}{dt^4} (\Delta t)^5 \quad (\text{D.7})$$

$$\text{CLOSED: } \epsilon^c = -\frac{19}{720} \frac{d^4 y}{dt^4} (\Delta t)^5 \quad (\text{D.8})$$

The open formula "predicts" a value $y_{\pi+1}^o$, based upon Δt and y_{π} , etc., which is then used in the closed formula to result in the final "corrected" value $y_{\pi+1}^c$ whose resultant error is ϵ^c . Now ϵ^o can be expressed as:

$$\epsilon^c = \left(\frac{\epsilon^c}{\epsilon^o - \epsilon^c} \right) (\epsilon^o - \epsilon^c) \quad (\text{D.9})$$

The first factor of Equation D.9 is found to be 14.2 by using Equations D.7 and D.8. Since the true value of the solution is

$$y_{\text{TRUE}} = y^o + \epsilon^o = y^c + \epsilon^c \quad (\text{D.10})$$

it follows that

$$\epsilon^o - \epsilon^c = y^c - y^o \quad (D.11)$$

Equation D.9 can be evaluated using the different forms of each factor:

$$\epsilon^c = \frac{y^c - y^o}{14.2} \quad (D.12)$$

Equation D.12 provides an estimate of the per-step error of the open-closed method which is dependent only upon the results of the two formulas, and it is used with some desired error limits as a criterion for varying time interval.

The open-closed method requires starting only if the best accuracy of the method is wanted. Thus, any time a discontinuity occurs in the equations (e.g., axis switching) the method should be restarted. This reasoning holds true for all open, closed, and open-closed formulas but, actually, if the method has favorable propagation characteristics and the best accuracy is not required, it is not necessary to start or restart.

The closed formula (Equation D.6) need not be used each computation cycle. In fact, in Reference D.4, it is suggested that the closed formula be used every tenth step. This would allow a substantial time saving.

D.2.4 Conclusion

The previous sections have presented some of the problems of numerical integration and the methods used during the study to overcome these problems. However, the techniques discussed here and others that were found during the study (see References D.5 and D.6) do not appear to be suitable for simulator use. In addition, the author's feeling is that the O₃₃ mod Gurk formula (see Reference D.7) may not be a suitable formula for simulator use with the equations of motion developed in Section III, especially if simulated re-entries are long enough for severe error accumulation. Unfortunately, O₃₃ mod Gurk was not tried with typical re-entry solutions, so that the "feeling" has little founding on fact.

D.3 OBTAINING SOLUTIONS OF EQUATIONS OF MOTION

D.3.1 Initial Condition Calculations for Cases II and III

The initial values of trajectory parameters for Cases II and III are given in Section 5.2.1 as:

$$\begin{aligned} x &= 300,000 \text{ ft} \\ v &= 24,000 \text{ ft/sec} \\ \gamma &= -1 \text{ deg} \\ \psi &= +30 \text{ deg} \\ \psi_T &= +120 \text{ deg} \end{aligned}$$

Other conditions which pertain are the earth's rotation with angular velocity, $\Omega = 0.004178 \text{ deg/sec}$, the 15° angle of attack to be held from zero time

At altitude $h = 300,000$ ft, and latitude $\psi = 30^\circ$, the inertial velocity component due to earth rotation is:

$$\begin{aligned} V_{en} &= \Omega r_{EB} \cos \psi \\ &= 0.00007292 (20.86 \times 10^6 + 0.3 \times 10^6) \cos 30^\circ \\ &= 1336.2661 \text{ ft/sec} \end{aligned}$$

Then, from Sketch A:

$$\begin{aligned} v &= V_{en} \sin 30^\circ \\ &= 668.13305 \text{ ft/sec} \end{aligned}$$

Sketch B shows that

$$V_n^2 + (V_T + V_{en} \cos 30^\circ)^2 = u^2 + w^2$$

which can be written as a quadratic in V_n :

$$V_n^2 + (V_n \cot 1^\circ + V_{en} \cos 30^\circ)^2 = u^2 + w^2$$

where

$$u^2 + w^2 = V^2 - v^2 = 575,553,598 \text{ (ft/sec)}^2$$

The physically realizable solution is

$$V_n = 398.501701 \text{ ft/sec}$$

It is now possible to evaluate the angle φ :

$$\varphi = \sin^{-1} \frac{V_n}{\sqrt{u^2 + w^2}}$$

$$\varphi = 0.9518 \text{ deg}$$

Then finally u and w are evaluated:

$$u = \sqrt{u^2 + w^2} \cos(\Theta + \varphi) = 23,178.450 \text{ ft/sec}$$

$$w = \sqrt{u^2 + w^2} \sin(\Theta + \varphi) = 6189.7513 \text{ ft/sec}$$

To check u , v , and w , find the sum of their squares and compare this sum with the square of the given V . The 8 digits given for u , v , and w are not an indication of the precision of the values.

D.3.2 Check Solutions and Accuracy

A number of solutions were obtained early in the study to check various portions of the computer program and to demonstrate the accuracy of the numerical integration methods over long time histories. For most of these special solutions, exact analytical answers could be obtained to compare with the numerical solution.

The types of check solutions and their purposes are listed here:

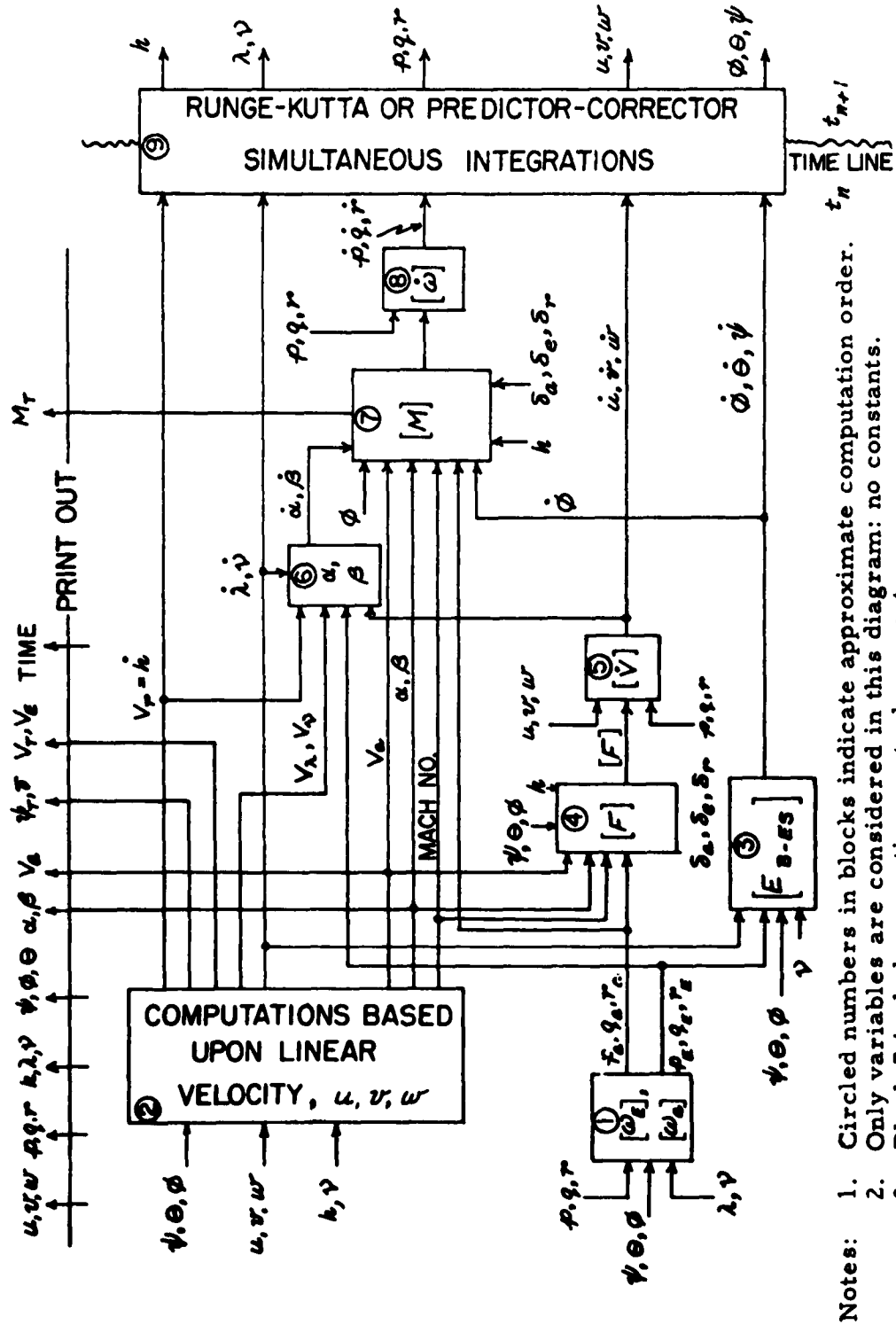
1. A force and moment free solution was obtained to check the rotational equations of motion only. This solution was patterned after the special integrable force-and moment-free solution on page 162 of Reference D. 8.
2. A circular orbit with $h = 300,000$ ft and the vehicle's attitude fixed in inertial space was obtained. This solution was designed to check the axis switching mechanism as the vehicle's attitude relative to earth changes. It also showed that the Runge-Kutta method could integrate orbits fairly well. The orbit did not close on itself but the error was only about -6 ft, nearly a half of which could be accounted for by the fact that the initial circular orbital velocity could not be programmed precisely enough with the 8 digit capacity of the IBM 704.
3. A highly eccentric (0.36) orbit was computed which is certainly not realistic for the earth of radius $R_0 = 20.86 \times 10^6$ ft. The altitude at apogee is 390,000 ft and at perigee, -10,860,000 ft. The vehicle was given angular velocity. This solution was another accuracy check with the vehicle undergoing more general motions. Again, the orbital accuracy proved good, but not so good as for the circular orbit in (2) above.
4. A constant $C_D S/m$ re-entry solution was obtained to check use of atmospheric models which, until this solution, were unused.
5. A solution was obtained with conditions set so that an exact second order response to an angle of attack step could be computed. This was, of course, designed to check the controller formulation and to determine the necessary Δt for reasonable accuracy. The solution for $\omega_n = 3$ rad/sec and $\zeta = 0.7$ required a time interval of 0.5 sec, an entirely unreasonable value from the point of view of computation time per solution.

Check solutions listed here proved very useful in finding programming errors. In addition, the last check solution above (5) showed that with $\Delta t = 0.5$ sec and a 2500 sec time history, the IBM 704, computing at a rate of 40 steps per minute, would require over 2 hours for each time history. Two hours was entirely too long when some dozens of solutions were required; therefore, a method for shortening the computation time per solution had to be devised.

D. 4 REFERENCES

- D. 1 Shed, W. H.: Program for IBM 704 Digital Computer Six-Degree-of-Freedom Re-Entry Vehicle. Cornell Aeronautical Laboratory FDM No. 318, 21 July 1961.
- D. 2 Urabe, M.: Theory of Errors in Numerical Integration of Ordinary Differential Equations. MRC Technical Summary Report No. 183, Mathematics Research Center, U. S. Army, The University of Wisconsin, October 1960.

- D.3 Gray, H. J., Jr.: "Numerical Methods in Digital Real-Time Simulation". Quarterly of Applied Mathematics, Vol. XII, No. 2, July 1954, P. 133.
- D.4 Murray, F. J.: "Planning and Error Considerations for Numerical Solution of a System of Differential Equations on a Sequence Calculator". Mathematical Tables and Other Aids to Computation, Vol. IV, No. 31, July 1950, P. 133.
- D.5 Forrington, C. V. D.: The Numerical Solution of Systems of Differential Equations Using a Different Step-Length for Each Equation. Technical Note No. M. S. 69, Royal Aircraft Establishment (Farnborough) England. September 1960, ASTIA 248-563. See also Technical Note No. M. S. 71 which is allied to this.
- D.6 Anderson, W. H.; R. B. Ball; and J. R. Voss: "A Numerical Method for Solving Control Differential Equations on Digital Computers". Journal of the Association for Computing Machinery, Vol. 7, No. 1, January 1960, P. 61.
- D.7 Rubinoff, M., et al: Universal Digital Operational Flight Trainers. University of Pennsylvania, Research Division, Report No. 54-45, 30 June 1954.
- D.8 Goldstein, H.: Classical Mechanics. Addison-Wesley Publishing Company, Inc., Cambridge, Massachusetts, 1953.



- Notes:
1. Circled numbers in blocks indicate approximate computation order.
 2. Only variables are considered in this diagram; no constants.
 3. Block 7 includes reaction control moment.

FIGURE D. 1 SIMPLIFIED DIAGRAM OF COMPUTER PROGRAM

NAVTRADEVCEEN 801A

DISTRIBUTION LIST

DEPARTMENT OF DEFENSE

The Secretary of Defense, The Pentagon, Washington 25, D. C. ATTN: Asst. Sec'y. (Research and Engineering)
Advanced Research Projects Agency, The Pentagon, Washington 25, D. C.,
MKD: Technical Library
Technical Library, Armed Services Technical Information Agency, Arlington Hall Station, Arlington 12, Virginia

U. S. NAVY

Office of Asst. Sec'y of the Navy (Research and Development), Navy Department, Room 4E-733, The Pentagon, Washington 25, D. C.
Director, Navy Publications and Printing Service, Navy Department, Washington 25, D. C.
Deputy Chief and Chief Scientist, Office of Naval Research (Code 102), Washington 25, D. C.
Chief of Naval Research, Department of the Navy, Washington 25, D. C.,
MKD: Code 130
Chief of Naval Research (Code 400), Navy Department, Washington 25, D. C.
Chief of Naval Research (Code 104), Research Coordinator, Washington 25, D. C.
Chief of Naval Research (Code 109), Technical Information Officer, Navy Department, Washington 25, D. C.
Chief of Naval Research, Navy Department, Washington 25, D. C.
Director of Research, U. S. Naval Research Laboratory (Code 700), Washington 25, D. C.
Library (Code 741), U. S. Naval Research Laboratory, Washington 25, D. C.
Chief of Naval Operations, Navy Department, Washington 25, D. C.
Chief of Naval Operations (Op-001), Navy Department, Washington 25, D. C.
Chief of Naval Operations (Op-07), Navy Department, Washington 25, D. C.
Chief of Naval Operations (Op-31), Navy Department, Washington 25, D. C.
Chief of Naval Operations (Op-34), Navy Department, Washington 25, D. C.
Chief of Naval Operations (Op-56), Navy Department, Washington 25, D. C.
Chief of Naval Personnel, Navy Department, Washington 25, D. C. ATTN: Code PERS-15
Asst. Chief for Education and Training, Bureau of Naval Personnel (PERS-CM), Washington 25, D. C.
Office of Liaison and Technical Information, Chief of Naval Personnel (PERS-16), Washington 25, D. C.
Chief of Naval Personnel (PERS-C14), Training Aids Branch, Washington 25, D. C.
Officer in Charge, U. S. Navy Training Publications Center, Bldg. T-63, U. S. Naval Station, Washington 25, D. C.
Superintendent, U. S. Naval Academy, Annapolis, Maryland, MKD: Head, Academic Sect. Executive Dept.
Superintendent, U. S. Naval Academy, Annapolis, Maryland, MKD: Library
Superintendent, U. S. Naval Postgraduate School, Monterey, California, MKD: Library
Superintendent, U. S. Naval Postgraduate School, Monterey, California

NAVTRADEVCEEN 801A

Chief, Bureau of Naval Weapons, Navy Department, Washington 25, D. C.
Chief Scientist, Bureau of Naval Weapons, Navy Department, Washington
25, D. C.
Chief, Bureau of Naval Weapons, Navy Department, Washington 25, D. C.,
MKD: Technical Library
Chief Scientist, U. S. Naval Air Development Center, Johnsville, Pennsyl-
vania
Commanding Officer, U. S. Naval Air Development Center, Johnsville,
Pennsylvania, MKD: NADC Library
Chief, Bureau of Ships, Technical Library (Code 335), Rm. 1532, Main
Navy Bldg., Washington 25, D. C.
Chief Scientist for R & D, Bureau of Ships (Code 315), Rm. 3018, Main
Navy Bldg., Washington 25, D. C.
Commanding Officer and Director, U. S. Navy Electronics Laboratory, San
Diego 52, California, MKD: Technical Library
Chief, Bureau of Medicine and Surgery, Navy Department, Washington 25,
D. C., MKD: Library
Asst. Chief for Research and Development, Bureau of Supplies and Accounts,
Washington 25, D. C.
Chief, Bureau of Yards and Docks, Navy Department, Washington 25, D. C.,
ATTN: Code D-400
Asst. Director R & D Division, Bureau of Yards and Docks, Navy Department,
Washington 25, D. C.
Scientific Director, U. S. Marine Corps, Rm. 2227, Arlington Annex,
Washington 25, D. C.
Commandant of Marine Corps, Headquarters, U. S. Marine Corps, Washington 25,
D. C., ATTN: Code A04E
Commander Naval Air Force, U. S. Pacific Fleet, U.S. Naval Air Station,
San Diego 35, California
Commander Naval Air Force, U. S. Atlantic Fleet, U. S. Naval Air Station,
Norfolk 11, Virginia
Commander, Fleet Airborne Electronics Training Unit, Atlantic, U.S. Naval
Air Station, Norfolk 11, Virginia
Commander, Fleet Airborne Electronics Training Unit, Pacific, U. S. Naval
Air Station, North Island, San Diego 35, California
Commander, U. S. Naval Air Test Center, Patuxent River, Maryland
Commanding Officer, U. S. Naval School of Aviation Medicine, U. S. Naval
Aviation Medical Center 54, Pensacola, Florida
Chief of Naval Air Advanced Training, U. S. Naval Air Advanced Training
Command, Naval Air Station, Corpus Christi, Texas
Chief of Naval Air Reserve Training, Naval Air Reserve Training Command,
Naval Air Station, Glenview, Illinois
Air Crew Equipment Laboratory, Naval Air Material Center, Philadelphia
Naval Shipyard, Philadelphia, Pennsylvania
Commanding Officer, U. S. Naval Air Technical Training Center, Naval Air
Station, Memphis 15, Tennessee
Superintendent, U. S. Naval Academy, Annapolis, Maryland, MKD: Head,
Aviation Department
Headquarters, Chief of Naval Air Training, Training Research Department,
Naval Air Station, Pensacola, Florida
Chief of Naval Air Basic Training, U. S. Naval Air Basic Training Command,
Naval Air Station, Pensacola, Florida

NAVTRADEVCCEN 801A

Office of Naval Research, Director, Air Programs, Department of the Navy,
Washington 25, D. C., MKD: For Code 461
Commander, Pacific Missile Range, Point Mugu, California
Officer-in-Charge, MDWP Contract Supervisory Staff, SACLANT ASW Research
Center, APO 19, New York, New York
Chief of Naval Personnel, Surface Warfare (PERS-C1411), Washington 25,
D. C.
Technical Director, U. S. Naval Underwater Ordnance Station, Newport,
Rhode Island
Technical Library, Naval Ordnance Test Station, China Lake, California
Technical Library, U. S. Naval Weapons Laboratory, Dahlgren, Virginia
Chief of Naval Personnel, Undersea Warfare (PERS-C1413), Washington 25, D. C.
Commanding Officer, U. S. Naval Underwater Ordnance Station, Newport, Rhode
Island
Commander, U. S. Naval Ordnance Laboratory, Technical Library, Silver Springs,
Maryland

U. S. ARMY

Deputy Chief of Staff for Military Operations, Department of the Army, The
Pentagon, Washington 25, D. C.
Commanding General, U. S. Continental Army Command, Fort Monroe, Virginia
Commandant, U. S. Army Primary Helicopter Training School, Camp Walters,
Texas
Chief of Research and Development, Department of the Army, The Pentagon,
Washington 25, D. C.
Assistant Secretary of the Army, Department of the Army, Washington 25, D. C.,
ATTN: Training Division
Army Library, TAGO, Room 1-A-518, Pentagon, Washington 25, D. C.
Special Service Division, Office of the Adjutant General, Washington 25,
D. C., MKD: Library
Commanding General, U. S. Continental Army Command, Fort Monroe, Virginia,
ATTN: G-3
TAG Research and Development Command, U. S. Army, Washington 25, D. C.,
MKD: AGTL
Office of Chief Signal Officer, HQ Department of the Army, Washington 25,
D. C., MKD: SIG PT-2
Assistant Chief of Transportation for R & D, Department of the Army
Washington 25, D. C.
Commandant, U. S. Army Command & General Staff College, Fort Leavenworth,
Kansas, MKD: ARCHIVES
U. S. Army War College, Carlisle Barracks, Pennsylvania, MKD: Library
Commanding General, U. S. Army Combat Development Experimental Center,
Fort Ord, California, MKD: NAVTRADEVCCEN Liaison Rep.
Library, U. S. Military Academy, West Point, New York
Army Signal School Library, Fort Monmouth, New Jersey
U. S. Army Signal Corps, R & D Laboratory, Fort Monmouth, New Jersey,
MKD: Library
Commanding Officer, Engineering Research & Development Lab., Fort Belvoir,
Virginia, MKD: Library

NAVTRADEVCEEN 801A

Military Information Section, Technical Information and Intelligence Office,
DCS/Operations, Arnold Engineering Development Center, Tullahoma,
Tennessee

Industrial College of the Armed Forces, Fort Lesley J. McNair, Washington
25, D. C., MKD: Library

U. S. Army Intelligence School, Baltimore, Maryland, MKD: Library

U. S. Army Security Agency Training Center, Fort Devens, Massachusetts,
MKD: Library

U. S. Army Medical School, Fort Sam Houston, Texas, MKD: Library

U. S. Army Aviation School Library, Fort Rucker, Alabama

Deputy Chief of Staff for Military Operation, Department of the Army,
Washington 25, D. C., ATTN: Army Aviation

Chief of Transportation, Department of the Army, Washington 25, D. C.
MKD: TCSOP-DB

Commanding General, U. S. Army Transportation Materiel Command, 12th and
Spruce Streets, St. Louis, Missouri, MKD: TCMAC QIT

Technical Library, White Sands Missile Range, New Mexico

Office of Chief Chemical Officer, Department of the Army, Washington 25,
D. C.

Office of the Chief of Engineers, Department of the Army, Washington 25,
D. C.

Office of the Chief Signal Officer, Department of the Army, Washington 25,
D. C.

Office of the Chief of Transportation, Department of the Army, Washington
25, D. C.

Office of the Chief of Ordnance, Department of the Army, Washington 25,
D. C.

Technical Documents Library, U. S. Army Ordnance Missile Command, Redstone
Arsenal, Alabama

Army Ordnance School Library, Aberdeen Proving Ground, Maryland

Technical Information Section, Feltman Research and Engineering Laboratories,
Picatinny Arsenal, Dover, New Jersey

Library, Army Artillery and Missile School, Fort Sill, Oklahoma

Air Defense School Library, Fort Bliss, Texas

Commanding General, U. S. Army Training Center, Air Defense, Fort Bliss,
Texas

Technical Laboratory, White Sands Missile Range, New Mexico

Springfield Armory Library, Springfield Armory, Springfield, Massachusetts

Watertown Arsenal Technical Info Center, Watertown 72, Massachusetts

Watervliet Arsenal Technical Laboratory, Watervliet, New York

Technical Laboratory, Army Electronic Training Command, Fort Huachuca,
Arizona

Technical Laboratory, Quartermaster Research and Engineering, Natick,
Massachusetts

Technical Laboratory, Quartermaster Research and Engineering Field, Evaluation
Agency, Fort Lee, Virginia

Army Armor School Library, Fort Knox, Kentucky

Army Infantry School Library, Fort Benning, Georgia

Army Audio School Library, Aberdeen Proving Grounds, Maryland

Technical Library, U. S. Army Chemical Corps, Proving Ground, Washington,
D. C.

NAVTRADEVCEEN 801A

Technical Library, U. S. Army Engineering District, Omaha, Corps of Engineers,
1709 Jackson Street, Omaha, Nebraska

Technical Library, Army Rocket and Guided Missile Agency, Redstone Arsenal,
Alabama

Quartermaster Training School Library, Fort Lee, Virginia

Transportation Corps Library, Transportation School, Fort Eustis, Virginia

U. S. AIR FORCE

Directorate of Training, DCS/F Headquarters, U. S. Air Force, Washington
25, D. C.

U. S. Air Force Office of Scientific Research, Washington 25, D. C.,

MKD: Technical Library

Headquarters, AFSC, Andrews Air Force Base, Washington 25, D. C., MKD:
Technical Library

Wright-Patterson Technical Library, Wright-Patterson Air Force Base, Ohio

Air Force Institute of Technology, Wright-Patterson Air Force Base, Ohio

MKD: Library

ASD (ASMT) Wright-Patterson AFB, Ohio

ASD (ASBST-5), Wright-Patterson AFB, Ohio

U. S. Air Force, Command and Control Devel. Div., Bldg. A, Stop 29,
Bedford, Massachusetts, MKD: Technical Library

USAFA (DLIB), U. S. Air Force Academy, Colorado

Air University, Maxwell Air Force Base, Alabama, MKD: Library

Rome Air Development Center, Griffiss Air Force Base, New York, MKD: Techni-
cal Library

Aeromedical Library, School of Aviation Medicine, Brooks Air Force Base,
Texas

Technical Library Branch (FTOTL), Air Force Flight Test Center, Edwards
Air Force Base, California

Technical Library, Air Force Missile Development Center, Holloman Air Force
Base, New Mexico

Base Library, Air Force Missile Test Center, Patrick Air Force Base,
Florida

Air Force Personnel & Training Research Center, Pilot Training Research
Field Section, Williams Air Force Base, Chandler, Arizona

GOVERNMENT

National Defense College & Canadian Army, Staff College, Fort Frontenac,
Kingston, Ontario, Canada

Department of Naval Defense Library, Rm. 1082, "C" Building, National
Defense Headquarters, Ottawa, Ontario, Canada

Department of Commerce, Office of Technical Services, Washington 25, D. C.

Division of Public Documents, U. S. Government Printing Office, Washington
25, D. C., MKD: Library

NASA Langley Research Center, Langley Air Force Base, Virginia, MKD:
Library

NASA American Research Center, Moffet Field, California, MKD: Library

NASA High Speed Research Center, Edwards Air Force Base, California,
MKD: Library

NASA, Assistant Director, Bio-Technical Manned Space Flight, 1520 "H"
Street, N. W., Washington 25, D. C.

Federal Aviation Agency, Bureau of Research and Development, Washington
25, D. C. MKD: Technical Library

NAVTRADEVCEEN 801A

Federal Aviation Agency, National Aviation Facilities Experimental Center,
Atlantic City, New Jersey, MKD: Technical Library
Federal Aviation Agency, Aeronautical Center, Oklahoma City, Oklahoma,
MKD: Director of Training
Officer-in-Charge, MDWP Contract Supervisory Staff, SACLANT ASW Research
Center, APO 19, New York, New York

CIVILIAN

National Science Foundation, 1520 "H" Street, N. W., Washington, D. C.
Massachusetts Institute of Technology, Cambridge, Massachusetts,
ATTN: Acquisitions Librarian
Cornell Aeronautical Laboratory, Inc., P. O. Box 235, Buffalo 21, New York,
MKD: Librarian
American Institute for Research, 410 Amberson Avenue, Pittsburgh 32,
Pennsylvania, MKD: Library
Brookhaven National Laboratory, Attention: Research Library, Upton, Long
Island, New York
Brown University, Providence 12, Rhode Island, MKD: Library
Carnegie Institute of Technology, Schenley Park, Pittsburgh 13, Pennsylvania,
MKD: Technical Processes
Columbia University Libraries, W. 114th Street, New York 27, New York,
MKD: Acquisitions Librarian
Cornell University, Ithaca, New York, MKD: Acquisitions Librarian
Franklin Institute, Parkway at 20th Street, Philadelphia 3, Pennsylvania,
MKD: Acquisitions Librarian
Harvard University, Cambridge 38, Massachusetts, MKD: Assoc, Librarian
for Resources & Acquisitions
New York University Libraries, Washington Square, New York, New York,
MKD: Acquisitions Librarian
Pennsylvania State University, Fred Lewis Pattee Library, University
Park, Pennsylvania, MKD: Acquisitions Librarian
University of Pennsylvania Library, Central Building, 34th & Walnut Street,
Philadelphia, Pennsylvania, MKD: Acquisitions Librarian
University of Pittsburgh Library, Fifth Avenue, Pittsburgh 13, Pennsylvania,
MKD: Acquisitions Librarian
Polytechnic Institute of Brooklyn, Spicer Memorial Library, 333 Jay Street,
Brooklyn 1, New York, MKD: Librarian
Princeton University Library, Princeton, New Jersey, MKD: Science & Technology
Rensselaer Polytechnic Institute Library, 110 Eighth Street, Troy, New York,
MKD: Librarian
University of Rochester Library, River Campus Station, Rochester 20, New
York, MKD: Librarian
Rutgers University Library, New Brunswick, New Jersey, MKD: Government
Documents
Yale University Library, 120 High St. (1603A Yale Station), New Haven,
Connecticut, MKD: Order Librarian
California Institute of Technology, Pasadena, California, MKD: Acquisitions
Librarian
Hughes Aircraft Co., Engineering Division, Culver City, California,
MKD: Technical Staff

NAVTRADEV CEN 801A

University of California at Los Angeles, 405 Hilgard Avenue, Los Angeles 24, California, MKD: University Library
Scripps Institution of Oceanography, University of California, 8601 La Jolla Shores Drive, Box 109, La Jolla, California, MKD: Library
Ohio State University Research Foundation, Columbus 8, Ohio, MKD: Library
University of Texas, Austin, Texas, MKD: U.S. Document Depository Library
University of Chicago Library, c/o Acquisitions Librarian, 1116 East 59th Street, Zone 37, Chicago, Ill.
University of Colorado Library, Boulder, Colorado, MKD: U.S. Document Depository Library
University of Illinois Library, Urbana, Illinois, MKD: U.S. Document Depository Library
University of Michigan Library, Ann Arbor, Michigan, MKD: U.S. Document Depository Library
Western Reserve University, Documentation and Communication Research, School of Library Science, Cleveland, Ohio.
Library of Congress, Washington 25, D.C., MKD: Exchange and Gift Division
Institute of Aeronautical Sciences Library, 2 East 64th Street, New York, New York
Man Machine Information Center, 2521 Connecticut Avenue, N. W., Washington 8, D. C.
Society of Automotive Engineers, Inc., 485 Lexington Avenue, New York 17, New York, ATTN: (SAE Committee GSE-3)
Technical Lab., Diamond and Fuze Laboratories, Conn. Avenue and North Van Ness Street, Washington, D. C.
Curtiss-Wright Corporation, Electronics Division, 35 Market Street, East Paterson, New Jersey
ACF Electronics Division, 48 Lafayette Street, Riverdale Plant, Riverdale, Maryland
Melpar, Inc., 3000 Arlington Boulevard, Falls Church, Virginia
Goodyear Aircraft Corporation, Research and Development Division, Department 20 Plant C Akron 15, Ohio
Bell Helicopter Corporation, P. O. Box 482, Fort Worth, Texas
Convair, A Division of General Dynamics Corporation, San Diego 12, California
Convair, A Division of General Dynamics Corporation, Fort Worth, Texas
Chance Vought Aircraft, Incorporated, Operational Factors and Reliability P. O. Box 5907 Dallas, Texas
Douglas Aircraft Company, Inc., El Segundo, California
Fairchild Astrionics Division, Wyandanch, Long Island, New York
Grumman Aircraft Engineering Corporation, Bethpage, New York
Link, Division of General Precision, Inc., Hillcrest, Binghamton, New York
Lockheed Aircraft Corporation Flight Simulators, California Division, Burbank, California
Lockheed Electronics Corporation, Plainfield, New Jersey
Lockheed Missile Systems Division, Sunnyvale, California
McDennell Aircraft Corporation, Box 516, St. Louis 3, Missouri
North American Aviation, Inc., Columbus Division, 4300 East Fifth Avenue, Columbus 16, Ohio
North American Aviation, Inc., International Airport, Los Angeles 45, California

NAVTRADEVCEEN 801A

Sikorsky Aircraft Division, Division of United Aircraft Corporation,
Stratford, Connecticut
Sylvania Electronic Systems, Data Systems Operations, 189 B Street Needham,
Massachusetts
The University of Michigan Analog Computer Laboratory, P. O. Box 2008, Ann
Arbor, Michigan
Electric Boat Division, General Dynamics Corporation, Groton, Connecticut
Boeing, Seattle, Washington
Republic Aviation Corporation, Farmingdale, New York, Attn: Library
United Airlines, Flight Simulator Engineering Denver, Colorado
Capitol Airlines, National Airport, Washington 1, D C., Attn: R. A Collins
American Airlines, Flight Simulator Engineering, 100 Park Avenue, New York, New York
Western Airlines, Synthetic Training, P. O. Box 45005, Los Angeles 45, California
Trans World Airlines, Systems Director, Transportation Training, 10 Richards
Road, Kansas City 5, Missouri
SAE GSE 3 Committee, 485 Lexington Avenue, New York 17, New York